THERMOPHOTOVOLTAIC APPLICATIONS IN THE UK: CRITICAL ASPECTS OF SYSTEM DESIGN

THOMAS BAUER

A thesis submitted in partial fulfilment

of the requirements of

Northumbria University

for the degree of

Doctor of Philosophy

Research undertaken in the

Northumbria Photovoltaics Applications Centre

in the

School of Computing, Engineering and Information Sciences

July 2005

Abstract

Almost 50 years of thermophotovoltaic (TPV) research from various sectors has resulted in a variety of potential applications and TPV technology options. In this work the potential of commercial TPV applications is assessed with specific reference to the UK. The assessment considers competing technologies for electricity generation, namely solar photovoltaics, external and internal heat engine generators, electro-chemical cells and direct heat-to-electricity conversion devices. Electricity generation by TPV conversion from waste heat of industrial high-temperature processes is identified as one of the most suitable TPV applications. This market is examined in more detail using three specific high-temperature processes from the iron and steel and the glass sectors. Results are extrapolated to the entire UK high-temperature industry and include potential energy and CO_2 savings. This work gathers knowledge from TPV and other literature sources and evaluates the technological options for the heat source, the radiator and the PV cell for a TPV system. The optical control in terms of the angular, spatial and in particular spectral radiation distributions in cavities is identified as a specific factor for TPV conversion and critical for a system design. The impact of simultaneous radiation suppression above and below the PV cell bandgap on an ultimate efficiency level is examined. This research focuses on fused silica (SiO_2) in TPV cavities and examines the aspects of radiation guidance by total internal reflection and spectral control using coupled radiative and conductive heat transfer. Finite volume modelling and experimental work have examined the radiator-glass-air-PV cell arrangement up to a SiO_2 thickness of 20 cm. Both show that the efficiency improves for an increased SiO_2 thickness. Finally, the novel concept of a TPV cavity consisting of a solid dielectric medium is assessed.

List of contents

List of tables

List of figures

List of abbreviations

1D, 2D or 3D	One, two or three dimensional
A	
AC	Alternating current
AFC	Alkaline fuel cell
Al_2O_3	Alumina
AM	Air mass
AMTEC	Alkali metal thermal-to-electric converter
APU	Auxiliary power unit
AR	Antireflective
B	
BASE	Beta alumina solid electrolyte
BSR	Back surface reflector
C	
Ce_2O_3	Ceria
CO	Carbon monoxide
CO_2	Carbon dioxide
CH_4	Methane
CH_3OH	Methanol
CHP	Combined heat and power
D	
DMFC	Direct methanol fuel cell
E	
EAF	Electric arc furnace
EU	European Union
F	
FF	Fill factor
FSF	Front surface filter
FSS	Frequency selective surface
G	
GaSb	Gallium antimonide
Ge	Germanium
H	
HfO_2	Hafnia
H_xC_x	Hydrocarbons
I	
ICE	Internal combustion engine
IEEE	Institute of Electrical and Electronics Engineers
InGaAs	Indium gallium arsenide
InGaAsSb	Indium gallium arsenide antimonide
InP	Indium phosphide
IR	Infrared
ISE	Fraunhofer Institute for Solar Energy Systems, Freiburg
ISFH	Institut für Solarenergieforschung GmbH Hameln/Emmerthal
ISET	Institut für Solare Energieversorgungstechnik, University Kassel
L	
LCD	Liquid crystal display
LPE	Liquid phase epitaxy
LPG	Liquefied propane gas
M	
MBE	Molecular beam epitaxy
MCFC	Molten carbonate fuel cell
MFI	Multi foil insulation
MgO	Magnesia
MIM	Monolithic interconnected module
MIS	Metal insulation semiconductor

MIT	Massachusetts Institute of Technology
MTPV	Micron-gap thermophotovoltaic
MOCVD	Metal organic vapour phase epitaxy
N	
N_2	Nitrogen
N/A	Not available
NREL	National Renewable Energy Laboratory
NPAC	Northumbria Photovoltaics Applications Centre
NO_x	Nitrogen oxides
O	
OC	Open circuit
P	
PAFC	Phosphoric acid fuel cell
PC	Personal computer
PID	Proportional intergral derivative
PV	Photovoltaic, Photovoltaics
psi	Pound per square inch (1 psi =6895 Pascal)
PSI	Paul Scherrer Institute
Q	
QE	Quantum efficiency
QWC	Quantum well cell
R	
RAGA	Radiator-Air-Glass-Air-PV cell
RCF	Refractory ceramic fibre
RGA	Radiator-Glass-Air-PV Cell
RG	Radiator-Glass-PV Cell
RTE	Radiative Transfer Equation
S	
SEC	Specific energy consumption
SiC	Silicon carbide
SiGe	Silicon germanium
SiO_2	Fused silica (quartz glass)
Si_3N_4	Silicon nitride
SC	Short circuit
SOFC	Solid oxide fuel cell
SO_x	Sulphur oxides
SPFC	Solid polymer membrane fuel cell
STPV	Solar thermophotovoltaic
T	
TCO	Transparent conducting oxide
TE	Thermoelectric
ThO_2	Thoria
TPX	Thermophotonic
TPV	Thermophotovoltaic, Thermophotovoltaics
U	
UE	Ultimate efficiency
UK	United Kingdom
UPS	Uninterruptible power supply
US	United States of America
W	
WS	WS-Wärmeprozesstechnik GmbH
Y	
YAG	Yttrium aluminium garnet
Y_2O_3	Yttria
Yb_2O_3	Ytterbia
Z	
ZrO_2	(stabilised) Zirconia

List of symbols

A	Area, cross section (m^2)
A	Thermionic constant (A K^{-2} m^{-2})
A_a	Aperture area of a solar concentrator (m^2)
A_r	Receiver area of a solar concentrator (m^2)
b	Constant of Wien's displacement law b = $2.898 \cdot 10^{-3}$ m K
c_0	Speed of light in vacuum $c_0 = 2.99792 \cdot 10^8$ m s^{-1}
c_p	Specific heat capacity (J kg^{-1} K^{-1})
$c_{p,w}$	Specific heat capacity of water $c_{p,w}$ = 4187 J kg^{-1} K^{-1} @ 298 K
d	Distance, diameter (m)
e_0	Elementary charge $e_0 = 1.60218 \cdot 10^{-19}$ A s
f	Sticking coefficient of the Hertz-Langmuir equation
f	Flow coefficient of the radiant tube burner (m^3 $hour^{-1}$ $mbar^{-1/2}$)
f_{air}	Air flow coefficient of the radiant tube burner f_{air} 2.4 m^3 $hour^{-1}$ $mbar^{-1/2}$
f_{gas}	Gas flow coefficient of the radiant tube burner f_{gas} = 0.25 m^3 $hour^{-1}$ $mbar^{-1/2}$
F_{h-c}	View factor from the hot to the cold plate (1)
h	Planck's constant h = $6.62617 \cdot 10^{-34}$ J s
hv	Photon energy (J)
hv_g	Bandgap energy (J)
H	Heat flux (W m^{-2})
H_u	Calorific value of a typical North Sea natural gas H_u = 34.91 MJ m^{-3}
i_b	Total blackbody intensity (W m^{-2})
$i_{b\lambda}$	Planck's function depending on wavelength (W m^{-2} μm^{-1})
i_{bv}	Planck's function depending on frequency (W m^{-2} s)
I_b	Total blackbody radiation intensity (W m^{-2})
$I_{b\lambda}$	Blackbody radiation intensity depending on wavelength (W m^{-2} μm^{-1})
I_{bv}	Blackbody radiation intensity depending on frequency (W m^{-2} s)
I	PV cell current (A)
I	Radiation intensity
$I_{0,\lambda}$	Initial radiation intensity (W m^{-2})
$I_{S,\lambda}$	Radiation intensity after path length S (W m^{-2})
I_{ph}	PV cell photocurrent (A)
I_s	PV cell saturation current (A)
I_s	Blackbody radiation - solar PV case (W m^{-2})
I_{sc}	PV cell short circuit current (A)
I_T	Blackbody radiation assuming the ultimate band model - TPV case (W m^{-2})
J_m	Current density at the maximum power point of the PV cell (A m^{-2})
J_{max}	Maximum photocurrent density (A m^{-2})
J_{ph}	Photocurrent density (A m^{-2})
k	Thermal conductivity (W m^{-1} K^{-1})
k	Boltzmann constant k = $1.38066 \cdot 10^{-23}$ J K^{-1}
k_R	Radiative conductivity of the Rosseland approximation (W m^{-1} K^{-1})
k_G	Thermal conductivity of SiO_2 (W m^{-1} K^{-1})
k_A	Thermal conductivity of air or vacuum (W m^{-1} K^{-1})
$k_{(\lambda)}$	Extinction coefficient (1)
L	Thickness (m)
L/R	Ratio of depth L to radius R of a cylinder (1)
M	Molecular weight (gram)
m	Mass (kg)
m_e	Electron mass $m_e = 9.1094 \cdot 10^{-31}$ kg
m*	Effective mass (kg)
n	Refractive index (1)
n_{ph}	Number of photons (1)
n_A	Refractive index of air or vacuum (1)
n_G	Refractive index of SiO_2 (1)
N	Number, Number of charge carriers (1)

p_v	Vapour pressure (torr)
ΔP	Differential pressure across the orifice (mbar)
ΔP_{gas}	Differential gas pressure across the orifice (mbar)
ΔP_{air}	Differential air pressure across the orifice (mbar)
P	Power (W), power density (W m^{-2})
P	Absolute pressure (mbar)
P_{el}	Electrical output power of the PV cell in the maximum power point (W)
$P_{el.net}$	P_{el} minus house keeping power (W)
$P_{el.meas}$	Measured electrical power density of the PV cell (W m^{-2})
P_{flue}	Thermal power in the flue gas (W)
P_{flux}	Measured power by the heat flux meter (W)
P_{heat}	Heat output of the PV cell (W)
P_{in}	Input power of the radiant tube burner (W)
P_{input}	Total input power of the TPV system (W)
P_{net}	Net heat transfer to the radiator (W)
P_m	Maximum power output of the PV cell (W)
$P_{peltier}$	Electrical input power of the Peltier element (W)
P_{PV}	Net absorbed power of the PV cell with conduction and convection (W)
$P_{PV\#}$	Net absorbed radiative power of the PV cell (W)
$P_{small.alu}$	Absorbed heat in the water of the small aluminium heat exchanger (W)
P_{solar}	Ultimate power density limit of solar PV conversion (W m^{-2})
P_{TPV}	Ultimate power density limit of TPV conversion (W m^{-2})
Q	Quality factor of the transparent conduction oxide filter
Q_s	Number of photons with energies greater hv_g - solar PV case (m^{-2} s^{-1})
Q_T	Number of photons with energies greater hv_g - TPV case (m^{-2} s^{-1})
r_s	Sun radius $r_s = 6.96 \cdot 10^8$ m
r_{se}	Sun-earth distance $r_{se} = 1.50 \cdot 10^{11}$ m
r+	Ratio of radiation in the upper spectral band divided by the total radiation above x_g (1)
r-	Ratio of radiation in the lower spectral band divided by the total radiation below x_g (1)
R_p	PV cell parallel resistance (Ω)
R_s	PV cell series resistance (Ω)
$\vec{s}$	Direction vector for the Radiative Transfer Equation (1)
S	Path length (m)
S	Seebeck coefficient (V K^{-1})
S_r	Radiation source term
t	Time (s)
ΔT	Differential temperature (K)
T	Temperature (K)
T_a	Absorber temperature (K)
T_A	Air temperature (K)
T_{AV}	Average temperature (K)
T_c	Cold side or cell temperature (K)
T_G	SiO_2 temperature (K)
T_h	Hot side temperature (K)
T_r	Radiator temperature (K)
T_s	Source or sun surface temperature (K)
v	Frequency (s^{-1})
v-	Frequency band limit below v_g (s^{-1})
v+	Frequency band limit above v_g (s^{-1})
v_g	Bandgap frequency (s^{-1})
v_p	Plasma frequency (s^{-1})
V	Flow rate (m^3 s^{-1})
V_{air}	Flow rate of the combustion air of the radiant tube burner (m^3 s^{-1})
V_g	Bandgap voltage (V)
V_{gas}	Flow rate of the natural gas of the radiant tube burner (m^3 s^{-1})
V_m	Voltage at the maximum power point of the PV cell (V)
V_{oc}	Open circuits voltage (V)
V_w	Flow rate water (m^3 s^{-1})

W	Evaporation rate (gram cm^{-2} s^{-1})
x	Substitution $x = hv/kT_s$ (1)
$x-$	Band limit below x_g (1)
$x+$	Band limit above x_g (1)
x_g	Normalised bandgap $x_g = hv_g/kT_s$ (1)
Z	Figure of merit for thermoelectric generator (K^{-1})

α	Absorption coefficient (m^{-1})
ε	Emissivity (1)
ε_a	Apparent emissivity (1)
ε_w	Wall emissivity (1)
ε_0	Dielectric constant in vacuum $\varepsilon_0 = 8.85418 \cdot 10^{-14}$ F m^{-1}
ε_b	Dielectric constant of the semiconductor (1)
η	Efficiency (1)
η_{cavity}	Efficiency of the cavity (1)
η_{source}	Efficiency of the heat source (1)
η_{PV}	Efficiency of the PV cell with conduction and convection (1)
η_{TPV}	Electrical thermophotovoltaic efficiency (1)
$\eta_{TPV,CHP}$	Combined heat and power thermophotovoltaic efficiency (1)
η_{house}	Efficiency of house keeping power sources (1)
η_{sys}	Electrical efficiency of the TPV system (1)
$\eta_{sys,CHP}$	Combined heat and power efficiency of the TPV system (1)
η_{OC}	Voltage factor (1)
η_{QE}	Collection efficiency (1)
η_{FF}	Fill factor (1)
η_{UE}	Ultimate efficiency (1)
η_{Array}	PV cell array efficiency (1)
θ	Angle, zenith angle (°)
θ_s	Opening half angle of the sun at the Earth's distance (°)
λ	Wavelength (μm)
λ_{max}	Wavelength where Planck's function becomes maximum (μm)
μ	Electron mobility of the semiconductor (m^2 V^{-1} s^{-1})
π	Constant $\pi = 3{,}14159$ (1)
ρ	Density (kg m^{-3})
ρ_N	Density of the gas (kg m^{-3})
ρ_w	Density of water $\rho_w = 1003$ kg m^{-3} @ 298 K
ρ_{gas}	Density of a typical North Sea natural gas $\rho_{gas} = 0.719$ kg m^{-3}
ρ	Reflection (1)
$\rho_\perp$	Reflection, polarisation perpendicular to plane of incidence (1)
ρ_{II}	Reflection, polarisation in plane of incidence (1)
σ	Stefan-Boltzmann constant $\sigma = 5.6705 \cdot 10^{-8}$ W m^{-2} K^{-4}
σ	Electrical conductivity (S m^{-1})
Φ	Work function (J)

Acknowledgement

First, I would like to thank my supervisors, Prof. Nicola Pearsall, Dr. Ian Forbes and Dr. Roger Penlington, for their guidance in this research project. In particular I wish to thank Dr. Ian Forbes for the support in innumerable discussions and the backing of Prof. Nicola Pearsall for all orders and the preparation and travelling for several conferences. The Northumbria Photovoltaics Applications Centre (NPAC) group was a very pleasant environment to work and many thanks to Kathleen Hynes who had always an open ear for the daily life hitches, Jayaraman Ramachandran and Dr. David Johnston for the enjoyable time inside and outside the university, and also Dr. Robert Miles, Ogah Ekechi and Paresh Nasikkar. Thanks are also due to James Scott from NPAC for all his effort and input in the construction of the experimental components. There have been several other people from Northumbria University, which assisted kindly the experimental work and I wish to thank all of them. They include Joe Allen who provided valuable knowledge about fused silica, Ed Lancely and others which organised a quick move of the radiant tube furnace, Bob Johnson from the fine art department who lent propane equipment, John Bagnall who machined some aluminium parts and Robert Best and Simone Rose from the Advanced Materials Research Institute which supported the work with liquid nitrogen, material characterisation and polishing equipment. I also thank John Marshall the glassblower from Newcastle University who kind-heartedly made the fused silica components. I would like to acknowledge the help of John Stanley from Tekniform Ltd for the custom-made refractory ceramic fibre tubes and silicon carbide cups, Dietrich Abel from WS-Wärmeprozesstechnik GmbH for the support in the radiant tube burner repair, as well as Atul Bakshi and Jonathon Hughes from Fuel Furnace Engineering LTD for the installation of the radiant tube furnace. I am grateful

to the North East development program for the financing of the radiant tube furnace and the UK PV network for sponsoring my attendance at the 5th Conference on Thermophotovoltaic Generation of Electricity.

Special thanks to Dr. Séan Danaher from Northumbria University, Dr. Eon O'Mongain from the University College Dublin, Prof. Dr. rer. nat. Hans-Ulrich Heß from the University of Applied Science at Heilbronn and Dr. Helmuth Thomas from the Royal Netherlands Institute for Sea Research for their discussions and stimulations to start a PhD degree.

Last but not least, I want to thank my wife, my parents and the friends for their support.

Author's declaration

The author declares that this work has not been submitted for any other award and that it is the work of the author alone. The Appendix A contains a list of publications and presentations, which were also part of this degree. The author also declares that the required training programme has been completed.

This work was funded by the School of Computing, Engineering and Information Sciences and the NPAC at Northumbria University.

1 Introduction

1.1 Importance of thermophotovoltaics

1.1.1 Energy aspect

In modern industrial society, the majority of energy is consumed in the sectors of transportation, building and industry, and fossil fuels are the primary sources of this energy. The use of fossil fuels has led to worldwide concerns about security of supply, increasing energy demand, limitation of resources and local and global environment impacts (e.g. acid rain and climate change). A consequence is increased interest in non-fossil fuel energy resources and the efficient use of fossil fuel. Thermophotovoltaics (TPV) converts heat directly into electricity and has been examined in all major energy sectors for both non-fossil fuel energy resources (e.g. radioactive, solar heat and biomass) and the efficient use of fossil fuel. Potentially TPV systems can convert heat into electricity with Carnot efficiency, which would make it an attractive alternative to existing electricity generation technologies. At the current stage of research high efficiencies have not been demonstrated and it is uncertain which practical efficiencies TPV systems can achieve. However, even moderate (partly) demonstrated efficiencies make TPV conversion already attractive for the efficient use of fossil fuel in

applications such as combined heat and power (CHP) and waste heat recovery. Currently, TPV systems are mainly developed for fossil fuel powered applications, which are not favourable from the energy saving aspect. However, the fuel flexibility of TPV systems allows the change from fossil fuels to bio-fuels in future, which may be more difficult for other technologies (e.g. fuel cells). Hence, TPV conversion could solve some of the fossil fuel constraints, if market and technology challenges can be overcome.

1.1.2 Technology aspect

TPV conversion has inherently some properties which makes it advantageous compared to existing methods to supply electricity. In industrial countries the vast amount of electricity is generated centrally in large power plants using internal and external heat engines (e.g. gas and steam turbines) together with a generator, and transmitted and distributed via the grid. One major disadvantages of central power generation is the waste of large amounts of heat, in the UK for example, fossil fuel powered plants discharge about 60% of their input as waste heat [1]. Other disadvantages include the system complexity, security of supply issues (e.g. black outs) and distribution and transmission losses. Hence, a rather distributed generation of heat and electricity would be genereally desirable. However, downscaling of central power technologies is critical in terms of reduced efficiency, high maintenance and noise. On the small-scale power, in the order of milliwatts to hundreds of watts, a large amount of non-grid connected electricity originates from (rechargeable) batteries, which have disadvantages in terms of lifetime, operation time and gravimetric energy densities (MJ/kg). Hydrocarbon fuels have in the order of 100 times higher gravimetric energy

densities and can be easily stored and continuously supplied [2]. Here, TPV conversion is a promising technology to convert hydrocarbon fuels into electricity.

It can be concluded that both batteries and large power plants using the grid have their own disadvantages to supply electricity. This is especially true for the intermediate power range (around 10 W to 10 kW). TPV conversion is one of several other technologies in a research and development stage that offer advantages over this existing electricity supply infrastructure. These include high reliability, low noise, high gravimetric and volumetric energy density, portability or long operation time, and can be expected to replace the existing infrastructure in the intermediate power range in future.

1.2 Solar PV and TPV conversion

Both solar photovoltaics (PV) and thermophotovoltaics (TPV) use photovoltaic cells to generate electricity from the radiation of a high-temperature thermal source. The key differences are the geometry and the temperature of the heat source [3].

1.2.1 Solar photovoltaics

The sun surface radiation corresponds approximately to 5800 K blackbody radiation. The intensity (W/m^2) drops over the large distance to a maximum value of approximately 0.1 W/cm^2 at the earth surface (Figure 1-1 upper part)[4,5]. The major part of the solar radiation is in the visible spectral range according to Planck's radiation law. Solar PV operates rather unsteadily in terms of intensity, spectrum and angle of solar radiation as well as PV cell temperature, because these parameters depend on location (latitude, longitude), different cycles (solar, annual, seasonal, daily), cloud cover and atmospheric absorption. For solar PV, the radiation intensity has a given

magnitude. Hence, choosing the ideal PV cell bandgap allows a simultaneous maximisation of the efficiency and the electrical power density. Assuming a solar intensity of 0.1 W/cm^2 and a conversion efficiency of 20% leads to a maximum electrical power density of about 0.02 W/cm^2. For non-concentrator solar PV, CHP operation is usually not utilised, so that the remaining heat is lost (for the assumption 0.08 W/cm^2).

1.2.2 Thermophotovoltaics

TPV conversion, on the other hand, can use a variety of heat sources, which usually heat up a radiator[1] to typically 1300 to 2000K (Figure 1-1 lower part). This temperature range leads to a theoretical hemispherical total radiation per unit area of approximately 16 to 91 W/cm^2 according to the Stefan-Boltzmann law (σT_s^4). Ideally no radiation is lost due to the close arrangement of radiator and PV cells. This has allowed demonstration of electrical power densities of the PV cell over 4 W/cm^2. The major part of this radiation is in the infrared spectral range according to Planck's radiation law. TPV systems typically operate steadily in terms of intensity, spectrum and angle of radiation as well as PV cell temperature. For example in waste heat recovery applications these systems may operate steadily 24 hours a day and 365 days per year, where these parameters may only alter due to some wear and ageing of the TPV system. Defining TPV efficiency is more complex compared to solar PV. The total input may be defined for example as the calorific value of a fuel or as a heat flux. Also, the high power densities in TPV conversion make CHP operation possible, so that the useful

[1] There are a few arrangements imaginable where no radiator may be required including the direct conversion of flame radiation and the conversion of waste heat where the process already radiates with a suitable spectrum.

output can be either purely electricity or electricity and heat. Therefore, the definition of TPV efficiency as useful output to total input is not unambiguous. TPV system design usually requires a spectral control concept and selection and design of the heat source, radiator and PV cell each with their own limitations and qualities. Figure 1-1 shows some examples of the various concepts and component options. Spectral control is a method to spectrally match the absorbed power of the PV cell in accordance to its bandgap and often includes additional components such as filters. In the solar PV case, photons with energies below the PV cell bandgap energy (out-of-band radiation) are lost. TPV systems, however, can suppress or recover these photons by some form of spectral control to increase the efficiency. The potentially higher efficiency of TPV conversion compared to solar PV conversion due to spectral control has been only partly demonstrated. CHP operation using TPV systems has been demonstrated and the high overall efficiency can be of interest in applications such as domestic micro CHP systems.

It can be summarised that TPV system design is more complex, but has advantages including steady operation, potentially higher efficiency and heat source flexibility, if compared to solar PV. Additionally, TPV conversion offers effective CHP operation and has demonstrated high electrical power densities compared to non-concentrator solar PV.

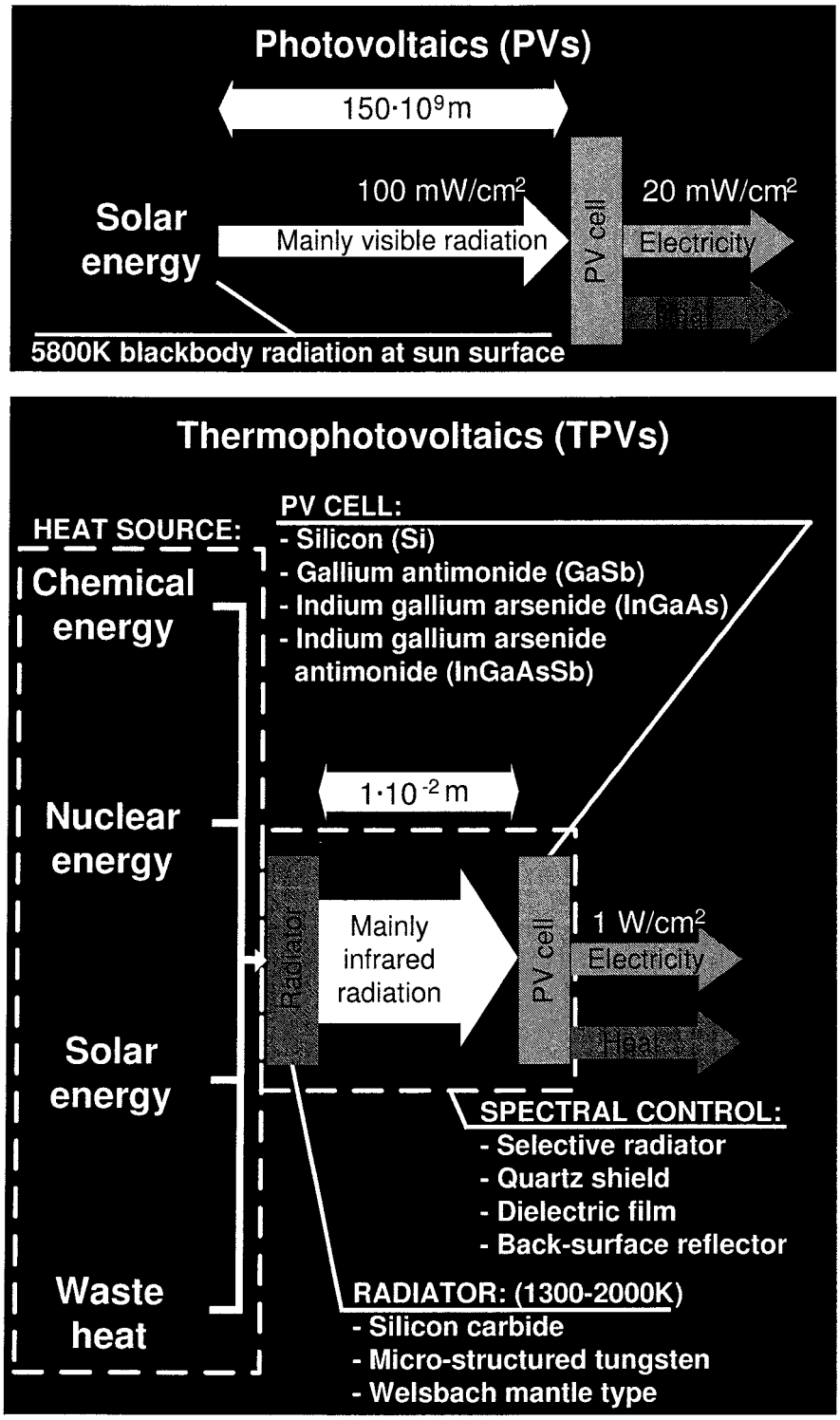

Figure 1-1: Comparison of solar photovoltaic and thermophotovoltaic conversion.

1.3 Objectives and methodology

In this research, there are two major objectives. Firstly, TPV technology options are reviewed with the focus on the most critical aspects. In addition, potential TPV applications are assessed for the UK, where promising applications are selected and discussed in more detail. This selection involves mapping of the capabilities of TPV technology and the requirements of UK applications. Secondly, for the selected applications a detailed system design is developed, where critical aspects are identified and examined by modelling and experiments.

1.3.1 Technology and application assessment

There has been some PV cell research for TPV at the Northumbria Photovoltaics Applications Centre (NPAC) previously. Published TPV research in the UK was carried out by the Imperial College of Science, Technology and Medicine (Quantum Photovoltaics Group), the University of Oxford (Nicholas Semiconductor Research Group), the University of Hull (The Optoelectronic Devices Research Group), Cardiff University and the University of Sheffield. These groups also focus on PV cell research, so that published work on TPV applications and system designs is limited in the UK.

Focusing of TPV research is challenging for several reasons. One reason is the limited number of published TPV survey or review articles. So far, there have been some book chapters about TPV conversion but no complete book, despite the large number of publications and almost 50 years of TPV research. The last comprehensive TPV review article dates back to 1999 by Coutts, which cannot include recent developments [3]. Focusing on a technological concept of TPV is also challenging. The major components of heat source, radiator and PV cell, as well as spectral control methods reveal a large number of technology options (see examples in Figure 1-1). The

TPV system performance is critically dependent on the combination of the components used, so that a large number of technology options in conjunction with each other have to be considered. The field of TPV has multiple disciplines and knowledge about the heat source, radiator and PV cell need to be gathered from other related research fields. The optical control in the cavity between radiator and PV cell impacts decisively on the TPV figures of merit, high efficiency and high electrical power density, and can be regarded as an TPV intrinsic research field. Aspects that need to be considered are for example absorbed photons by the PV cell with energies below the bandgap, the incident angle of the radiation at PV cell and the uniformity of PV cell illumination. Hence, the cavity component options need to be selected such, that the radiative heat transfer in the cavity is optimised in terms of all the spectral, angular and spatial radiation distributions. Additionally, TPV technology options and applications become diverse due to a variety of interest groups all with their own focus. They include the US military, the US space industry, the gas industry, the automotive industry, the CHP community and the PV community. Finally, competing technologies need to be considered, so that TPV applications do not focus on areas, where other technologies may be superior.

The following methodology is chosen to meet the first major objective. In a TPV technology review information sources are identified and the major development milestones are placed in a historical perspective (Chapter 3). This chapter then presents an individual assessment of the major TPV components (heat source, radiator and PV cell). Recently suggested novel TPV concepts are also briefly discussed. The concepts of optical control including related components, such as filters, are identified as a critical aspect of TPV system designs in this work and are reviewed in more detail in

Chapter 4. Out of the optical control approaches, fused silica (SiO_2) shields are of particular interest (also called quartz glass). Reasons for this interest include its common usage in TPV systems and the limited research how these shields participate in the spectral control of the cavity. Also during the period of this project, another group reported modelling work that indicated that spectral control using SiO_2 shields could be improved by increasing the shield thickness. Hence, this work focuses on SiO_2 in TPV cavities and their impact on the spectral control.

Technologies competing with TPV conversion have been collected and sorted into groups relating to their conversion process. The groups were as follows, heat engine generators, electro-chemical cells, direct heat-to-electricity conversion devices and solar PV (Chapter 5). Figures of merit, which allow a technological comparison among competitors and with TPV, are identified. This enables the determination of the specific advantages and disadvantages of TPV conversion.

In Chapter 6 potential TPV applications are identified and assessed. First the applications from TPV and competing technology literature are collected and grouped. For the applications groups, a rating system and figures of merits are defined. The assumptions made in this step result in a pre-selection of applications. Knowledge about specific TPV advantages and disadvantages can help to define these assumptions. The rating system then identifies the applications with the highest potential.

The application of industrial high-temperature heat recovery is selected for this work and is discussed in more detail in Chapter 7. The detailed discussion focuses on aspects already identified in the rating system of the previous chapter. The diversity of this application limits the examination to specific processes in selected industries and findings can then be extrapolated.

1.3.2 Critical aspects of system design

The second major objective is outlined in the following. The quality of spectral control methods can be described using the underlying theory of PV cell conversion and heat transfer. Of the three heat transfer modes, radiation, conduction and convection, the spectral radiation distribution in relation to the PV cell bandgap is of particular importance for TPV conversion. In this work, spectral control methods are defined as means to suppress photons with energies below the PV cell bandgap energy being absorbed by the PV cell. This work selects SiO_2 shields as a spectral control approach. Cavity heat transfer in a practical TPV system is generally complex, if for example a common TPV cavity consisting of the arrangement Radiator-Air-Glass-Air-PV cell (RAGA) is considered. A number of groups have presented a variety of analytical and computational heat transfer models, all with their own simplified assumptions about the cavity heat transfer. Various aspects of the SiO_2 shield are thought to influence the spectral control, such as the boundary conditions (e.g. shield thickness, shield surface reflection, external cooling), the mechanisms within the SiO_2 (e.g. absorption and re-emission of radiation, coupled radiation and conduction) and the material properties (e.g. refractive index, absorption coefficient, thermal conductivity). Past TPV modelling work focusing on the SiO_2 shield has not examined the impact of these aspects in detail. One objective of this work is to review and select a suitable model to study how the shield affects the spectral control in a typical TPV cavity.

In this work it is found that the efficiency improves for an increased shield thickness and that surface reflections reduce the electrical power density. Hence, an alternative arrangement Radiator-Glass-Air-PV cell (RGA) is proposed instead of the RAGA arrangement. Modelling results indicate that a SiO_2 thickness of around 10 cm is

required. For such a thickness, total internal reflection seems to be the mechanism that minimises side losses. Although earlier TPV research has experimentally applied such radiation guidance and high power densities could be achieved, however the losses of such radiation guidance were not quantified. Hence, another objective of this work is to compare an experimental RGA arrangement using total internal reflection and different SiO_2 thicknesses with 1D modelling results in terms of efficiency and electrical power density. Power density results then allow statements about the quality and losses of the radiation guidance. Also the experiments can give valuable information about difficulties that may occur for an implementation of a TPV heat recovery system in a high-temperature industrial process.

It is known, that total blackbody emission into a medium with higher refractive index than 1 scales with the refractive index squared. Recently for micron-gap TPV (MTPV) system it was suggested that the photon flux is limited by the lowest refractive index in the photonic cavity and scales with the minimum refractive index squared. Hence, work reported in this thesis proposes and models the Radiator-Glass-PV cell (RG) arrangement. The aim is to determine, by modelling, whether the power density and/or efficiency can be enhanced compared to the RAGA and RGA arrangements.

The following methodology is adapted to meet the second major objective. In Chapter 3, a Sankey diagram of a general type of a TPV system is composed and partial efficiencies are defined. It is found that the ultimate efficiency is the decisive partial efficiency in terms of the spectral control. Hence, the modelling assumed all other partial efficiencies are ideal. The ultimate efficiency is well known for solar PV conversion and is extended to the more general TPV case. This allows insights into spectral control in general and can give an upper limit for the efficiency and electrical

power density. Here, also the impact of the simultaneous above and below bandgap suppression is considered.

Chapter 8 presents all computational heat transfer modelling to verify experimental results. The literature review presents past modelling in the order of increasing complexity. This also illustrates the historical development in TPV heat transfer modelling. Then, the modelling methodology and the assumptions are presented. Finally, results of all three arrangements RAGA, RGA and RG are analysed.

The concepts of TPV cavity design including total internal reflection are discussed in Chapter 4. Chapter 9 selects a suitable cavity design and discusses the experimental implementation of the RGA arrangement using total internal reflection. Initial tests on a temporary furnace aim to determine the feasibility of light guidance and identify critical issues before proceeding to a more sophisticated design that utilises a radiant tube furnace. Then this chapter proceeds with the characterisation and implementation of the RGA arrangement in the radiant tube furnace. Modelling and experimental results are also compared in Chapter 9. In the conclusion (Chapter 10), findings about the implementation of the experimental RGA arrangement in an industrial high-temperature heat recovery process are presented. Here also limitations, future work and implications of this work are presented.

The next chapter (Chapter 2) gives some background theory about conductive, convective and radiative heat transfer focusing on the latter.

2 Theory of heat transfer

2.1 Introduction

Heat transfer is concerned with the transport of thermal energy due to a temperature difference and can occur in three modes. These modes are conduction, convection and radiation. In general, for a TPV system, both conductive and convective heat transfer from the radiator to the PV cell and to the surroundings is parasitic and needs to be minimised. In contrast to this, radiative heat transfer in the cavity needs to be optimised in terms of the spectral, angular and spatial radiation distribution in order to achieve high electrical power densities and efficiencies. Figure 2-1 shows schematically the arrangement of a typical TPV system.

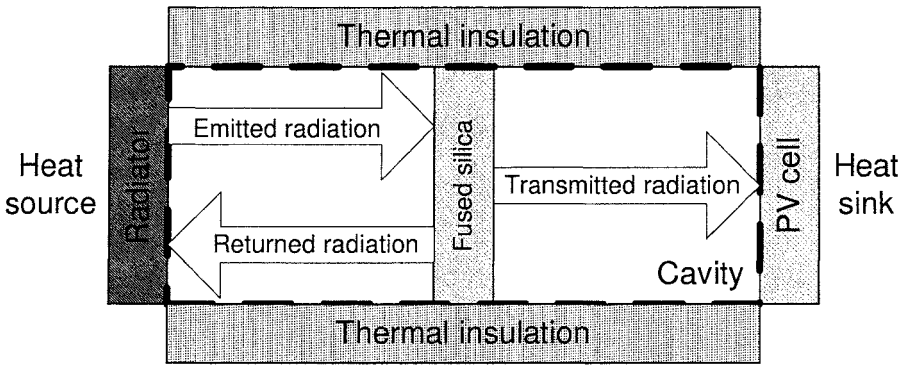

Figure 2-1: Schematic of a typical TPV system with cavity.
The system consists of a heat source thermally connected to the radiator and a heat sink thermally connected to the PV cells, as well as thermal insulation with a reflective surface. Radiator, reflective thermal insulation and PV cell form the TPV cavity.

2.2 Conduction

In the process of heat conduction, energy is transferred in the collision of randomly moving molecules, where the mean position of the molecule is fixed. Equation 2-1 gives the conductive steady state heat flux H (W/m^2), for the simplified one-dimensional (1D) assumption of a homogeneous body of thickness L and the temperature difference T_h - T_c, where k is the thermal conductivity of the material.

$$H = k \cdot \frac{T_h - T_c}{L} \tag{2-1}$$

For TPV conversion, conduction is undesirable and occurs from the radiator to the PV cell through the air (or gas) layer, as well as from the radiator to the surroundings. One location where high conductivity in a TPV system is desirable is the radiator, where a high conductivity results in a uniform radiator surface temperature, so that the emitted radiation tends to become uniform too. Another location of interest for high conductivity is the PV cell mounting on the heat sink, where heat has to be conducted effectively away in order to keep the PV cell temperature low.

2.3 Convection

In the process of heat convection, macroscopic movement of matter transfers energy. It can be distinguished between forced heat convection and free heat convection. Different densities of matter at different temperatures cause free (or natural) heat convection. Parasitic free convection heat transfer may occur in the TPV cavity through gases from the radiator to the PV cell. Cells are usually cooled by forced convection. Often PV cells are cooled by forced water systems, however cooling by forced air [6] and by the thermo-syphon-principal using water seems to be feasible [7].

2.4 Radiation

All materials continuously emit or absorb electromagnetic waves, or photons, by lowering or raising their molecular energy levels and heat transfer by radiation does not require a medium unlike heat transfer by conduction and convection [8,9].

2.4.1 Absorption of radiation

When radiation travelling through a medium strikes the surface of a second medium, radiation may be reflected (either partly or totally), and any non-reflected part will penetrate into the second medium [8]. While passing into the second medium, the **Lambert-Beer law** describes the radiation reduction assuming 1D radiative heat transfer, a non-scattering medium and a constant absorption coefficient $\alpha(\lambda)$ along a path length S, where $I_{0,\lambda}$ is the initial radiation intensity and $I_{L,\lambda}$ the radiation intensity after a path length S (Equation 2-2).

$$I_{L,\lambda} = I_{0,\lambda} \cdot e^{-\alpha_{(\lambda)} \cdot S} \tag{2-2}$$

Here, three cases for the optical thickness $\alpha(\lambda) \cdot S$ can be distinguished [9]:

- Opaque or optically thick: $\alpha(\lambda) \cdot S >> 1$
- Transparent or optically thin: $\alpha(\lambda) \cdot S << 1$
- Semitransparent: for all other cases of $\alpha(\lambda) \cdot S$

Metals tend to require a small path length S to become opaque, although very thin metal layers behave as transparent for some wavelengths. For TPV, gold layers with thicknesses from 15 to 25 nm have been used within dielectric filters [10]. Non-metals generally require much larger thicknesses before they become opaque [8]. For an opaque medium, although radiation penetrates into the medium, interaction with radiation can be treated as a surface phenomenon. For semitransparent media, there are

radiation interactions with the surface and within the medium. Examples in a TPV system are filament ceramic radiators, glass shields or PV cells.

2.4.2 Emission of radiation

The upper limit of radiation emitted at every wavelength λ (or frequency v) and in every direction into a medium with refractive index n is given by a blackbody as described by **Planck's functions** (Equation 2-3)[2] [8,9,11]. The function depends on the radiator temperature T_s.

$$i_{b\lambda(\lambda,T_s)} = \frac{2hc_0^{\,2}}{n^2\lambda^5}\cdot\frac{1}{e^{\frac{hc_0}{kT_s n\lambda}}-1} \qquad i_{bv(v,T_s)} = \frac{2n^2hv^3}{c_0^{\,2}}\cdot\frac{1}{e^{\frac{hv}{kT_s}}-1} \tag{2-3}$$

Wien's displacement law gives the wavelength where this function $i_{b\lambda(\lambda,Ts)}$ becomes maximum (Equation 2-4) [8]. For TPV the implications of this law are that higher radiator temperatures result in a shift of radiation towards shorter wavelengths, where PV cell with a higher energy bandgap can be used.

$$\lambda_{max} = \frac{\lambda_{max,0}}{n} = \frac{b}{n\cdot T_s} \tag{2-4}$$

Integration of $i_{b\lambda(\lambda,Ts)}$ (Equation 2-3) over all wavelengths results in the **total blackbody intensity** (Equation 2-5) [8]. As a result of this law, a higher radiator temperature in a TPV system usually results in higher electrical power densities, because the total emitted radiation increases with the fourth power of the temperature.

$$i_{b(T_s)} = \int_0^\infty i_{b\lambda(\lambda,T_s)}d\lambda = \frac{n^2\sigma T_s^{\,4}}{\pi} \tag{2-5}$$

---

[2] The refractive index n is assumed wavelength and temperature independent. The wavelength λ to frequency v conversion uses the relation: $v\cdot n\cdot\lambda=c_0$. Sometimes the wavenumber is used and this is defined as the reciprocal of the wavelength in vacuum [8].

2.4.3 Radiation interaction at surfaces

Blackbody surfaces are by definition diffuse, so that the directional emitted radiation decreases with polar angle θ away from normal, which is known as the **Lambert's cosine-law** (Equation 2-6) [9]. This law is of less importance, where the radiator is approximately a point source and radiation rays are parallel (e.g. the sun for solar PV[3]), but becomes important for TPV conversion. Assuming a TPV system consisting of two infinite plates, one a blackbody radiator and the other one a PV cell, it becomes clear that radiation is incident at all angles at the PV cell, whereas the cell surface can only absorb radiation under certain angles.

$$I_{b\lambda(\lambda,T_s,\theta)} = i_{b\lambda(\lambda,T_s)} \cdot \cos(\theta) \tag{2-6}$$

Integration of Planck's function (Equation 2-3) over one hemisphere leads to **Planck's radiation law** (Equation 2-7), which defines radiation emitted from a blackbody surface into a second medium with refractive index n over one hemisphere.

$$I_{b\lambda(\lambda,T_s)} = n^2 \cdot \pi \cdot i_{b\lambda(\lambda,T_s)} \qquad I_{bv(v,T_s)} = n^2 \cdot \pi \cdot i_{bv(v,T_s)} \tag{2-7}$$

Integration over all wavelengths λ of Equation 2-7 results in the total hemispherical radiated power $e_{b(Ts)}$, which is known as the **Stefan-Boltzmann law** (Equation 2-8).

$$I_{b(T_s)} = \int_0^\infty I_{bv(v,T_s)} dv = n^2 \frac{2\pi^5 k^4}{15h^3 c_0^{\,2}} T_s^{\,4} = n^2 \sigma T_s^{\,4} \qquad I_{b(T_s)} = \int_0^\infty I_{b\lambda(\lambda,T_s)} d\lambda = n^2 \sigma T_s^{\,4} \tag{2-8}$$

The **emissivity** is then defined as the ratio of real to blackbody radiation varying from 0 to 1, where the definition can be directional spectral (e.g. commonly for normal direction), directional total, hemispherical spectral or hemispherical total [9]. Additionally the surface emissivity depends on temperature, material composition (e.g.

[3] Diffuse solar radiation is not considered here.

oxide films) and physical structure (e.g. rough, polished or engineered microstructures). For example for TPV selective radiators such as tungsten, surface structures have been fabricated in the same order of dimension as the radiation wavelength. The surface can be not only engineered spectrally but also to be directionally selective [8]. This could be useful for TPV radiators, since PV cell surfaces become increasingly reflective for angles away from normal. Only one TPV paper could be found which discuss directionally selective emitting radiators [12]. Surfaces with spectrally constant emissivity are known as grey surfaces. Pure polished metals tend to have high emissivity for short wavelengths (1 to 2 μm). The emissivity for long wavelengths decreases approximately proportional to $\sqrt{T/\lambda}$ [13]. This natural spectral selectivity makes metals suitable for TPV radiators, but the equation also shows that long wavelength emissivity increases with temperature [14]. Ceramics tend to have fairly constant and intermediate emissivity for short wavelengths, followed by a sharp increase at wavelengths around 4 to 10 μm, where lattice and molecular vibration are resonant with long-wavelength photons [13,15]. The temperature dependence of the emissivity of ceramics is rather weak [13].

The **absorptivity** is defined as the ratio of incident to absorbed radiation, where the definition may be directional or hemispherical, as well as spectral or total [8]. Often Kirchhoff's law is valid, which states that the absorptivity is equal to the emissivity. The conditions for this law are discussed elsewhere [8,9].

The **reflectivity** of a surface depends not only on the direction of the incoming radiation (as for the absorptivity), but also on the direction of the reflected radiation. Two ideal cases of reflection can be defined, which are diffuse (equal reflection in all

directions) and specular (mirror like). Real surface reflection can be often approximated by specular, diffuse or combined specular-diffuse reflection.

The **radiative heat transfer** between surfaces can be calculated using view factors. For two infinite parallel plates with blackbody surface characteristics (view factor 1, emissivity 1) the radiative heat flux H (W/m^2) from the hot T_h to the cold T_c plate is given by Equation 2-9, assuming no other modes of heat transfer (conduction and convection) and a transparent medium in between the surfaces [8].

$$H = n^2\sigma \cdot \left(T_h^4 - T_c^4\right) \tag{2-9}$$

This equation can be used as a simple model of radiative heat transfer from the radiator to the PV cell.

2.4.4 Radiation interaction within participating semitransparent media

For semitransparent media, emission and absorption of radiation are bulk, rather than surface, phenomena. The spontaneous spectral emission of radiation in all directions by an isothermal volume element is $n^2 \cdot \alpha \cdot 4\pi \cdot i_{b\lambda(\lambda,T_s)} dV d\lambda$ [9], where α is the absorption coefficient and T_s the temperature of the volume element. Radiation is then absorbed on its way towards the surface. **Lambert-Beer law** describes the radiation reduction for 1D radiative heat transfer (Equation 2-2).

Radiation within the semitransparent medium with refractive index n_1 (e.g. glass) incident on a surface of a second medium with refractive index n_2 (e.g. air) is either internally reflected or refracted across this surface. For optically smooth surfaces the refraction across the surface can be described by **Snell's law** (Equation 2-10).

$$\frac{\sin\theta_2}{\sin\theta_1} = \frac{n_1}{n_2} \tag{2-10}$$

Fresnel's equations give the specular reflection for polarised ($\rho_\perp$ and ρ_{II}) and non-polarised (ρ) radiation depending on the angle of incidence for optically smooth surfaces (Equation 2-11)[8]. Placing Snell's law in Fresnel's equations can reduce the unknowns (n_1, n_2, θ_1 or θ_2) by one.

$$\rho_{II} = \left(\frac{n_1\cos\theta_2 - n_2\cos\theta_1}{n_1\cos\theta_1 + n_2\cos\theta_1}\right)^2 \quad \rho_\perp = \left(\frac{n_1\cos\theta_1 - n_2\cos\theta_2}{n_1\cos\theta_1 + n_2\cos\theta_2}\right)^2 \quad \rho = \frac{1}{2}\rho_{II} + \frac{1}{2}\rho_\perp \tag{2-11}$$

2.5 Summary

This chapter reviewed the theory about the three heat transfer modes: conduction, convection and radiation. In additions, typical examples of heat transfer in TPV systems have been related to the theory. In particular the discussion about radiation will form the basis for the discussion about optical control in Chapter 4. The next chapter reviews and assesses the technological components of TPV systems.

3 Assessment of TPV technology

This chapter incorporates a literature review with a description and discussion of the three major TPV components: heat source, radiator and PV cell. PV cells are reported and compared in terms of the fill factor, collection efficiency and voltage factor, where these partial efficiencies have been calculated from reported values in the literature. The interdisciplinary nature of TPV conversion requires not only referring to TPV literature but also to sources from other technology fields. A discussion took place in context with the literature review rather than a discussion at the end of this chapter because of the large diversity of components in TPV systems.

This chapter starts with some TPV background about information sources, historical developments and efficiency definitions (Section 3.1-3.3). Then the three major TPV components as well as remaining components and advanced TPV concepts are presented (Section 3.4-3.7).

3.1 TPV information sources

Book chapters or sections are useful sources to introduce TPV technology. In particular these include one chapter [16] and one section [17] by Coutts. Fahrenbruch and Bube [18], Green [19] and Würfel [20] mostly focus on solar thermophotovoltaic

(STPV) conversion. Additionally direct energy conversion books discuss TPV conversion, such as by Decher [21] or an older book by Angrist [22].

There have been several PhD and MSc theses at different institutions related to TPV. Available for this work were theses from Massachusetts Institute of Technology (MIT) [23,24], Imperial College of Science, Technology and Medicine [25,26], Karlsruhe University [27], Albert-Ludwigs-Universität Freiburg im Breisgau together with Fraunhofer Institute for Solar Energy Systems (ISE) [28], Swedish University of Agricultural Science, Uppsala together with Solar Energy Research Center (SERC) at Dalarna University [29], Institut für Solarenergieforschung GmbH Hameln/Emmerthal (ISFH) [30] and the Institut für Solare Energieversorgungstechnik at Kassel University (ISET) together with the Robert Bosch company [31]. Schmid from Kassel University also gives a TPV introduction in his energy conversion script [32].

In 1995, Broman published a bibliography of TPV, which contains 180 entries on TPV conversion of energy for the time period from 1950 to 1994 [33]. A comprehensive TPV review article is available from Coutts, which was published in 1999 [3].

Currently the Conference on Thermophotovoltaic Generation of Electricity is the major international event on TPV research. The first four conferences were held under the auspices of the National Renewable Energy Laboratory (NREL) in Colorado, US. The fifth conference was held in Rome in 2002 and the sixth conference in Freiburg in 2004. All of the six proceedings, published by the American Institute of Physics, were available for this work. Other conferences with TPV contributions include the European Photovoltaic Solar Energy Conference, the IEEE Photovoltaic Specialists Conference and the Intersociety Energy Conversion Engineering Conference.

TPV articles can be found in various photovoltaics, physics, material and energy journals. In 2003, the journal Semiconductor Science and Technology released a special issue about TPV [34].

Additionally more than 100 patents can give some insight in TPV [35,36].

3.2 Historical development of TPV technology

Literature about the historical development of TPV includes work by Coutts [3], Ralph and FitzGerald [37], Noreen and Honghua [38] and Nelson [2,39].

The invention of TPV dates back to about 1956. Most literature references cite Aigrain as the inventor of TPV, who proposed the concept during a series of lectures at the MIT in 1956 [3,40]. Nelson reported about a demonstration TPV system at the MIT Lincoln Laboratory by Kolm in the same year [39,41]. Early US research until the mid 1970s focussed on stand alone military power generators using fossil fuel combustion as a heat source. In this early period the three principal heat sources (solar, nuclear, combustion) and spectral control options (selective radiator, filter, PV cell front and back surface reflector) had been identified [39,42-44]. Of the available PV cell materials, both silicon and germanium had their own difficulties. The high silicon bandgap usually requires high radiator temperatures, where engineering difficulties occur. Germanium PV cells require lower radiator temperature but have usually a low performance [3]. In the mid 1970s, the pace of TPV development slowed significantly when the US Army chose thermoelectric technology as a power source and General Motors discontinued TPV research, because of business challenges during the oil crises [39].

However, TPV research overall profited from the research effort after the energy crisis. Solar energy had been identified as one important non-fossil fuel source.

Advances were made in solar TPV (STPV) in the US and Europe, and TPV research has also profit from progress in solar PV. Improvements were made in PV cells using III-V materials and PV concentrator systems, where these III-V PV cells are now commonly used in TPV systems, such as gallium antimonide (GaSb) and indium gallium arsenide (InGaAs) [39] and experience from PV concentrator systems with high radiation densities can be applied to TPV systems (e.g. grid design). TPV research has also benefited from research in the efficient use of fossil fuel and in particular in the area of efficient and durable radiant burners for heating purposes. For example, fibrous rare earth oxide burners [45] and ceramic radiant tube burners [46] have been initially developed for other purposes and could be successfully applied in combustion-powered TPV systems to efficiently convert fuel into radiation.

In the early 1990s there had been a renewed TPV interest for military and space power in the US and two companies were founded to produce GaSb cells (JX-Crystals Inc. and EDTEK Inc.). JX-Crystals developed a propane powered CHP stove (Midnight Sun®) of which 20 units were sold for beta testing [47]. TPV power generators using radioisotope heat sources were considered for deep space missions, where solar PV is not attractive because of the low light level. The Vehicle Research Institute at Western Washington University demonstrated successfully a combustion TPV generator in a hybrid car [48,49].

Recently, TPV development seems to have slowed down in the US, but there is some renewed interest in Europe mainly for the micro CHP application, such as at the ISE and the Paul Scherrer Institut (PSI). Industrial waste heat recovery using TPV conversion is another promising research area, which was proposed by Coutts [3] in the late 90's.

3.3 TPV efficiency definitions

The efficiency of a TPV system depends generally on the definition of the boundaries and is discussed in the following using Figure 3-1.

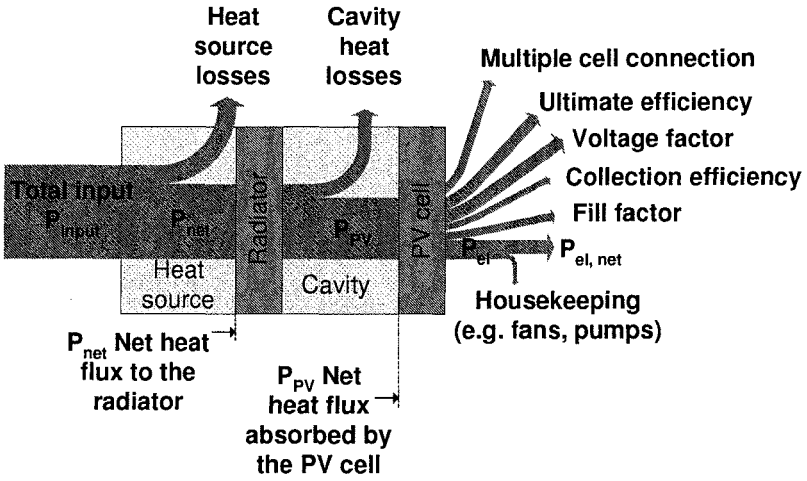

Figure 3-1: Sankey diagram of a general type of TPV system.

Efficiency is generally defined as the ratio of the useful output to the total input. The useful output for a TPV system may be either the generated electrical power or the generated power **and** the useful heat for CHP operation. This makes a TPV system using purely electricity inherently less efficient than a CHP system. Furthermore the output power may or may not include power necessary for system housekeeping (for example fuel pump or electric control). The total input depends on the heat source and can be defined in different ways. Four heat sources are distinguished here, namely chemical energy (e.g. hydrocarbon combustion), nuclear energy (e.g. radioisotope heat), solar energy and waste heat (e.g. from industrial high temperature processes). In a radioisotope, solar or waste heat recovery TPV system the total input may be defined as a heat flux (W/m^2), where heat source losses can often be neglected. In a hydrocarbon combustion system the total input may be defined by the fuel flow rate (e.g. kg/hour). This rate can be converted into an input power (W) assuming gross or net calorific

values of the fuel, where some MJ/kg values are given in Subsection 3.7.2. Efficient high-temperature radiant burners, that operate with natural gas for example, can have heat losses as little as 20% [46]. This heat is mostly lost through the hot flue gas. The percentage value suggests, that high efficiency hydrocarbon powered TPV systems can be configured. On the other hand it can also be pointed out that radioisotope, solar and waste heat recovery TPV systems are inherently more efficient compared to combustion systems. The heat source efficiency can be defined as the ratio of radiator net heat transfer to the total input (e.g. product of fuel flow rate and calorific value), as also shown in Figure 3-1 (Equation 3-1).

$$\eta_{source} = \frac{P_{net}}{P_{input}} \tag{3-1}$$

Practical TPV systems have losses to the surroundings. Loss mechanisms include parasitic absorption by mirrors as well as conduction heat losses from the radiator. The cavity efficiency can be defined as the ratio of net absorbed power by the PV cell to net heat transfer to the radiator (Equation 3-2).

$$\eta_{cavity} = \frac{P_{PV}}{P_{net}} \tag{3-2}$$

In some cases it may be not feasible to separate between heat source and cavity losses, as shown in Figure 3-1, because the heat source with the combustion products and the cavity are spatially not separated (e.g. for hydrocarbon combustion using a Welsbach mantle radiator).

The net absorbed heat flux of the PV cell P_{PV} can consist not only of radiation, but also of parasitic air conduction and convection. These losses can be minimised in a vacuum system. In practice the net absorbed heat flux of the PV cell can then be determined by measuring the total output of the PV cell (Equation 3-3, electricity plus

heat). The PV cell efficiency can be defined as the ratio of electricity output to the net absorbed heat flux. This efficiency depends on several operational conditions including the PV cell temperature, the radiation intensity, as well as the spectral, angular and spatial radiation distribution. So far these operation conditions have not been standardised in order to characterise PV cells for TPV systems. Therefore any PV cell efficiency has to be seen in conjunction with the operation conditions in the TPV system. For example, the efficiency of a specific PV cell can be expected to be high for a spectrally matched radiator and cell, but low for the spectrally unmatched case.

$$\eta_{PV} = \frac{P_{el}}{P_{PV}} = \frac{P_{el}}{P_{heat} + P_{el}} \tag{3-3}$$

The reduction due to house keeping power is expressed in terms of the house keeping efficiency (Equation 3-4).

$$\eta_{house} = \frac{P_{el,net}}{P_{el}} \tag{3-4}$$

The overall efficiency of a TPV system is then a product of all partial efficiencies. Hence, a high system efficiency requires maximisation of all partial efficiencies (Equation 3-5) [50].

$$\eta_{sys} = \eta_{source} \cdot \eta_{cavity} \cdot \eta_{PV} \cdot \eta_{house} = \eta_{source} \cdot \eta_{TPV} = \frac{P_{el,net}}{P_{input}} \tag{3-5}$$

3.4 Heat source

TPV conversion can be classified, by the kind of reaction of the heat source, which is either a chemical reaction (rearrangement of the outer electrons of the atoms) or a nuclear reaction (rearrangement of the nucleus of the atoms). Nuclear reactions are of fusion or fission type. This classification results in three major TPV heat sources (Figure 3-2), which are the combustion of fuels (usually hydrocarbons), solar heat and nuclear sources (radioisotopes and nuclear reactors).

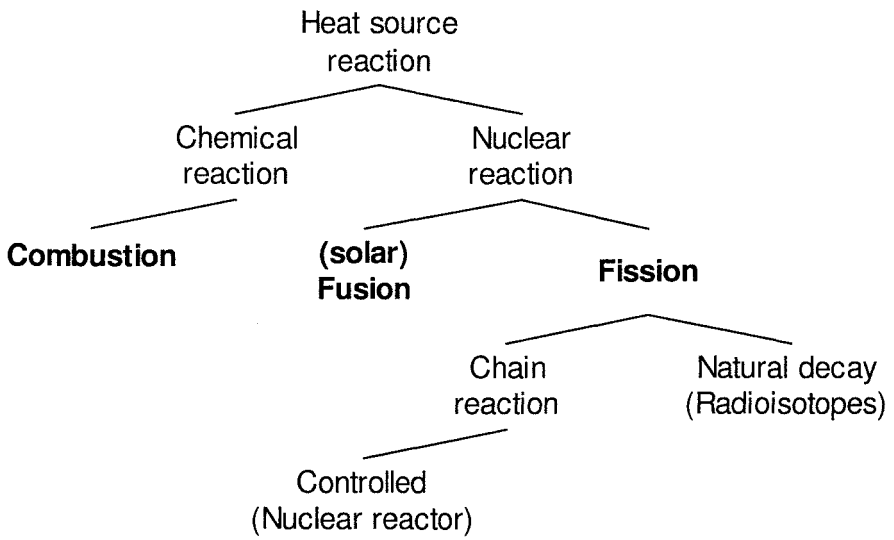

Figure 3-2: Heat sources of TPV conversion classified by their reactions

This work defines a fourth general heat source, waste heat, such as from industrial high-temperature processes. This heat derives mostly from fossil fuel combustion and in some cases from electrical heating, where the major purpose is the provision of process heat. In the following four sections nuclear, solar, combustion and waste heat sources are discussed in more detail.

3.4.1 Nuclear heat source

Two nuclear fission sources have been of interest for TPV conversion, namely nuclear reactors [51,52] and isotopes with half-life periods shorter than the naturally occurring isotopes [47,52-59]. Details about nuclear fission can be found elsewhere [60-63]. One of the major attractions of nuclear sources is their high gravimetric energy density (MJ/kg) [63]. This results in long refuelling periods and makes them attractive for remote area supply (e.g. naval, space). Drawbacks are usually high costs and safety aspects, such as fuel processing and transport, operation, decommissioning, waste disposal and weapon capability. **Radioisotopes** have been used for long-term power for space, remote area and pacemaker supply with a typical heat range from mW to kW. Potentially there are over 1300 radioisotopes [62]. Most commonly Plutonium 238 and Strontium 90 are used. The first publications for TPV nuclear space research date back to the 1980s. Radioisotope temperatures around 1273 to 1473 K have been reported in TPV literature [47,53-59], where the standard Plutonium 238 sources give the upper temperature limit. The minimum size of a **nuclear reactor** is limited by the critical mass of the fissionable material used. The smallest reactors developed for space exploration had a thermal power in the order of tens of kW heat [61]. At the upper end of the power range are civilian nuclear power stations with GWs of heat. In the reactor, fission heat is removed by a coolant and these include (heavy) water, gases (e.g. helium or carbon dioxide) or liquid metals (e.g. sodium or lithium). In a TPV system the coolant would circulate and transport heat from the reactor to the radiator, where liquid metal and gas coolants have been proposed for TPV conversion [51,52]. Gas cooled reactors, such as the developmental Pellet Bed Reactors are predicted to achieve radiator temperatures as high as 1800 K [51].

3.4.2 Solar heat source

The nuclear fusion[4] in the sun is a powerful and durable heat source. The sun radiates approximately $4 \cdot 10^{26}$ W according to blackbody laws from its surface[5], where about $2 \cdot 10^{17}$ W incident on the earth [5,64]. This can be compared with the world primary power demand of around $1 \cdot 10^{13}$ W. The solar radiation can be approximated by blackbody spectrum with 5800 K, where the radiation is often standardised as air mass (AM), e.g. AM0 in space and AM1.5 for the terrestrial radiation (Figure 3-3).

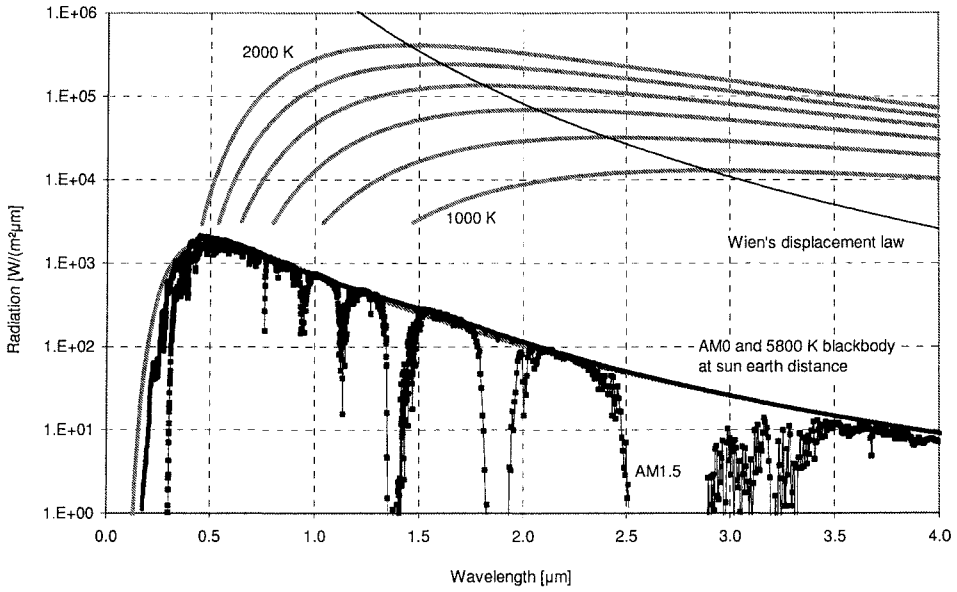

Figure 3-3: Comparison of solar spectra at sun earth distance and blackbody spectra. The AM1.5 and AM0 solar radiation spectrum is plotted as black dots with a grey line and as a black line, respectively. A 5800 K blackbody spectrum reduced by a factor r_s^2/r_{se}^2 (grey line) can approximate the AM0 spectrum (black line), where r_{se} is the sun earth distance and r_s the sun radius. For comparison the blackbody radiation increasing from 1000 to 2000 K in 200 K steps is also shown (grey line, small values overlapping with the solar spectra are not shown) with the maximum given by the Wien's displacement law (black line). The diagram has been computed within this work and the AM spectra are from [65,66].

---

[4] Terrestrial power generation by nuclear fusion is not considered in this work, because cost effective exploitation seems to be decades in the future.

[5] The sun radiates approximately as a blackbody sphere with radius $r_s = 696 \cdot 10^6$m and temperature T_s = 5800 K. The power emitted by the sun is approximately given by $4\pi r_s^2 \sigma T_s^4$, where $4\pi r_s^2$ is the sun surface and σT_s^4 the Stefan-Boltzmann law.

Compared to other heat sources (e.g. combustion, nuclear), the solar source has advantages such as cost free availability, no pollution and no weight gain through the heat source. The major drawback of the sun as a heat source for TPV is the unsteady availability and the low intensity. The incident solar radiation on a surface varies in terms of its spectrum, angle and total intensity depending on factors such as location (e.g. latitude), orientation (e.g. tilt), operation environment (e.g. reflected radiation), cloud cover and different cycles (sun, annual, seasonal and daily). At optimum condition (no clouds and optimum tilt angle) the intensity of the terrestrial solar radiation is about 0.1 W/cm^2. The low intensity of solar radiation requires solar concentration in order to achieve suitable radiator temperatures for TPV (> 1300 K).

The principle of **solar concentration** to increase the temperature has long been known (e.g. Archimedes) and recently, solar concentrators have been also extensively used for thermal and electrical solar systems [67]. Solar concentrators are devices, which concentrate the solar radiation from a large aperture area A_a onto a smaller receiver area A_r facing the sun. Equation 3-6 defines the maximum concentration A_a/A_r, where the sun-earth distance is $r_{se} = 150 \cdot 10^9$ m, the sun radius is $r_s = 696 \cdot 10^6$ m, n is the refractive index and θ_s is the opening half angle of the sun at the Earth's surface [68].

$$\left(\frac{A_a}{A_r}\right)_{max} = \frac{r_{se}^2}{r_s^2} n^2 = \frac{n^2}{\sin^2 \theta_s} = 46448 \cdot n^2 \qquad (3\text{-}6)$$

The blackbody temperature of the sun surface gives an upper theoretical temperature limit of the receiving area of 5796 K [5], where experimental temperatures as high as 3273 K could be achieved [67]. The thermodynamic efficiency limit of solar TPV conversion is given by Equation 3-7, where a maximum of 85% at an absorber temperature of $T_a = 2478$ K occurs, assuming $T_s = 5800$ K and $T_c = 300$ K [5].

$$\eta = \left[1 - \left(\frac{T_a}{T_s}\right)^2\right]\left(1 - \frac{T_c}{T_a}\right) \tag{3-7}$$

Different **concentrator types** have been considered for solar TPV operation. Work has been reported about (parabolic) dish concentrators [69-73], Fresnel lens concentrators [74] and central power receivers [69,71]. Absorber temperatures in STPV systems of 1623 K have been demonstrated [71,72]. Concentration levels in the range from 100 [75] to 25000 [76] have been considered. In general, the UK climate is less suitable for solar concentration due to a high share of diffuse sunlight.

Solar concentrator PV is defined here as the direct conversion of concentrated solar radiation, whereas solar TPV is the conversion of radiation from an intermittent radiator heated by concentrated solar radiation

The low availability of the sun can be overcome in a solar TPV system by using two strategies, which may also be combined. Firstly, the high temperature heat can be **stored thermally** and supplied at times when less or no solar radiation is available. Secondly, **hybrid systems** can be designed using solar radiation and an additional heat source, such as combustion to supply heat for times with no or low availability of solar radiation [69,70,72,75-81].

Solar TPV systems have some advantages compared to other heat sources. Potentially these systems can operate at high radiator temperatures, where temperatures above 2000 K have been predicted [72,82,83]. Also the radiator can be completely surrounded by an inert gas or vacuum and this should allow simple system construction (e.g. similar to a light bulb) without challenging high-temperature seals [82-84].

3.4.3 Combustion heat source

Currently, the major part of the world's energy consumption originates from combustion. Combustion as a heat source for TPV has been considered for a wide range of powers. Combustion systems that generate heat as small as about 1 W have been researched [85]. For small power applications, battery substitutes in the order of 100 W heat have been reported [6,86-89]. For large power applications, CHP plants in the order of 100 kW to 1 MW heat were considered [90,91].

In general, combustion heat sources achieve suitable radiator temperatures for TPV operation (1300 - 2000 K). Combustion chamber temperatures depend on the type of fuel (e.g. calorific value, moisture content or aggregate state), type of oxidiser (e.g. air or oxygen), the type of flue gas heat recovery and several other factors (e.g. type of fuel-oxidiser mixing). For TPV, all major methods of flue gas heat recovery have been considered. These include air preheating using recuperator [46,92] and regenerator [93-95] devices, as well as fuel preheating [92] and flue gas recirculation using flame tubes [46,96]. Lower calorific value fuels tend to generate radiator temperatures at the lower temperature limit of TPV operation. For example for wood powder a radiator temperature of 1400K has been demonstrated [90]. The combustion temperature of these fuels may be enhanced by the use of flue gas recirculation [97]. For common fuels combustion temperatures up to 2500 K are feasible [97]. However at these temperatures, difficulties in terms of thermal engineering (e.g. heat exchanger, thermal insulation) and pollution by thermal nitrogen oxides must be taken into account.

Hydrocarbon **fuels** have high gravimetric energy density values (e.g. compared to secondary batteries) [2]. This makes them attractive for portable applications (e.g. petrol in automobiles) and they can be considered safe (e.g. cigarette lighter) [98].

Hydrocarbon combustion has disadvantages in terms of local and global pollution. Excess local pollution including oxides of nitrogen (NO_x) and oxides of sulphur (SO_x) can cause acid rain. Globally the level of carbon dioxide (CO_2) has been found to increase due to the combustion of previously stored (fossil) fuels and the increased atmospheric CO_2 is causing climate change. On the other hand biomass fuels can be regarded as CO_2 neutral.

The most important fuel elements, in terms of heat generation, are carbon and hydrogen (hydrocarbons), which react with oxygen (usually in air) to produce CO_2 and water. For TPV, most commonly gaseous fuels, such as methane (or natural gas), propane or butane, have been used. TPV systems using kerosene and diesel have also been designed [92,96,99]. Combustion of liquid fuels usually requires a fuel feed system (e.g. pump) and atomiser, which can make system design more complex compared to gas fuelled systems (gas system can operate solely from a pressurised tank). Solid fuels are often associated with sophisticated combustion techniques. No published TPV work could be found, except the combustion of wood powder [90].

Williams et al. [89] demonstrated the **direct conversion of flame radiation** with a PV cell without using a radiator. The infrared radiation of hydrocarbon flames is composed of major spectral emission bands at around 2.7 and 4.4 μm [9,100] and greybody radiation from carbon particles within the flame (soot) [89,101]. The ratio of radiative heat transfer to the total heat released by the combustion depends on fuel type and burner design as well as other parameters. For natural gas this ratio can reach values as high as 30% for modern industrial burners [101] and Gaydon stated a ratio of 2 to 20% in an earlier literature reference [102]. It can be concluded that the direct conversion of flame radiation is unsuitable for TPV conversion because of the small

ratio of radiant heat to the total combustion heat and the unsuitable radiation spectrum. Therefore, means to increase the radiation intensity and to tailor the spectrum are required [103].

Radiant burners have been developed for both lighting and heating applications. The historical development of spectrally selective radiant burners for **lighting** is of interest, since the mechanisms applied to enhance visible radiation for lighting can also be applied to enhance near-infrared radiation for TPV conversion. In 1826, Thomas Drummond heated a monolithic block of calcia (lime) to incandescent temperature by flame impingement using a hydrogen/oxygen flame, where the calcia block could enhance visible radiation [103]. Subsequent work focused on different radiator materials and geometries [103]. In the early 1890s, Carl Auer (Baron von Welsbach) perfected both the material compositions and the geometrical structure by using fibres of around 10 μm in diameter consisting of 99.3% of thoria (ThO_2) and 0.7% of ceria (Ce_2O_3) by weight. This structure, known as the Welsbach mantle, continues to be the most efficient converter of gas combustion heat to visible light and is still being used for example in camping lanterns [45,103]. The Welsbach mantle is optically thick in the visible spectral range and optically thin in the infrared range (1-8μm) [45]. For most spectral regions the combustion flame is also optically thin, except some spectral bands mainly at around 2.7 and 4.3 μm, so that the Welsbach mantle emits most radiation in the visible range where the mantle is optically thick. The physically small fibre diameters can achieve temperatures close to that of the flame and the combustion products, because their small physical size allows high heat transfer rates. The thin fibres are tolerant to thermal stress and can be heated up quickly [103]. However scaled up Welsbach mantles have proved to be fragile [104].

Radiant burners for **heating** can be broadly classified into direct and indirect radiant burners. Indirect-fired burners spatially and optically separate the combustion and heating zone, whereas direct-fired burners do not separate these two zones.

Direct radiant burners may operate on flame impingement or utilise porous structures in the combustion zone. For TPV, physically small porous structures that are of interest are those that can be designed to achieve high temperatures and convert fuel efficiently into radiation. Materials considered are mainly **oxide type ceramics**. TPV radiant burners have been designed that use a modified Welsbach mantle, which consists of ytterbium and erbium oxides. Generally suitably high temperature operation (more than 1700 K) and highly selective spectral emission was achieved [104]. However, the modified Welsbach mantle also suffered from scaling and fragility difficulties. Hence alternative structures have been examined including composite fibres and foams. These structures currently overcome the scaling and fragility issues of the Welsbach mantle but at the expense of spectral selectivity. Direct radiant burners using **metals** (e.g. wires) have been used in TPV systems. Metals are generally limited to lower temperatures due to oxidation in the flame atmosphere compared to ceramic oxides. One disadvantage of all direct radiant burners is that PV cell surfaces would be contaminated from combustion products. Hence, usually additional means are required to protect the cells. This is usually achieved using transparent shields (e.g. fused silica). No work on the long-term contamination of these shields by the combustion products could be found in literature, although this could affect the shield transparency. Another drawback of direct radiant burners is that at least some unsuitable flame radiation is inherently in the emitted spectrum (at 2.7 and 4.3 μm). Furthermore, an optically thin radiator used in direct radiant burners can usually not be used for other heat sources

than combustion. Finally, in this work no commercial direct radiant burners with a suitable performance (high efficiency, selective spectrum) for TPV systems could be identified.

Indirect radiant burners spatially enclose the combustion zone and have also been used in TPV systems. These burners utilising gaseous hydrocarbon fuels are commercially available for space and industrial heating applications and are of metal or ceramic type. Ceramic burners are usually of interest for TPV because of their higher operation temperature. These burners typically have a tubular form in various shapes including U, W, P, double P, A or single tube [105]. Single tube burner types include straight-through, single ended recuperative or single ended recirculating recuperative [101,106]. For TPV the latter one made of silicon carbide (SiC) has typically been utilised. These burners were either commercially acquired [46] or custom-designed [96]. Using efficient recuperators, as much as 80% of the chemical energy can be converted to radiant energy (Figure 3-1)[47]. Additional coatings have been applied in order to achieve a spectrally selective emission. The various selective radiator options are discussed in Section 3.5, since selective radiators for indirect radiant burners (non-transparent substrate) can also be applied for other heat sources.

3.4.4 Waste heat source

A waste heat source is defined as a process where the major purpose is heat generation and some of the heat is available for electricity conversion by TPV.

In the large power range, the recovery of **industrial high-temperature waste heat** by a TPV system has been proposed by Coutts [3]. In particular the glass industry has been suggested [107,108]. Fraas et al. [91,107,108] partly developed TPV generator tubes. These tubes could be inserted in high-temperature processes in order to generate

electricity and low-grade heat in the form of hot water. Yamaguchi et al. [109,110] assessed industrial high-temperature waste heat recovery using TPV in the flue gas location for Japan. Additional TPV literature regarding industrial waste heat recovery by TPV could not be identified within this work.

There should also be a niche market for **self-powered** operation of industrial processes using a TPV heat recovery system. In the power range from 1 to 40 kW, self-powered heating systems have also been of interest, such as for a combined camping heater and generator [111], an off-grid stove [112] and self-powered central heating units [113,114].

In the low power range, some work by Goldstein and DeShazer et al. suggests, that radiation can be extracted from a process by **high-temperature resistive dielectric solid radiation guides** [115-117]. It seems likely that such arrangement could be also used to convert small amounts of waste heat for applications such as self-powered sensors.

Applications using waste heat sources have the advantage of free or low cost of heat. Also the availability of the heat can be high (e.g. industrial high-temperature processes operating throughout day and night). Finally the efficiency is often not a decisive factor in these applications where heat is generated in any case.

This section dealt with the four different heat sources and the next section discusses the radiator options for TPV conversion.

3.5 Radiator

Radiators (also called emitters) may be classified according to several aspects including the following:

- Emissivity (spectral, angular)
- Transparency
- Material composition
- Thermo-physical properties (e.g. upper operation temperature, evaporation rate)
- Electrical conductivity (Metal, Semiconductor, Non-metal)
- Physical structure (e.g. bulk, porous, filaments, film, microstructured surface)

TPV radiators have been reviewed by Coutts [3], Gombert [14], Licciulli et al. [15], Adair et al. [100] and Nelson [103]. Radiators may be broadly classified in spectrally broadband and selectively emitting, or alternatively into metal and ceramic radiators. Two basic mechanisms allow spectral alteration of the emissivity. These are the material composition and the physical structure. The emissivity of radiators is also angle and temperature dependent.

The following subsection first reviews some theory about radiator evaporation. Then the radiator concepts have been classified in broadband ceramics, selective ceramics and metals (Subsection 3.5.2-3.5.4).

3.5.1 Radiator evaporation

In general there is limited TPV literature available about the mass transfer from the hot radiator to the PV cell or other components (e.g. heat shield) in a TPV cavity. It was pointed out that above 1500 K, most materials, including rare-earth oxides, show evaporation rates well above 100 μm per year [118] and this could contaminate PV cells and glass shields. Also metal radiators may apply an antireflection coating to enhance the emissivity in the short wavelength range, where evaporation of this coating can shift

the peak of the emissivity enhancement to other wavelengths [27]. The Hertz-Langmuir equation has been used in the TPV community. This equation can predict the maximum evaporation rate from the solid radiator surface into a vacuum (Equation 3-8), where W is the evaporation rate (grams/cm^{2}s), p_v the vapour pressure (torr), T the absolute temperature (K), M the molecular weight (gram) and f the sticking coefficient (or de-absorption constant) [27,119-121]. Evaporation rates for increased gas pressure (other than vacuum) are lower [121]. For TPV applications, Equation 3-8 shows that generally radiator materials with low vapour pressure, such as tungsten, are of interest. The vapour pressure generally increases with temperature and this usually limits the upper temperature of a TPV radiator. The sticking coefficient f varies in a wide range from typically $1 \cdot 10^{-2}$ to $1 \cdot 10^{-6}$ and must be experimentally determined for each material [119].

$$W = 5.83 \cdot 10^{-2} \cdot p_v \cdot f \cdot \sqrt{M/T} \tag{3-8}$$

Knowledge about the evaporation rate is available from other research areas, where this mass transfer may be desired (e.g. vapour deposition of films) or undesired (e.g. darkening of electric light bulbs by the filament evaporation) [122]. Conduction and convection heat losses through the TPV cavity are generally unwanted and need to be minimised. This can be achieved by reducing the gas pressure (vacuum conditions). Hence, there is a trade-off between conduction and convection losses and the radiator evaporation rate.

3.5.2 Broadband ceramic radiators

There are several requirements for ceramic broadband radiators for TPV including high-temperature stability in an oxidising environment, good thermal shock resistance and high availability. High emissivities are usually required in order to achieve high radiative heat transfer rates. High thermal conductivities result in low temperature

differences from the heat source and a uniform temperature distribution in the radiators. High-temperature resistant ceramics can be classified into oxide and non-oxide based.

Typical high-temperature **oxide based** ceramics are stable in oxidising atmospheres [123] and oxides include alumina (Al_2O_3), stabilised zirconia (ZrO_2), magnesia (MgO), silica (SiO_2), beryllia (BeO), hafnia (HfO_2), thoria (ThO_2) and yttria (Y_2O_3). High-temperature oxide based ceramics may consists of one or more of these oxides, such as mullite (Al_2O_3 SiO_2), cordierite (MgO Al_2O_3 SiO_2) or steatite (MgO SiO_2). The most commonly used high-temperature oxide based ceramic is Al_2O_3. Al_2O_3 is stable in oxidising atmosphere up to 2173 K, which is close to its fusion temperature of 2323 K [123]. Similarly ZrO_2 ceramics can withstand temperatures close to their fusion temperature of 2823 K [123]. A theoretical study has considered Al_2O_3 and ZrO_2 as a TPV broadband radiator, where the major difficulties of these materials have been seen in the poor thermal shock resistance and the low emissivity [38].

Non-oxide based high temperature ceramics include the groups of carbides (e.g. C, SiC, B_4C, WC, HfC), nitrides (e.g. Si_4N_3, BN, AlN) and borides (e.g. TiB_2) [27,124].

Silicon nitride (Si_3N_4) can be used up to about 1473 to 1773 K in an oxidising atmosphere and has been proposed as broadband radiator for TPV [38,124], but no system development using Si_3N_4 could be identified within this work.

Graphite (C) has a high thermal conductivity and shows high thermal shock resistance [123]. It has a high emissivity over the spectral range of interest [122], but can only be utilised in an oxidising atmospheres up to about 723 K [124]. Hence graphite is of interest for non-oxidising atmospheres for TPV (e.g. space systems) [47]. The surface of graphite can be converted into SiC, which allows operation at higher

temperatures in oxidising atmospheres [123]. Höfler reported an evaporation rate for graphite about 2000 times higher than that of tungsten [27].

Silicon carbide (SiC) decomposes at around 2873 K and can operate in oxidising atmospheres up to around 1923 K due to a protective oxidation layer, which consists of silicon dioxide (passive oxidation) [123,124]. The oxidation resistance of SiC degrades in atmospheres containing water vapour [38]. In rare cases, silicon monoxide gas forms in atmospheres with a low partial pressure of oxygen (active oxidation) and consumes the SiC [123]. The emissivity of SiC is generally high and, in the wavelength range of interest (1-3 μm), the values range from 0.7 to 0.94 depending on author and measurement methodology [125]. The thermal conductivity of SiC is generally high, but smaller than that of graphite [123]. High-temperature application examples of SiC are heat exchangers, gas turbine components and heating elements (electric or gas) [123]. Manufacturing methods of SiC include ceramic-bonded, reaction bonded, silicon nitride bonded, carbon bonded, recrystallised, sintered, hot pressed and chemical vapour deposition [124]. SiC has been applied almost exclusively as a broadband radiator for TPV systems. The evaporation rate of SiC is high. Fraas calculated a mass transfer rate from the radiator at 1425 K to the PV cell of 1 μm per 300 hours in vacuum [47]. Guazzoni also presented some work on coated SiC radiators, which could suppress some mid-infrared radiation [126].

3.5.3 Selective radiators based on transition metal oxides

This subsection first reviews some theory about transition metals and then discusses different arrangements of optically thin and optically thick ceramics.

In the periodic table, transition metals can be further categorised into inner-transition metals (or rare earth elements), which are made up of the lanthanide and actinide series.

For selective TPV radiators some elements of the lanthanide series (f-transition metals) and some of the element numbers 21 to 30 (d-transition metals) are of interest (marked grey in Table 3-2).

The **f-transition metals** have partly filled deep lying 4f shells shielded by filled 5s and 6p orbitals (Table 3-2) [127]. Therefore, electrons in the 4f shells interact little with neighbour ions and emit radiation similar to gases (line emission). Line emission is caused by discrete energy levels, which can be described by quantum mechanics. Work on the spectra and discrete energy levels of rare earth ions in crystals has been summarised by Dieke [128,129]. The chemical properties of the f-transition metals are similar, generally having three valence electrons ($6s^2$, $5d^1$) [15]. Guazzoni was the first to propose high temperature spectrally selective infrared emittance for monolithic ceramics of Er, Sm, Nd and Yb for TPV conversion [43,103]. Since then most work focused on Ho, Er and Yb [3]. Table 3-1 sums up the emission peak wavelengths.

Element	Peak wavelength (μm)	Source
Nd	2.5	[43,128]
Sm	High emissivity from 1.8 - 5.0	[43]
Ho	(1.2) 2.0-2.1	[14,15,128]
Er	1.55	[14,15,43,103,128,130]
Tm	1.8	[15]
Yb	0.98	[15,43,103,128,130]

Table 3-1: Emission peaks of f-transition metals.

The **d-transition metals** have a similar unique electron configuration compared to f-transition metals, where the partly filled 3d orbitals are shielded by the 4s orbitals (Table 3-2). In general, the f-transition elements emit in narrower lines and are less affected by the host material compared to d-transition elements [127]. For TPV, cobalt (Co) and nickel (Ni) have been used with magnesia (MgO) used as a host material and emission peaks at 1.13, 1.27 and 1.49 μm (Co in MgO) and 1.12, 1.26 and 1.41 μm (Ni in MgO) were observed [127].

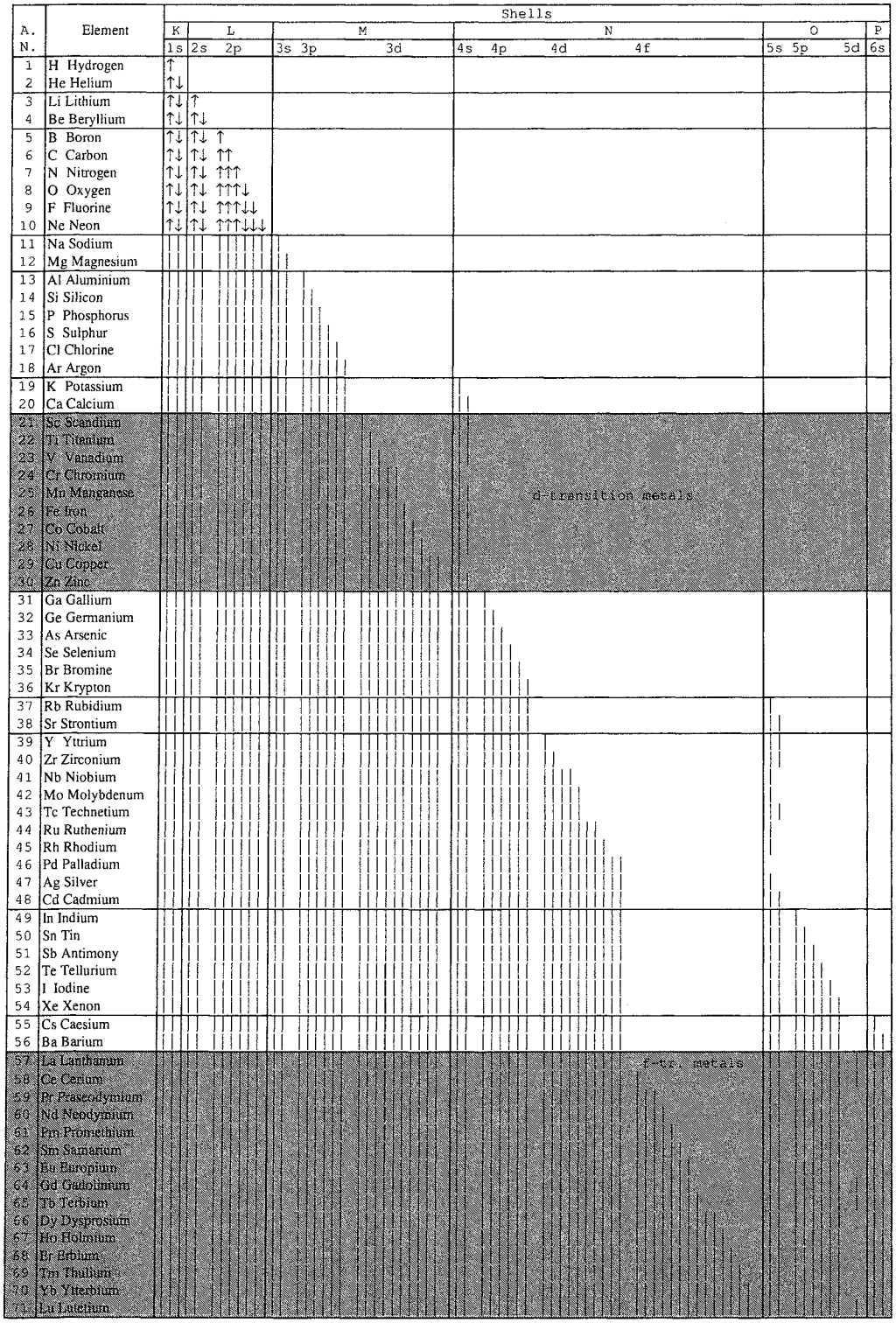

Table 3-2: Ground state of shell fillings, f- and d-transition metals are marked grey.

Guazzoni reported about the selective emission of monolithic f-transition metal ceramic oxides [43]. The ceramics were **optically thick** (no flame radiation was transmitted through the sample) and erbium and ytterbium showed improved selective emission with emissivities from approximately 0.2 to 0.3 in a wavelength range from 0.5 to 5 μm with an enhanced emissivity at the peak wavelength of around 0.6 [43]. Emissivities for longer wavelengths have been not reported, but it is known that for high-temperature resistant glasses and ceramics the absorption coefficient typically increases considerably for wavelengths longer than about 5 μm due to lattice vibrations [15,127,131]. Consequently these materials also emit long-wavelength radiation, which is generally undesirable for TPV operation [15]. Another difficulty with monolithic f-transition metal ceramic oxides is the poor thermal shock resistance. Also, although f-transition metal ceramic oxides show some spectral selective emissivity, there is still a large share of undesirable radiation below and above the peak emission wavelength [100]. Several attempts have been made to overcome thermal shock and emissivity challenges of monolithic radiators and they are summarised in the following.

The classical form of an **optically thin** ceramic oxide radiator using f-transition metals is the Welsbach mantle. For TPV, ytterbia (Yb_2O_3) and erbia have been utilised and there are literature reports about high-temperature stable mantles (e.g. more than 1700 K) with spectrally selective emission [104]. However, other sources report about scaling, fragility and durability difficulties for such Welsbach mantle [14,15,132]. Hence various optically thin ceramic oxide radiator structures, containing f-transition metals, have been investigated [15,133]. These include ceramic foams [134], matrixes constructed of long fibres [15,100,135,136], supported fibres [103,137], ceramics consisting of short fibres [132], films on (polycrystalline) sapphire [138], doped silica

glass [15,139], doped garnets [140,141,115] and small rare earth oxide particles suspended in a hot carrier gas and enclosed by sapphire [135,142].

Optically thin ceramic ribbons have also been made using magnesia doped with d-transition metals (cobalt and nickel) [127,133,143]. As already discussed, optically thin radiators are limited to the use in combustion or hot gas streams, require protective transparent shields and emit some flame radiation. Hence, structures on non-transparent substrates are of interest.

Optically thick and thermally stable ceramics (e.g. SiC or Al_2O_3) can be coated **with a porous coating containing f-transition metals**. For this approach the thickness of the coating is critical, where too small a thickness results in undesired transmission of substrate radiation through the coating [15]. Large thicknesses on the other hand can become optically thick and can have a temperature drop across them. In this case the volumetric emission of radiation at the lower temperature regions is usually undesirable. Erbium oxide and cobalt oxide [144], as well as porous erbium aluminium garnet [145] coatings in the order of ten to hundreds of micrometers have been applied to a SiC substrate. It has been found that scattering in the porous coatings can improve suppression of substrate radiation [15,145].

Generally metals have inherently a desired spectral selectivity with an intermediate emittance for short and low emittance for long wavelengths. Optically smooth metal surfaces have a low total emittance and can be used as reflectors [144]. **Metal films**, such as platinum [131,144] or molybdenum [27,146], have been used **as a substrate for f- and d-transition metal ceramic oxide films**. In this configuration the oxide films are heated by conduction through the metal substrate where substrate radiation can be low, because of the high metal reflectivity. Oxide film materials included erbia with thulia

and holmia as well as cobalt doped spinel [144], ytterbia (Yb_2O_3) [27,146] and erbium, holmium and thulium aluminum garnets [131,147]. For the latter it was found that film thickness, material composition, scattering within the film and the temperature gradient across the film are all parameters that influence the (spectral) emittance of the radiator.

It has been pointed out, that the emission bandwidth of a single f-transition element is relatively narrow, which could result in low electrical power densities [15]. Hence, the superposition of emissivities from different f-transition elements has been examined to broaden the spectral radiation output [15,148].

From the literature review in this subsection, it is concluded here, that in general limited work has been carried out on the durability and evaporation rate of selective ceramic radiators.

3.5.4 Metal radiators

Flat metal surfaces tend to have intermediate emissivity in the near infrared and low emissivities in the mid and far infrared (see Subsection 2.4.2). This natural selectivity makes metals an attractive option for TPV radiators.

Noble metals are known for their high resistance to oxidation in air, whereas most other metals are unstable in high-temperature oxidizing atmospheres. **Gold** does not oxidise up to its melting point of 1336 K, but does not support its own mass at elevated temperatures and has a high reflectivity [149,150]. Gold on specially prepared ceramic foils has been used very close to its melting point as reflector between the radiator and the PV cell [31]. Elements of the **platinum group** (platinum, palladium, iridium, rhodium, osmium and ruthenium) are oxidation resistant, have high strengths at elevated temperatures and have high melting points (>2030 K) [149]. For TPV, platinum has been used as a mirror material between the radiator and PV cell [31] and as a radiator

[151]. One major disadvantage of platinum is the high material cost. Hence no single metal element seems to fulfil the requirements for a TPV radiator in oxidising environments so that alloys are of interest.

Some high temperature resistant **alloys** form protective oxide layers at their surface and these layers can prevent further oxidation. For example, commercial metal fibre burners are available up to around 1300 K using alloys such as FeCrAlYSiMnCuC [152] or NiCrFe (Inconel) [153]. For TPV, high-temperature, oxidation-resistant metal alloys have been inserted in the combustion zone. These alloys operate at the lower end of typical TPV radiator temperatures. They include the alloys of FeCrAlNi[6] used at about 1200 K [28] and FeCrAlCoC tested at around 1500 K [28,154]. Advantages of metal alloys as radiators for TPV include their spectral selectivity [154] and their high thermal conductivity resulting in uniform radiator temperatures [31]. Alloys with oxidised surfaces can also have high emissivities compared to non-oxidised surfaces [28,154,155].

Refractory metals (e.g. tungsten, molybdenum) have high melting points and a high thermal stability, but poor oxidisation resistance at elevated temperatures. For example **tungsten** has the highest melting point (3683 K) of any metal and a low vapour pressure (or low evaporation rate), but oxidises in air at temperatures above about 773 K [14,27,149]. Hence, TPV systems using tungsten as the radiator operate with a vacuum or inert gas atmosphere to avoid oxidation. The intermediate emissivity in the near infrared of tungsten can be enhanced using **antireflective (AR) coatings**. Theoretical emissivity values up to 95% in the wavelength range from 1 to 1.7 μm have been

[6] Supplied by the company Kanthal.

calculated using an AR coating thickness of 138 nm [14]. AR coating materials considered have included Al_2O_3, ThO_2, ZrO_2 and HfO_2 [27,151,156,157]. AR coatings also allow some control of the spectral and angular emission characteristics [12].

Surface gratings with periods in the order of micrometers have been fabricated using tungsten [14,158-160] and other materials [161]. Several phenomena influence the spectral emissivity of these radiators including surface plasmon resonance, vertical standing waves in deep cavities and AR sub-wavelength gratings [14]. The optimum dimension of the surface gratings for high in-band and low out-of-band radiation can be found by modelling these structures (e.g. rigorous coupled-wave analyses). The durability of tungsten surface gratings is limited by surface diffusion and the gratings become almost planar after a few hours at temperatures above 1500 K [14]. It was found that a 25 nm surface coating with HfO_2 could reduce surface diffusion considerably [14,159]. It is noted here, that tungsten lamp filaments need to retain their fibrous grain microstructure to accommodate the stresses and strains at operating temperatures of around 2500 to 3370 K. This stability is achieved through additions of thoria or a combination of potassium, silicate and alumina (also called AKS dopants) [122]. Hence, one might expect that the thermal stability issues of TPV radiators at lower temperatures can be overcome using knowledge from the light bulb development.

Photonic bandgap crystals have been also of interest for TPV conversion. In photonic bandgap crystals the lattice structure is on a scale with optical wavelengths and is based on alternating materials with high and low dielectric constants. The lattice periodicity is spaced such that bandgap wavelengths destructively interfere, thereby preventing their passage through the crystal. Constructive interference enhances wavelengths outside the bandgap and allows them to propagate through the crystal with

little attenuation. This phenomenon is well known for example for 1D multilayer films. In 1991, the first 3D photonic bandgap crystal structure was found, where photons can be blocked at the crystal bandgap regardless of the direction the photon travelled or their coherence, polarization or angle of incidence [162]. For TPV, 3D photonic crystal radiators from tungsten have been suggested. The crystal bandgap prevents mid and far infrared radiation and the near infrared emissivities can be high [14,163].

Photonic structures of alternating layers of ultra-thin metallic films in-between dielectric layers have been also examined for radiators [164].

3.5.5 Other radiator materials

Other radiator materials than those summarised in the three previous subsections (broadband ceramics, selective radiators based on transition metals and metal radiators) have also been proposed. These include inter-metallic materials such as $TaSi_2$ [15], semiconductor materials such as silicon [27,165] and a variety of coatings applied to molybdenum, niobium and nickel base metals [119,166].

3.6 Photovoltaic cell

PV cells for TPV conversion have been reviewed by Coutts [3], Andreev [167], Bath et al. [168] and Iles [169]. In the following, first partial PV cell efficiencies are defined (Subsection 3.6.1). These definitions are then used to compare PV cells based on group IV (Subsection 3.6.2) and group III-V semiconductors (Subsection 3.6.3).

3.6.1 Theory of PV cell efficiency

The PV cell efficiency can be divided into five sub-efficiencies, which are the voltage factor η_{OC}, the collection efficiency (also called mean quantum efficiency) η_{QE}, the fill factor η_{FF}, the ultimate efficiency η_{UE} and the PV cell array efficiency η_{Array} (Equation 3-9) [168,170-175].

$$\eta_{PV} = \frac{P_{el}}{P_{PV}} = \eta_{OC} \cdot \eta_{QE} \cdot \eta_{FF} \cdot \eta_{UE} \cdot \eta_{Array} \tag{3-9}$$

The first three efficiencies (η_{OC}, η_{QE} and η_{FF}) are mainly related to the characteristics of the PV cell. The ultimate efficiency η_{UE} describes losses due to the spectral match of the absorbed illumination spectrum in relation to the PV cell bandgap. The efficiency η_{Array} includes losses due to multiple cell connections and heat absorption by conduction and convection.

The maximum voltage, which may be obtained from the PV cell, is the bandgap voltage V_g defined as the ratio of the PV cell bandgap energy hv_g to the elementary charge e_0 [170]. The open circuits voltage V_{oc} is less than V_g by the **voltage factor** η_{OC} (Equation 3-10) [168]. As Shockley and Queisser pointed out, the voltage factor η_{OC} is a function of several parameters [170]. The voltage factor η_{OC} decreases for lower bandgaps [172] and η_{OC} increases for higher illumination intensities. Comparing a silicon cell (1.1 eV) operating under non-concentrated solar radiation (AM1.5) with a

GaSb cell (0.72 eV) operating under concentration (1473 K blackbody) similar voltage factors have been achieved due to the compensation of the two effects. The voltage factor is usually the lowest and most critical efficiency of the PV cell related efficiencies (η_{OC}, η_{QE} and η_{FF}) [172]. This is particularly true for the lowest bandgaps currently investigated.

$$\eta_{OC} = \frac{V_{oc}}{V_g} = \frac{e_0 \cdot V_{oc}}{h\nu_g} \tag{3-10}$$

The maximum photocurrent density J_{max} is given by the number of photons with energies above the bandgap energy $h\nu_g$ presented in the radiation spectrum multiplied with the elementary charge e_0 (Equation 3-11). The actual photocurrent density J_{ph} is smaller, where the reduction can be described by the **collection efficiency** η_{QE} [168]. The collection efficiency η_{QE} can be generally close to 100% for optimised cells. For non-concentrator silicon solar cells a value of 97% has been achieved [176]. GaSb cells operating in a TPV system may have values around 80% [167,177].

$$\eta_{QE} = \frac{J_{ph}}{J_{\max}} = \frac{J_{ph}}{e_0 \int_{\nu_g}^{\infty} n_{ph(\nu)} d\nu} = \frac{J_{ph}}{e_0 \int_{\nu_g}^{\infty} \frac{P_{PV\#(\nu)}}{h\nu \cdot A} d\nu} \tag{3-11}$$

The current-voltage curve of the PV cell under illumination has an exponential characteristic (diode curve). The maximum electrical power density obtained $J_m \cdot V_m$ is less than the product of $J_{ph} \cdot V_{oc}$, which is described by the **fill factor** (Equation 3-12). The fill factor η_{FF} usually decreases for lower PV cell bandgaps, higher series resistances, lower parallel resistance and higher cell temperatures [4,168,174,178]. Most of these negative factors can occur for PV cells operating in TPV systems, so that usually lower fill factors can be expected than for non-concentrator solar PV.

$$\eta_{FF} = \frac{J_m \cdot V_m}{J_{ph} \cdot V_{oc}} \tag{3-12}$$

The **ultimate efficiency** η_{UE} describes how the absorbed radiation power[7] $P_{PV\#(v)}$ matches the PV cell bandgap energy hv_g. There are two loss mechanisms. The first of these is due to photons with energies $hv < hv_g$ which are usually not converted and this mechanism is named **free carrier heating** here. The second mechanism is due to photons with energies $hv > hv_g$ which can only contribute to the energy output hv_g, where the excess energy ($hv - hv_g$) is lost as heat and this is named here **hot carrier heating** [170,179]. Section 4.2 in the next chapter discusses the dependency of the ultimate efficiency for different illumination spectra (suppression of radiation above and below the bandgap).

The discussed efficiencies all relate to single cell performance. PV cells connected in series and parallel and built into TPV systems have generally lower efficiencies than a single cell, because of the following reasons:

- Distribution of different individual cell properties, so that each cell cannot operate at its own maximum power point. Also a group of cells and not only the best performing cells is used.
- Cells within a group of cells operating at different temperatures.
- Non-uniform absorption of radiation due to the spatial and angular distribution of the radiation in a TPV cavity.
- Packing of the PV cells (for TPV, the packing factor has been optimised using shingling [180]).
- Heat absorbed by conduction and convection

For TPV, many of these factors (e.g. cell temperature and incident angle of the radiation) are time constant compared to solar PV and can be minimised due to suitable system engineering.

---

[7] The absorbed radiation power $P_{PV\#(v)}$ does not include conduction and convection losses, whereas the absorbed radiation power $P_{PV(v)}$ includes these losses.

3.6.2 Group of IV semiconductors

Bitnar reviewed silicon and germanium cells [181]. Several TPV systems have been developed using **silicon** PV cells [39,103,114,182]. Silicon cells operating under high illumination are commercially available for solar concentrator PV systems [183]. Laser grooved buried contact silicon cells, widely used for non-concentrator solar conversion, have been reported to be suitable for the adaptation of higher concentrations [16]. Silicon has an indirect bandgap of $hv_g = 1.12$ eV at 300 K (responds up to 1.11 μm) [4]. This bandgap is usually regarded as high for TPV conversion. Typically silicon cells have been used with an ytterbia (Yb_2O_3) radiator (e.g. Welsbach mantle type), which has a suitable selective emission for the silicon bandgap [181]. References about back surface reflector (BSR) work in conjunction with silicon cells have been summarised by Charache et al. [184]. Recently, Hampe et al. reported about a metal insulation semiconductor (MIS) silicon PV cell using a BSR [30,185]. A recent record silicon PV cell has been identified to have approximately the following performance: $\eta_{PV} = 25\%$ with $\eta_{OC} = 63\%$, $\eta_{QE} = 97\%$, $\eta_{FF} = 83\%$ and $\eta_{UE} = 49\%$. This calculation assumed the global AM1.5 spectrum with a total intensity of 0.1 W/cm^2 [176][8].

In the early stages of TPV system development, **germanium** PV cells were utilised. However, these cells suffered from poor cell performance [39]. Recently, more advanced germanium PV cells have been developed as a bottom cell for multi-bandgap solar converters. For TPV, single junction germanium cells are being developed

[8] The values were calculated within this work. The value η_{OC} was calculated as $e_0 \cdot V_{OC} / hv_g = 0.706/1.12 = 0.630$. Using AM1.5 data from [5] the maximum photocurrent of $J_{max} = 43.6$mA/cm^2 was computed (also given in [178]). This results in $\eta_{QE} = 42.2/43.6 = 0.968$. The ultimate efficiency was computed as $\eta_{UE} = 0.488$ for the global AM1.5 spectrum. This value is slightly higher than the blackbody value of 0.44 [170].

[186,187]. The costs of germanium substrates are reported to be lower than those of GaSb by a factor of 6 to 7 [181]. Germanium has an indirect bandgap of $hv_g = 0.66$ eV at 300 K and responds up to 1.88 μm [4]. Germanium cells spectrally match the selective emission of erbia radiators [181]. A germanium cell recently reported (seen as amongst the best in literature) has the following performance: $\eta_{PV} = 6.7\%$ with $\eta_{OC} = 37.1\%$, $\eta_{QE} = 75.2\%$, $\eta_{FF} = 59.6\%$ and $\eta_{UE} = 40.2\%$. The calculation assumed the global AM1.5 spectrum and an intensity of 0.1 W/cm^2 [186][9]. These partial efficiencies show that in particular high voltage factors are difficult to achieve for germanium cells [188]. BSRs are seen generally feasible for germanium cells and are discussed elsewhere [167,187].

SiGe structures are used for high-frequency semiconductor devices. SiGe alloys allow changing the bandgap by varying the Ge content (Figure 3-4). Bitnar reviewed work on SiGe PV cells, where only a few papers have been recently published [181].

In summary it is concluded, that currently IV semiconductor PV cells are less suitable for TPV conversion due to the high bandgap of silicon, the low voltage factor of germanium cells and the early research stage of SiGe cells.

[9] The value η_{OC} was calculated through $e_0 \cdot V_{OC} / hv_g = 0.245/0.66 = 0.371$ using AM1.5 data from [5]. A maximum photocurrent of $J_{max} = 60.9$ mA/cm^2 was computed (also given in [178]), which gives $\eta_{QE} = 45.8/60.9 = 0.752$. The ultimate efficiency was computed as $\eta_{UE} = 0.402$ for the global AM1.5 spectrum.

3.6.3 Group of III-V semiconductors

PV cells based on III-V semiconductors have currently the highest conversion efficiencies (e.g. developed for space applications) [176], but high cost is a major hindrance to their widespread use. For cost reduction polycrystalline cells [112], thin film cells [189-191] and growth on other substrates [192] have been examined [188]. For TPV conversion the major low bandgap materials currently of interest are gallium antimonide (GaSb), indium gallium arsenide (InGaAs) and indium gallium arsenide antimonide (InGaAsSb). Figure 3-4 shows possible bandgaps of III-V semiconductors compounds versus the lattice constant.

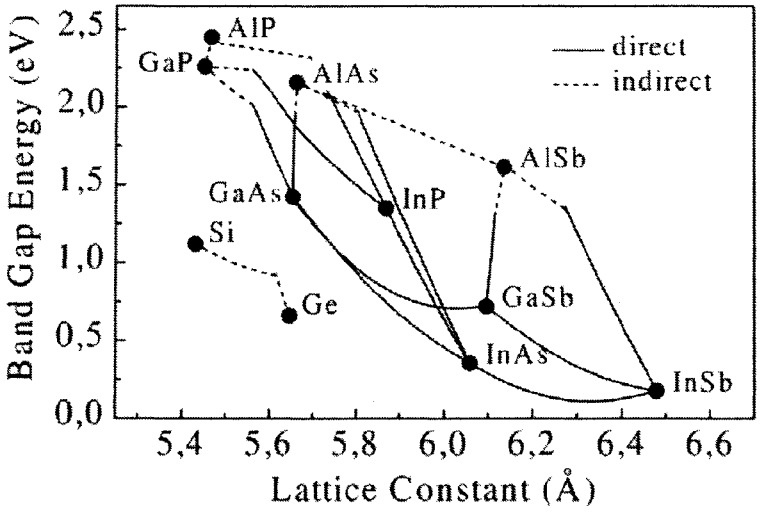

Figure 3-4: Energy bandgap versus lattice constant of III-V semiconductors. The bandgap of silicon and germanium is also shown for comparison [193].

At present, **GaSb** PV cells can be regarded as the most suitable choice for modern TPV generators [194]. Historically, GaSb cells have been developed as a bottom cell for mechanically stacked multi-bandgap solar PV converters with high performances [176]. This material has a direct bandgap of 0.72 eV (1.72 μm) at 300 K [4]. Several research groups and companies have manufactured GaSb cells using diffusion or epitaxial

technologies. The latter include metal organic vapour phase epitaxy (MOCVD) and liquid phase epitaxy (LPE) [167,194]. In the early 1990s two companies were founded (Fraas at JX-Crystals Inc. and Horne at EDTEK Inc.). Both companies started to produce Boeing's Zn-diffused GaSb cell technology under license [39]. Spectral control approaches for GaSb cells have included (also in combination) selective radiators (erbia, matched cobalt radiator), thick SiO_2 windows, filters and PV cell front surface filters (FSF). The difficulties in incorporating BSRs into GaSb cells are discussed by Charache et al. [184]. In the work reported here, the performance of a typical GaSb cell under 1473 K blackbody radiation has been calculated[10]: η_{PV} = 3% with η_{OC} = 65.6%, η_{QE} = 47%, η_{FF} = 73.3% and η_{UE} 13.6%. The value for the cell efficiency η_{PV} can be also approximately confirmed by the measured electrical power density and the total blackbody radiation $\eta_{PV} = P_{el,mess}/\sigma T_s^4 = 0.82/26.7 \cdot 100\% = 3\%$ [177]. This efficiency value shows the vital importance of spectral control for TPV. Assuming all radiation below the bandgap energy (0.72 eV) can be recovered (not absorbed in the cell), the ultimate efficiency, and hence the cell performance, improves significantly: η_{UE} = 80.9% and η_{PV} = 18%. It can be seen that high fill factors η_{FF} and high voltage factors η_{OC} can be achieved for GaSb cells (e.g. compared to Ge). The low collection efficiency of η_{QE} = 47% is believed here, to be the result of the cavity design (view factor, radiation angle), where incident photons under low angles are totally reflected at the cell surface and other photons may have been lost in between the radiator and the PV cells. From the quantum efficiency vs. wavelength curve [167,177] a value around η_{QE} = 80%

[10] The value η_{OC} was calculated through $e_0 \cdot V_{OC} / h\nu_g = 0.472/0.72 = 0.656$. Using a 1473 K blackbody spectrum the maximum photocurrent of J_{max} = 5.06 A/cm^2 was computed, which gives η_{QE} = 2.36/5.06=0.47. The ultimate efficiency was computed as η_{UE} = 0.136 for the 1473 K blackbody spectrum and the bandgap of 0.72eV.

can be expected, which yields an even higher cell efficiency: η_{PV} = 31%. In summary, it can be said that the cell related efficiency (product of η_{OC}, η_{QE} and η_{FF}) is currently usually smaller for GaSb operating in a TPV system (39%) compared to high-performance silicon cells converting solar radiation (51%). However, the total cell efficiency η_{PV} can be higher for TPV due to a higher ultimate efficiency achieved by using suitable spectral and angular control methods.

The bandgap of **$In_xGa_{1-x}As$**, also called GaInAs, can be varied in a wide range from 1.42 to 0.36 eV (0.87 to 3.44 μm) by varying x from 0 to 1 [168,195] (Figure 3-4). **Lattice matched $In_{0.53}Ga_{0.47}As$** cells on Indium phosphide (InP) substrate (bandgap 0.74 eV, 1.68 μm) have been manufactured mainly by epitaxial methods (MOCVD and LPE) [167], but also some by diffusion methods [196]. Fabrication of cells based on InGaAs is a mature technology and applications include infrared photo detectors (e.g. fibre optic communication), laser power converters and bottom cells in solar tandem converters [167,168]. Wilt et al. reported the performance of a 0.74 eV InGaAs cell under the AM0 spectrum [197]. The efficiency values are calculated in this work as follows[11]: η_{PV} = 11.9% with η_{OC} = 53.9%, η_{QE} = 75.3%, η_{FF} = 71.5% and η_{UE} = 40.9%. Ginige et al. reports about the adaptation from laboratory to industrial batch manufacturing [198]. For TPV conversion lower bandgap **lattice mismatched InGaAs** cells are of interest. These cells can be produced by increasing the indium and decreasing the gallium content. Different lattice mismatched $In_xGa_{1-x}As$ cells on an InP substrate with bandgaps from 0.6 eV (2.07 μm) to 0.55 eV (2.25 μm) have been grown

[11] The value η_{OC} was calculated through $e_0 \cdot V_{OC} / h\nu_g$ = 0.3988/0.74 = 0.539. Using AM0 spectrum data from (1353 W/m^2) a maximum photocurrent of J_{max} = 74.8 mA/cm^2 was computed, which gives η_{QE} = 56.35/74.8=0.753. The ultimate efficiency was computed as η_{UE} = 0.409 for the AM0 spectrum.

by MOCVD [167,199]. A high performance has been demonstrated for the 0.6 eV $In_{0.68}Ga_{0.32}As$ cell (η_{OC} = 59% and η_{FF} = 73.4%) under concentration [200]. Cells with higher lattice mismatch (lower bandgaps) on InP substrates appear to be difficult to manufacture with high performance.

Monolithic Interconnected Modules (MIMs) have been designed using lattice matched and mismatched $In_xGa_{1-x}As$ cells since 1994 [197,201,202]. These MIMs are typified by an InP semi-insulating substrate [197]. This substrate provides two key advantages: electrical isolation for the component cells and near perfect optical transparency for sub bandgap photons. The former allows series connection to increase the voltage and the latter allows spectral control using a BSR [197]. Wilt et al. discusses other advantages of the MIM structure [197]. Tandem cells using the MIM structure have also been developed. They consist of a 0.72 eV lattice matched and a lower bandgap mismatched cell [201]. MIMs are generally suitable for broadband radiators due to the incorporation of back surface or buried reflectors [167,202-204].

InGaAsSb (also called GaInAsSb) cells can be lattice matched on a GaSb substrate with bandgaps ranging from 0.29 to 0.72 eV are theoretically possible, however the miscibility gap limits the lower bandgap to about 0.5 eV [188]. InGaAsSb cells on GaSb substrates have been fabricated with bandgaps from approximately 0.5 to (2.48 μm) to 0.6 eV (2.07 μm) using diffusion and epitaxial growth processes including LPE, MOCVD and Molecular beam epitaxy (MBE)[167,188]. InGaAsSb cells (0.52 eV) with voltage factors of η_{OC} = 57.7% and fill factors of η_{FF} = 70% have been reported [205]. The difficulties in designing InGaAsSb MIM structures are discussed elsewhere [188,201]. Tandem cells consisting of a 0.72 eV GaSb top and a 0.56 eV InGaAsSb

bottom cell have also been reported [188]. For InGaAsSb cells buried reflectors have also been examined [206,207].

3.6.4 Other PV cell compounds and concepts

As already reported together with the individual cell, tandem cells offer a further enhancement of the cell efficiency. In particular series connected tandem cells should be beneficial to raise the low voltages of the low bandgap cells. Work on tandems has started on different material combinations:

- GaSb/InGaAsSb (0.72/0.56 eV) [154,167,188]
- InGaAs/InGaAs (0.74/0.63 eV) [201,208]
- InGaAsP/InGaAs (0.72/0.60 eV) [209].

Since 1990 **quantum well cells** (QWCs) have been examined. QWCs are reported to have advantages in TPV applications in terms of temperature, voltage and variable absorption edge characteristics [26,210]. InGaAsP on InP cells have been developed as QWCs (0.72 eV)[26,210].

Other tertiary and quaternary materials examined for TPV cells include **InAsSbP** (0.3-0.5 eV) [167,188,211], **InAsSb** on GaSb (0.29 eV) [188] and $\mathbf{Ga_{1-x}In_xSb}$ (also called InGaSb) [168,188,211]. Vertical junction cells [212] and II-IV thin film cells [3,190,191] have been also proposed for TPV conversion.

The following section discusses components other than the heat source, the radiator and the PV cell.

3.7 Remaining components

3.7.1 Thermal insulation

Typical radiator temperatures ranges from 1300 to 2000 K and PV cell temperatures from around 300 to 330 K. For some TPV systems it may be feasible to cover the entire radiator area with PV cell (e.g. radioisotope systems [56]), but usually low thermal conductivity insulation of the TPV cavity between the radiator and the PV cell is essential to minimise heat losses (Figure 2-1). Figure 3-5 shows a selection of thermal insulation options collected from various sources [213-218].

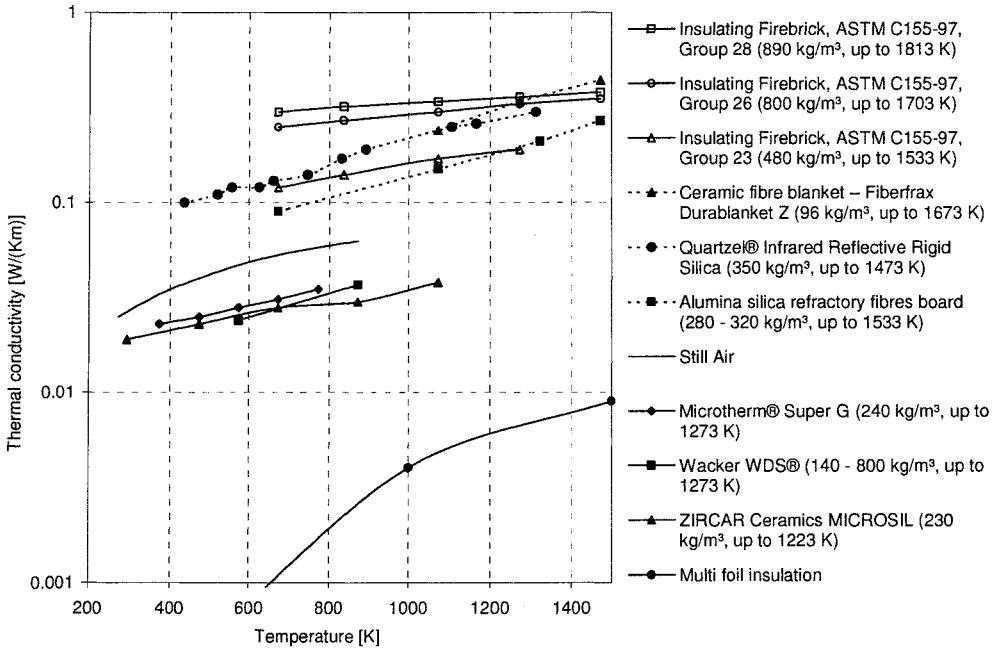

Figure 3-5: Thermal conductivity versus temperature of various insulation materials.

Multi foil insulations (MFIs) utilise reflective metal foils separated by spacers, where the space in between is usually evacuated. MFIs were originally developed for cryogenic applications but are also applicable for high-temperature applications. For radioisotope TPV systems, an MFI using 60 layers of 0.008 mm thick molybdenum foil

separated by zirconia (ZrO_2) spacers has been considered [56]. Such MFIs can withstand hot side temperatures up to 1500 K [219], but commercially are not widely available.

Microporous insulation is commercially available in different shapes and has also low thermal conductivities (Figure 3-5)[213-215]. For TPV, microporous insulation has been used as an insulation frame between radiator and PV cells [31]. However, currently commercial versions of this insulation are limited to about 1300 K for continuous use [213-215].

Figure 3-5 shows the thermal conductivity of still **air** for comparison. Solar TPV systems where the radiator is held with a few contact points in a **vacuum** chamber have been considered [74,82-84], where thermal conduction would be even lower than for still air.

Another potentially interesting insulation option for TPV systems could be **sintered fused silica fibre insulation** (e.g. Quartzel® [217]), since this material has inherently a high infrared reflectivity and good insulation properties. Hence, for example Quartzel® may replace the challenging high temperature mirror design in a TPV system, but no TPV work could be identified.

Fibre insulation made mainly from silica and alumina is available in several forms (e.g. rigid board or blanket) for different temperature ranges. One disadvantage is the health and safety issue associated with the fibre dust. **Insulating firebricks** are less health and safety critical and have similar thermal conductivities (Figure 3-5).

3.7.2 Energy storage

Energy is stored to match energy supply and demand, as well as for transportation. Energy storage systems may be classified into four types, each with their own characteristics in terms of stored energy (J), charge and (self) discharge rates (W), capital costs (£/J), as well as volumetric (J/m^3) and gravimetric energy density (J/kg):

- Mechanical (e.g. compressed air, pumped hydro, flywheel)
- Thermal (e.g. boiler)
- Chemical (e.g. hydrocarbon fuel tank)
- Electrical (e.g. capacitor, superconductor, electro-chemical)

For TPV, the last three energy storage options are of particular interest. **Thermal** energy storage systems can be further classified into sensible and latent heat storages [220,221]. Water is widely available and has one of the highest **sensible** heat contents of any liquid around ambient temperatures [221]. In CHP systems the PV cells are usually cooled by water and the sensible heat of the water can be stored in boilers as in some conventional central heating systems. **Latent** heat storages utilise the phase change energy, so that approximately isothermal systems can be designed. For TPV, latent heat storages have been considered for radiator heating in intermittently operating solar concentrator systems [75]. Silicon has been identified as suitable latent heat storage with a solid-liquid phase change temperature of 1680 K [75].

The **chemical** storage of energy is of interest for TPV systems using hydrocarbon combustion as a heat source. Hydrocarbon fuels are advantageous in terms of availability, long-term storage and transport characteristics. Liquid and gaseous hydrocarbon fuels share high gravimetric energy densities (Table 3-3) with values more than 100 times higher compared to secondary batteries [2]. Some gaseous fuels can be liquefied in order to achieve similar volumetric and gravimetric energy densities to oils

(Table 3-3) [2,222-224]. These liquid fuels (diesel, kerosene, liquefied propane) with both high volumetric and gravimetric energy density have been utilised for portable TPV applications [2,96,99,225].

Fuel/Battery	Type	Density (kg/m^3)	Volumetric energy density (MJ/m^3)	Gravimetric energy density (MJ/kg)
Primary battery	Carbon zinc	1565	360	0.23
	Alkaline	2640	1188	0.45
	Silver oxide	4186	1800	0.43
	Lithium	2386	1980	0.83
Secondary battery	Lead acid	1938	252	0.13
	NiCd	2492	324	0.13
	NiMH	3500	630	0.18
	Li ion	2250	720	0.32
Gaseous	Hydrogen	0.09	12.76	142.0
	Methane	0.716	39.8	55.6
	Air (for comparison)	1.293	-	-
	Ethane	1.342	69.7	51.9
	Propane	1.968	99.1	50.4
	n-Butane	2.596	128.3	49.5
	Natural gases	0.75-0.84	33-43	40-52
Liquid	Oils	790-970	36700-41800	42.5-46.5
	Propane (liquefied)	512	26266	51.3
	Butane (liquefied)	575	28463	49.5
	Methanol	793	23790	30
Solid	Coals	N/A	N/A	26-37
	Wood powder	215	4300	20

Table 3-3: Volumetric and gravimetric energy density of some selected fuels. Higher calorific values are given. For methanol the higher calorific value was estimated from the lower calorific by adding 10%. Primary and secondary batteries are also shown for comparison.

Currently TPV systems are usually designed for constant **electrical** power output. For some application this operation mode may be suitable (e.g. industrial waste heat recovery system) and for others not (e.g. portable power supply with varying load). Electrical energy storage can overcome this limitation. To date, secondary batteries have been considered as a supplement [6]. In principle, other options are also feasible, such as (super) capacitors.

3.7.3 Miscellaneous components

PV cells are typically **cooled** by a forced convection water cycle, where heat is transferred sometimes to the ambient. Such configuration usually requires a pump and a cooler. In Section 2.3 other concepts for PV cell cooling have been discussed. Heat removal by heat pipes and utilisation of the Joule Thomson Effect of expanding liquefied fuel may be also utilised for cell cooling. Generally, knowledge about PV cell cooling is available from solar concentrator PV systems.

TPV systems also require a **maximum power tracker** in order to operate the PV cell array at its maximum power point. Different trackers are available from solar PV applications. The operation conditions are usually less critical for steady illuminated cells in TPV systems compared to the fluctuating illumination conditions experienced for solar conversion.

Often, the additional components are heat source and application dependent. For example combustion TPV systems require air and fuel conditioning (e.g. pumps, blowers, atomisers), flue gas recuperation, as well as burner ignition and control. Portable systems often require a fuel tank, ignition and load levelling (secondary battery). CHP systems may include a thermal storage system for hot water. Solar TPV systems using a latent thermal storage require a controlled shutter mechanism to minimise heat losses from the storage.

3.8 Novel TPV concepts

Besides photonic bandgap crystals (see Subsection 3.5.4), other novel concepts are discussed within this subsection.

In the late 1990's research in the field of **micron-gap TPV** (MTPV) started. The blackbody radiation law can be derived from Maxwell's equations under the assumption of large separation of the hot radiation source and the cold sink [226]. This assumption applies to nearly all TPV systems using typical distances in the centimetre range. However, the blackbody radiation law is not longer valid, when the separation decreases to a sub-micron-gap. It was concluded that the photon flux is limited by the lowest refractive index in the photonic cavity and scales with the minimum refractive index squared. Close separation allows partial coupling of the enhanced radiative heat transfer by n^2 while the vacuum gap thermally insulates. The advantage is that both the PV cell and the radiator can have a high refractive index, so that an enhancement of about 10 in the radiative heat transfer seems to be feasible [227]. The challenges of this concept include the engineering aspects of a gap in the order of 0.1 μm and the spectral control of radiation [227,228].

Ashcroft and DePoy proposed **high-temperature heat pipes** (e.g. filled with lithium or sodium) to transport energy from the heat source to the radiator. This arrangement should allow a TPV system design with high volumetric power densities (W/cm^3) [229].

Qiu et al. proposed a **cascaded** radiant burner with two temperature zones using silicon cells at the high-temperature zone and GaSb at the low temperature zone [182]. TPV systems operating cascaded with another energy conversion device have been also considered. In such systems the TPV converter may operate in the top cycle (e.g. together with a lower temperature fuel cell reformer [230]) or bottom cycle (e.g. using

the exhaust gas of a gas turbine [231]). Cascaded systems of a TPV converter with another conversion device can be associated with complex system design and are mainly of interest for large power systems, where additional complexity can be justified. It is concluded here, that there is generally a limited scope for cascaded operation with other technologies due to the high hot and the low cold side temperature of typical TPV systems.

Hybrid systems consisting of a TPV system combined (not cascaded) with another energy conversion device have been also of interest. Examples include TPV generators combined with a secondary battery providing high peak power [6] or combined with a renewable generator (e.g. solar PV or wind) [232]. As already discussed, hybrid systems with more than one heat source (e.g. solar and combustion) are also of interest (Subsection 3.4.2).

For most TPV systems, the PV cell temperature is maintained below 370 K. One major difficulty for systems used in space is the removal of heat from the PV cells. Low temperature cell operation would require large cooling fins, since heat can be only be removed by radiation in space. Hence, TPV systems using **PV cells with temperatures up to 500 K** have been examined [233-235]. The major efficiency limitation originates from the decrease of the cell fill factor and voltage factor with increasing temperature. One advantage is that available, higher bandgap, PV cells can be utilised, since these higher bandgaps decrease to suitable bandgaps at high operation temperatures. TPV high-temperature cell research may also gain from solar PV developments for near-sun missions.

The principle of **thermophotonics** (TPXs) is based on the idea that light emitting diodes can be developed that emit photons having a higher energy than the bandgap

energy, where the excess energy is provided by a heat source [19,236]. This radiation could then be converted by PV cells with higher bandgaps than the usual bandgaps utilised for TPV. One major limitation of TPXs is that high efficiency light emitting diodes for high-temperature operation are not available.

Different approaches currently under investigation for solar PV conversion may also impact on TPV conversion in future, if these approaches can be fully demonstrated. Examples are **luminescent up and down converters** [237], as well as **antenna-rectifier PV areas** [238,239]. Antenna-rectifiers have demonstrated highly efficient conversion of microwave radiation into electricity. For example systems capable of converting more than 80% of monochromatic microwave radiation into electricity have been demonstrated. For conversion of solar radiation one major challenge is the requirement of small physical structures. Infrared (IR) radiation would allow larger structures and the radiator spectrum may be also tailored narrowly. Hence, antenna-rectifier PV areas may be rather suited for the direct conversion of heat into electricity, but no literature could be identified within this work.

This chapter addressed the technological options for the heat source, the radiator and the PV cell. Information sources, history, efficiency definitions, novel concepts and other components for TPV conversion were also reviewed and discussed. Chapter 4 examines optical control and the PV cell ultimate efficiency in detail.

4 Optical control in TPV cavities

4.1 Importance of optical control

The important TPV figures of merit, high efficiency and high electrical power density critically depend on the heat transfer between the radiator and the PV cell in the TPV cavity (see Figure 2-1). Conductive and convective heat transfer from the radiator to the PV cell or the surroundings is parasitic and needs to be minimised. Radiative heat transfer in the cavity needs to be optimised in terms of the spectral, angular and spatial radiation distributions.

For optimum PV cell performance, usually the cells need **spatially uniform** illumination [28]. Typically the cells are series connected to increase the voltage. A lower current from one cell, due to spatially non-uniform illumination, reduces the power output from the whole string.

The **angle** of the radiation in the TPV cavity is also of significance. Flat surfaces of dielectric materials increasingly reflect radiation with incident angles away from the normal (or large zenith angles) according to Fresnel's equations and Snell's law (see Subsection 2.4.4). This can result in lower radiative heat transfer rates from the radiator to the PV cell. An example would be a PV cell facing a blackbody radiator, where from the definition, radiation leaves the blackbody radiator at all angles (diffuse surface).

However, radiation incident at the PV cell surface[12] with large zenith angles is increasingly reflected and this leads to a lower radiative heat transfer compared to two blackbody surfaces facing each other. Similarly, radiation is reflected on heat shields or filters placed in the cavity. Collimators can align diffuse radiation so that radiation incident at surfaces can have smaller zenith angles. As a result, TPV systems may be designed with higher radiative heat transfer rates. In addition to the angle dependent surface reflection, the radiative surface properties (e.g. emissivity, reflectivity) of real components (e.g. radiator, SiO_2 or PV cell) usually have both angular **and** spectral dependences. Examples are selective radiators and dielectric filters. Typically these components become spectrally less selective for angles away from normal. This dual dependency adds to the complexity of spectral control in the TPV cavity.

The **spectrum** of the absorbed radiation by the PV cell has a major impact on the cell conversion efficiency and the remaining discussion in this chapter focuses on this spectral control. In the review and discussion about PV cells (Section 3.6), the PV cell efficiency was split into partial efficiencies. The PV cell related efficiencies (η_{OC}, η_{QE} and η_{FF}) and the PV cell array efficiency η_{Array} need to be optimised for a specific PV cell type and TPV system design. In such optimised systems, the spectral match of the absorbed power by the PV cell to its bandgap (spectral control) is of interest and this is described by the ultimate efficiency discussed and modelled in the next section.

[12] This assumes a flat PV cell surface without light trapping.

4.2 Ultimate efficiency and power density

Several models have been developed to predict efficiency, power density or ideal PV cell bandgap. Coutts gives an overview of these models [3,179] and Cody compares efficiencies for different models without spectral control [240]. Some models are based on empirical values for the reverse saturation current density including work by Woolf [241,242], Wanlass et al. [243,244], Caruso and Piro [245] and Iles et al. [246]. TPV systems using specifically the sun as a heat source were also investigated by Würfel and Höfler et al. [20,27,247,248] and others [249-252]. De Vos modelled the solar PV conversion as an endoreversible heat engine [253-255]. This model has been adapted for TPV conversion using different assumptions by Gray and El-Husseini [256] and Heinzel et al. [257,258]. In general, there is limited work on the combined effect of above and sub bandgap suppression. Usual assumptions include no above and no sub bandgap suppression (full spectrum case) [168,240,251], only suppression of sub bandgap radiation [168,171,251,257,258], perfect sub bandgap and variable above bandgap suppression [249] and specific percentage or band assumptions about the sub and above bandgap suppression [3,246,256]. One difficulty in modelling TPV efficiency and electrical power density is the number of parameters. These include mainly the radiator temperature T_s, the PV cell bandgap hv_g, as well as the suppression of sub and above bandgap radiation. Some TPV work used the substitution $x = hv/kT_s$ (respectively $x_g = hv_g/kT_s$) to reduce the number of parameters by one [18,128,171,179].

This work focuses on the simultaneous above and sub bandgap suppression on an ultimate efficiency level, where the discussed substitution is adapted. This allows insights into spectral control in general and can give an upper limit for the efficiency and electrical power density.

The assumptions made in this modelling are a single bandgap PV cell illuminated by a blackbody, where parts of the spectrum sub and above the PV cell bandgap energy are suppressed. The loss mechanisms of free and hot carrier heating are considered and all other partial efficiencies are assumed ideal (η_{OC}, η_{QE}, η_{FF}, η_{Array} and η_{Cavity}, Section 3.3). For the modelling, the following methodology is used. First, the ultimate efficiency of the solar PV conversion process as presented by Shockley and Queisser is repeated [170]. Second, this modelling is extended to the more general TPV case.

4.2.1 Solar PV conversion

The sun can be approximately modelled as a blackbody radiator with a temperature T_s = 5800 K. Equation 4-1 gives the number of photons with energies greater than hv_g leaving this blackbody per unit area and per unit time [170].

$$Q_{s(v_g,T_s)} = \frac{2\pi}{c_0^2}\int_{v_g}^{\infty}\frac{v^2}{e^{\frac{hv}{kT_s}}-1}dv = \frac{2\pi}{c_0^2}\cdot\left(\frac{kT_s}{h}\right)^3\int_{x_g}^{\infty}\frac{x^2}{e^x-1}dx \tag{4-1}$$

Integration of Planck's radiation law yields the Stefan Boltzmann law given in Equation 4-2 (see also Subsection 2.4.3) [21,170].

$$\begin{aligned} I_{s(T_s)} &= \frac{2\pi h}{c_0^2}\int_0^{\infty}\frac{v^3}{e^{\frac{hv}{kT_s}}-1}dv \\ &= \frac{2\pi h}{c_0^2}\cdot\left(\frac{kT_s}{h}\right)^4\int_0^{\infty}\frac{x^3}{e^x-1}dx = \frac{2\pi h}{c_0^2}\cdot\left(\frac{kT_s}{h}\right)^4\frac{\pi^4}{15} = \frac{2\pi^5k^4}{15h^3c_0^2}T_s^4 = \sigma T_s^4 \end{aligned} \tag{4-2}$$

Assuming the sun as a hot sphere with radius r_s, Q_s and I_s drop by a factor of r_s^2/r_{se}^2 at sun-earth distance r_{se}. Equation 4-3 gives the PV power density and Equation 4-4 the PV cell efficiency at the outer earth atmosphere, assuming each photon with energy greater than hv_g contributes to the electricity output hv_g. The ultimate solar efficiency η_{solar} has a maximum of about 44% at the approximate value x_g = 2.2 [170]. For this

simplified model, one may also calculate the ideal bandgap for solar PV conversion as 1.1 eV using the definition of the substitution $x_g = hv_g/kT_s$.

$$P_{solar} = \frac{r_s^2}{r_{se}^2} \cdot hv_g \cdot Q_{s(v_g,T_s)} \tag{4-3}$$

$$\eta_{solar} = \frac{hv_g \cdot Q_{s(v_g,T_s)}}{I_{s(T_s)}} = \frac{\int_{x_g}^{\infty} \frac{x^2}{e^x - 1} dx}{\int_0^{\infty} \frac{x^3}{e^x - 1} dx} \tag{4-4}$$

4.2.2 TPV conversion without spectral control

For TPV conversion, the radiator and the PV cell can be closely arranged so that ideally no radiation is lost, so that the factor r_s^2/r_{se}^2 in Equation 4-3 is assumed unity for TPV conversion. On the other hand, Q_s values are smaller for TPV compared to non-concentrator solar PV conversion, because of the lower radiator temperatures for TPV conversion. Overall, higher power densities are usually obtained for TPV conversion (Watts/cm^2) compared to non-concentrator solar PV conversion (0.01-0.02 W/cm^2).

It has been pointed out that the ultimate solar efficiency η_{solar} (Equation 4-4) is also valid for TPV conversion with the assumption of no spectral control [3,259]. It becomes clear that the ideal PV cell bandgap energies for TPV are smaller compared to solar PV conversion, since the substitution $x_g = hv_g/kT_s$ becomes maximum at the constant value of about 2.2 and the radiator temperatures are lower for TPV conversion. Using T_s values in the range from 1300 to 2000 K results in hv_g values from 0.25 to 0.38 eV. Currently it is challenging to obtain $\eta_{OC} > 0$ from such low bandgap cells.

4.2.3 TPV conversion with spectral control

TPV offers the possibility to suppress or recover photons using spectral control. It is assumed here that all photons absorbed by the PV cell be within a spectral band, with

some blackbody radiation below and some above the PV bandgap hv_g. Figure 4-1 shows an example of this band model using the normalised Planck's radiation law (Eq. 4-5) and the substitution $x = hv/kT_s$, where x- is the lower and x+ the upper band limit. The normalised bandgap x_g is assumed to be in between these two boundaries.

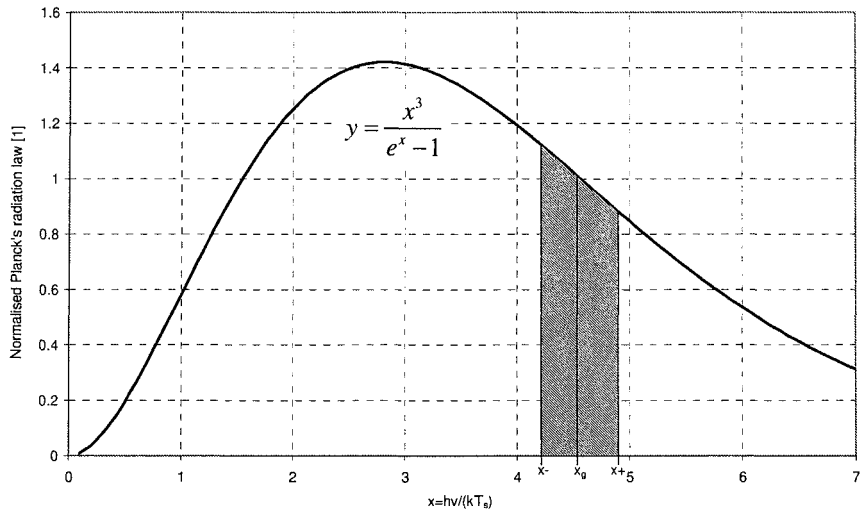

Figure 4-1: Plot of the normalised Planck's radiation law. The substitution x=hv/(kT$_s$) was used. An example of the band model is also shown.

$$I_{bv(v,T_s)} = \frac{2\pi h}{c_0^2}\frac{v^3}{e^{\frac{hv}{kT_s}}-1} = \frac{2\pi h}{c_0^2}\left(\frac{kT_s}{h}\right)^3 \frac{x^3}{e^x-1} \qquad (4\text{-}5)$$

It is mentioned here that a change in radiator temperature T_s does not change the shape of the plotted function in Figure 4-1, but scales the function equally for all values of x (Equation 4-5).

Practically, the absorbed radiation by the PV cell will differ from the band model. Nevertheless, the band approach can be justified since for other spectra an equivalent spectral band can be calculated, which generates the same amount of heat and electricity as the absorbed spectra (see Appendix D).

Similar to the solar PV case, Q_T can be defined as the number of photons with energies greater than hv_g and below the band limit (Equation 4-6). The radiation

absorbed by the PV cell I_T can be defined for the TPV case using the spectral band model (Equation 4-7).

$$Q_{T(\nu_g,T_s,\nu+)} = \frac{2\pi}{c_0^{\,2}} \int_{\nu_g}^{\nu+} \frac{\nu^2}{e^{\frac{h\nu}{kT_s}}-1} d\nu = \frac{2\pi}{c_0^{\,2}} \cdot \left(\frac{kT_s}{h}\right)^3 \int_{x_g}^{x+} \frac{x^2}{e^x-1} dx \tag{4-6}$$

$$I_{T(T_s,\nu_+,\nu-)} = \frac{2\pi h}{c_0^{\,2}} \int_{\nu-}^{\nu+} \frac{\nu^3}{e^{\frac{h\nu}{kT_s}}-1} d\nu = \frac{2\pi h}{c_0^{\,2}} \cdot \left(\frac{kT_s}{h}\right)^4 \int_{x-}^{x+} \frac{x^3}{e^x-1} dx \tag{4-7}$$

The spectral band limits x+ and x- are less meaningful values. A more meaningful value is the ratio of radiation within the spectral band below the bandgap divided by the total radiation below the bandgap (r-). For the above bandgap radiation, similarly r+ is defined (Equations 4-8).

$$r+ = \frac{\int_{x_g}^{x+} \frac{x^3}{e^x-1} dx}{\int_{x_g}^{\infty} \frac{x^3}{e^x-1} dx} \qquad r- = \frac{\int_{x-}^{x_g} \frac{x^3}{e^x-1} dx}{\int_{0}^{x_g} \frac{x^3}{e^x-1} dx} \tag{4-8}$$

The relation between r+ and x+ depending on x_g can then be computed numerically from Equation 4-8 (see Appendix C). With this consideration the power density and efficiency of TPV can be defined (Equation 4-9 and 4-10). Computation of values between r- and x- is not necessary, since the definition of r+ and r- (Equation 4-8) can be inserted into the definition of I_T by splitting the integral at x_g (Equation 4-7).

$$P_{TPV} = h\nu_g \cdot Q_{T(T_s,x_g,x+)} = \frac{2\pi h}{c_0^{\,2}} \left(\frac{kT_s}{h}\right)^4 x_g \int_{x_g}^{x+} \frac{x^2}{e^x-1} dx \tag{4-9}$$

$$\eta_{TPV(\nu_g,\nu-,\nu+,T_s)} = \frac{h\nu_g \cdot Q_T}{I_T} = \frac{x_g \int_{x_g}^{x+} \frac{x^2}{e^x-1} dx}{\int_{x-}^{x+} \frac{x^3}{e^x-1} dx} = \frac{x_g \int_{x_g}^{x+} \frac{x^2}{e^x-1} dx}{r_- \int_{0}^{x_g} \frac{x^3}{e^x-1} dx + r_+ \int_{x_g}^{\infty} \frac{x^3}{e^x-1} dx} \tag{4-10}$$

In the following computed results of the Equation 4-9 and 4-10 are presented. The x-axis has been always used to plot the normalised bandgap $x_g = hv_g/kT_s$ and the parameters r- and r+ are altered parametrically.

The **power density** does not depend on the sub bandgap suppression (Equation 4-9) and this has been also pointed out by Coutts [3]. Hence, the ideal normalised bandgap for the maximum electrical power density is $x_g = 2.2$. This is the same value as for the ultimate efficiency for solar PV conversion. Equation 4-4 and Equation 4-9 give the same maximum for x_g, because the denominator integral of Equation 4-4 is simply the constant $\pi^4/15$ [21]. Figure 4-2 shows how the electrical power density decreases and the ideal normalised bandgap shifts to even smaller values for above bandgap suppression.

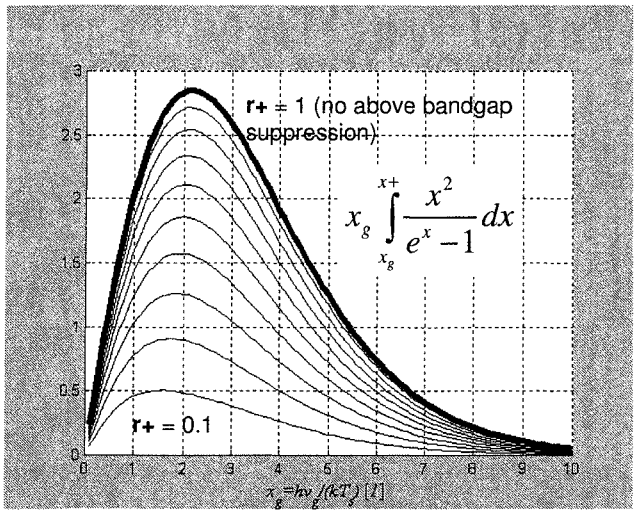

Below bandgap suppression (r-) does not influence the electrical power density

Figure 4-2: Plot of the power density as a function of x_g and r+.
The bold line shows the normalised power density without above bandgap suppression (r+=1). The above bandgap suppression varies parametrically in steps of 0.1 from r+=0.1 to r-=1.

As discussed, the value $x_g = 2.2$ already results in low ideal PV cell bandgap energies. For these reasons, it can be concluded that above bandgap suppression is not desirable from the viewpoint of electrical power density. Bearing in mind that typical combinations of GaSb cells and radiator temperatures result currently in x_g values from

4.8 to 5.4 [46,96,138,143] and Si cell based systems from 5.4 to 7.5 [115,260-262], it can be said that higher power densities are feasible if radiator temperatures can be increased or lower PV cell bandgaps being developed (see Appendix D).

The **efficiency** depends on all three modelled parameters, the normalised PV cell bandgap x_g, the above bandgap suppression r+ and the sub bandgap suppression r-. The three plots in Figure 4-3 vary in terms of the above bandgap suppression among each other. Other assumptions remain the same between these plots. Several conclusions can be drawn. Both above and sub bandgap suppression can increase the maximum efficiency. The theoretical case of monochromatic illumination with the bandgap energy of the PV cell may be considered (r+=0, r-=0) in such a case the ultimate efficiency could become 100% at an electrical power density of zero (not shown). Hence, full above bandgap suppression is unrealistic. Also full sub bandgap suppression (r-=0) leads to unrealistic results. Here, the efficiency function increases monotonically with the normalised bandgap x_g (Figure 4-3) [171]. Woolf highlighted the impact of small parasitic sub bandgap absorption on the TPV efficiency [241]. The importance of sub bandgap suppression can be strengthened using a typical TPV example. A TPV system using a GaSb cell (hv_g = 0.72 eV) and a radiator temperature of 1500 K result in x_g = 5.57. Assuming no above and no sub bandgap suppression the ultimate efficiency is slightly higher than 10% (Figure 4-3 top, solar PV case). Assuming that 10% of the sub bandgap radiation is absorbed by the PV cell (or 90% of the sub bandgap radiation is suppressed), the ultimate efficiency increases considerable to a value of more than 50% (Figure 4-3 top, r-=0.1).

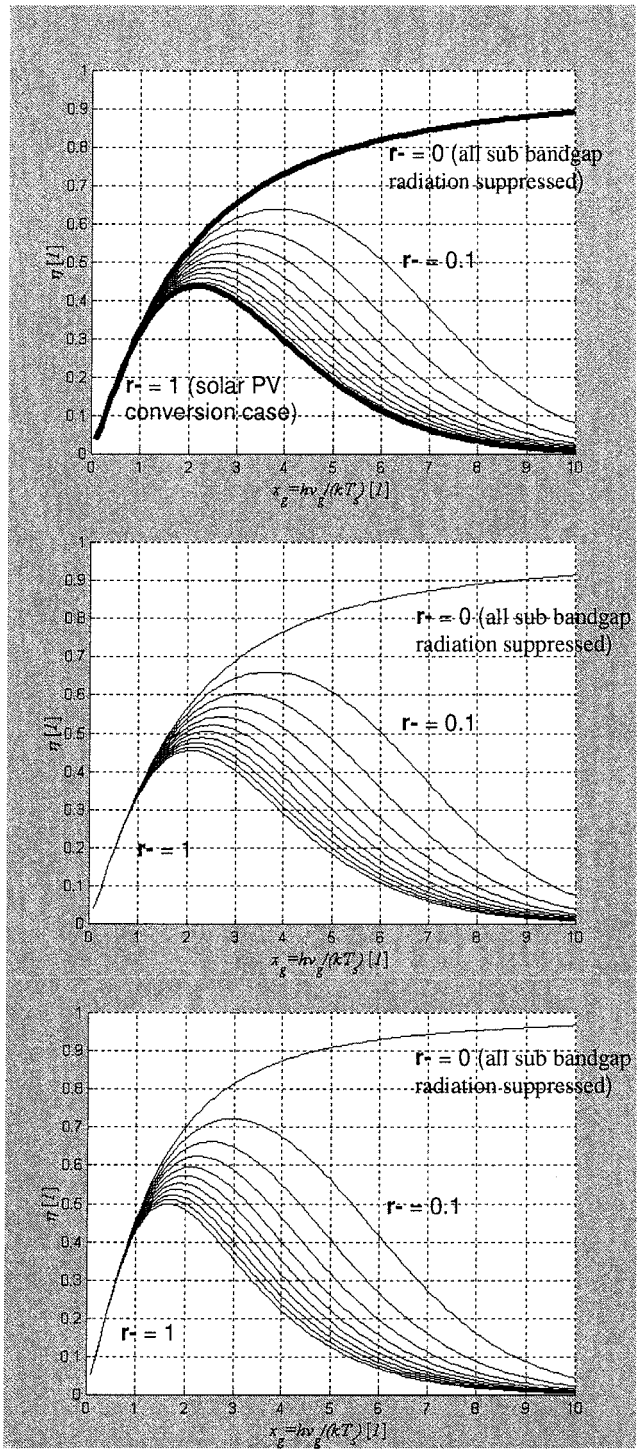

No above bandgap suppression (r+ = 1)

Additional suppression of some above bandgap radiation (r+ = 0.9)

Half of the above bandgap radiation is suppressed (r+ = 0.5)

Figure 4-3: Three plots of the ultimate efficiency as a function of x_g, r- and r+. For each plot the sub bandgap suppression varies parametrically in steps of 0.1 from r-=1 (solar PV case shown bold for the first plot) to the r-=0 (all radiation suppressed also shown bold for the first plot). Above bandgap radiation has been additionally suppressed for the two pictures at the bottom.

In the case of simultaneous above and sub bandgap suppression (Figure 4-3 bottom, r-=0.1) the ultimate efficiency even decreases below the case with sub bandgap suppression only. This is the result of a shift of the efficiency function to smaller normalised bandgaps for additional above bandgap suppression. Also the sub bandgap suppression broadens and the above bandgap suppression sharpens the efficiency curve compared to the solar PV case (r-=1, r+=1). A broader efficiency curve is generally desirable, because this can result in high efficiencies even if x_g values are not in the maximum of the function as discussed for the example $x_g = 5.57$.

4.2.4 Summary

Generally, the ultimate efficiency shows that ideal sub and/or above bandgap suppression (r- = 0, r+ = 0) lead to unrealistic results, so that higher r- and r+ values need to be considered. Both efficiency and electrical power density should increase for smaller PV cell bandgaps hv_g or higher radiator temperatures T_s compared to the typical situation currently with values of x_g higher than 5. Historically, there has been also a trend to smaller bandgaps in TPV cell development and this trend may be expected to continue. However, the ultimate efficiency cannot be seen as isolated from the other partial efficiencies. For example, the fill factor and voltage factor can be expected to decrease for smaller PV cell bandgaps (see Subsection 3.6.1). Hence, for smaller bandgaps the trade-off between an increase of the ultimate efficiency and a decrease of other partial efficiencies needs to be considered.

Coutts pointed out that the efficiency of TPV conversion might be enhanced further by not only suppressing sub bandgap radiation, but also above bandgap radiation [3]. In this work it is concluded, that sub bandgap suppression can enhance the ultimate efficiency considerably assuming currently utilised x_g values. This is for the reason that

the maximum of the efficiency function shifts to higher normalised bandgaps x_g and the function broadens. It is concluded that for these x_g values, above bandgap suppression is usually not desirable unless almost all sub bandgap radiation can be suppressed (r-values well below 0.1 would be required).

Assuming no above bandgap suppression, it needs to be considered that the maximum of the power density function remains the same. Therefore, there is no common ideal PV cell bandgap to maximise the ultimate efficiency and the electrical power density simultaneously. Hence, a trade-off between high efficiency and high electrical power density can occur due to sub bandgap suppression.

As a result of the assessment of simultaneous sub and above bandgap suppression, this work defines the figures of merit for the spectral control as follows:

- High share of in-band radiation absorbed by the PV cell
  (or low above bandgap suppression)
- Low share of out-of-band radiation absorbed by the PV cell
  (or high sub bandgap suppression)

4.3 TPV cavity design

There have been several geometric configurations of TPV cavities and these are discussed in the following using Figure 4-4.

In the **first** configuration (Figure 4-4) the radiator is completely surrounded by the PV cells. Although currently not considered, such configuration is theoretically feasible for radioisotope sources [47]. Also solar TPV systems may be designed similar to the first configuration using only a small inlet aperture for the solar radiation and a centred radiator [81,263]. One advantage of this configuration is that heat leaving the radiator is transferred necessarily to the PV cell and mirror areas are minimised. A drawback is the limitation in power density, since the area ratio of radiator to PV cell is always smaller

than one. In addition practical implementation should pose some engineering challenges, such as holding of the radiator, spherical system design or non-uniform PV cell illumination for a cube design. Half spherical systems have been also proposed for solar TPV conversion [27,73].

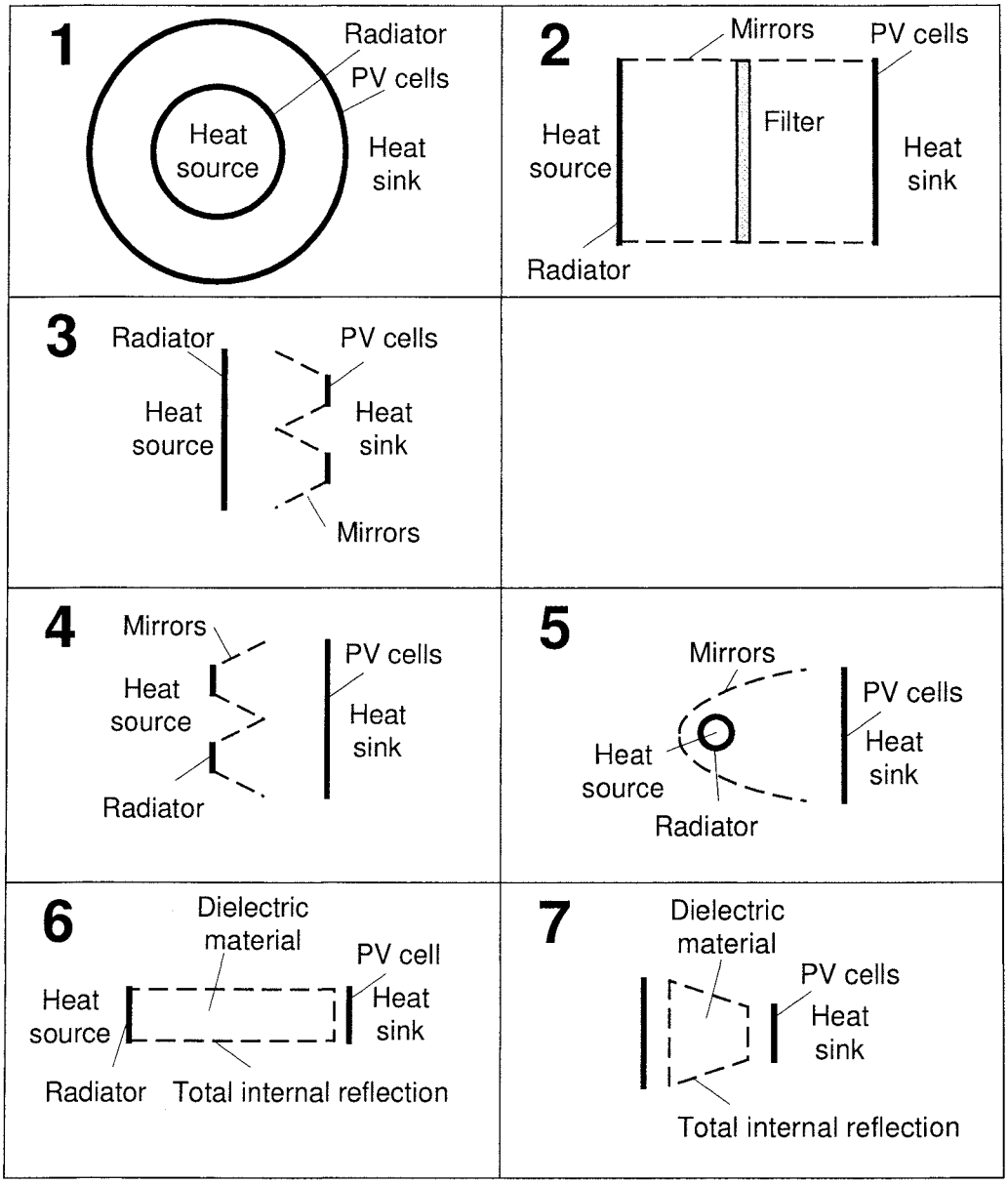

Figure 4-4: Eight schematics of geometric configurations for TPV cavities.

For combustion systems, as well as other heat sources, **concentric** tubes for the radiator and the PV cells have been usually preferred. Most commonly the PV cells surround the radiator [6,42,46,49,77,88,92,111,113,126,136,154,231], but also the inverse configuration has been examined [91,264]. Also systems using a **planar** design for the radiator and the PV cell facing each other have been designed [31,71,74,85,134,182]. The differences of concentric and planar configurations have been also examined [28,265]. The **second** schematic (Figure 4-4) is representative for all of these configurations in two dimensions. Often a SiO_2 shield has been placed in between the radiator and the PV cells for this configuration. The mirror area can be minimised by making the area of radiator and PV cell large compared to their distance. Mirrors can minimise cavity losses and direct the radiation to the PV cell. Engineering of a mirror operating on one side at radiator temperatures and mounted on a substrate with low thermal conductivity can be regarded as challenging [31].

The **third** configuration (Figure 4-4) offers the advantage of radiation concentration in the TPV cavity compared to the second configuration. This potentially can replace expensive PV cell area with cheaper mirror area (cost saving). The mirrors may extend to the radiator [264], consist of one large concentrator [266] or several small concentrators [267,268]. An experiment by Fraas et al. pointed out that mirror area decreases the efficiency due to parasitic air conduction and convection and it was concluded that mirror areas should be minimised [180].

Usually the radiator emits diffuse radiation, whereas most filters perform better for a radiation distribution with small zenith angles. Hence, collimator configurations have been proposed to direct the diffuse radiation. Configuration **four** (Figure 4-4) has included one large collimator [29], as well as light-emitting groove radiators consisting

of a high emissivity back and cone shaped reflective sidewalls [8,12]. Using a tubular radiator surrounded by a parabolic mirror has been also proposed for conversion of radiation into a parallel beam (Figure 4-4 configuration **five**) [51].

TPV systems where radiation is guided by total internal reflection in dielectrics have been also demonstrated. Goldstein et al. used a 20 cm long yttrium aluminium garnet (YAG) rod and this is shown schematically in configuration **six** [115-117]. Recently, Horne et al. successfully demonstrated 4 times concentration using SiO_2 prisms, sketched in configuration **seven** (Figure 4-4)[269].

Often the configurations shown in Figure 4-4 have been combined with a filter, where various filter concepts exist. The **location of the filter** can be considered as critical. For close location to the radiator, overheating of filters has been reported [28,269]. Hence, there has been a historical preference to place the filter on the front surface of the PV cell, where the filter can be cooled via the PV cell [270,271]. On the other hand, SiO_2 could generally withstand the temperatures in the TPV cavity.

The three major possibilities for spectral control are selective radiators, filters and PV cell design [3,47,172,270]. The former one has been already discussed together with other radiator concepts (Section 3.5), where a high emissivity for the short wavelength range (in-band) and a low emissivity for the long wavelength range (out-of-band) need to be achieved. The following sections discuss filters (Section 4.4) and PV cell design (Section 4.5) for spectral control.

4.4 Filter types for spectral control

Good et al. [272], Chubb et al. [273], Gruenbaum et al. [274] and Horne et al. [275] give some overview about filters in the TPV cavity. With the figures of merit defined in this work, filters with a high short wavelength (in-band) transmission and high long wavelength (out-of-band) reflection are required. For high efficiencies, usually out-of-band reflectivity of 90% and higher is required assuming currently used bandgaps and radiator temperatures, as pointed out by Baldasaro et al. [172] and in Subsection 4.2.4.

4.4.1 Frequency selective surface (FSS) filters

FSSs are essentially array structures which consist of a plurality of thin conducting elements, often printed on a dielectric substrate for support [276]. Examples of element shapes are dipole, tripole, jerusalem cross, square loop, cross dipole and circular loop [276]. Frequently, FSSs can form band-pass filters, also called resonant array or metallic mesh filters, which consist of a conducting plate with periodic apertures (inductive type). The complementary structure with periodic metal patches forms a band-rejection filter (conductive type) [275]. FSSs are well known for the sub millimetre and micrometer electromagnetic wavelength range [3]. For example they are familiar from the door of a common microwave oven where they reflect long wavelength electromagnetic radiation (microwaves) and transmit short wavelength radiation (light) [277].

For TPV, band-pass filters are of interest. These reflect most radiation except photons with energies in a band above the PV cell bandgap energy. The challenge of these filters applied for the near infrared wavelength range is the fabrication of the physically small structures with dimensions smaller than the peak transmission

wavelength [278]. Hence, nanofabrication techniques such as electron beam lithography, ion beam lithography or nanoimprint lithography are required [277,279].

Horne at EDTEK Inc. has developed inductive FSSs using about 420 million cross dipoles per cm^2 [96,269,275,280,281]. Initially each dipole has been fabricated individually by direct-electron-beam lithography, which has been replaced by a masked-ion-beam lithography process to reduce costs. The peak transmission at resonance frequency has been optimised for a wavelength of 1.45 μm for GaSb cells responding up to 1.8 μm. Disadvantages of this filter include high costs (0.55 £/cm^2 for masked-ion-beam lithography were estimated) and the transmission vs. wavelength performance (approximately Gaussian shape). The transmission characteristic leads to an in-band transmission of less than 100% that reduces the power density. The Gaussian shape transmission characteristic also has no sharp cut-off wavelength so that some out-of band transmission occurs. Nevertheless, systems using this filter are among the most efficient TPV systems being build. This filter has been incorporated or considered for combustion, solar and nuclear TPV systems [54,269]. The high performance is achieved due to a reflectivity of mid and long wavelength radiation similar to a gold mirror (98 to 99% reflectivity) [275] and the suitable angular performance of the filter. The transmission peak wavelength (or resonant frequency) of this filter remains the same for incident radiation with large zenith angles, although the filter increasingly reflects this radiation (specular surface behaviour) [275].

Kristensen et al. also examined other element structures than the cross dipole for TPV FSS filters [282].

4.4.2 Transparent conducting oxide (TCO) filters

TCOs are highly doped semiconductors with a high bandgap such as indium oxide, tin oxide, indium tin oxide, zinc oxide and cadmium stannate [3]. TCOs transmit in the short wavelength and reflect radiation in the long wavelength range. The reflectance vs. wavelength behaviour can been modelled using the classical Drude theory, where the reflectance can sharply increase for wavelengths higher than the plasma wavelength. Equation 4-11 defines the plasma frequency v_p, where N is the number of charge carries, e_o the elementary charge, ε_0 the vacuum dielectric constant, ε_b the dielectric constant associated with bound carriers at very high frequency, m* the effective mass and Y the relaxation frequency of the semiconductor [28,283,284].

$$v_p = \sqrt{\frac{N \cdot e_0^2}{\varepsilon_b \varepsilon_0 m^*} - Y^2} \tag{4-11}$$

$$Q = \frac{N\mu^2 m^*}{\varepsilon_b \varepsilon_0} - 1 \tag{4-12}$$

In order to get a steep transition from transmittance to reflectance the quality factor Q, given by Equation 4-12 needs to be maximised, where μ is the electron mobility [283,284].

TCOs are widely used in applications such as flat-panel displays, architectural heat reflecting coatings and PV panels [3], where they transmit visible light and reflect infrared radiation. For TPV, plasma wavelengths need to be shifted into the infrared and TCOs have been considered on the heat shield [285,286], as PV cell front surface filter (FSF) [287] and as an integral part of III-V semiconductors (e.g. InGaAs) [3,288]. The advantages of TCOs are potentially low costs and broad reflectance in the mid and far infrared. One major disadvantage of TCOs is the absorption near the plasma frequency [275]. Cadmium stannate filters demonstrated mid and far infrared reflectance over 90%

[289]. Further improvements of TCOs may or may not allow reaching the high mid and far infrared reflectance of FSS filters [289]. Arsenic, phosphorus and boron doped silicon TCOs were also examined for TPV [290].

4.4.3 All-dielectric filters

All-dielectric filters, also called interference or dichroic filters [274], consist of multiple thin layers of material having different refractive indices (e.g. $n_{ZnS} = 2.3$ and $n_{MgF2} = 1.4$ [3,27]). Generally, all dielectric filters have low absorption and are well understood [3]. They can be flexibly designed as bandpass or edge filters. Software packages allow optimisation of the transmission and reflection vs. wavelength characteristics of the filters for given optical material constants (e.g. refractive index versus wavelength) [3].

All-dielectric filters have several disadvantages when they are applied for spectral control in a TPV system. These filters are typically optimised for smaller wavelength ranges than required for TPV operation (typically 0.5 to 10 μm) [27]. The TPV requirements of out-of-band reflectivity over a **wide wavelength range**, a high in-band transmissivity and sharp transition behaviour can only be met using a large number of dielectric layers, where costs and the control of film thickness are seen as challenging [3]. Also combining more than one all-dielectric filter could not overcome this challenge due to interference between the filters [27,274].

In addition, it is well known that the transmission and reflection vs. wavelength of dielectric filters are a function of the **incident angle**. Hence, optical systems have been designed for TPV to bundle the radiation so that the incident radiation at the filter has small zenith angles (see Section 4.3).

4.4.4 Metal-dielectric filters

Metal dielectric filters (also called induced transmission filters [274]) consist of a thin layer of metal, such as silver or gold. For TPV a thickness of around 10 to 30 nm has been considered, in between one or more dielectric layers on each side [27,77,291,292,293]. Metal films have the advantage of high reflectivity in the mid and far infrared wavelength range. These filters have successfully transmitted visible light and reflected infrared radiation [283,284]. Unfortunately shifting the transmission range further into the infrared has been found to increase the absorption within these filters [274].

4.4.5 Bulk dielectrics in the cavity (heat shields)

Heat shields made of fused silica (SiO_2) are commonly used in TPV systems [77,114,138,180]. Fused silica has the highest melting point of any glass and is widely available. For lower temperatures other high-temperature glasses have been also considered including Duran® [114] and Pyrex® [77]. Hottel pointed out that the glass shield acts as a thermal protection for the PV cells but also reduces in-band transmission in TPV cavities [50]. Pierce and Guazzoni measured different 1 mm thick SiO_2 shields and they concluded that participating glass shields in a TPV system emit radiation in both directions (to the PV cell and the radiator) [138]. Physically thick dielectric media with thicknesses of several centimetres have been also considered in TPV cavities. This research area is of special interest to the work reported here and past TPV research by Goldstein et al. [115-117] and Hanamura et al. [93-95] will be discussed further together with the computational modelling in Subsection 8.2.5.

4.4.6 Other filter concepts

Another promising filter is a **tandem filter** consisting of an all-dielectric and a TCO filter. Recently, this tandem filters have achieved high performance as PV cell FSFs [270-272,275]. **Rugate filters** are based on interference coatings with a continuously varying refractive index. This filter has been proposed as FSF in full-spectrum cavity solar converters [294,295].

Spectral splitters apply different principles such as reflection/transmission [294,295], refraction (e.g. prism) and holography. Only TPV work on the latter could be identified [83,51]. Although direct solar spectral splitting systems may use the same low bandgap PV cells as TPV systems, such as hybrid lighting or full-spectrum cavity converters [294,295,296], they are not considered as a TPV system in this work, because of the absence of a radiator.

At the Paul Scherrer Institute (PSI) a 5 mm thick **water** layer held by two concentrical SiO_2 tubes has been considered as a long wavelength absorption filter (above 1.4 μm) [7,286]. Advantages of this design include simplicity, high absorption of mid and far infrared radiation and the use of the hot water for a CHP system. Disadvantages include reduced in-band transmission (or power density) and reduction of electrical conversion efficiency due to the absorbed and lost heat in the water.

The **inverse filter** concept, in which undesirable long wavelength radiation (out-of-band) is transmitted and convertible short wavelength radiation (in-band) is reflected, has also been considered for TPV [27]. Such filters are known as cold mirrors and are used for example in dichroic lamps. It has been pointed out that TPV systems utilising cold mirrors would require a complex design with an additional mirror [27].

Recently, **photonic crystal** FSFs have been proposed [270].

4.5 PV cell design with spectral control

4.5.1 Front surface filters (FSFs)

Commonly PV cells are antireflection coated to couple radiation from a low refractive index media (air or vacuum) into the semiconductor with high refractive index. This can be seen as a simple FSF [275]. For TPV, FSFs need to transmit in-band radiation and reflect mid and far infrared radiation. One advantage of FSFs is that they are cooled together with the PV cell, in contrast to filters placed in the TPV cavity, which may require additional cooling. All dielectric FSFs have been examined since the 1960s for germanium cells [275]. There are examples of all major filter types used as a FSF: all-dielectric [47], tandem [47,270], metal-dielectric [293] and FSS [270].

4.5.2 Back surface reflectors (BSRs) and buried layer reflectors

The technology of BSRs is partly available from space solar cells or silicon cells, where multiple passes of photons can increase cell efficiency [297]. The principle of the BSR is that out-of-band radiation penetrates into the PV cell, passes through the device layer and substrate, is then reflected at the back surface mirror, returns via the same path and then leaves the PV cell to be returned to the radiator [3]. Hence, this concept requires low absorption of sub bandgap radiation by the device layer and substrate. Low absorption due to free carriers can be achieved using low-doped substrates such as GaSb, InP and Si [3,30,206]. However, making an ohmic contact to a lightly doped substrate is generally difficult [3,30,31]. PV cells operating in TPV systems usually operate under high illumination intensities and this requires a particularly low series resistance to minimise ohmic losses. Besides a low resistance contact and low substrate absorption of the cell, other requirements for BSRs are high specular reflection, good

adhesion, as well as good chemical and thermal stability [3,184]. These requirements have lead to various PV cell designs including buried layer structures for the InGaAs and InGaAsSb cells, where the reflector is located within the MIM. The potential of combining BSRs and FSFs has been pointed out by Coutts [3].

4.6 Summary

This chapter highlighted the importance of radiative heat transfer in TPV cavities in terms of the angular, spatial and spectral radiation distributions. The work then focused on spectral control, where the combined sub and above bandgap suppression was examined using an analytical model. It was found that spectral control methods applying sub but no above bandgap suppression are desirable assuming current radiator temperatures and PV cell bandgaps. Hence, the figures of merit of high in-band radiative heat transfer and high out-of-band suppression were defined for this work. Then, principles of TPV cavity designs have been discussed. Here, the mirror design in TPV cavities has been identified as critical and total internal reflection in dielectrics is regarded as a promising alternative concept to overcome this difficulty. Subsequently, filter concepts have been reviewed, where each concept has been found to have its own strengths and challenges. Advances in both the PV cell performance (discussed in the previous chapter in Section 3.6) and spectral control engineering at the cells have been made over the last several years. There has been limited work on bulk dielectrics, although most TPV systems use SiO_2 heat shields in their cavity.

5 Competing technologies to TPV systems

5.1 Introduction

In general it can be assumed that there exists a potential market for TPV systems anywhere that an electrical power source is required [37]. Hence, in order to identify suitable TPV applications, this chapter reviews other deployed and emerging electricity generating technologies.

In TPV literature, competing technologies discussed have included internal heat engine generators [2,109,110,298,299], solar PV systems [109,110], electro-chemical cells and direct heat-to-electricity converters. The last category includes thermoelectric, thermionic and alkali metal thermal to electric converters (AMTECs)[2,109,110,298-300]. The three electro-chemical cell types are primary (battery), secondary (rechargeable battery) or tertiary (fuel cell)[2,109,110,298,300]. Other literature also gives details about these technologies [21,22,32,106,301-303]. These sources indicate that external heat engine generators, and in particular Stirling generators, are another potential competitor group.

This review of competing technologies has been limited to a range of technologies. From the various potential technologies to generate electricity only those have been considered which also convert one of the four sources considered in this work. This has

led, for example, to the exclusion of renewable conversion technologies other than solar PV (e.g. wind). Technologies above 1 MW have also not been considered in this work, because TPV cell costs are currently high and the largest demonstrated TPV systems have powers in the order of kilowatts. Also other conversion technologies can have high efficiencies above 1 MW. Only direct heat-to-electricity converters commonly found in recent literature have been considered [2,109,110,298-300], some other conversion technologies exist and are discussed elsewhere [22].

The technology options are summarised in Figure 5-1, which illustrates that the heat sources have to be taken into account when comparing TPV to its competitors. Power densities (e.g. W/kg, W/m^3, W/cm^2) and efficiencies are important performance indicators to compare these technologies. The next four sections discuss heat engines, electro-chemical cells, direct-heat-to-electricity converters and solar PV systems (Section 5.2-5.5). Afterwards a comparison of these technologies and TPV technology is made (Section 5.6).

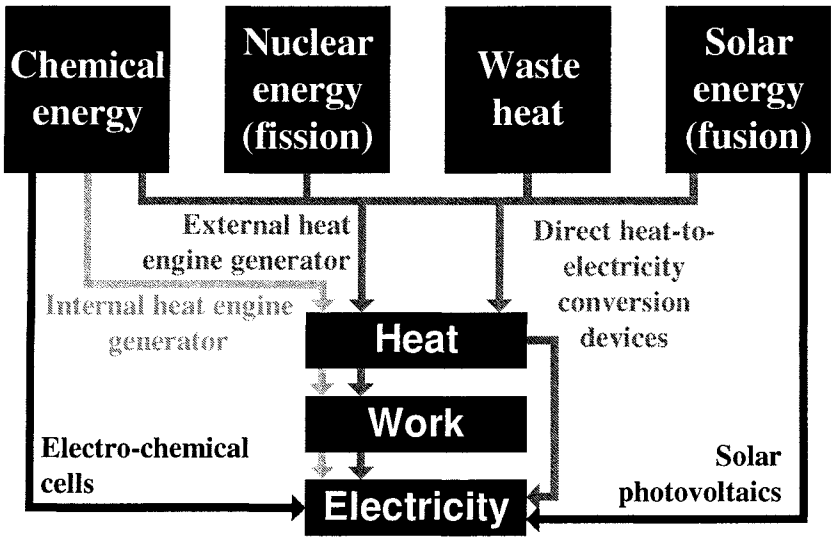

Figure 5-1: Summary of competing technologies to TPV systems.
The figure defines four types of heat sources and five classes of energy converters and has been composed in this work.

5.2 Heat engine generators

These generators utilise a two-step conversion process. The first conversion into mechanical energy limits the efficiency. The second conversion from mechanical energy into electricity can be generally efficient with values greater than 95% [298]. The requirement for moving parts can be associated with complex starting, noise, weight, high complexity, high maintenance and short lifetime compared to TPV conversion. In general, internal and external heat engines can be distinguished [302].

5.2.1 Internal heat engine generators

In an internal heat engine, the heat source is also the working fluid in thermodynamic terms and thus they compete with TPV generators only for combustion heat sources (Figure 5-1). Internal combustion engines (ICEs) tend to have few components, although not necessarily moving parts, and therefore higher volumetric and gravimetric power densities compared to external heat engines [302]. ICEs can have an **intermittent** (reciprocating engines) or a **continuous** flow and combustion process (e.g. gas turbine). In intermittent engines combustion occurs during a limited part of the cycle only, so that component temperature exposures tend to be less severe in intermittent compared to continuous engines [302]. This usually results in higher efficiencies but higher pollution (CO, NO_x and unburned H_xC_x) of intermittent engines compared to continuous engines [302,303]. The flow rate can be higher for continuous engines, so that these engines tend to have higher volumetric power densities [303]. The major **intermittent** heat engines are reciprocating spark ignition (Otto cycle) and compression ignition (Diesel cycle) engines. Generators based on ICEs are established and are commercially available at low prices.

Table 5-1 shows the performance and cost range of the smallest commercial gasoline generators [298,304,305]. Yamaguchi et al. [109,110] reported portable generator efficiencies of 10 to 20% in the range from 1 kW to 10 kW and efficiencies below 10% for generators smaller than 1 kW. Above 10 kW the efficiencies can exceed 30%, where engines are available from vehicles at low prices (lower than about 0.03 £/W) and high power densities [110][13].

Characteristics	Data
Electrical output power	150 - 5500 W
Efficiency fuel to electricity[14]	3 - 10%
Gravimetric power density[15]	12 - 84 W/kg
Volumetric power density	8.5 - 31 kW/m^3
Capital cost vs. electricity output	0.2 - 1.8 £/W

Table 5-1: Performance of a variety of small portable Honda generators.

Currently **gas turbine** (Brayton cycle) generators are mainly used in the MW power range, such as for central power stations in conjunction with steam turbines. Gas turbines can operate in a closed or open cycle. The closed cycle configuration results usually in higher efficiencies at the cost of increased complexity [303]. Table 5-2 plots the performance and costs of a small currently commercially available CHP open cycle turbine [306,307]. Micro turbines as small as 10 W are in a research stage [308].

Characteristics	Data
Electrical output power	30 kW
Efficiency fuel to electricity	26%
Gravimetric power density	74 W/kg
Volumetric power density	13.4 kW/m^3
Capital cost vs. electricity output	0.64 £/W

Table 5-2: Performance of the CHP micro-turbine CAPSTONE C30.

---

[13] In this work currency values have been converted using an average 2004 interbank rate of £1 = $1.833 and £1 = 1.475 Euro.

[14] In this work, the efficiency has been calculated by the ratio of electricity output divided by fuel input at ¼ of the nomial power. The fuel input power has been calculated by the product of tank capacity and the volumetric fuel energy density of 40 MJ/litre divided by the ¼ load operation time.

[15] In this work, the gravimetric power density has been calculated by the ratio of nominal electricity output divided by the weight without fuel.

5.2.2 External heat engine generators

An external heat engine has a separated heat source and working fluid. The use of an external combustor, often associated with heat exchangers for the working fluid, adds usually some complexity and results in lower volumetric and gravimetric power density than ICEs, but allows heat to be derived from all four sources (Figure 5-1). The major external heat engines apply the Rankine and Stirling cycle.

Steam turbines (Rankine cycle) tend to be used in large centralised power stations. The Rankine cycle can be of closed (e.g. nuclear power plant) or open type (e.g. steam locomotive) [303]. The open cycle requires a constant water source. The closed cycle usually results in complex system designs with moderate efficiencies and low power densities for power outputs considered in this work [303]. Hence these engines are not considered further here.

Stirling engine generators have been researched for a wide power range from artificial heart power to military submarine propulsion. They usually have good part load behaviour, can operate with low noise (free piston engine) and potentially achieve Carnot efficiency. Stirling engine generators have been considered for all four heat sources and similar applications as TPV. There are several Stirling CHP units emerging commercially (Table 5-3). Disadvantages of Stirling engines often include low power densities [303]. Past challenges in terms of working fluid leakages and seals may or may have not been completely overcome in current systems.

Characteristics	WhisperGen AC [309,310]	Solo Stirling 161 [311]	STM PowerUnit [312]
Manufacturer	Whisper Tech	Solo Stirling	STM power
Electrical output power	1.2 kW	2 - 9.5 kW	55 kW
Efficiency fuel to electricity	12% (calculated)	22 - 24%	30%
Gravimetric power density	8.7 W/kg	4.3 - 20.6 W/kg	34.6 W/kg
Volumetric power density	4.7 kW/m^3	2.3 - 10.8 kW/m^3	14.3 kW/m^3
Capital cost vs. electricity output	2.5 £/W	N/A	N/A

Table 5-3: Performance and costs of stationary CHP units using Stirling engines.

5.3 Electro-chemical cells

There are primary (battery), secondary (rechargeable battery) and tertiary cells (fuel cells), which are discussed in the following two subsections.

5.3.1 Primary and secondary cells (batteries)

Batteries are available from small primary button cells (from 10 J) up to large secondary batteries for underwater propulsion and load levelling (up to 100 MJ) [16]. Advantages include low maintenance (no moving parts), good part load behaviour and efficient charge/discharge performance. Currently, the major primary cell types are zinc-carbon, alkaline-manganese, mercury-oxide, silver-oxide and zinc-oxide, as well as lithium-based cells [313]. The major secondary cell types are nickel-cadmium, nickel-metal hydride and lead-acid [313]. Secondary batteries tend to have higher gravimetric and volumetric **power densities** compared to primary batteries. Secondary nickel-cadmium batteries have the highest power densities with values of around 500 kW/m^3 and several hundreds of watts per kilogram [314,315]. These values can be regarded as high compared to other technologies. On the other hand, the **energy density** of primary and secondary batteries is low compared to hydrocarbon fuels (see Table 3-3) [314]. Lithium batteries are expected to reach values as high as 3.6 MJ/kg in future [298]. Often battery disadvantages include the use of environmentally critical materials, limited shelf life and high electricity costs [314]. For example, the cheapest primary batteries are usually alkaline-manganese cells, where for a typical AA-battery a capital cost energy price of around 270 £/kWh can be estimated[16]. This value can be compared

[16] Assuming for example data of 1000 mAh, 1.5 V and a capital cost of £0.40.

to current utility gas and electricity prices of several pence per kWh in the UK. Hence, cost and energy density constraints of batteries make a replacement consisting of a low cost hydrocarbon fuels together with a fuel-to-electricity converter (e.g. TPV) attractive. This arrangement has also the advantage of a simpler refuelling compared to the recharging process of secondary batteries.

5.3.2 Tertiary cells (fuel cells)

Fuel cells compete directly with TPV in the conversion of fuel into electricity (Figure 5-1). Fuel cell research can be found for a wide power range from mW to MW. They can be classified by different criteria including fuel type (e.g. hydrogen or hydrocarbon), fuel processing strategy (external or internal reforming), operation temperature, catalyst material, charge carrier or type of electrolyte. Usually the latter one is commonly used for classification. Table 5-4 has been composed from different sources [316-319] and sums up the major fuel cell types and their performance. One major advantage of fuel cells is the demonstrated high efficiency, which can be around 40 to 60% based on lower heating values for the major fuel cell types [317,320]. The efficiency also remains high at part load and over a wide power range. Another advantage is the solid-state operation (e.g. low noise). CHP operation is generally feasible and the operation temperature of the fuel cell influences the heat grade. Hence Solid polymer membrane fuel cells (SPFCs) can only generate low-grade heat.

	Solid polymer membrane (SPFC)[17]	**Alkaline (AFC)**	**Phosphoric acid (PAFC)**	**Molten carbonate (MCFC)**	**Solid oxide (SOFC)**
Catalyser	Platinum	Platinum	Platinum	Nickel	Perovskites
Temperature	323-383 K (50-110 °C)	323-473 K (50-200 °C)	463-483 K (190-210 °C)	903-923 K (630-650 °C)	923-1273 K (650-1000 °C)
Cell fuels	H_2, CH_3OH	H_2	H_2	H_2, CO	H_2, CO, CH_4
Cell poisons	CO (>10 ppm) Sulphur (>0.1ppm)	CO_2 is a poison which more or less rules out its use with reformed fuels	CO (>0.5%) Sulphur (>50ppm)	Sulphur (>0.5ppm)	Sulphur (>1ppm)
Reformer	External or direct CH_3OH		External	External or internal	External, internal or direct CH_4
Reformer fuels	CH_3OH, alcohols, LPG, gasoline, diesel, jet fuel		Natural gas, alcohols, gasoline, diesel, jet fuel	Gas from coal or biomass, natural gas, gasoline, diesel, jet fuel	Gas from coal or biomass, natural gas, gasoline, diesel, jet fuel
Typical application	Commercial and residential CHP, distributed power, portable power, transport	Transport, space	CHP power generation	Commercial and residential CHP, power generation, ship propulsion, trains	Commercial and residential CHP, power generation, ship propulsion, trains
Advantages	High power density, rapid start-up and good load-following characteristics, direct methanol cell without reformer	Simple design, cheap electrolyte, high power density	Advanced technology, commercial system available (e.g. PC25C)	Internal reforming, cheap catalyst, CO as fuel, CO_2 rich fuels	Internal reforming, cheap catalyst CO as fuel, CO_2 rich fuels, impervious to gas cross-over
Disadvantages	CO removal, water management, membrane cross-over and costs	Limited to hydrogen	External reforming, expensive catalyst	Poor start-up, poor load following, high temperature design issues	Poor start-up, poor load following, high temperature design issues

Table 5-4: Comparison of the main fuel cell types.

SPFCs and advanced space AFCs have demonstrated area power densities (W/cm^2) roughly a factor ten greater than that observed of other fuel cells [320]. This can result in high volumetric and gravimetric power densities. The power density generally

[17] The solid polymer fuel cell (SPFC) is also known as proton exchange membrane (PEM) fuel cell.

increases with increasing power output. For example for automotive applications SPFC stacks have demonstrated power densities of 1000 kW/m^3 and 700 W/kg [319,321,322]. Selecting the operation point of a fuel cell, using its voltage versus current density characteristic, requires a compromise between a highly efficient but large cell and a low efficient but high power density cell [317]. One key disadvantage of fuel cells is the use of hydrogen, which is commercially not available for the mass market and fuel storage and handling is immature and can be dangerous [298]. The high gravimetric energy density of hydrogen is generally advantageous, whereas the volumetric energy density of 12.8 MJ/m^3 compares low to oils with values around 40000 MJ/m^3 (Table 3-3). Compression of hydrogen increases the volumetric energy density. Using a common laboratory gas cylinder at 2200 psi results in a volumetric energy density of 1600 MJ/m^3 and higher pressures can increase the density further (e.g. 5300 MJ/m^3 at 10000 psi). Liquid hydrogen has a volumetric energy density of about 10000 MJ/m^3 and this is still lower than oils. Another storage option is the use of solid-hydride storages (e.g. lanthanum nickel hydride), which are capable of a slightly higher volumetric energy density at the expense of gravimetric energy density, compared to liquid hydrogen [323,324]. Currently there are challenges with all hydrogen storage technologies [323,324]. Non-hydrogen fuels require usually internal or external reforming. The difficulties of reforming are discussed elsewhere [317,319].

SPFCs converting directly methanol without reformer are known as direct methanol fuel cells (DMFCs). There has been some renewed interest since the 1990s in DMFCs due to advances made in the membrane of the SPFC [319]. DMFCs are attractive, because methanol can be economically and efficiently produced. In addition methanol storage is simple and safe compared to hydrogen. It seems that the first large-scale fuel

cell products will be the replacement of secondary batteries by DMFCs (e.g. laptop, mobile phone). In these applications the secondary battery lifetime is low, so that the DMFCs lifetime is not highly critical. Currently the DMFC market develops dynamically and several start-up companies have been formed [325].

Table 5-5 sums up the characteristics of some fuel cells, which emerge commercially or operate in field trials.

	SFC A25, SFC A50 [326,327]	**VE100 v2, VE1000 [328,329]**	**AirGen [330,331]**	**Ebara Ballard [332,333]**	**Independence 1000 [334]**	**Auto fuel cell stacks [110,321]**	**PC25C [335,336]**
Application	Portable	Portable	Portable	μCHP Japan	Stationary backup	Vehicle propulsion	Stationary CHP
Fuel	Methanol	Hydrogen	Hydrogen	Natural gas	Hydrogen	Hydrogen	Natural gas
Technology	DMFC	SPFC	SPFC	SPFC & reformer	SPFC	SPFC	PAFC & reformer
Manufacturer	SFC Smart Fuel Cell AG	Voller Energy	Ballard	Ebara Ballard	ReliOn, Inc., Avista Lab. Inc.	N/A	UTC Fuel Cells
El. power	25-50 W	0.1-1 kW	1 kW	1 kW	1 kW	50-100 kW	200 kW
Efficiency fuel to electricity	~10-12%[18]	34-36% [19]	~30%[20]	~34%	~ 31%	N/A	~40%
Gravimetric power density	8 - 11 W/kg	17 - 56 W/kg	20 W/kg	N/A	12 W/kg	~1000 W/kg	11 W/kg
Volumetric power density	1.1-3.4 kW/m^3	6.3-6.7 kW/m^3	7.6 kW/m^3	N/A	3.0 kW/m^3	1000-1800 kW/m^3	3.6 kW/m^3
Capital cost vs. electricity output	47-76 £/W	5.5-20 £/W	3.6 £/W	3.3-5.5 £/W	2.3 £/W	5.5 £/W	4.5£/W installed

Table 5-5: Commercially available and field trial fuel cell systems.

[18] A methanol calorific value of 23790 MJ/m^3 and a consumption of 1.3 and 1.5 litre methanol per kWh electricity have been assumed [224].

[19] A hydrogen calorific value of 12.76 MJ/m^3 and a consumption of 1.3 litre hydrogen per minute to generate 100 W have been assumed [224].

[20] It has been assumed that the AirGen product is based on the Nexa product with a fuel consumption of 18.5 litres per minute. A hydrogen calorific value of 12.76 MJ/m^3 has been assumed. The actual efficiency can be expected lower due to the housekeeping power [224].

5.4 Direct heat-to-electricity conversion devices

Besides TPV, there are other direct heat-to-electricity conversion technologies including thermoelectric converters, alkali metal thermal-to-electric converters (AMTECs) and thermionic converters. All these technologies use a hot source and a cold sink. The heat flux from the source to the sink can be partly converted into electricity by the direct heat-to-electricity conversion device. Thus important characteristics of these devices are the electricity output per area (power density in W/cm^2) and the efficiency (ratio of electricity output to total heat flux). All technologies share potentially similar solid-state properties, such as simple design, no moving parts, low maintenance, high reliability, good scalability and modularity. Solid-state is a macroscopic statement. In fact, movement or transport of energy must always involve motion of a physical entity with energy [21]. For the direct heat-to-electricity conversion device these are ions (AMTEC), electrons (thermoelectrics, thermionics) or photons (TPV). Also all technologies can convert heat from any source with a suitable temperature (Figure 5-1) into direct current electricity. Major aspects where the devices differ from each other include the heat source and sink temperature, the commercial status, the efficiency and the power density.

5.4.1 Thermoelectric converter

Electricity generation in a thermoelement is based on the Seebeck, Peltier and Thomson effect. A thermoelectric generator usually consists of a large number of thermoelements connected electrically in series (Figure 5-2). Of the direct heat-to-electricity conversion devices, thermoelectric generators are the most developed devices and are used in niche market applications such as for space and remote power. Hot side

temperatures range from very low (e.g. body temperature powered wrist watch) up to around 1300 K (e.g. space applications). Also the power output varies widely from nW to more than 100 kW [337]. Similar thermoelectric modules can be used for cooling as well for power generation from low-grade (e.g. geothermal, ocean power, low-grade waste heat) and high-grade heat (e.g. combustion). In this work only thermoelectric generators using high-grade heat are considered, since these generators directly compete with TPV converters.

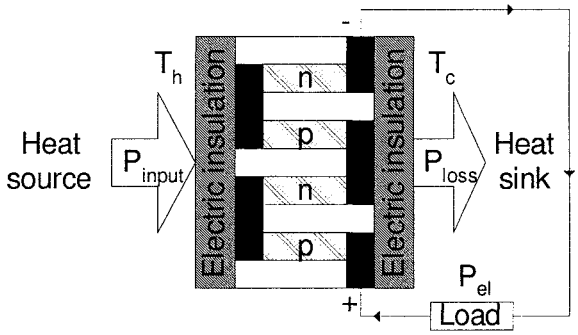

Figure 5-2: Schematic of the operation principle of a thermoelectric generator. The n-type and p-type semiconductor legs are electrically connected.

$$\eta_{\max} = \eta_{Carnot} \cdot \frac{\left(1+Z \cdot T_{AV}\right)^{1/2} - 1}{\left(1+Z \cdot T_{AV}\right)^{1/2} + T_c / T_h} \tag{5-1}$$

Calculations of thermoelectric generator efficiency and power density have been discussed by Cobble [338]. The generator can be optimised for maximum power density **or** efficiency. Equation 5-1 gives the maximum efficiency of a single-stage generator, which is optimised for maximum efficiency, where $T_{AV} = (T_h - T_c)/2$ [338]. The figure of merit Z is defined as $S^2\sigma/k$ (1/K) for a single-stage converter using one junction material, where S is the Seebeck coefficient (V/K), σ the electrical conductivity (S/m) and k the thermal conductivity (W/mK). It follows from Equation 5-1, that a high efficiency η_{max} requires a large temperature difference from the hot to the cold side T_h - T_c and a high figure of merit Z. Currently bulk semiconductor materials have maximum

ZT values of close to or less than 1 [339,340]. This results in a low efficiency, which is one of the major drawbacks of thermoelectric generators. Global Thermoelectric Inc. is the major manufacturer of combustion based thermoelectric systems [339,341] and the performance of their generators is shown in Table 5-6 together with a single thermoelectric module for power generation [342,343]. It has been estimated that more than 12,000 combustion powered thermoelectric generators have been placed into operation for niche market applications [344]. There has been funding for large-scale thermoelectric heat recovery in Japan [339,345], with current funding in the US [346] and possible future funding in the EU [347]. Heat to electricity efficiencies of below or around 5% can be expected [339]. Future thermoelectric generators may show higher performance using various concepts to increase the figure of merit Z (e.g. using nanostructured materials) [339,340]. Other promising concepts include symbiotic and multistage generation. For the former one - symbiotic, the thermoelectric generator is part of a counter-flow heat exchanger [339,348].

Characteristics	**Combustion generator**	**Bismuth Telluride Module HZ20**
Manufacturer	Global Thermoelectric	Hi-Z Technology
Electrical output power	15 - 500 W	19 W
Efficiency	2.3-3.5% (fuel to electricity)[21]	~4.5%[22]
Gravimetric power density	0.7 - 5.4 W/kg	165 W/kg
Volumetric power density	217-515 W/m^3	N/A
Area power density	N/A	0.43 W/cm^2
Capital cost vs. el. output	~ 27 £/W	4.4 £/W

Table 5-6: Performance of thermoelectric combustion generators and a module.

[21] For the combustion generator efficiency, a higher calorific value of propane of 50.4 MJ/kg has been assumed [224]. This efficiency includes flue gas losses, so that higher heat-to-electricity efficiency values can be expected.

[22] For the module efficiency, a hot side temperature of 503 K (230 °C) and a cold side temperature of 303 K (30 °C) have been assumed.

5.4.2 Alkali metal thermal-to-electric converter (AMTEC)

The AMTEC is a thermally regenerative, electro-chemical device, where an alkali metal flows in a closed loop cycles its aggregate state between liquid and vapour [21,298,349]. Of the alkali metals, sodium has mainly been used. There has also been some work on potassium. Cycling of the alkali metal is obtained using devices such as electromagnetic pumps and capillary wicks [349]. The only remaining moving part in AMTECs using capillary wicks is the enclosed alkali metal (solid-state device behaviour). The electricity is generated in an anode, cathode and electrolyte configuration, where alkali metal ions flow through the electrolyte and electrons bypass the electrolyte (Figure 5-3)[21,349,350]. Usually AMTECs use a beta alumina solid electrolyte (BASE), which is commonly fabricated as a dense microcrystalline ceramic consisting of the elements sodium, lithium, aluminium and oxygen [21]. The BASE limits the hot side temperature to around 1300 K, since the electrolyte becomes chemically reactive at higher temperatures [21]. The cold side temperatures typically range from 400 to 800 K [21]. The two main types of AMTEC cycles, liquid-anode and the vapour-anode, are discussed elsewhere [349].

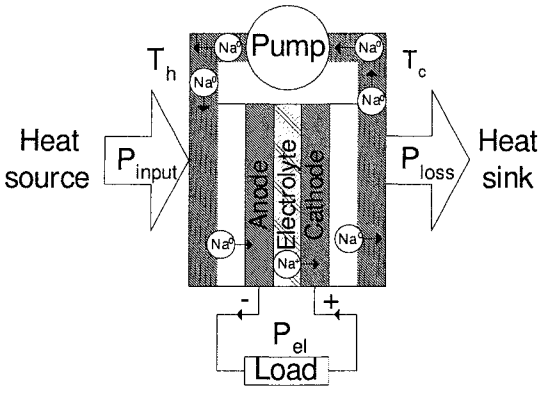

Figure 5-3: Schematic of the operation principle of an AMTEC. The generator uses the alkali metal sodium, which is ionised in the electrolyte. The figure has been composed from different sources.

The specific advantages of AMTECs are high efficiency, high power density and the use of potentially low cost materials [349]. Electrical power densities of 1 W/cm^2 have been achieved [349] and gravimetric power densities up to 500 W/kg are thought to be feasible [298,349]. One of the major difficulties of current AMTECs is the deterioration of efficiency over time. For example an AMTEC, which could only produce about half its initial output power after two years of operation has been reported [349]. Another drawback of AMTECs is that conversion efficiencies larger than 20% of heat into electricity seem to be feasible but this has not been demonstrated [349].

There are several similarities between AMTECs and TPV converters. Both technologies share a potentially high power density, a similar demonstrated and anticipated efficiency and a similar power range [298,349,351]. For radioisotope powered space applications, both are considered as a possible upgrade for the low efficient thermoelectric generators at present [351]. A basic literature search indicates that the AMTEC research community is smaller than the TPV community and that AMTEC work has focused on space applications [349]. However, AMTEC work on terrestrial applications, similar to TPV, has also been reported. These include remote power, portable power, micro CHP and auxiliary power units (APUs) [352].

5.4.3 Thermionic converter

In a thermionic converter electrons are emitted (or "boiled") from the heated cathode (also called emitter) and collected by a cooler anode (also called collector). The electrons return to the cathode by means of an external load (Figure 5-4)[21,106]. The maximum electron current that an emitting surface can supply per unit area is given by the Richardson-Dushman equation (Equation 5-2)[21,22]. From this equation it becomes clear, that the electron flux increases rapidly with increasing temperatures, and

is large for metals with a small work function Φ (e.g. tungsten). The work function of a material is defined as the amount of energy required for an electron with a certain energy to overcome and escape the binding attractive charge (or surface potential) of a material's surface. The constant A is ideally a collection of fundamental constants, where real materials yield lower values [21,353].

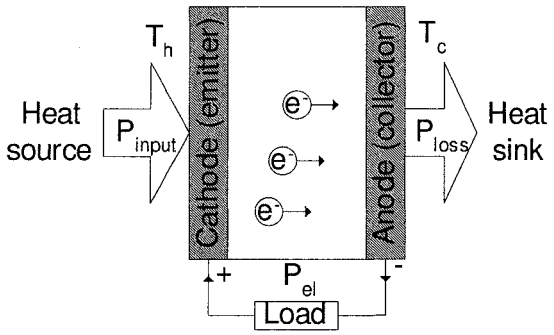

Figure 5-4: Schematic of the operation principle of a thermionic generator. Electrons are transferred from the hot cathode to the cold anode by the Edison effect.

$$J = A \cdot T_h^2 \cdot e^{-\frac{\Phi}{kT_h}} \qquad \text{with } A = \frac{4\pi e_0 m_e k^2}{h^3} \tag{5-2}$$

One major attraction of thermionic conversion is the high power density with potential values of 10s of W/cm^2 [22,106]. Practically, values in the order of 1-5 W/cm^2 have been achieved [21]. The heat rejection (cold side) temperature of thermionic converters can be high with temperatures from around 900 to 1300 K [106,353]. This should allow cascading with other conversion technologies and the use of small radiator fins for space applications. Another benefit of thermionic generators is the capability to provide peak power above the continuous rating, for a limited time [353].

One challenge in thermionic converter design is that electrons leaving the emitter surface sense the negative space charge in the interelectrode gap and are forced to return to the emitter surface [353]. There have been different attempts to reduce this space charge including closed spaced anodes and cathodes, filling of the space with positive

ions for neutralisation (e.g. the alkali metal caesium), the use of electric or magnetic fields to conduct the electrons from the cathode to the anode and the use of a grid to accelerate the electron flow [106]. Another major challenge is the high hot side temperature, which is typically around 1800 to 2000 K [353]. At these temperatures major engineering challenges occur which can be associated with high costs. Similar to TPV systems, radiative heat transfer, proportional to T_h^4-T_c^4, occurs from the hot (cathode) to the cold (anode) side, whereas this heat transfer is undesirable and degrades the efficiency in thermionic converters. Also cathode evaporation has been reported for thermionic converters. This can cause contamination and limits the lifetime [21,353].

Thermionic generators have been considered for a wide power range stretching from miniature radioisotope powered converters (mW) to top cycle converters for terrestrial central power stations (MW) [22]. Currently thermionic research focuses mainly on space applications using solar and nuclear heat sources [353]. The objectives of thermionic space nuclear reactors have been reported as follows: power range from 10 to 100 kW and beyond, emitter temperature of 2000 K, collector temperature from 880 to 1000 K, power density from 3.5 to 13 W/cm^2, efficiency from 10 to 15% and lifetime from 7 to 10 years [354].

Recently there has been also some work on semiconductors using combined thermoelectric and thermionic conversion operating at lower temperatures [355].

5.5 Solar photovoltaic systems

Generally solar TPV and solar concentrator PV systems share similar properties. The difference between solar (concentrator) PV and solar TPV has been already defined in Subsection 3.4.2. Figure 5-1 also shows this difference of an intermediate radiator. Both technologies share radiation concentration, the feasibility of CHP operation and similar

electrical power densities. Hence, the solar concentrator PV systems are regarded here as a closer competitor compared to non-concentrator solar PV systems. The combination of solar PV and solar TPV has been proposed [80,356], but is not considered here further.

Potential advantages of solar TPV include continuous operation using other heat sources (hybrid systems) and/or thermal storages, low sensitivity to the solar spectrum and high potential efficiency, when compared to solar concentrator PV conversion. High solar TPV efficiencies have not yet been demonstrated. Also solar TPV system could have disadvantages in terms of high-temperature engineering and system complexity compared to solar PV systems.

5.6 Summary, discussion and comparison with TPV

The discussion in this chapter delivered some insight of the benefits and limitations of various electricity generating technologies in terms of power density (W/m^3, W/m^2, W/kg) and efficiency, as well as other aspects such as heat source (or fuel) flexibility, reliability, lifetime and market status.

TPV electrical power densities up to 4.2 W/cm^2 have been demonstrated [357-359]. The potential TPV power density increases sharply for higher radiator temperature. For example, assuming a PV cell converting 40% of the radiation up to 2.5 μm (e.g. multi-junction InGaAsSb cell) and a 2000 K blackbody radiator would result in a theoretical electrical power density of about 23 W/cm^2. The power density could be further increased using radiation concentration or high refractive index materials in the cavity (e.g. MTPV). Gravimetric power densities for combustion-powered systems greater than 100 W/kg appear to be feasible [301]. Hence, TPV can be regarded as a high power density technology amongst its competitors.

Demonstrated TPV system efficiencies on the other hand have been moderate. The combustion system efficiencies of up to around 8% [31,269] have been achieved, which can be translated into a heat to electricity conversion efficiency of around 10% assuming a combustion efficiency of 80%. In-cavity PV cell efficiencies of around 20% have been reported for InGaAs and InGaAsSb cells [360,361,362]. For optimised spectral conditions GaSb cell efficiencies of around 30% can be expected (see Subsection 3.6.3). Hence, a 20 to 30% efficient conversion of heat into electricity can be regarded as feasible and competitive (especially to other direct heat-to-electricity converters).

Currently one of the major cost constraints of TPV conversion are the cell costs. In 2004, GaSb cells were commercially available at a single piece price of 22 £/W, assuming a typical power density of 1 W/cm^2 [177]. Similar to solar PV, the cell price is expected to decrease considerably with higher production volumes. Fraas et al. projected capital GaSb cell costs of 1.1 £/W for a production volume of 300 kW/year (30 m^2/year) and below 0.3 £/W for 100 MW/year (10000 m^2/year). It has been pointed out, when expressed in £/W, that the GaSb cells could be almost 100 times less expensive than non-concentrator silicon cells at a given production volume, because the production processes could be similar and GaSb cells could generate 1 W/cm^2 [363].

Besides capital cell costs, the operation time is another decisive factor that determines the payback period. Within Europe the mean annual energy production of a non-concentrator PV array is 700-1100 kWh/kW$_p$ per year [364]. For example, a heat recovery TPV system in the high-temperature industry could operate continuously and generate up to 8760 kWh/KW$_p$ per year.

Across the conversion technologies, engineering challenges are reported for operation temperatures around or above 1300 K. These include cracks due to differences in the thermal expansion of materials, contamination degrading the system performance due to material evaporation, thermal insulation losses and radiation effects. Hence, it can be expected that TPV systems will also need to overcome these engineering challenges.

The solid-state technologies discussed in this work can be alternatively classified by their charge carrier: electrons (thermoelectrics, thermionics), ions (primary, secondary and tertiary cells, as well as AMTEC) and photons (solar PV, TPV). The technologies considered in this work indicate that "electron-based" technologies mainly require materials with suitable properties to increase the efficiency (e.g. figure of merit for thermoelectrics, workfunction for thermionics). On the other hand "ion-based" technologies generally have a requirement for increased lifetime. One may argue that "photon-based" technologies have demonstrated a high lifetime and an intermediate efficiency for solar PV conversion and a similar behaviour may be expected for TPV conversion.

Table 5-7 sums up the potential advantages and drawbacks of TPV conversion.

Disadvantages	**Advantages**
- High hot side temperature (T> ~1300K)	- Solid-state
- Low cold side temperature (T< ~350 K)	- Little or no moving parts
- Overall system design required	- Low noise
- Inter-related research areas	- Low maintenance
- High-temperature engineering	- High reliability
- Low demonstrated conversion efficiencies	- Heat source (fuel) variety
- Part load behaviour	- Continuous combustion
- High PV cell costs	- Low pollution, simple ignition
	- Long operation time (e.g. industrial waste heat)
	- Rapid start-up
	- Good scalability (also modular systems)
	- Possibility of CHP operation
	- Components available and tested
	- High electrical power density demonstrated

Table 5-7: Potential advantages and disadvantages of TPV conversion.

6 Assessment of TPV application in the UK

6.1 Introduction

Within this chapter the most promising TPV applications for the UK are assessed and selected. Section 6.2 reviews application literature using TPV and competing technology sources. This allows identification of potential TPV applications and competitors, as well as indicators for comparison of both. Section 6.3 then defines the assumptions made in this assessment and excludes some applications. The most promising applications are then discussed and identified in the following five sections (Section 6.4-6.8). The heat source and the CHP mode have been used as classification criteria. For each selected application, the discussion focuses mainly on the following aspects: past TPV research, grid connection, interest groups, specific example applications, component requirements, fuel supply, load demand and lifetime/reliability requirements.

The most suitable applications for the UK have been identified by an equally balanced rating system using five indicators (Section 6.9, Table 6-6). This methodology required grouping of the applications and the indicators and resulted in an iterative assessment in order that the specific differences between the applications could be identified.

6.2 Literature review

6.2.1 TPV literature

In this subsection literature about TPV applications is reviewed in chronological order. **Ralph et al.** identified near-term and long-term applications for TPV [37]. Near-term markets were characterised by small-scale use, high price and specific TPV advantages. The identified applications were leisure power for applications such as recreational vehicles, boats and cabins (simplicity, quiet and reliable operation, prestige value), battery charges for applications such as military man-packs and portable generators (lightweight), isotope space power for applications such as deep space missions and grid-independent self powered heaters for applications such gas furnaces and water heater. Potential long-term applications were seen in the vehicles (green car, hybrid electric, military), nuclear (submarines, space reactor) and utility sectors (off-grid, cogeneration, hybrid renewable back-up) [37].

Krist [365] listed potential TPV applications for the gas industry. Self-powered gas heating and cooling devices have been identified as the major applications, such as residential and commercial furnaces, absorption coolers, water heaters, industrial dryers and fireplace power devices (heat circulating, decorative logs). The following advantages were reported: operation during power faults, surplus electricity generation for back-up power, simpler installation (no electrical grid connection required), higher on-site gas consumption (higher gas sales) and energy conservation through on-site generation. In long-term, CHP systems with a minimum gas-to-electric efficiency of 20% and remote power systems for cathodic protection were seen as potential applications. No statement about the power range was made.

Rose [298] gave examples of potential portable TPV applications arranged by their power range (Table 6-1). The power range was not specified in detail [298].

>Watts	>Kilowatt	>10 Kilowatts	>100 Kilowatts
Telephones Home electronics Computers Navigational buoy Soldier systems	Tools Recreational vehicles Wheelchairs Actuation	Yachts Remotely piloted vehicles Golf carts Electric cars	Advanced radar Spacecraft Electric bus Weapons

Table 6-1: Rose's examples of portable TPV applications by power range.

Table 6-2 redraws the result of the application analysis by **Ostrowski et al.** [366]. Three classes of applications had been identified: near-term (recreational, military), medium-term (commercial, remote) and long-term (remaining applications).

Application (example)	User need	Market value	Market size	External funding	Competing technology	Required system cost
Recreational (yacht, RV units)	High	High	Small	N/A	ICE generator, recharg. battery	2.7 £/W
Commercial (emergency backup)	High	Medium	Small	N/A	Diesel generator	1.1 £/W
Residential (CHP)	Medium	Medium	Large	Yes	Electric grid	0.55 £/W
Military	High	High	Medium	Yes	ICE generator	2.7 £/W
Remote (transmitter, cathodic protection, water pumping)	Medium	Medium	Medium	N/A	Solar PV, diesel generator	1.1 £/W
Transportation (low emission fleet, hybrid)	Medium	Low	Large	Yes	ICE generator, fuel cells	0.55 £/W
Electric power (peak loading, grid extension)	Low	Low	Large	N/A	Electric grid	0.55 £/W
Space mission (satellite)	Low	High	Small	N/A	solar PV, fuel cell, nuclear	0.55 £/W

Table 6-2: Ostrowski's application assessment assuming a 10 kW system for costs.

Johnson [299] predicted that TPV conversion should be advantageous for applications below 5 kW and that there is strong competition above this power. The work defined a hypothetical TPV device in order to assess potential markets. The specifications were assumed as follows: variable power output of 500 to 5000 W, an efficiency of 10%, cost of 0.55-1.1 £/W and a size of $0.6 \cdot 0.6 \cdot 0.9$ m^3 (~ 15 kW/m^3). The four application groups identified were recreational vehicles, homes without grid connection, uninterruptible power and military.

Yamaguchi et al. [109,110] assessed the applications of solar TPV, industrial high-temperature waste heat recovery, micro CHP and portable generators for the commercial Japanese market. Their work selected portable power and micro CHP as the most promising applications. The major requirements for portable generators were identified as high power density, high system efficiency, fuel flexibility, low noise and low price. Competitors (fuel cells, ICE generators, batteries) were also considered and TPV was found to have specific advantages in the power range below 5 kW (especially fuel flexibility, power density and low noise). A micro CHP TPV system with an electrical power of 1 kW and 10 to 20% gas-to-electric efficiency was also modelled in terms of cost and energy savings, where the TPV system supplied the total heat demand using a thermal storage system [109,110].

6.2.2 Literature from technologies competing with TPV conversion

Table 6-3 sums up relevant applications for several competing technologies.

Technology	Applications
Internal heat engine generator [304,367]	Lighting, electronics (e.g. TV, filming, laptop), garden, forest and construction tools (e.g. hedge trimmer, drill, cement mixer, crane and elevator, circular saw, welding), outdoor events (e.g. music, shops), mains backup (home, medical), auxiliary power for vehicles (e.g. ships, trucks)
Stirling engine generator [368]	Artificial heart power, underwater power unit, space power, remote power sources, military ground power, solar thermal generator, CHP
Battery [369]	Entertainment (lighting, toys & games, photography), vehicle (starting, lighting, ignition, electric/hybrid propulsion, mining, recreational, personal mobility), personal communications devices (portable computers), power tools, backup power (telecommunications, industrial, utility-related)
Fuel cell [317,370]	1-10 W: camcorder, micro-satellite, palm-top computer, safety lamps & flashlights 10-100 W: battery re-charger, hand-held power tool, mobile/variable road sign, outdoor/camping supply, portable PC, radio communication, surveillance camera 100-500W: domestic gardening equipment, domestic power supply backup, heavy duty battery re-charging, professional power tools, telecommunication field equipment 1kW-1MW: distributed generation (optionally with CHP) 10kW-200kW: road vehicle 1-10kW: auxiliary power units (APUs) for vehicles Space (satellite) and military (submarine)
Thermoelectric generator [371,372]	Oil and gas (cathodic protection, supervisory control and data acquisition, offshore), telecom use (relay station, military communication, emergency services), self-powered heating devices, power from vehicle exhaust, power from waste heat
Thermionic generator [353]	Space solar systems (30 to 70 kW), space nuclear reactor (20 kW - MW), terrestrial applications had little attention over the last two decades
AMTEC [349]	Hybrid electric vehicle, portable power (military, battery charger), micro CHP, remote power (lighting, residential), utility power, recreational vehicle, air conditioning power, self-powered furnaces, radioisotope space power
Solar PV [373]	Utility power, recreational vehicles (e.g. boats), remote housing, forest & parks, military, telecommunication, oil & gas (cathodic protection), highway, railroad & marine, agriculture, original equipment manufacturers, outdoor lights, refrigerators, computers, lighting, monitoring and instrumentation, remote weather stations, telemetry systems, navigational aids, water pumping

Table 6-3: Summary of applications identified from competing technologies.

6.3 Preliminary assumptions and selections

As already discussed in Section 3.8, cascaded systems consisting of a TPV generator and another conversion device are not considered.

In this assessment, space and military applications, as well as applications using nuclear sources are briefly discussed to give a comprehensive overview, but have been not selected, since this work focuses on the commercial and industrial sectors.

Firstly, a target power (Subsection 6.3.1) and a target efficiency range (Subsection 6.3.2) are assumed. Subsection 6.3.3 then introduces the rating system of this assessment.

6.3.1 Electrical power range

The target power range of the applications has been expressed on a logarithmic scale in steps of ten. The smallest electrical power currently under consideration for TPV is around 10 mW [85]. A standard upper power range limit of 10 kW has been assumed, because competing technologies above this power have high efficiencies (larger than 20%). Also, currently PV cells for TPV systems are only available in limited quantities at high costs. In addition, the maximum demonstrated power of a TPV system has been in the kilowatt range. The absolute upper power range limit has been extended up to 1 MW, if TPV conversion is found to have unique advantages over its competitors. This power range definitions have lead to the exclusion of applications with a power above 1 MW (e.g. centralised power stations).

6.3.2 Efficiency range

Efficiency is usually defined as the ratio of the useful output to the total input. The useful output has been assumed either as electricity, or heat **and** electricity (CHP

mode). Two input modes have been assumed, which were either the product of calorific value and flow rate for a combustion system or a heat flux for all other sources (waste heat, solar). This resulted in four efficiency groups (Table 6-4).

	Fuel to Electricity Conversion (Combustion)		Heat to Electricity Conversion (Solar, waste heat)	
	ηsys	ηsys,CHP	ηTPV	ηTPV,CHP
(System cost reduction)	<5%	80%	<6%	100%
Demonstrated	5%	80%	6%	100%
Near-term	10%	80%	13%	100%
Medium-term	15%	80%	19%	100%
Long-term	20%	80%	25%	100%
(Excluded)	>20%	80%	> 25%	100%

Table 6-4: Summary of efficiency assumptions for the applications assessment. The table shows from left to right the combustion efficiency, the combustion CHP efficiency, the solar and waste heat efficiency, and the solar and waste heat CHP efficiency.

The **combustion system efficiencies** of around η_{sys} = 8% have been reported [31,269]. In this work a demonstrated value η_{sys} = 5% has been assumed taking some housekeeping power into account and making cautious assumptions. Applications with lower efficiencies than 5% should allow simple system design at reduced costs. Efficiency targets of 10% (near-term), 15% (medium-term) and 20% (long-term) have been assumed. The medium-term efficiency target has been considered as a standard upper limit for the selected applications. The CHP combustion efficiency has been generally assumed with $\eta_{sys,CHP}$ = 80% [47].

For waste heat and solar applications, the efficiencies have been derived from the combustion efficiencies by excluding the 20% flue gas loss (combustion efficiencies divided by 80%). Furthermore, it has been assumed that cavity losses and all heat output from the PV cell can contribute to the useful heat output. This can be seen on the CHP efficiency with a value of 100% in Table 6-4 (see also Section 3.3).

Applications with efficiency requirements higher than the long-term efficiency target (η_{sys} > 20%, η_{TPV} > 25%) have been excluded from the assessment (e.g. series hybrid electric vehicles, CHP plants above 100 kW power, centralised power stations).

6.3.3 Rating

Five indicator groups have been finally identified in this iterative assessment. For each indicator group specific questions have been raised and a rating from 0 to 3 has been introduced. Applications with a 0 rating have been excluded in the iterative assessment. The considered ratings were 1 (negative), 2 (balanced) and 3 (positive).

The first indicator group questions the TPV technology constraints prohibiting the use and the **research and development effort** for a specific application. Three ratings have been defined: negative (1), balanced (2) and positive (3). Factors contributing to a negative rating have been: no TPV system development, complex overall design, operation under part load, operation in a hostile environment (e.g. temperature, humidity or vibration) and high efficiency requirements (15 - 20%). Positive factors have been: TPV system development of at least one institution, operation partly demonstrated, efficiencies smaller than 5% sufficient and simple overall design.

The second indicator group assesses the benefit of TPV compared to **competing technologies** in a deployed (current technology) or emerging state (likely future technology). The following rating has been used:

0. TPV has disadvantages over one or more other deployed technology
1. The disadvantages and advantages of TPV and competing deployed technologies are balanced
2. TPV has advantages over **either** competing deployed **or** emerging technologies
3. TPV has advantages over competing deployed **and** emerging technologies

The following factors have been regarded as important for this indicator:

- Noise
- Reliability, maintenance, dormancy, lifetime
- Modularity, scalability
- Efficiency, power density (W/m^3, W/kg)
- Heat source consideration (e.g. fuel storage or flexibility)
- Direct or alternating current power requirements

The third indicator group **market and cost** has been rated negative (1), balanced (2) or positive (3). The following aspects have been taken into account and each individual positive, balanced or negative rating has been summed up to the overall rating:

- Three is a large potential market and a niche market. The niche market allows for higher costs to launch TPV
- There is interest from the TPV community (market push)
- There is a market requirement (market pull)
- Long operation hours allow cost effective operation
- TPV system costs could match the application
- Funding has been available or is seen feasible

The fourth indicator group identifies specific advantages of TPV **applications in the UK** compared to other industrial countries. Usually a balanced rating (2) has been applied and only exceptionally negative (1) or positive (3) ratings have been given.

The **human impact** is the fifth indicator. Special attention has been paid to potential primary energy savings (or CO_2 reductions), but also local human impact factors have been considered. Local factors include low pollution (SO_x, NO_x), low noise, security of supply improvements and user friendliness (e.g. low maintenance). The following rating has been used:

0. TPV operation makes the current human impact worse
1. TPV operation makes the current human impact neither worse nor better
2. TPV operation could improve **either** global **or** local human impact factors
3. TPV operation could improve both global **and** local human impact factors

6.4 Nuclear applications

The major requirements for **space** applications are high power densities (translating into lower launch costs), high conversion efficiencies, high reliabilities and the survivability in the space environment. The only long-duration heat sources are solar and nuclear sources [354], and this is where TPV systems have been considered among other conversion technologies. In unsuitable illumination conditions for PV cells (e.g. near sun, deep space) nuclear sources are used. **Nuclear reactors** for space are considered in a heat range from 10 kW to MWs [61,353]. Competing conversion technologies include Stirling engine [368], thermionic [353] and thermoelectric generators [61]. TPV space nuclear reactor systems have been proposed [37,51]. However, the major TPV space research focuses on **radioisotope** systems [53-59]. Currently space radioisotope systems utilise thermoelectric converters and for future missions also AMTEC, Stirling engine and TPV generators have been considered [349,374]. TPV radioisotope system efficiencies above 20% are currently projected [47]. TPV systems have the disadvantage of the fins required to cool the cells in space.

Terrestrial centralised nuclear power stations would require large sized TPV generators and this currently seems not to be feasible. Smaller **nuclear generators** can be found for naval (submarines, aircraft carriers) and remote applications (e.g. repeater station, navigation aids). In the smaller power range Stirling engine generators have been utilised for heat-to-electricity conversion [368]. There are also a few niche markets for terrestrial **radioisotope generators**, where neither batteries nor combustion systems have sufficient operation times. Examples include very remote power supply (e.g. polar region) and artificial heart power. In these applications TPV would compete with Stirling engine and thermoelectric generators [368].

6.5 Combustion applications without CHP

In the majority of cases TPV combustion systems have utilised hydrocarbon fuels, although hydrogen has been also burned in converters with small powers [88]. Hydrocarbon fuels are widely available, can be easily stored, transported and recharged. Additionally they have high gravimetric energy densities [2]. Competing technologies for hydrocarbon-powered applications are mostly batteries in the smaller power range and ICE generators in the larger power range. Fuel cells are emerging for these applications and are seen here as the major future competitor.

For future fuel powered **space missions**, it has been pointed out that advances in hydrogen storage need to be made to meet the requirements. TPV systems have been proposed as an alternative to fuel cells for space applications [375]. However, most TPV space research focuses on radioisotope systems (Section 6.4).

6.5.1 Portable power

Past TPV research and development of portable power generators included a battery charger combined with a torch with about 1-3 W [2], a battery substitute with 20-25 W [6,151], a portable generator with 5-20 W [154], a propane generator with 100-150 W [262] and a multi-fuel (diesel, kerosene) generator with 500 W [92,96,99,376]. For portable applications with a power in the order of 10 mW, a micro-mechanical TPV system has been also designed [85]. Such small power systems have not been considered further for this application, because of their early research stage. Hence, the power range of interest has been defined from 1 W to 1 kW including the referred TPV systems. Batteries are predominant in the lower power range and can be regarded superior below 1 W. Portable heat engine generators have advantages in the higher

power range and can be regarded superior above 1 kW. The upper limit of 1 kW has also been identified by Yamaguchi et al. [109,110].

In the US, there has been **military** interest for portable power generators from the early phases of TPV research up to now [39,301,377]. The relevant advantages of TPV for military applications are quiet operation, high power densities, no moving parts, fuel flexibility, capability of CHP operation, tolerance to low temperature, simple start-up, excellent dormancy and direct current output [37,299,300,304,349,366-368,377]. Challenges were seen in the low demonstrated efficiency, the thermal signature due to the high-temperature operation, sensitivity to temperature changes (temperature control required), poor system experience, radiator ruggedness and up-scaling [377].

Yamaguchi et al. concluded, that **civilian** portable generators are one of the most promising TPV applications [109,110]. Portable generators with an intermediate **power** from 10 to 100 W within the examined range from 1 W to 1 kW and with a long operation time are regarded in the work reported here as particularly promising, because of low competition from other technologies. Example applications are battery chargers, lighting equipment, portable electronics (e.g. laptop, TV, filming), power tools (e.g. garden, agriculture, forest, construction), camping, temporary outdoor events (e.g. shops, music) and mobile road signs [298,317,370].

High conversion **efficiencies** are desirable in order to achieve long refuelling intervals. Portable hydrocarbon-powered TPV systems with efficiencies (fuel-to-electricity) of a few percent can be superior to current primary and secondary batteries in terms of overall energy density due to the high energy densities of hydrocarbon fuels (J/kg, J/m^3) [2]. A minimum efficiency target of 5% has been assumed here, accounting

for some weight of the TPV converter in addition to the fuel and assuming that improved energy densities compared to batteries are of interest.

The indicator for **technology constraints** and the research and development effort has been rated as balanced. Several institutions have, at least partly, demonstrated TPV operation for this application [92,96,99,376]. However, a general-purpose generator would need to operate under various operation conditions (part load, hostile environment). Efficient part load operation could be possible using a TPV system in on/off mode and an additional secondary battery, but this has not been demonstrated.

Major **competitors** are secondary batteries in the small power range and ICE generators in the large power range. ICE generators have disadvantages in terms of high maintenance, starting in the cold and noise. Major disadvantages of secondary batteries are low lifetime, poor dormancy, slow recharging and limited capacity (or low volumetric and gravimetric energy densities). Fuel cells (emerging) have the advantage of a high efficiency and a good part load performance. On the other hand, TPV generators are predicted to be superior in terms of power density, lifetime and fuel flexibility, compared to fuel cells [109,110]. It has been concluded that portable TPV generators have some advantages over deployed technologies and balanced properties compared to fuel cells.

There are niche **markets** in portable power that have special requirements for low maintenance, low noise, low weight and long operation time. The entire battery market and heat engine generator market is potentially a large long-term market. In the TPV community there has been interest in military and civilian portable power generators (positive market push). There is also generally a market requirement (positive market pull), since currently secondary batteries often limit the system operation time (e.g.

laptop). Funding for civilian portable generators may be regarded as unlikely, but overall market and cost issues have been rated positive.

The **local human impact** has been rated positive. Batteries can be regarded as bulky and heavy and difficult to refuel. Compared to heat engine generators, TPV generators should be less noisy and the continuous combustion is generally cleaner. Major CO_2 saving can be not expected for this market and this resulted in a negative **global human impact**. Hence overall the human impact has been rated balanced.

6.5.2 Uninterruptible power supply (UPS)

UPSs[23] are used in sectors such as computer, communication (e.g. telephone network), domestic, military, security (e.g. banks, elevator), industry (e.g. power failure critical processes), medicine, emergency and lighting (e.g. airport) [299,304,317,366,367,369,370]. An industrial study shows that there is a wide power range for UPSs from below 1 kW (e.g. single computers) to above 150 kW (e.g. industrial production line) [378]. UPSs for large computer suites can be even in the order of MWs [379]. TPV technology is particularly suitable for the lower power range up to 10 kW. Other technologies compete above this power. In the low power range UPSs are likely to operate within buildings and utilise batteries. Indoor operation of a hydrocarbon based TPV UPS would require usually flue gas extraction, which is assumed to be not justifiable below an electricity output of 100 W. It is assumed that the power is usually supplied from the grid and the TPV UPS covers occasional faults. After a power fault the TPV UPS could be refuelled. This operation mode is unlikely to

[23] Uninterruptible power supplies may be also known as backup power or emergency power supplies.

require high TPV system efficiencies and a target range from 5 to 15% has been assumed. Costs and reliability are likely to be more important aspects.

The indicator for the **technology constraints** and the research and development effort has been rated as negative due to the complex overall design. A TPV UPS system design typically includes an inverter (not required for DC systems), switches, a means to monitor the grid and a buffer battery. Also no UPS system development could be identified in the TPV community.

Competition arises from batteries in the small power range and ICE generators in the large power range, where disadvantages have been discussed previously (see Subsection 6.5.1). For UPSs, secondary batteries often immediately provide power for several minutes and bring a standby diesel generator on the load for long-term backup [380]. Flywheels or capacitors in conjunction with heat engine generators may also be utilised as short-term electrical storage options [379]. UPSs using fuel cells are emerging [334]. Fuel cell lifetime is not critical because of the low operation time (only during power fault). Hence, a TPV UPS system is regarded here to have advantages over deployed technologies, but limited advantages over fuel cells in this application.

In general the UPS **market** is large and growing. There are potentially niche markets for reliable, low noise and fuel flexible solid-state TPV UPSs. Some power failure critical applications make use of a redundant UPS, which may also be a market for TPV. Yet no market push from the TPV community could be identified. As a result the market and cost indicator has been rated as balanced.

Regarding the local **human impact** a positive rating has been given, since local pollution and security of supply could improve. Also a TPV system could be more user-

friendly (e.g. no regular checks as for heat engine generators or batteries) and operate quietly. A minor global human impact can be expected due to the short-term use.

6.5.3 Remote power

For remote power applications, the power density of the generator is usually uncritical, because operation is typically stationary. In the smaller power range the load has been assumed to be typically constant (e.g. telecommunication repeater), whereas in the large power range the load has been assumed to vary (e.g. non-grid connected households). The fuel for a remote TPV combustion system may be available on-site (e.g. gas and oil exploration) or supplied through regular site visits. Similar to thermoelectric on-site generators [371], it can be assumed that TPV generators operate reliably with a long-lifetime. Remote generators typically have to operate under hostile environment conditions (e.g. temperature, humidity).

Figure 6-1 summarises the options for remote power supply identified in this work. Currently, primary batteries can supply low power and long operation applications (e.g. battery powered radio temperature sensor) and secondary batteries are suitable for higher power and shorter operation applications (e.g. electric wheelchair or model-making). In applications requiring both high power and long operation secondary batteries are typically recharged using a renewable source (e.g. solar PV, wind). Alternatively combustion-powered thermoelectric generators can be used. These generators can be advantageous in application with the following factors in their favour: fuel is on-site (e.g. gas and oil exploration), limited availability of renewable sources, high reliability requirement or long-lifetime need. TPV generators promise higher efficiencies than thermoelectric generators in this niche market. Hence, the replacement

of these thermoelectric generators is considered here as one potential remote TPV application and named **unmanned remote power** (Figure 6-1, No. 2)

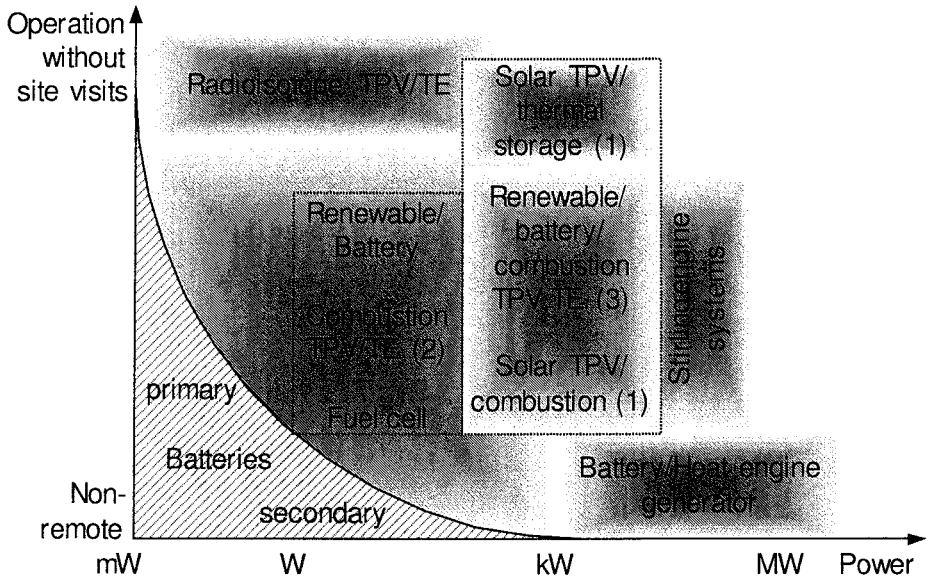

Figure 6-1: Plot of the identified technology options for remote power supply. The dotted boxes are the areas of interest for this assessment. The three TPV options considered are solar TPV systems with thermal storage or an additional combustion source (1), combustion TPV systems (2) and combustion TPV systems combined with a battery and a renewable source such as a solar PV or a wind system (3). Thermoelectric generators have been abbreviated with TE and applications with a low number of site visits are considered as non-remote.

Very remote applications (e.g. in polar regions) may have limited renewable sources and no fuel on-site. Also battery lifetime may be too short and regular refuelling unfeasible. In such applications radioisotope sources may be utilised together with a thermoelectric or TPV generator. This option has been excluded, since nuclear sources are not considered in this assessment, but is shown for completeness in Figure 6-1. Another remote system option with long autonomous operation is a solar TPV system with thermal storage (Figure 6-1, No. 1). Such system is not limited by battery lifetime and the (stored) heat can be converted into electricity by direct-heat-to-electricity devices (e.g. TPV) or external heat engine generators (e.g. Stirling). Stirling engines are assumed to be suitable around and above the 10 kW power range. For smaller systems it

can be assumed that these generators show disadvantages in terms of complexity compared to TPV. Also the Stirling engine efficiency is likely to decrease for the smaller power range (see Subsection 5.2.2). Heat engine generators are readily available for less remote applications (Figure 6-1), where regular maintenance is not critical. In the intermediate power range centred around 1 kW two TPV system configurations have been identified. The first configuration is solar TPV conversion (Figure 6-1, No. 1), which is discussed in more detail in the Subsections 3.4.2 and 6.7.1. The third configuration (Figure 6-1) consists of a renewable generator (e.g. solar PV, wind) combined with a secondary battery and a combustion driven generator (e.g. TEs, TPV). This configuration has the advantage, that both the PV cell output power and the battery capacity can be scaled down considerably, when compared to the renewable/secondary battery configuration only. In this case, the combustion generator acts as a backup power supply if the renewable source is not available.

6.5.4 Remote power - unmanned

Applications of unmanned remote power include the areas of water supply (e.g. monitoring, pumping), oil/gas exploration and distribution (e.g. cathodic protection, valve operation, data acquisition), stationary telecommunication (e.g. repeater), environmental monitoring (e.g. weather, air quality, scientific measuring) and navigational aids (e.g. aircraft, shipping, road and rail signalling) [298,317,365,366,370-372]. These applications have typically a constant load. The reliability requirements depend on the specific application. A large share of these applications can be supplied by a hybrid system consisting of a renewable generator and secondary batteries. There are, however, applications supplied by combustion thermoelectric generators and these are also the niche applications of interest for TPV.

The power range has been identified from approximately 1 W to 1 kW using competing technology literature [342,368,370,381]. The thermoelectric generator is the major direct competitor for this small niche market. Hence the minimum efficiency has been assumed with the same value as current combustion-powered thermoelectric generator (Table 5-6). Systems with such low efficiency may be used where the fuel is cheaply available on-site, such as for oil/gas exploration and distribution. The near-term target of 10% has been selected as an upper efficiency limit. This value would be about a 3 times improvement over the efficiency of current thermoelectric generators and this may also open new markets.

The indicator for the **technology constraints** and the research and development effort has been assessed as negative. The low efficiency requirements have been regarded positive. However, negative aspects have been identified as dominating. No TPV systems development for this application could be identified and the operation in hostile environments also contributed negatively.

Overall the **competition and benefit** has been rated positive compared to deployed and emerging competitors. TPV systems have demonstrated higher efficiency than thermoelectric systems (deployed). Fuel cells have demonstrated higher efficiencies than TPV, but other TPV advantages are believed to outweigh fuel cells. They include fuel flexibility and storage, as well as the potentially higher lifetime of TPV.

Market and cost issues have been rated balanced. The TPV community identified the unmanned remote power as a niche market [366], but no work towards a system development could be identified. Another constraint is likely to be the lack of funding of this application. Potential advantages are long operating hours and the allowance for

premium capital costs in this market. Portable generators and uninterruptible power supplies may be seen as a similar and potentially large market.

The use of unmanned remote power systems in the **UK** has been rated negative. In the UK the majority of the non-grid connected countryside areas can be connected with short links to the grid. Also the UK has usually suitable renewable resources for a remote supply with a renewable/secondary battery system considered to cover the same power range (Figure 6-1). The export market is also limited for this small niche market.

No major improvements in terms of the human impact can be expected by using TPV instead of a thermoelectric generator in this application. Hence, the **human impact** of unmanned remote generators has been rated as neither better nor worse.

6.5.5 Remote power - renewable hybrid

A major drawback of renewable sources (e.g. solar PV, wind, hydro) is the fluctuation in output power (e.g. daily, seasonally). Hence, using a combined renewable and secondary battery system for non-grid connected supply requires large sizing of both secondary batteries and renewable sources to meet the (varying) demand at all times. A possible solution to this is the use of an additional combustion-powered generator. It has been simulated that the size of the PV system can be reduced to a third of that required for an exclusively PV based system, if only 10% of the annual demand is met by the combustion-generator, assuming a constant load and Central Europe climate [232]. It has been also suggested that this redundancy arrangement can improve the overall reliability [232].

A target **power range** from 100 W to 10 kW has been assumed here for the combustion TPV generator and the renewable generator would usually be larger than the TPV generator. Below this power range the complexity of this renewable hybrid

system can be regarded as a hindrance in terms of the number of components, optimisation of the size of each component and the energy management. Above 10 kW power major competition arises from heat engine generators (e.g. ICE, Stirling). Examples of hybrid remote power applications may be similar as unmanned remote applications discussed previously (see Subsection 6.5.4). In addition to these unmanned applications, larger power applications could include remote housing (e.g. developing world) or larger telecommunications installations. Varying load demand could be met by a secondary battery. It is also feasible that the combustion TPV system would operate with on-site fuel (e.g. biomass).

For the hybrid remote power system an efficiency range with a higher upper limit of 5 to 15% has been adopted, compared to the previously discussed unmanned remote application. It is believed that the higher power range makes the number of site visits for refuelling and fuel costs more important issues.

The complexity of this approach has led to a negative rating of the indicator for **technology constraints** and the research and development effort. Although TPV has been suggested for this application [232], no system development could be identified.

The **competition** has been rated as advantageous and is generally regarded as similar to the previously discussed application on unmanned remote power (Subsection 6.5.4).

Market and cost issues have been rated as balanced and are also regarded similar to the previous application, where differences should be a shorter operation time (negative) and a larger market (positive).

The use in the **UK** has been rated as balanced. Although the vast area of the countryside can be connected with short links to the grid, there are niche markets for

this application in the UK. Also the market is generally larger than for the unmanned remote systems. The large developing world market may allow export.

Currently, supplementary combustion generators are likely to be ICE based. Hence a TPV system could improve local **human impact** factors (e.g. reduced pollution due to continuous combustion, lower noise, lower maintenance). Potentially primary energy savings are feasible in the developing world using this application. Hence, the highest rating for the human impact has been given.

6.5.6 Transport applications

In 2001 in the UK, the transport sector consumed about one quarter of the total primary energy consumption and only the domestic sector had a higher share [1].

One major route to reduce energy consumption in the transport sector is the improvement of the poor current energy efficiency of this sector. For example an automobile engine converts typically not more than 30% (Otto engine) to 40% (Diesel engine) from the fuel energy into useful work (maximum brake thermal efficiency) [302]. These values are for optimum load conditions and decrease further for normal operating conditions. **Hybrid electric automobiles** are considered a major technology option in order to improve this propulsion efficiency. TPV generators in the power range from 6 to 10 kW have been examined for series hybrid automobiles in the US [48,49] and within a project funded by the EU ("The REV") [382]. Potentially, a TPV generator could have advantages in terms of noise, fuel flexibility, power density, reliability and maintenance, when compared to internal combustion generators and fuel cells. The major challenge for TPV generators in hybrid vehicles is the high efficiency requirement. For example in the EU project the fuel-to-electric efficiency target has

been set to 35% [382]. In the work reported here, it is concluded that major technological progress would be necessary to meet such an efficiency target.

Harvesting and conversion of exhaust gas energy into electricity could also improve propulsion efficiency, since electricity is typically generated from the shaft power of the propulsion engine. Thermoelectric generators are considered as an option to convert the energy from the heat engine exhaust gas into useful electricity [372,383]. A TPV system has been designed to convert exhaust gas from a gas turbine into electricity. Here, problems have been reported to meet the desired radiator temperature of around 1600 K [231]. Automobile flue gas temperatures vary up to a maximum of around 1300 K [383]. It is concluded here, that exhaust gas power harvesting may be of future interest, if advances in TPV conversion towards lower radiator temperature systems are made (e.g. micron-gap systems or lower bandgap PV cell materials). For this assessment exhaust gas power harvesting has been excluded because temperatures are typically too low.

Other TPV applications, considered in this work are small power propulsions (see Subsection 6.5.7) and auxiliary power units (see Subsection 6.5.8). In general, the component and system requirements in the transport sector are challenging. There is a need for reliable operation in hostile environments (e.g. temperature, humidity, vibrations), as well as requirements for low weight and low maintenance.

6.5.7 Transport applications - small power propulsion

Some vehicles in the road, air and water sector can have special requirements in terms of low noise, high reliability or low complexity. A TPV generator could meet these needs and is considered competitive in the smaller power range. Examples are the following [37,298,369,384,385]:

- Land (e.g. electric wheelchair, electric bike/trike, power assisted bicycle, luggage/pallet trolley, electric cart, recreational vehicle, sweeper, scooter, golf cart, forklift, lawnmower, snowmobile, all terrain vehicle, airport vehicle, station car, robot, remotely piloted vehicle)
- Air (e.g. small aeroplane, unmanned aeroplane)
- Water (e.g. small ship, jet-ski, unmanned submarine)

Currently either secondary batteries together with an electric motor or ICEs typically power these applications. Heat engines tend to be used in the larger and batteries in the smaller power range. In the intermediate power range, assumed here from 100 W to 10 kW, both concepts have their weaknesses. The battery concept tends to have disadvantages in terms of energy density (weight, operation range), recharging (refuelling) and cold temperature operation. On the other hand, the heat engine concept has drawbacks in terms of noise, maintenance, local pollution and starting reliability. Hence it is assumed, that a combustion TPV generator together with an electric motor for propulsion could have advantages compared to both existing concepts. Optionally a secondary battery may be applied to supply peak propulsion demand and to store recovered brake energy. In general high TPV conversion efficiencies are required, since high efficiencies reduce fuel to be transported resulting in a long operation range. The electric propulsion motor and possibly a battery will add additional weight. Hence, the efficiency target range has been set to the highest range of this assessment (15 – 20%).

The **technology constraints** and the research and development effort of this application are generally challenging. No TPV system development could be identified specifically designed for small propulsion power and there are high efficiency requirements. Other negative aspects are complex overall design requirement (energy management, battery, power electronics) and the operation in changing environmental conditions.

As already discussed TPV should have specific advantages over deployed **competing** technologies (batteries, heat engines). Fuel cells are identified as the major emerging competitor. It has been assumed that TPV advantages (fuel storage and flexibility, high power density) outweigh the high efficiency of fuel cells.

The largely diverse **market** should have niche applications allowing for higher costs and large potential markets at lower costs. Negative market aspects are seen to prevail and they include minor TPV community interest, the short operation time and the unlikelihood of funding. Hence a negative rating has been given.

The local **human impact** has been seen as positive. Currently reciprocating heat engines are noisy and polluting (TPV would have continuous combustion) and batteries can be regarded as not user-friendly (recharging, limited operation range, safety). Large energy saving can be regarded as unfeasible in this niche market application.

6.5.8 Transport applications - auxiliary power unit (APU)

In the transport sector there is a large variety of auxiliary (non-propulsion) power consumers for comfort, safety and control functions. Examples are ignition, lights, starters, navigation devices, electric windlasses, alarm system control, fans, heated windows, TV, Radio and by-wire technologies (e.g. fly-by-wire, break-by-wire and steer-by-wire) [37,301,304,366,367,369]. The electricity required for these applications may be generated coupled or decoupled from the propulsion engine.

Typically **coupled** systems use a generator and the shaft power of the propulsion heat engine. This can be regarded as a simple configuration with a generator as the major component. Other coupled systems may utilise the exhaust gas heat of the propulsion engine, which is preferable in terms of the overall efficiency but not commonly used for the small power range (e.g. automobile). Exhaust gas conversion with steam turbines in

large ships or thermoelectric generators are rare examples. Of course the disadvantage of all coupled systems is that the power is only generated as long as the propulsion engine is operating. Hence propulsion engine idling for electricity generation can be common (e.g. trucks), but this is undesirable in terms of fuel consumption. Electrical storage systems can only partly overcome idling. The secondary battery concept in the transport sector has disadvantages in terms of energy density, self-discharge, low temperature performance and constant "key-off" load supply. For example in the automobile, "key-off" loads (e.g. keyless entry, theft alarm, clock) are sufficient to drain the battery in a state-of-the-art car when left parked for long periods (e.g. at an airport for several weeks) [386]. For some applications the security of electricity supply can be another concern. Systems coupled to a propulsion heat engine are susceptible to a propulsion engine failure. For all these reasons electricity generation decoupled (auxiliary) from the propulsion is of interest.

There are several technology options for **auxiliary power units** (APUs), such as reciprocating engine generators, fuel cells or direct heat-to-electricity devices. Transport applications with a large power requirement may apply for example gas turbines as APUs (e.g. aeroplane, ship). As already mentioned in the previous paragraph, smaller power applications typically rely on a propulsion engine coupled generation (e.g. automobile, trucks). This smaller power range, assumed here up to a power of 10 kW, has been identified as a potential market for TPV. TPV APUs could be also of interest down to very small powers in the order of watts to supply "key-off" loads in automotive applications [386,387]. This "key-off" power is small compared to the propulsion power and the operation time may be limited (e.g. to an airport visit), so that the importance of

the efficiency can be regarded as secondary. Hence, a typical thermoelectric generator efficiency of 2% has been assumed as a lower limit.

The **technology constraints** and the research and development effort have been assessed as balanced. The MIT together with a car consortium currently considers TPV APUs [388], no other published work could be identified. Another positive aspect is seen here in the low efficiency requirements (fuel on-site) for the small powers. The major challenge is seen in the harsh operation environment (e.g. automobile with a wide temperature and humidity range, as well as vibrations).

Fuel cells are identified as one major emerging **competitor**. It can be assumed that TPV advantages, and in particular the flexible operation on any propulsion fuel, outweigh the high efficiency of fuel cells. In the small power range there is some competition from deployed thermoelectric generators with a low efficiency. Hence, TPV should have advantages over deployed and emerging technologies.

Market and cost issues have been rated balanced. In general there is a market requirement for reliable APUs. The automotive market is a large potential market [386] and niche markets are also feasible (e.g. TPV generator working in CHP mode for truck idling). On the other hand funding is regarded as less likely. In general hybrid vehicles are more likely to be funded due to their energy saving potential.

The local **human impact** has been rated as positive, because local pollution, noise, security of supply and user friendliness can be expected to improve. No major primary energy saving can be expected (global human impact negative).

6.6 Combustion applications with CHP

The concept of combined heat and power (CHP), also known as cogeneration or total energy, is the simultaneous generation of heat and electricity[24] [389,390]. CHP is an attractive energy saving option because of its high overall efficiency (typically 80 to 90%) defined as the ratio of useful heat and electricity output to the fuel energy input. This efficiency value can be compared with low efficiency centralised fossil fuel power stations (see Subsection 1.1.2). Cost effective operation of CHP systems typically requires a runtime of several thousand hours per year and decisive economic factors are the capital cost of the CHP system, as well as the fuel and electricity prices [391,392].

The generated heat varies from low-grade (e.g. hot air or water for space heating) to high-grade (e.g. steam for industrial applications). TPV systems are currently limited to low-grade heat generation, because the heat originates from PV cell cooling. TPV systems operating with cell temperatures up to about 360 K have been reported [393], where a typical cell temperature may be around 320 to 330 K. Generally, remaining flue gas heat leaving the TPV system using an additional heat exchanger could upgrade the heat output [109,110]. Hence, overall efficiencies higher than the assumed 80% of this assessment are regarded as feasible if required by the application.

CHP systems tend to be built on-site and matched to the heat load, because transportation of heat over long distances is usually difficult. Short-term time varying heat demand can be bridged by thermal storage systems, whereas long-term variations do not usually allow matching to all demand cases and often results in a larger sized and

[24] Mechanical and cooling power is not considered here, although it may be also defined as CHP.

shorter operating CHP system. An example is the space heating demand, where seasonal variations result in an oversized system in the summer. The electricity output tends to be less critical compared to the heat output, since electricity can be consumed on-site and surplus electricity can be exported to the grid. Electrical output powers of traditional CHP plants typically range from 100 kW to 100 MW using primary movers such as steam turbines, gas turbines or reciprocating engines combined with a generator [389]. Recently, several emerging technologies allow smaller-sized systems with output powers as small as around 1 kW. These systems have been named micro CHP [392,394,395]. Table 6-5 summarises the reported CHP TPV research. In this work three applications groups were identified. These are micro CHP (Subsection 6.6.1), district heating and industrial CHP (Subsection 6.6.2) and self-powered heating devices (Subsection 6.8.1).

Application	Institution	R & D status	PV cells	Output power	Efficiency target	Source
Micro CHP	JX-Crystals, WS	Partly built	GaSb	1.5 kW_{el} 12.2 kW_{th}	η_{el}=12% η_{sys}=80%	[46,376]
Self-powered heating (Midnight Sun®)	JX-Crystals	Beta testing of 20 units	GaSb	7.3 $kW_{th\#}$ 0.1 kW_{el}	η_{el}~1-2%#	[47,112]
District and industrial heating	JX-Crystals	Partly built	GaSb	147 $kW_{th\#}$ 20 $kW_{el\#}$	η_{el}~ 10-15%	[91,107]
Self-powered heating	Quantum Group	Demonstrated	Si	0.2 kW_{el} 19.2 $kW_{th\#}$	η_{el}~1%# η_{sys}>83%	[113]
Self-powered heating, Micro CHP	PSI, Hovalwerk AG	Partly built	Si	0.2-1.5kW_{el} 10-20 kW_{th}	η_{el}=1-5%	[114]
Micro CHP	ISE, Freiburg	Partly built	GaSb	0.13 $kW_{el\#}$ 1.1 $kW_{th\#}$	η_{el}=7% η_{sys}=60%	[396]
Back-up, Micro CHP	ISET, Kassel	Demonstrated	GaSb	60 W_{el} 1.2 $kW_{th\#}$	η_{el}=4% η_{sys}=86%	[397]
Micro CHP	Dutch Energy Research Found.	N/A	Si	N/A	N/A	[134]
CHP	British Gas Research & Techn. Centre	N/A	N/A	0.3 kW_{el}	N/A	[134]
Micro CHP, District heating	SERC, Sweden	Partly built	InGaAs GaSb	10-1000 kW_{th}	N/A	[223]

Table 6-5: CHP TPV developments by different institutions.
The table lists the research and development status, the PV cell material, the thermal and electrical output power, the efficiency and the literature source. Efficiency and power values marked with # have been calculated in this work.

6.6.1 Micro CHP

Micro CHP systems aim to replace conventional boilers in a dwelling and provide both electricity and heating to that dwelling. To make CHP suitable as a boiler replacement the size of traditional CHP systems needs to be reduced. There are requirements in terms of high reliability, low local pollution, low noise and low cost [392,398]. Both US and European studies have identified an efficiency target from fuel to electricity in the range from 10 to 25% and an overall efficiency target of 80% or higher [392,398]. The 10% electrical efficiency has been adopted as a minimum target in this assessment.

Generally, no deployed technology can fulfil all these requirements and there are several candidates under active investigation as micro CHP systems each with their own drawbacks and strengths. **Reciprocating engine** systems have been traditionally the CHP systems with the smallest output power among the traditional CHP technologies. Adapted reciprocating engine generators are under development to improve noise, local pollution and maintenance. Systems with 5 kW output power are commercially available in Europe (e.g. SenerTec, Ecopower) and 1 kW systems based on a Honda generator have been sold in Japan (Ecowill) [399]. Currently, one **Stirling engine** system has become commercially available in the UK (WhisperTech commercialised by E.ON) and others being developed (e.g. Enatec consortium 1.1 kW, Sigma, Microgen within the BG Group 1.1 kW) [399]. Stirling engines can have the advantage of a clean and fuel flexible combustion compared to reciprocating ICEs. The WhisperTech system has an electrical efficiency in the lower target range (12%). **Rankine** systems are also emerging from research and development laboratories. Examples are systems from the Baxi Group (1.1 kW), Cogen Microsystems (2.5 kW) or Enginion (4.6 kW) [398,399].

Traditionally steam engines have been mainly used for large-scale centralised power generation, such as steam turbines for nuclear power stations. Hence there is generally experience with the technology. Generally the advantages are similar to Stirling systems (also external heat engine). Rankine systems for micro CHP are in a less developed stage compared to Stirling systems and may be also limited to low efficiency for the low output powers of interest. There are two major **fuel cell** types for micro CHP. These are SPFC (e.g. Vaillant 5 kW_{el}) and SOFC (e.g. Sulzer Hexis 1 kW_{el}) [399]. Both types operate in field trials. The major advantage of fuel cells in comparison to other micro CHP technologies is the high electrical efficiency. The major drawbacks have been identified to be capital cost, overall efficiency (e.g. for SPFC) and lifetime [399,400].

AMTEC micro CHP systems have been also proposed [349]. **Thermoelectric** systems have been also considered for systems with a low electrical efficiency (self-powered operation) [401]. Future advances in thermoelectric system efficiency may also allow micro CHP operation.

For micro CHP TPV systems a target **power range** from 1 to 10 kW has been identified from the reviewed competing systems. A typical TPV system may aim for a power output of around 1 kW with stronger competition from other technologies in the power range close to 10 kW [110].

No major **technology constraints** could be identified. There have been system developments by more than one institution and system performances could be partly demonstrated. The inverter and grid-connection issues have been assessed for solar PV systems previously and have been also demonstrated for TPV operation [7].

There are no fully deployed **competing** technologies for micro CHP, but several emerging technologies as discussed previously. The long-term strength of TPV is

thought to be the solid-state operation. This should allow building micro CHP systems with the same maintenance requirements and reliability performance as existing boilers. The long-term energy efficiency of buildings is likely to improve, so that smaller sized systems would be required. However, heat engine efficiencies tend to decrease for smaller sizes [391] and scaling to various sizes could be also simpler for a TPV system. Fuel cells are also solid-state devices, have demonstrated high efficiencies and can be also scaled flexibly. Nevertheless, even if all current fuel cell problems for micro CHP could be overcome (e.g. reformer, lifetime, costs), there could be still a long-term market for oil and biomass based micro CHP TPV systems, since the fuel flexibility is another challenge of fuel cells. This discussion points out that there are specific TPV benefits over emerging competitors. On the other hand there is a number of emerging technologies and they are closer to the market. This is considered to outweigh specific TPV advantages. Hence, overall TPV has been not rated advantageous over its emerging competitors.

There is a huge mass **market** for micro CHP. For example in Great Britain a gas boiler market of 13.5 million is potentially suitable for micro CHP [395]. There are also niche markets for non-grid connected systems and self-powered boilers allowing for higher capital costs. Funding is generally feasible, since the promise of primary energy saving has stimulated political interest (e.g. UK, EU). TPV cost estimations indicate that TPV could compete with fuel cells and heat engines [114]. Hence, market and cost issues have been rated as positive.

The **UK** market has been identified as one of the most promising markets among a few other Western European countries [392,399]. Reasons include the high total dwelling stock with central heating (around 80%), the extensive natural gas distribution

network, the high annual boiler sales, the liberalised gas and electricity market, suitable heating loads and regulatory changes currently taking place to facilitate the connection of embedded generation [392,399].

The **human** impact has been identified as very positive (rating 3). Micro CHP has the potential of considerable primary energy savings, if large numbers of central heating boilers could be replaced [392]. The slight increase in local energy consumption (or local pollution) of a micro CHP system compared to current conventional boilers is not seen as a major disadvantage. In long-term micro CHP systems promise cost savings with a slight increase of fuel costs but major savings in electricity costs for the user. Micro CHP is also a potential technology for grid independent backup power in case of a power failure.

6.6.2 District heating and industrial CHP

In addition to micro CHP (1 - 10 kW) there has been also interest in larger sized TPV systems. Systems have been proposed with thermal powers of over 100 kW and even up to 1000 kW for apartment, district and industrial heating [91,107,223]. This results in an electrical **power range** from about 10 to 100 kW assuming the same **efficiency** range as for micro CHP (10 - 15%).

Scaling-up of the TPV output power has not been demonstrated yet. However, TPV systems can operate modular as proposed by Fraas et al. [91], so that **technology constraints** similar to those for micro CHP can be expected.

Competition arises from both deployed and emerging technologies. Deployed reciprocating ICE CHP systems are commercially available. Maintenance and noise of these engines have been regarded as acceptable for the large CHP range compared to micro CHP systems (e.g. installation in a separate room may be common). Small gas

turbines, known as microturbines, are an emerging technology [391]. The Stirling engine with an output power of tens of kWs is another emerging technology [402] It is concluded that there is strong competition from both deployed and emerging technologies and no clear overall benefit could be identified using TPV (rating 1).

The **UK** has currently a small CHP penetration and a climate with high heating demand compared to other Western European countries [391,392]. This should result in a considerable market for commercial and residential space heating in the UK. Industrial processes operating with low-grade heat are an additional potential market. Hence the usage in the UK is considered as positive.

Promising niche **markets** are applications with a steady heat demand over the course of a year. Examples are swimming pools, leisure centres or industrial processes [403]. There has been some cooperative research of the industry and a TPV company (ABB with JX-Crystals). The feasibility of primary energy saving should allow funding. In terms of capital system costs per output power, in needs to be considered that ICE systems become increasingly cheaper for larger output powers. TPV systems are likely to be mainly determined by PV cell costs. Hence, £/W values can be expected relatively constant for increased output powers. However, industrial and distributed heating CHP systems could have longer operation hours to improve economics compared to micro CHP systems. Overall the market and cost indicator has been rated balanced with generally suitable market conditions available but some cost constraints.

Similar considerations have been made for the **human impact** as for micro CHP.

6.7 Solar applications

The first publications for solar TPV **space** research date back to the 1980s. In the majority of cases, solar power is preferred over nuclear power for space applications [374]. Space applications with intermittent solar radiation (e.g. low earth orbit) usually utilise secondary batteries as energy storages [374], where batteries have disadvantages in terms of energy density and lifetime. One attraction of solar TPV for space is the potential of high efficiencies and high power densities. Solar TPV systems using a high-temperature thermal storage have been also proposed to replace PV cell/battery space systems [69]. A specific technological drawback is the requirement for a low PV cell operating temperature resulting in cooling challenges in space. Other technologies considered include Stirling engines and thermionic generators [353].

For **terrestrial** solar applications, the UK climate is less suitable for solar concentration as discussed earlier (Subsection 3.4.2). For Japan, solar TPV conversion has been considered unsuitable for this reason [110]. Potential advantages of solar TPV include the high efficiency due to spectral control and the insensitivity to changes in the radiation spectrum, compared to solar concentrator PV systems. Practical solar TPV systems face difficulties in terms of high-temperature engineering with an ideal radiator temperature of around 2500 K (Subsection 3.4.2). Both solar concentrator PV systems and Stirling generators have demonstrated high efficiencies [368,404]. For example, multi-bandgap solar PV concentrator cells (GaInP/GaAs/Ge) with efficiencies of 35% have been reported [176]. A recent solar TPV system was reported that aimed for a solar-to-electric efficiency of 30%, however, extrapolation from measurement resulted in an efficiency of only 22% [269]. Also basic PV cell efficiency calculations suggest that single bandgap GaSb can currently not achieve heat-to-electric efficiencies higher

than around 30% in a TPV system (Subsection 3.6.3). These considerations show that currently solar PV concentrator systems using multi-bandgap cells outperform solar TPV system using a single-bandgap cell. In the long-term multi-bandgap solar TPV systems may be competitive, but these cells are currently in an early research stage for TPV. Hence in this assessment, simple solar TPV systems have been excluded. Solar TPV hybrid or thermal storage systems have other specific advantages compared to solar PV concentrator systems, which can make efficiency considerations secondary.

6.7.1 Hybrid and thermal storage solar system

One possibility is the design of a hybrid solar-combustion TPV system. Such system has been designed using natural gas as a fuel and with an electrical output power of around 500 W [269]. This system could also operate in CHP mode. Solar TPV systems using a thermal storage system have been examined for space applications and may be also applicable for terrestrial use. Thermal storage based systems could potentially supply heat and power continuously and autonomously with long lifetimes (e.g. no refuelling required and no moving parts). In the short-term such storage and hybrid systems could be used for non-grid connected applications. Civilian applications may include remote manned (e.g. developing countries) or unmanned power supplies (e.g. relay station, data acquisition, weather stations, navigational aids). For an unsteady load such systems may require an additional electrical storage capability (e.g. secondary battery). In the long-term hybrid solar-combustion TPV systems may be utilised as grid-connected distributed CHP systems [401]. For the thermal storage or hybrid system without secondary battery (constant load) a long lifetime and a high reliability can be expected.

The required **efficiency** of solar TPV conversion has been assumed with the medium to long-term demonstration aim for this application (13 to 25%). This assumed efficiency range also includes an extrapolated efficiency of 22% predicted from measurements [269]. For combustion-based systems, the combustion efficiency target has been assumed from the demonstrated (5%) to the medium-term research aim (15%), where the higher efficiency value was also the aim for an examined TPV hybrid system [269]. In general, high combustion conversion efficiencies are desirable to extend the refuelling cycle period and keep operation fuel costs low. However, for remote applications, thermoelectric converters have been also applied in niche market applications with low efficiencies (smaller 5%). Hence, currently demonstrated TPV systems efficiencies (5% target) can be regarded as competitive for some applications.

In the small **power range**, hybrid or thermal storage systems could be of interest for unmanned remote applications. In remote, non-grid connected, applications the time interval of site visits and the power requirements are decisive parameters for the selection of a suitable technology (Figure 6-1). Small power applications may be also supplied by a flat plate PV cell/battery system or a combustion driven thermoelectric generator. Such systems are thought to be less complex compared to a TPV hybrid or thermal storage solar systems. Hence, a minimum power of 100 W has been assumed to justify the more complex hybrid solar TPV approach. Large power installations are likely to allow more maintenance and monitoring, thus permitting the use of deployed diesel engine generators. In this work the maximum competitive power has been assumed with 10 kW.

Overall, the **technology constraints** and the research and development effort were rated as negative. The funded research of a TPV hybrid generator has been rated as

positive [269]. Negative aspects included the complex overall design, the operation in hostile environments and the operation under part load for some applications.

A solar TPV hybrid or thermal storage system is likely to have advantages over both deployed and emerging **competing** technologies. Deployed technologies are solar PV/battery systems, diesel generators and thermoelectric generators. All of them have all their own disadvantages in terms of lifetime and costs (solar PV/secondary battery), maintenance and noise (diesel generator) or efficiency (thermoelectric generator). Another potential system may be the combination of a PV cell, an electrolyser, a hydrogen storage system and a fuel cell. Such system can be regarded as complex and costly. Fuel cell systems operating purely from a fuel tank would have high fuel requirements (large tanks, frequent site visits). Solar/combustion hybrid systems using Stirling engines have been also researched, but are considered here to suit the power range around or above 10 kW [405].

Market and cost issues can be regarded as positive. There have been at least two funded TPV projects [269]. In addition, this application has a potential niche market (e.g. off-grid supply) and a large potential market (distributed generation). Depending on the application and the detailed system design, solar TPV hybrid or thermal storage systems could operate up to 24 hours per day. The **use in the UK** has been considered less suitable, because of the high fraction of diffuse sunlight. Nevertheless, the application has been not excluded due to a large potential export market (e.g. developing countries). The **human impact** can be regarded as positive in terms of global and local human impact factors.

6.8 Waste heat applications

Waste heat applications are defined in this work as those where the major purpose is heat generation. In such applications TPV systems can converts some of the waste heat into electricity. Three applications are identified, which are self-powered heating (Subsection 6.8.1), industrial waste heat recovery (Subsection 6.8.2) and applications based on radiation guidance (Subsection 6.8.3).

6.8.1 Self-powered heating

In this application hydrocarbon based heating devices without grid connection are of interest (e.g. for space heating, hot water, drying). Examples are self-powered central heating units, district heating units, space heaters with fan, portable heaters, tent heaters, independent vehicle heaters or self-powered furnaces [37,112,365,349,372]. Typically heating devices have a large thermal power compared to the electrical power requirements necessary for control and heat distribution. Usually heat is distributed by forced convection (e.g. pumps, fans). The smallest thermal power has been assumed around 1 kW (hairdryer size). District heating units with thermal powers up to 1 MW also could have a need for grid-independent operation and have been assumed as an upper power range limit. From different sources [112-114,406] it becomes clear that these devices typically have an electricity requirement in the order of 1% of their total energy consumption. Consequently an electrical power range from 10 W to 10 kW has been calculated from the thermal range.

The **technology constraints** and the research and development effort have been rated as positive. Positive factors were the low efficiency requirements and beta tests of the Midnight Sun® system [112].

Deployed **competitors** could not be identified in this work. Self-powered heating systems using thermoelectric generators have been also considered [303,372]. On the one hand the implementation of commercial thermoelectric modules in these applications seems to be simpler compared to a TPV system using typically an optical cavity design. On the other hand it is currently challenging to design a thermoelectric generator with 2% efficiency [342]. In long-term TPV cells may be produced at lower prices per generated watt than thermoelectric modules. Currently thermoelectric modules seem to have advantages for this application with low efficiency requirements.

Self-powered heating devices are used in niche **markets**, where higher system capital costs could be justified. In long-term this application could grow into the large micro CHP market. The US Gas Research Institute identified self-powered devices as the major future market for TPV [365] and there is general interest in the TPV community for this application (e.g. Midnight Sun® system). Hence, market and cost issues have been rated as positive.

TPV could improve security of electricity supply and human comfort. This resulted in a positive local **human impact** rating. The total energy consumption is largely unaffected for the small share of electricity generated.

6.8.2 Industrial high-temperature waste heat recovery

The potential industries for high-temperature waste heat recovery are the iron and steel, non-ferrous, bricks, refractories, cement, ceramics and glass. JX-Crystals received funding from the US Department of Energy and researched TPV heat recovery tubes each with an output power of 5 kW [91,108]. These tubes could be inserted in high-temperature processes in order to generate electricity and low-grade heat in the form of hot water. Two applications have been proposed, which are high-temperature waste heat

recovery in the manufacturing industry and CHP supply for apartment buildings [91,108]. Yamaguchi et al. [109,110] assessed the potential of waste heat recovery in Japan. They found that waste heat recovery from flue gas for large industrial processes is already utilised for large furnace using steam turbines based systems and hence they concentrated on small furnace where they found temperatures to be too low for TPV operation. However, it was pointed out, that it is possible to upgrade small-scale flue gas heat using premium heat produced by an additional combustion process. Heat recovery from other locations than the flue gas was not considered in their work [109,110]. In the UK the situation is different. In the high-temperature industry electricity generation from waste heat is rarely used [407]. One major attraction of industrial waste heat recovery is that the heat is freely and often steadily available and that the electricity generated can be typically used at the industrial site. The low-grade heat generated by the TPV system may also be utilised for space heating if a demand can be identified.

For thermoelectric systems it has been pointed out that **efficiency** is not a serious drawback in the conversion of free waste heat and that the capital cost per watt is the decisive economic factor [408]. These considerations can also be brought forward for TPV and thus the lower efficiency target range has been assumed with the demonstrated efficiency (6% for non-combustion systems).

The use of 200 5kW tubes has been suggested in a glass furnace [108]. This would result in an electricity output **power** of 1 MW. This value has been assumed as an upper power range limit for this assessment. Small high-temperature furnaces could also have a requirement for self-powered operation, which would result in a minimum electrical power of 1 kW assuming 1% of a 100 kW thermal furnace.

A partly demonstrated TPV system indicates that there should be no major **technology constraints** [91]. Also a TPV heat recovery system does not require the design of an efficient combustion unit. This should result in a simpler system design. Industrial inter and intra process temperature variation require some further technology consideration. Hence, a balanced rating has been given for the technology constraints and research and development effort.

One deployed **competing** combination of technologies could generate electricity from heat in the flue gas. This combination consists of a heat exchanger, a high-pressure steam boiler, a condensing steam turbine and a generator [407,409]. However, the complexity of this approach associated with high capital and maintenance costs limits applications to large industrial plants using only the flue gas heat. TPV systems could be scaled in a wide power range to not only recover flue gas heat, but these systems could also convert heat of hot products leaving the process and heat lost through walls. Emerging competing technologies include heat engine concepts based on the organic Rankine [410], the Stirling [312] and the air-bottom cycle [409], as well as thermoelectric systems [408]. Heat engines are usually limited to the conversion of flue gas heat. Also, typically the heat needs to be piped to the heat engine, which inevitably leads to some heat degradation. Laboratory thermoelectric conversion modules are currently limited to hot side temperatures below 1300 K. However, for these high temperatures, sufficient and reliable electrical contacts and mechanical properties are difficult to achieve [340]. Hence, no direct competitor could be identified and TPV systems should offer flexibility in terms of scaling and location applicability.

In 1999 in the UK classified by type of use, high-temperature processes accounted for about one quarter of the industrial energy consumption. High-temperature processes

can be further classified by sector. Most of these sectors have energy-intensive processes operating at temperatures above 1300 K and which are suitable for TPV operation [411]. This indicates a large **market** for industrial waste heat recovery. Niche markets could be self-powered furnaces and backup power supplies in the industry. Funding has been available in the US [108] and very long operation hours should keep payback periods low. From these considerations a positive market and cost rating has been given.

The local and global **human impact** has been rated as positive. Primary energy savings are feasible and no additional pollution due to TPV operation should occur. Electricity generation would be expected to require low maintenance and would generate low noise. On-site use of electricity is another environmental advantage.

6.8.3 Waste heat application based on radiation guidance

Goldstein and DeShazer et al. examined high-temperature resistive dielectric solid radiation guides (e.g. yttrium aluminium garnet, erbium aluminium garnet) together with PV cells for TPV conversion [115-117]. In this arrangement one side of the dielectric solid light guide is in the high-temperature heat source environment, where radiation is coupled into the guide, and the other end can have a low temperature and illuminates the PV cell. Using total internal reflection allows radiation guidance. It can be assumed that this arrangement is simpler than other TPV systems using a cavity with challenging high-temperature mirror design. The arrangement could be inserted into each high-temperature process with a suitable temperature. This could allow applications such as self-powered heating devices (e.g. powering of displays or thermostats), self-powered sensors or fire energy converters for camping. Goldstein also

proposed the conversion of jet engine heat into electricity using dielectric solid light guides [116].

The variety of potential applications results in a wide **power range**, which has been assumed from mW to kW. Especially in the small power range (e.g. self powered sensor) the efficiency is likely to be not a critical factor. Hence, the demonstrated efficiency of heat into electricity conversion has been assumed as 6%.

The simplicity of the light guidance arrangement suggests that **technology constraints** and research and development effort would be low compared to the ordinary TPV cavity designs. Some research and development may be required for the radiation guides (e.g. material selection, losses of radiation guidance by total internal reflection). Overall, the limited TPV research [115-117] has lead to a balanced rating.

Thermoelectric generators, as a **competitor**, typically utilise conduction to transfer heat to the thermoelectric modules. Thermal conduction can be associated with temperature gradients. Hence thermoelectric modules need to be typically placed close to the heat source in order to achieve high hot side temperatures. Radiation, on the other hand, can be transferred over long distances with little losses (e.g. optical fibres in telecommunication applications). Also thermoelectric generators usually have lower efficiencies than TPV generators. Hence, TPV conversion is seen superior over its competitors in this configuration.

The **market and cost** indicator has been rated as negative. The applications are rather niche markets without a large potential market. Also the currently considered crystalline radiation guides are expensive. Amorphous materials (e.g. fused silica) could be cheaper, but have usually a lower maximum operation temperature.

No major improvement in the local or global **human impact** could be identified.

6.9 Results and conclusions

The assessment has been an iterative process, which considered the availability of different heat sources, the capabilities of TPV and competing conversion technologies, as well as the application requirements. The applications have been classed by heat source and CHP mode. Table 6-6 gives the final result of this assessment. Figure of merit ranges for both efficiency and electrical power output of each application have been identified. The five indicator groups have been rated from 1 to 3. The applications with the highest potential were identified by summing these indicators for each application (Table 6-6).

In CHP systems both heat and the electricity output are utilised. **Micro CHP** systems aim to replace conventional boilers in a dwelling and have been identified as the most suitable TPV application of this assessment. In Western Europe and the US there is some major interest in micro CHP. Generally TPV technology capabilities match the micro CHP requirements, namely high reliability, low maintenance and low noise. Currently, there are several other emerging technologies with similar capabilities operating in field trials and this competition is seen as the major challenge for the TPV micro CHP application. Industrial and distributed CHP systems could have longer operation hours to improve economics and have also been identified as a promising application. However, competition in the larger power range arises not only from emerging technologies, as for micro CHP, but also from deployed ICE CHP systems. In addition, self-powered heating devices have been identified as a promising application. Examples include water boilers, space heaters, tent heaters and independent vehicle heaters. These applications can be regarded as a suitable high value niche market for micro CHP systems.

Applications by heat source and CHP mode	Figures of merit ranges		R & D effort	Comp. & benefit	Market & cost	Use in the UK	Human impact	Final result
	Efficiency	Power						
Combustion non-CHP								
Portable generator	5-15%	1 W-1 kW	2	3	3	2	2	**12**
Uninterruptible power supply	5-15%	100 W-10 kW	1	2	2	2	2	**9**
Unmanned remote power	2-10%	1 W-1 kW	1	2	2	1	1	**7**
Renewable hybrid system	5-15%	100 W-10 kW	1	2	2	2	3	**10**
Small vehicle propulsion	15-20%	100 W-10 kW	1	3	1	2	2	**9**
Vehicle auxiliary power units	2-15%	1 W-10 kW	2	3	2	2	2	**11**
Combustion – CHP								
Micro CHP	10-15%	1-10 kW	3	2	3	3	3	**14**
District/industrial CHP	10-15%	10-100 kW	3	1	2	3	3	**12**
Solar								
Solar TPV storage/combustion	13-25% (5-15%)	100 W-10 kW	1	3	3	1	3	**11**
Waste heat								
Self-powered heating	1-2%	10 W-1 kW	3	2	3	2	2	**12**
Industrial waste heat recovery	6-19%	100 W-1 MW	2	3	3	2	3	**13**
Radiation guidance system	6-19%	1 mW-1 kW	2	3	1	2	1	**9**

Table 6-6: Summary of the application assessment.
The applications are classified by heat source and CHP mode. For each application figures of merit for the efficiency and power range have been identified. The five indicators are summed up to the final result.

Hydrocarbon fuels are widely available, can be easily stored, transported or refuelled, and have high energy density. Combining fuel with TPV technology capabilities results in several potential applications in this assessment. Competing technologies for these applications are mostly batteries in the smaller power range and internal combustion generators in the larger power range. Here, fuel cells are seen as the major future competitor. **Portable power** applications have been identified as promising. Strong military interest and another TPV assessment for Japan also indicate the potential. **APUs** operating independently of the vehicle propulsion have had less attention in the TPV community, but are regarded here as a high potential application. In particular, applications with low noise, high reliability or low complexity requirements should hold promise. Potentially, **solar TPV systems** using a thermal storage system or additional hydrocarbon combustion could allow autonomous power supply. However, the requirement of concentrators makes such system less attractive for the UK with a high diffuse sun light fraction.

TPV **high-temperature industrial waste heat recovery** has been identified as the second most suitable application of this assessment. Potential advantages are primary energy savings, high operation time, low competition from other technologies and moderate efficiency requirements due to the free or low cost of the thermal input. Also, many high-temperature processes are susceptible to power failures, where TPV could act as a backup power source. This high value backup market could be used to launch the TPV heat recovery systems. Industrial inter and intra process temperature variations need some further technology consideration. Hence, this work focuses on the high-temperature industrial waste heat recovery application, because of the high potential and limited TPV research work. The next chapter discusses this application in more detail.

7 Evaluation of industrial heat recovery

7.1 Introduction

The manufacturing industry is one of the major primary energy sectors alongside transportation and building. The improvement of energy efficiency in the manufacturing industry is the major means to reduce fossil fuel dependence. Energy efficiency can be measured by economic or physical indicators. The manufacturing industry, and especially the energy-intensive (or high-temperature) industry commonly applies the specific energy consumption (SEC) as a physical indicator [412]. The SEC is defined as the energy requirement per output of the process (e.g. GJ/tonne). Reduction of the SEC in the manufacturing industry can be achieved by various measures such as process optimisation or change, improved combustion, CHP, energy management, improved insulation and heat recovery. The capital and operation cost of the measure can be compared with reduced energy costs (achieved through reduced SEC) and both costs will decisively determine the payback period. It is a fundamental principle of thermodynamics that almost all of the energy entering an industrial process is discharged as waste heat [413]. An exception is energy stored in the chemical transformation of materials (e.g. smelting of ores into metals, forming of glass). In the high-temperature industry these energies are often small compared to the total energy

use. Hence, the recovery of the waste heat leaving the process is of vital importance in order to improve process energy efficiency.

As already pointed out, there has been limited work in the field of industrial heat recovery by TPV conversion (Subsection 6.8.2). Past work included proposals by Coutts [3], an assessment among other applications for Japan by Yamaguchi et al. [109,110] and some system development by Fraas et al. [91,107,108]. Hence, this chapter will first review some background of the industry with focus on the traditional high-temperature industries in the UK (Section 7.2). After that, other existing heat recovery methods are reviewed. This allows the placing of TPV heat recovery in context (Section 7.3). Three principal locations for high-temperature heat recovery are identified within this chapter (product, flue gas and wall heat recovery). Then the use of TPV in the high-temperature industry is assessed (Section 7.4), where one example process for each of these three locations is discussed in more detail. Conclusions are drawn in Section 7.5.

7.2 The UK high-temperature industry

In 1999, classified by end-use, high-temperature processes accounted for one fourth of the energy consumption in the UK industry (Figure 7-1)[1].

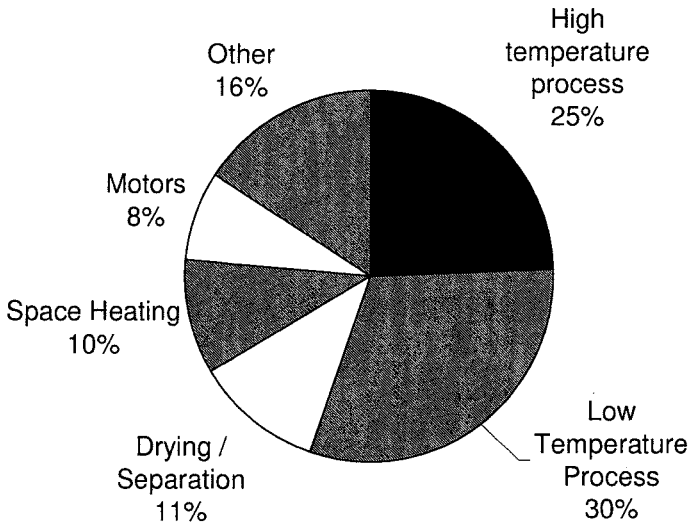

Figure 7-1: UK industrial energy consumption by type of use in 1999.

These high-temperature processes can be further classified by sector and process (Table 7-1)[414][25]. Most energy-intensive processes operate at temperatures above 1300 K [411]. Hence these processes can be regarded as generally suitable for TPV operation. The main energy users in high-temperature processing are coke ovens, blast and other furnaces, kilns (e.g. cement rotary), metal smelters, and glass tanks [1,414]. Most high-

[25] No newer detailed breakdown of the industrial energy consumption in the UK could be identified within this work. For example data in [414] have been used to project industrial energy consumption until 2010 in the same reference. This suggests publishing time frames of one to two decades of such detailed assessments. The total industrial energy consumption has drop by about 10% from 1990 to 2001 [1]. The share of the high-temperature processes decreased from about 34% in 1990 [414] to 25% in 1999 [1]. Dissimilarities in statistical methods may have also contributed to some of these differences.

temperature sectors show a large diversity in terms of production volume, fuel type, furnace type, existing heat recovery method, specific process and process temperature.

Industrial consumption by end-use in the UK in 1990	**Energy (*PJ/y*)**	**Sector**	**Energy (*PJ/y*)**	**High-temperature Process**	**Energy (*PJ/y*)**
High-temperature processes	524.52	Iron and steel	312.25	Sinter strands	25.10
				Electric arc furnaces	16.19
				Basic oxygen furnaces	5.50
				Blast furnaces	198.80
				Continuous reheating	32.00
				Ladle/tundish dishes	3.20
				Batch furnaces	13.50
				Cupolas	7.14
				Remelting and holding	4.52
				Heat treatment	6.30
		Bricks	21.28	Tunnel kilns	16.16
				Intermittent kilns	3.45
				Driers	1.67
		Refractories	5.08	Rotary kilns	1.98
				Tunnel kilns	1.93
				Intermittent kilns	1.08
				Driers	0.09
		Cement	63.82	Rotary kilns	63.82
		Aluminium alloy & non ferrous	74.13	Heat treatment	4.15
				Secondary refining	4.98
				Smelting and holding	33.14
				Reheating furnaces	2.65
				Melting and holding	9.10
				Other processes	20.11
		Ceramics and glass	47.96	Tunnel kilns	6.85
				Intermittent kilns	1.05
				Driers	5.09
				Large tanks for glass	21.26
				Small tanks for glass	8.64
				Glass conditioning	5.07
Low temperature processes	384.36	Paper	41.00		
		Textiles	33.15		
		Rubber	7.12		
		Food	112.54		
		Chemicals	190.55		
Engineering	109.61				
Space heating	263.12				
Other industrial end use	263.39				
Total industrial energy	1545.00				

Table 7-1: Industrial energy consumption for high-temperature processes in the UK. The data refer to the end-use per year. The table has been composed using data from [414].

Nearly all of the high-temperature processes coincide with a general type of process considered in this work (Figure 7-2). The energy entering the process chamber derives from electrical heating, combustion, a hot feedstock, or any combination of the previous

sources. Within the process chamber the temperature exceeds 1300 K and the combustion and feedstock/product may sometimes show interactions. Examples are the formation of CO_2 from glass forming reactions and the use of coke in a blast furnace as feedstock and fuel. The feedstock can be charged in different modes including batch, tap and charge or continuous type. The feedstock can consist of raw materials, recycled products or a mixture of both. Typically the SEC of processes using recycled products is lower if compared with raw materials. The important parameters to specify an industrial high-temperature process are the process temperature and pressure, fuel requirements, insulation losses and thermal efficiency, as well as the flow of mass and energy in the process [411]. The energy flow can be visualised in a Sankey diagram. Hence, this diagram can be used to identify major heat losses for possible heat recovery locations.

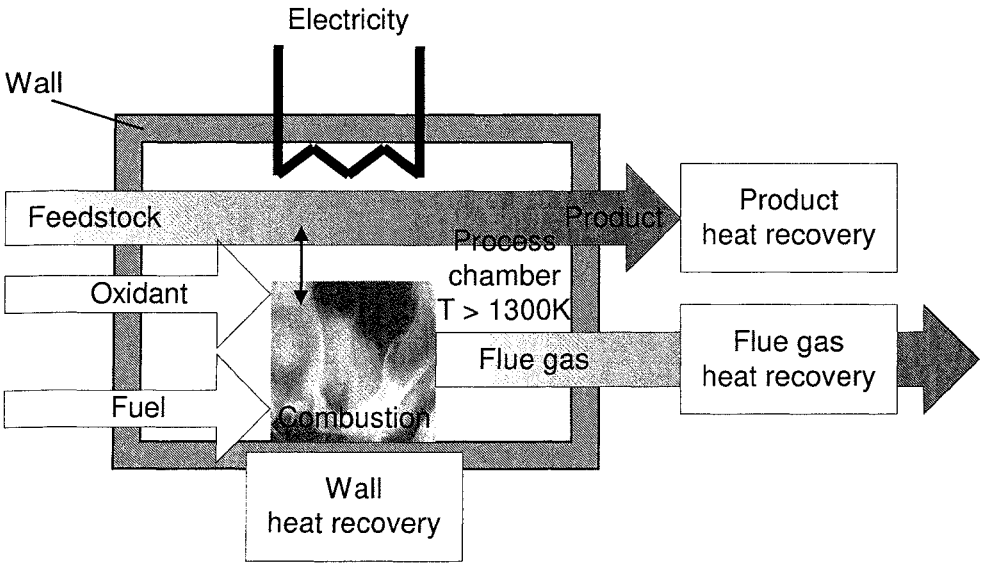

Figure 7-2: Schematic of a general type of industrial high-temperature process. The schematic has been produced within this work.

7.3 Heat recovery in the high-temperature industry

For the general type of high-temperature process considered (Table 7-1, Figure 7-2), there are three principal locations for heat recovery, namely product (1), flue gas (2) and wall heat recovery (3). Heat recovery in the chemical and petrochemical industry and in CHP plants may also show some potential, but these areas are not considered further here [407]. Existing heat recovery methods most commonly utilise the flue gas location (e.g. glass furnaces regenerators, pig iron blast furnaces) followed by the product and by-product[26] (e.g. cement clinker cooler, blast furnace slag recovery [415]). Insulation heat losses are rarely recovered and a rare example is the recovery of radiation losses from a shell of a cement rotary kiln [414].

Once potential sources of waste heat are identified, the **end-use** of the recovered energy needs to be considered. The use of the recovered energy in the same process (e.g. combustion air pre-heating, feedstock preheating) has several advantages, such as minimising the process SEC, avoiding long distance transport of heat and usually matching of energy supply and demand [407]. However, the use of waste heat within the process is not always feasible and therefore this heat is available for external use (e.g. space heating, electricity generation). External use of energy may be classified by the type of energy conversion: heat-to-heat (e.g. steam or hot water production), heat-to-chemical energy (e.g. forming methane from blast furnace slag) or heat-to-electricity. Heat-to-heat conversion, mostly associated with heat exchangers, has simplicity, but is limited to applications where heat recovery and demand coincide since heat can only be

[26] In this work only the recovery of the sensible and latent heat of products and by-products is considered. Other technologies use the calorific value of by-products, such as coke oven, blast furnace and basic oxygen furnace gas in the steel industry [415].

transported and stored to a limited extent. Additionally, heat exchangers may have problems with leaks, low efficiencies and fouling from flue gas, especially for temperatures higher than 1300 K [407,414]. Heat recovery technologies that generate electricity offer more flexibility since electricity can be transmitted with lower losses than for heat, the grid can act as storage and electricity can be converted to other energy forms at high conversion efficiencies.

A combination of deployed technologies allows electricity generation from heat in the flue gas using a high-pressure steam generator, a steam turbine, a condenser and a generator [407,409]. This approach has been adopted for flue gas heat recovery for large high-temperature processes in Japan [109,110]. However, there was no known UK example of a retrofit power generation system using high-temperature waste gas streams in 1999 [407]. Reasons for the low penetration in the UK include the complexity of this approach, associated with high capital and maintenance cost, as well as the present power cost. Other technologies are mostly in a research and development stage operating in different temperature ranges. These technologies can be classified into two groups, external heat engine based systems and direct heat-to-electricity conversion devices (see Chapter 5).

External heat engine based systems operate with different thermodynamic cycles, such as the Rankine or Stirling cycle. These cycles can use different working fluids and may be of open or closed type. This results in a variety of potential recovery systems using external heat engines [409,410]. For high-temperature waste heat sources of interest here (above 1300 K), the inlet temperature at the heat engine is usually lower than 1300 K. There may be different reasons for this including high-temperature engineering difficulties, collection and piping heat losses or deliberate cooling for the

conversion (e.g. because the heat engine operates at a lower inlet temperature). Product and wall heat losses are typically not converted into electricity using external heat engines.

Direct heat-to-electricity conversion devices have advantages in terms of low maintenance, high reliability, good power scalability and low complexity compared to heat engines. In addition, they could be used directly at any heat source (flue gas, wall, product) so that collection and piping losses could be avoided. The major direct heat-to-electricity conversion devices currently of research interest are thermoelectric generators [408,416]. However, these generators can commonly convert only low-grade heat with hot side temperatures of around 400 K or lower temperatures [340,408,416]. High-temperature thermoelectric generators are feasible but there are still engineering challenges to be overcome (Subsection 6.8.2).

It is concluded, that direct-heat-to-electricity conversion devices have specific advantages over external heat engine generator systems in the industrial waste heat recovery application. Furthermore, thermoelectric does not compete with TPV conversion, because both technologies operate in a different hot-side temperature range.

7.4 TPV conversion in the high-temperature industry

In 1990 in the UK, the total estimated technical potential energy savings in the high-temperature industry using deployed and demonstrated heat recovery devices for product, flue gas and wall heat recovery were calculated as 49.5 PJ/year and it was estimated that a value of 7 PJ/year has been achieved. The major reasons for the differences between technical potential and implemented saving were doubts over the cost effectiveness and the difficulty of the utilisation of the waste heat [414]. Electricity generation from this waste heat using TPV conversion could not only improve the

process energy efficiency, but also act as an independent power supply, since a lot of high-temperature processes are susceptible to power failures and therefore require a backup power source. However, electricity generation from waste heat is usually only considered if no use of the heat within the process or outside the process can be found. This makes TPV somewhat dependent on changes of the high-temperature process. In some cases, less high-grade heat may become available for TPV due to these process alternations (e.g. improved pre-heating of combustion air or higher refractory durability). In other cases the feasibility of high-temperature heat recovery may increase (e.g. oxygen-fuel instead of air-fuel combustion). In the following three subsections product, flue gas and wall heat recovery are discussed using one example process to estimate energy savings. The glass tank furnace is discussed into more detail in order to gain insights in a complete high-temperature process. The flue gas location of the glass furnace is then identified as the most promising location and assessed in depth.

7.4.1 Product heat recovery on a continuous curved caster

Most high-temperature industries have a product leaving the process at temperatures above 1300 K. By cooling the product down from a higher temperature to 1300 K, a specific enthalpy will be available from the hot product (Figure 7-3) [415,417-420]. This enthalpy could be converted by a TPV heat recovery system. Sometimes the enthalpy of the product is accessible only partly in the process, because of restrictions including other heat recovery methods (e.g. clinker cooler for air preheating in the cement industry), other following processes operating at high product temperature or discontinuously operating processes (e.g. slag from a blast furnace). However, there are examples where the product leaves continuously and is accessible at high temperatures. From the historical development it can be expected that the number of continuous

processes is likely to increase. For example, a potential future process may be a strip caster replacing discontinuous casting in moulds [415].

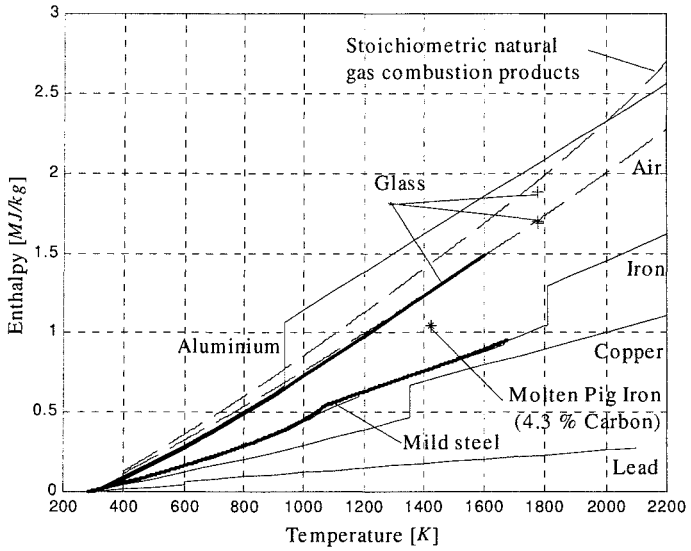

Figure 7-3: Examples of the enthalpy of some selected media versus temperature. Glass and steel are drawn as a bold line, since they do overlap with some other data. The enthalpy of combustion products and air is shown for comparison. The melting point temperature can be recognised by a large change in the enthalpy. Ideally, a TPV generator could also convert this phase change (latent) energy. The diagram was developed from various literature sources.

A **continuous curved caster** is discussed as an example process. Over the last decades continuous casting methods have largely replaced the casting of ingots with subsequent reheating in soaking pits and rolling. The most common type of continuous casting machine is curved in shape and forms billets, blooms and slabs [421]. Assuming an enthalpy of the liquid steel of 1.4 MJ/kg [415], a minimum TPV operation temperature of 1300 K and the enthalpy data in Figure 7-3, it is estimated that an energy of about 0.7 MJ/kg steel, or 11 PJ/year for continuous casting in the UK in 1996, is in principle available for TPV conversion [422]. There may be three potential locations for TPV operation. These are the water-cooled copper mould to form a solid skin of the strand, the support area and the guide area. It is thought that the low temperature of the hot face of the copper moulds, far below the 1300 K required for TPV conversion [421],

precludes the use of TPV in these moulds. In the support area, the strand with its solidified skin and the liquid core is supported by rollers and cooled by water sprayers. The support area can vary over a wide range and may not be required at all (e.g. for billets with low casting speed) or extend over the full length of the machine (e.g. for a slab caster). The guide area uses less support and cooling, when compared to the support area. A role for TPV is seen in the replacement of water sprayers, however limitations may arise due to closed arrangement of rollers and quality changes may occur due to changes in the heat transfer rate in the cooling process. The steel surface heat transfer rate and temperature varies along the curved caster depending on parameters such as product cross-section, casting speed, mould system and support system. Hence, individual caster designs would need to be assessed in order to determine the TPV energy saving potential. An upper electricity potential of 2.2 PJ/year (20% of 11 PJ/year) is estimated here for the UK.

Other potential processes with large areas for product heat recovery by TPV are float glass baths and in future possibly strip casters.

7.4.2 Flue gas heat recovery on a regenerative glass tank furnace

In the UK in 1990, the emitted flue gas energy from high-temperature processes was estimated as 100 PJ and as 65 PJ for waste gas above 673 K compared to a total consumption of 525 PJ (Table 7-1)[407]. Most of the high-temperature processes considered have flue gas temperatures above 1300 K [411] and typically already use heat recovery methods for combustion air or product preheating and reject flue gas still at relatively high temperatures (65 PJ/year above 400 °C). It is thought that TPV flue gas heat recovery would typically operate in a cascaded manner, where the TPV system would make use of the high-grade heat from the actual flue gas temperature down to

1300 K and other heat recovery methods would utilise the remaining heat. Operation of the heat exchanger has partly proved to be difficult due to flue gas contamination [407,414]. These engineering challenges may also occur for TPV heat recovery systems.

Flue gas heat recovery on a **regenerative natural gas-powered glass tank furnace** is used as an example process. This furnace type represents the major part of the glass market by primary energy use [423]. Smaller intermittently operating furnaces are likely to operate in a 24-hour cycle consisting of batch feeding, melting and extraction of the glass. Although there are some opportunities for TPV in regard to these furnaces, they are not considered here because of their small primary energy consumption.

Figure 7-4 shows a typical end-fired regenerative glass tank furnace, adapted from [424]. The largest of these regenerative glass tank furnaces are side-fired float glass furnaces, with a daily production volume of up to 1000 tonnes of glass. Such furnaces can contain up to 2500 tonnes of molten glass.

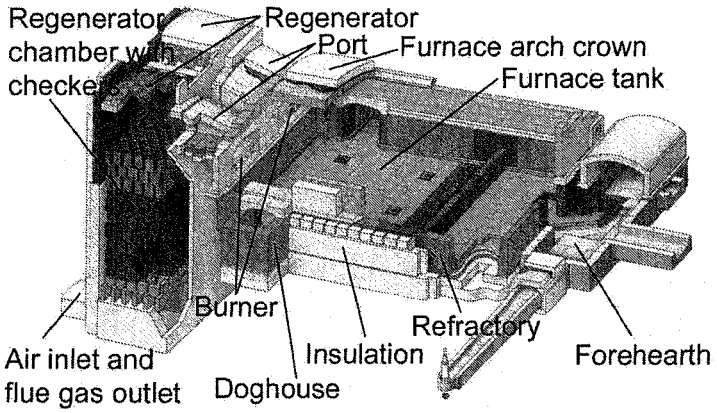

Figure 7-4: Drawing of a typical end-fired regenerative glass tank furnace. The components of the picture from [424] were named within this work.

The material consisting of the raw material (batch), cullet (recycled glass) or a mixture of both is fed continuously into one side of the furnace (doghouse), the melting, the refining and conditioning process takes place throughout the furnace and the molten glass is extracted at the other end (forehearth). Typically, these furnaces operate with no

interruption for about a decade and are heated by natural gas. Sometimes electrical boosting is used and some furnaces are entirely electrically heated. For electrical heating, rods are usually introduced into the furnace and the molten glass acts as an electrical conductor.

The following discussion concentrates on the commonly used natural gas heated regenerative tank furnaces. For these furnaces, the energy distribution (Sankey diagram) has been composed here for a modern type furnace from two different literature sources (Figure 7-5)[425,426][27].

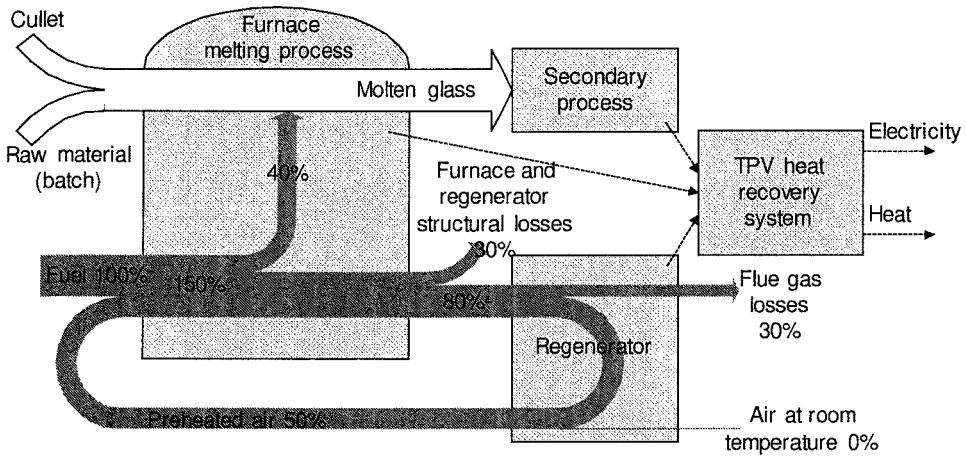

Figure 7-5: Sankey diagram of a natural gas-powered regenerative tank furnace. The three potential TPV heat recovery location, product, wall and flue gas are shown.

As can be seen in Figure 7-5, of the total input heat, around 40% leaves through the hot product, around 30% through the walls and around 30% through the hot flue gas. There is a potential to recover heat by TPV from all three locations. For wall heat recovery, the principal problem is seen as the small wall heat flux (commonly in the

[27] The theoretical requirement to heat glass from room temperature to 1500 °C is about 1.7 GJ per tonne. The energy required for the chemical reaction of the raw material is about 0.6 GJ per tonne [425]. This value can differ for different glass compositions [418]. For a modern furnace with an efficiency of 40% operating without cullet, these values result in an energy consumption of 5.75 GJ/tonne.

range of 0.1 to 0.3 W/cm² [418,427]) compared to the typical heat flux utilised in TPV, which could be for example 5 W/cm² for an electrical power density of 1 W/cm² assuming 20% conversion efficiency. To overcome this, it may be possible to accept higher wall losses (resulting in higher fuel consumption), to accept lower power densities for TPV conversion (resulting in higher TPV costs) or possibly to include a means to concentrate the heat flux locally whilst ideally keeping the average wall flux at the previous heat loss level. In continuously operating furnaces the molten glass is distributed via the forehearth. The glass temperature at the forehearth outlet is around 1400 K [425] and the forehearth wall heat fluxes are also low for TPV operation (around 0.1 W/cm^2 [427]). An exception is the float glass process, which does not require a forehearth. However, the glass inlet temperature of about 1300 K is relatively low for TPV operation. Hence, flue gas heat recovery is considered here.

Regenerators improve the energy efficiency of a tank furnace by transferring flue gas heat to the combustion air. The regenerator uses an alternating cycle of combustion air and flue gas. The combustion air is heated in the first regenerator (Figure 7-4). Afterwards, natural gas together with the preheated combustion air is burned above the molten glass bulk and the flue gas leaves the furnace through the second regenerator. After 15 to 30 minutes the direction of firing is reversed and the second regenerator preheats the combustion air [428,429]. Figure 7-5 shows the typical efficiency of regenerators with 50% reused energy. The theoretical maximum limit of reused energy is about 58%, estimated from data provided in [426], but this is not achieved in practice, because of increased costs for large regenerators and increased production of NO_x due to high air preheating temperatures. In the UK, stringent NO_x emission limits lead partly to lower air-preheating. This increases the waste heat from the regenerator. The fact that

flue gas heat leaving the regenerator is wasted is also reflected in the high flue gas temperature with typically values of around 800 to 900 K [425]. It can be concluded that around 38% of the flue gas heat is, in principle, suitable for TPV conversion. This assumes a flue gas temperature equal to the glass temperature of around 1800 K, a minimum TPV operation temperature of 1300 K and the enthalpy diagram (Figure 7-3). This percentage value can be translated for the Sankey diagram (Figure 7-5) into a value of around 30% (38% of 80%). In this idealised case a TPV system would make use of all the high-grade heat and the remaining heat would be utilised for combustion air preheating and no heat would be lost. Taking into account that very low flue gas temperatures are impractical (large sized regenerators) and that a combustion air of 1300 K is at the lower end for glass furnace operation, the amount of heat available for TPV conversion from the regenerator in the Sankey diagram has been assumed as 20% instead of 30%. It needs to be considered that this would still require a larger sizing of the regenerator, since heat transfer to and from the regenerator checkers would be reduced for lower temperatures. Furthermore, assuming a TPV efficiency of 20%, the resulting generated electricity would be equivalent to 4% of the total energy input (20% of 20%). Assuming this energy distribution for a modern 100 tonnes per day furnace with a total input energy of 5.75 GJ/tonne would result in a TPV power output of about 270 kW (100 tonnes/day · 5.75 GJ/tonne · 0.04). The PV cell area for such arrangement would be 27 m^2 assuming a TPV electrical power density of 1 W/cm^2. Such areas are thought to be generally available in the regenerator.

Recently, there is a trend to switch from air-fuel to **oxygen-fuel fired furnaces** [425]. Oxygen-fuel firing usually has advantages in terms of a higher efficiency through the reduction in the flue gas volume (about 1/5 compared to air) and a reduction of NO_x

emission [425]. Oxygen-fuel combustion can result in higher furnace temperatures (enhanced crown refractory corrosion can occur [425]). Hence, flue gas heat that previously preheated the combustion air is usually available for heat recovery. There is also a requirement of flue gas cooling for cleaning processes operating at low temperatures. Hence, oxygen-fuel fired furnaces are considered to have a high potential for TPV heat recovery.

Other potential processes for flue gas heat recovery are blast, re-melting, holding, heat treatment, secondary refining and reheating furnaces.

7.4.3 Wall heat recovery on a 3-phase AC current electric arc furnace

In 1990 in the UK, the total potential technical energy savings in the high-temperature industry for improved insulation was estimated as 9 PJ/year, which is a relatively low value if compared to other measures: improved combustion processes (50 PJ/year), process development (80 PJ/year), furnace and kiln design (65.5 PJ/year) and heat recovery (49.5 PJ/year) [414]. No total value of energy losses through walls was available for this work. It is conservatively assumed here that at least 10% of the total energy consumption of high-temperature processes (Table 7-1, 525 PJ/year) is lost through walls. The 10% value would result in about 53 PJ/year for the UK and can be compared, for example, to a value of 30% for a glass tank furnace (Figure 7-5). This consideration shows that even if the total potential technical energy savings methods for improved insulation are applied, there is still a large amount of energy lost through insulating walls (44 PJ/year). Direct energy conversion devices, namely thermoelectrics and TPV should be advantageous technologies for wall heat recovery, because of their modularity and the direct use of the wall heat flux without any further intermediary energy conversion or heat transport process. Typically, a high-temperature wall consists

of a refractory layer at the hot side to withstand the process chamber environment and one or more insulation layers on the outer surface. If the insulation thickness is increased, the temperature in the refractory will increase resulting in accelerated refractory degradation. This mechanism and the insulation cost are the major limiting factors for improved insulation.

A 3-phase **alternating current (AC) electric arc furnace** (EAF) is discussed as an example process. EAFs are cylindrical refractory lined vessels with usually three carbon electrodes that can be raised or lowered through a removable furnace roof. They are used to produce carbon and alloy steels in a batch process. Cycles range from about 1.5 to 5 hours to produce carbon steel and from 5-10 hours or more to produce alloy steel. The feedstock is mainly scrap steel and waste pig iron from steel works. Power is supplied mainly by 3-phase AC electricity, which creates arcs between the electrodes that melt the metallic charge. Additionally oxygen-fuel burners are widely employed to assist melting. Water-cooling on the roof and sidewall panels of EAFs is becoming common practice. It is thought that these panels could be replaced by a TPV heat recovery system, where the already available water supply could be used for PV cell cooling. About 4% of the total energy input of an EAF (0.65 of 16.2 PJ/year in the UK) could be recovered as electricity by using TPV in the roof and sidewalls. This assumes extrapolated data from a case study of a typical 80 tonne furnace [430], a TPV efficiency of 20% and a TPV power density of 1 W/cm^2.

Other potential processes are the metallurgical reactor for secondary refining in the steel industry, the conditioning zone of glass furnaces (especially float glass) and blast furnaces. In particular water cooled walls usually have high heat fluxes and are regarded here as suitable locations for TPV wall heat recovery systems.

7.5 Conclusions of the heat recovery evaluation

The UK high-temperature industry has been reviewed and the potential of TPV heat recovery systems to improve energy efficiency in the industrial sectors has been investigated. Three principal locations of heat recovery have been identified, namely the locations of the product (1), flue gas (2) and wall (3). In this chapter example processes for each identified location have been assessed. These were product heat recovery on a continuous curved caster, flue gas heat recovery on a regenerative glass tank furnace and wall heat recovery on a 3-phase electric arc furnace.

The traditional heat recovery technique of electricity generation based on a steam turbine is mostly limited to the flue gas location and large energy consuming processes. Direct energy conversion devices could be used in all locations. Thermoelectrics could recover low-temperature heat (<400 K) and TPV the high-temperature heat (>1300 K). Advances in both technologies may allow the entire temperature range to be covered using direct energy conversion devices.

An overall assessment of TPV in the high-temperature industry is complex, mainly because of the large process diversity and because an individual assessment for each process in terms of TPV use is required. Also, the identification of major primary energy consuming processes does not allow statements about major energy losses within the processes. For example, the energy input of a continuous curved caster originates from the previous melting process and not from primary energy consumption within the casting process. Hence, the entire high-temperature process chain has to be assessed. The Sankey diagram of these processes can be used for identification of potential heat recovery locations.

Three major TPV technology challenges were identified. Firstly, a TPV system would need to be designed for a specific hot side temperature. However, this temperature would depend on the process, where intra and inter process variation have to be taken into account. Secondly, for the same hot side temperature the heat flux could vary for different heat recovery locations. For example, an insulating wall of a glass furnace may have a small heat flux compared to a water-cooled wall of a 3-phase electric arc furnace. Ideally, a TPV system could be matched in a flexible way to the hot side temperature and heat flux of a heat recovery location. This assumes that the use of a TPV system would not alter the current process. Thirdly, in some heat recovery locations the temperature changes with time. Examples of these heating cooling cycles are glass tank regenerators (tens of minutes) or electric arc furnaces (hours). Shorter cycle periods may allow TPV operation at a constant radiator temperature using a thermal storage system to bridge the temperature variations. These storage systems would be also part of a TPV system design and hence add to the system complexity.

Two processes studied in this chapter, both indicate that a TPV system could generate around 4% electricity of the total process energy consumption. For example in the US, around 10 to 24% of the energy used on a glass site is statistically electricity and this does not include generation and distribution losses [425]. Similar values around 10% are reported for the US steel industry [431]. For the UK in 1992, the fossil fuel and (non-primary) electricity demand of different high-temperature sectors has been reported [432]. From this source the share of electricity to the total energy demand of different industrial sectors can be given: iron and steel 8%, non-ferrous metals 40%, other minerals 31%, bricks 8%, cement, lime, plaster 8% and glass and glassware 14%. Hence, it is concluded here that electricity generated by TPV could usually be directly

consumed at the high-temperature process site. This would avoid transmission and distribution losses of the electricity generation and for some sites it may also be possible to use the heat generated by the TPV system. Also, from the historical development perspective it can be expected that the electricity share in the high-temperature industry is likely to increase. For example, this has been reported for the US steel industry [431].

It is concluded here, that there should be a large potential for energy savings in the high-temperature industry using TPV. For example in the UK, 30% (21 of 70 PJ/year) of the electricity consumed in the entire high-temperature industry could be covered by TPV heat recovery, assuming the 4% result of the two example processes can be extrapolated to the entire high-temperature industry, a UK consumption of the high-temperature industry of 525 PJ/year in 1990 and an electricity consumption of 70 PJ/year of the high-temperature industry in 1992 [414,432].

The work reported here estimates a potential saving of about 2.6 million tonnes of CO_2 using TPV heat recovery in the UK high-temperature industry. This calculation is based on the assumption of a conversion factor of 122.2 $kgCO_2/GJ$ for electricity generation from primary energy [423] and 21 PJ/year generated electricity by TPV conversion as outlined in the previous paragraph. The saving value of 2.6 million tonnes can be compared with the total UK CO_2 emission of 164 million tonnes in 1990 [433]. This potential saving in energy and CO_2 are generally comparable with other measures to improve the energy efficiency of the high-temperature industry [414]. Also, for the UK in 2001 the climate change levy came into force and includes CO_2 trading of the high-temperature industries [433]. This levy may help to introduce TPV heat recovery as a CO_2 reducing measure.

In general, continuously operating high-temperature processes have been identified as advantageous for TPV heat recovery (e.g. glass tank furnace). Such processes allow a long TPV operation time, which would translate into short payback periods. Another advantage is the free availability of the waste heat, assuming that the TPV system does not alter the process. This limits the cost mainly to the TPV system capital costs (e.g. rated in £/W). In this case the conversion efficiency is not a decisive factor [408]. Continuously operating processes are often power-failure critical so that a backup power supply is required and this power supply could be replaced by the TPV heat recovery system (self-powered process). In future continuous processes, associated with high product output and low SEC, are likely to increase in number. It may be expected that NO_x legislation will become stricter and oxygen-fuel combustion gain in importance. These developments should increase the potential of TPV heat recovery.

Finally, PV cells for TPV with lower bandgaps are being developed, as pointed out in Subsection 3.6.3. These cells are potential candidates to operate in TPV systems with lower radiator temperatures.

In the following chapter, typical radiator temperatures and PV cell bandgaps are assumed to model fused silica (SiO_2) in TPV cavities. In this work, physically thick SiO_2 using total internal reflection is considered as a promising arrangement to extract waste heat from a process and guide suitable radiation to the PV cell for conversion into electricity.

8 Computational modelling of heat transfer

8.1 Introduction

As already pointed out in Chapter 4, optimisation of heat transfer in general, and radiative heat transfer in particular in terms of the spectral, angular and spatial radiation distributions, is required in order to achieve high efficiencies and high electrical power densities for TPV conversion. The requirements have been defined as high in-band and low out-of-band radiative heat transfer. Cavity conductive and convective heat transfer from the radiator to the PV cell and the surrounding is usually parasitic and needs to be minimised.

In general, modelling of heat transfer in TPV systems is complex. For example radiative surface properties of cavity components are temperature, angle and spectrum dependent and these components usually interact by the three heat transfer modes (conduction, convection and radiation). Hence, simplifications need to be made, if heat transfer is modelled for TPV systems. For example, modelling can be limited to the dominating heat transfer mode, surfaces can be approximated as either diffuse or specularly reflective in terms of their angular dependence and spectral dependences can be simplified by assuming constant values within spectral bands.

Section 8.2 contains a literature review and some background theory of radiative heat transfer modelling for TPV. This literature is then discussed in Section 8.3 and a suitable technique for investigating the participating media (e.g. fused silica) in TPV applications is selected. The modelling methodology and assumptions are discussed in Section 8.4, where three principal arrangements are defined: Radiator-Air-Glass-Air-PV cell (RAGA), Radiator-Glass-Air-PV Cell (RGA) and Radiator-Glass-PV Cell (RG). The modelling results are presented in Section 8.5, before the conclusions (Section 8.6).

8.2 Theory and literature review

The importance of radiative heat transfer modelling for TPV has been highlighted by Hottel et al. [50]. Subsequent TPV heat transfer modelling was summarised by Coutts [3] and Aschaber et al. [434-436]. Fundamental treatments of radiative heat transfer can be found elsewhere [8,9,11,437]. A number of other authors have modelled various geometries for TPV. These are discussed in the following subsections starting with the simplest models and continuing with the more complex models.

8.2.1 Radiative heat transfer between two surfaces

Equation 8-1 gives the net radiative heat transfer from a hot plate to a cold plate. This equation assumes two isothermal blackbody surfaces with the temperature T_h and T_c and no participating medium between the two surfaces [8,9,11]. The view factor $F_{h\text{-}c}$ depends on the arrangement of the plates (distance, angle and size) and reaches unity for an infinite parallel plate arrangement. The view factor may be also known as configuration factor, radiation shape factor or angle factor. View factor equations for simple geometries can be found in literature [8,9].

$$H = \sigma \cdot \left(T_h^4 - T_c^4\right) \cdot F_{h-c} \tag{8-1}$$

Equation 8-1 allows simplified radiative heat transfer calculations from the radiator (T_h = 1500 K) to the PV cell (T_c = 300 K). For the temperature of interest in TPV, the term σT_h^4 is usually much larger compared to σT_c^4, so that the latter term can be in a first approximation neglected. The term σT_c^4 defines an upper limit of radiative heat transfer in a TPV system and is tabulated in the Appendix B for a range of temperatures. Equation 8-1 has been used as a base for past TPV models discussed in the following.

Hottel computed the radiative heat transfer through glass shields for an infinite plate arrangement using an analytical model. He included spectral dependences of the radiator emissivity (ε) and the reflectivity of PV cell and glass shield. Glass shield absorption was assumed to be wavelength independent and participation of the glass was neglected. The reflectance for different angles was assumed constant. One conclusion made was that the shield reduces in-band transmission [50]. Burger [438] and Schroeder et al. [266] developed their own models based on the Hottel model.

8.2.2 Net radiation method for a TPV cavity

A TPV cavity is often composed of a radiator, PV cells and reflector surfaces as shown in Figure 2-1 [260,434]. In some cases the assumption can be made that the medium within the enclosure (e.g. vacuum) shows no interaction with radiation and is non-conductive and non-convective. In such cases the radiative heat transfer between all surfaces depends only on the absolute temperature of the surfaces and the geometry. TPV cavities containing non-participating media with diffuse surfaces have been modelled by the net radiation method using view factors to calculate the radiative heat transfer between surfaces [8,9,11,260,261,265,434-436]. The surfaces are usually subdivided until they can be approximated as having a uniform temperature. The net radiation method also allows the definition of spectrally selective surfaces. Enclosures

with partially specular boundary conditions can be treated using specular view factors [8]. Generally the treatment of spectrally dependent and specularly reflective surfaces is complex, so that numerical models are usually required [9].

8.2.3 Ray tracing for a TPV cavity

Specularly reflective surfaces in a TPV system can include mirrors, PV cells and glass surfaces. For (partially) specular surfaces, ray-tracing methods have been applied for TPV modelling using statistical methods. These methods are typically, but not exclusively based on Monte Carlo techniques [29,46,436,439-443].

8.2.4 Radiative heat transfer with participating media

Many TPV systems use a transparent high-temperature heat shield made from fused silica (SiO_2) between the radiator and the PV cells. Such heat shields perform several roles including minimisation of non-radiative heat transfer, as well as the protection of metal radiators from oxidation and PV cells from combustion products. It is well known that SiO_2 with a thickness of a few millimetres is largely transparent to visible and near infrared (in-band) radiation, but increasingly absorbs longer wavelength infrared (out-of-band) radiation. Hence, unless cooled, deliberately or due to parasitic losses, these shields are heated up to elevated temperatures due to the absorption of out-of-band radiation. At these temperatures absorption and re-emission of radiation within the glass becomes important. As Gardon proposed [444], for semi-transparent materials, unlike the more familiar opaque materials, the emission and absorption of radiation are bulk, rather than surface, phenomena. Each volume element of glass radiates in proportion to $\alpha \cdot n^2 \cdot \sigma T^4$, where α is the absorption coefficient, n the refractive index, σ the Stefan-Boltzmann constant and T the absolute temperature. Radiation is then absorbed on its way towards the glass-air surface, some is internally reflected at this surface, and some

refracted across the surface [444]. The **radiative transfer equation** describes the conservation of radiative energy for an infinitesimally small volume [8]. Exact analytical solutions of this equation can only be found for idealised situations. For most other situations approximate solution methods are required. Howell and Mengüç compared these for multidimensional complex problems and regarded the Monte Carlo and Discrete Ordinates methods as having the best and a similar overall performance [11]. The four major approximation methods currently used are given by Modest and marked grey in Table 8-1 [8]. This work selects the Discrete Ordinates method.

Method	Angular resolution	Spatial resolution	Spectral resolution
Flux methods			
Multi flux approaches	Acceptable	Very good	Very good
Discrete transfer method	Acceptable	Very good	Very good
Discrete Ordinates (Sn)	Good	Very good	Very good
Moment methods			
Moment method	Not good	Very good	Very good
Spherical Harmonics (Pn)	Acceptable	(Very) Good	Very good
Zone methods	Acceptable	Good	Acceptable
Monte Carlo techniques	Very good	Good	Good
Numerical approaches			
Finite difference technique	Acceptable	Very good	Good
Finite element technique	Acceptable	Very good	Good

Table 8-1: Approximation methods of the Radiative Transfer Equation.

8.2.5 Radiative coupled with conductive heat transfer

For example, heat transfer in glass consists of radiation **coupled** with conduction. For greybody media with combined radiative and conductive heat transfer, there are two boundary cases: optically thin and optically thick. Optically thin is defined as $\alpha \cdot S << 1$ and optically thick as $\alpha \cdot S >> 1$ assuming no scattering and a constant absorption coefficient α along a path length S [9]. In an enclosure with **optically thin** media, radiative heat transfer is dominated by surface-to-surface exchange [437]. In this case, radiative and conductive heat transfer can be decoupled, so that the total heat transfer between the surfaces is the sum of the two [9,436]. For the **optically thick** approximation, radiative heat transfer within the medium can be treated as a localised

phenomenon, little affected by surface boundaries, so that radiation emitted by a volume element is absorbed within another volume element before it can reach these boundaries. In this case, the diffusion (or Rosseland) approximation can be derived[28] [8] and has the same form as the Fourier conduction law [9]. This enables a radiative conductivity to be defined ($k_R = 16n^2\sigma T^3/3\alpha$) that has the same format as the (molecular) conductivity with the unit W/mK. The effective conductivity is then the sum of both conductivities [8,436,444]. Hence, coupling of conduction and radiation occurs purely for an intermediate optical thickness $\alpha \cdot S$ [437].

For TPV conversion, **Fraas** et al. [445] have pointed out that out-of-band radiation is absorbed in the SiO_2 shields and re-emitted in both directions. They concluded that N shields reduce out-of-band radiation by 1/(N+1).

Pierce and Guazzoni [138] measured different 1 mm thick SiO_2 shields. They also concluded that participating glass shields in a TPV system emit radiation in both directions. Measurements were made of two (non-infrared grade) SiO_2 shields with temperatures fixed at 1073 and 723 K. This arrangement could suppress some of the out-of-band radiation. However, in-band transmission was also reduced when the number of SiO_2 shields was increased.

Physically thick semitransparent media have also been considered for TPV. Such media need not to be cooled but have a temperature gradient across their thickness. **Goldstein and DeShazer** et al. [115-117] in an experiment used single crystals of yttrium aluminium garnet (YAG) as a light guide using total internal reflection with a length of 20 cm. YAG has absorption coefficients below 5 cm^{-1} in the spectral window

[28] The Rosseland approximation needs to be used with care near the boundaries [8].

from 0.19 to 6 μm. Different rare-earth aluminium garnet radiators were applied and the light pipe acted as a partial thermal insulator between the radiator and the PV cell. Both the radiator and the YAG are optically thin and out-of-band radiation was not suppressed within the participating media in the intermediate wavelength range.

Hanamura and Kumano [93-95] modelled and examined experimentally piled SiO_2 sheets as filters for GaSb PV cells. The 1D finite element model (see Table 8-1 for the performance) indicated that in-band radiation is mainly transmitted. They concluded that the remaining attenuation of radiation with wavelengths shorter than 2.2 μm was due to surface reflections of the SiO_2. Out-of-band radiation is absorbed in the glass and provides the facility for regenerative combustion-air preheating [93]. The SiO_2 temperature profile was mainly determined by the flue gas and combustion-air temperature for the direct radiant burner. Experimental results [94] fell short of some modelling results [93]. The radiation output was approximately spectrally broadband up to 4.5 μm, which was attributed to the radiation absorbed and re-emitted by the non-reflective insulation between the SiO_2 sheets [94]. Also, in-band radiation was largely reduced compared to 1500 K blackbody radiation due to multiple glass surface reflections [94,95]. They concluded that a physically thick SiO_2 medium with antireflection coating would be required for improved system performance [94].

8.2.6 Radiative heat transfer enhanced by the refractive index

It is well known, that total blackbody emission into a medium with higher refractive index than n = 1 (other than vacuum or in good approximation air) scales with the refractive index squared, so that the total hemispherical emission becomes $n^2\sigma T^4$ according to the Stefan-Boltzmann law (see Section 2.4) [8,11,437]. It has also been shown that the radiative heat transfer between two infinite opaque blackbody

boundaries comprising a dielectric non-scattering and non-absorbing medium with refractive index n would be $n^2\sigma(T_h^4-T_c^4)$ [8]. Examples where the enhanced radiative heat transfer in a dielectric medium is important are glass tank furnaces [444] and solar concentrators using total internal reflection in a dielectric [68]. A recent experiment demonstrated that this enhancement is also of interest for TPV [227], where a high in-band radiative heat transfer translates into high electrical power densities. In the experiment a PV cell was illuminated by a light emitting diode, where the gap in between was filled with either air (n = 1) or oil (n = 1.5) and the radiative heat transfer increased by about n^2 = 2.25 due to the use of oil [227]. It was concluded that the photon flux is limited by the lowest refractive index in the photonic cavity and scales with the minimum refractive index squared [227,228]. This enhancement was termed Dielectric Photon Concentration in [227] and two approaches were considered. These are the closed space concept (MTPV) and the dielectric insulator concept, where most work has concentrated on the former [228].

The **closed space concept** [227,228] utilises a sub-micron vacuum gap. This gap allows **partial** coupling of the enhanced radiative heat transfer by n^2 while the vacuum gap thermally insulates. The advantages and disadvantages of this concept have been discussed in Section 3.8.

No published work on the **dielectric insulator concept** except the experiments using oil at a low temperature [227] could be found within this work.

8.3 Literature review discussion and focus of this work

8.3.1 Discussion of the literature review

Heat shields, usually made of SiO_2, are commonly used in TPV cavities. In general, there have been only a few publications assessing how these shields situated between radiator and PV cell influence the radiative heat transfer. Modelling by Hottel [50] has not included re-emission of radiation of these shields. However, experimental work by Pierce et al. [138] and Fraas et al. [445] indicates that re-emission of the hot shields needs to be taken into account. It has been pointed out that hot shield re-emits radiation in both direction to the radiator and the PV cell [138,445]. This allows suppression of some out-of-band radiation, but the quality of this suppression can be regarded as limited. External cooling can keep the shield at a lower temperature to minimise re-emission of radiation. However, this can be regarded as generally undesirable, since the energy absorbed and lost by the shield degrades the overall efficiency of the TPV system. Hence, operation of the heat shield in radiative equilibrium with its environment (radiator, PV cells) is of interest.

Another option is the use of multiple shields to improve out-of-band suppression [445,93-95]. However for multiple shields it has been found that not only out-of-band, but also in-band radiative heat transfer is reduced [93-95,138], where reduced in-band transmission, associated with low electrical power densities, is usually not desirable.

Recent modelling of SiO_2 by Hanamura et al. [93-95] suggests that an increased SiO_2 shield thickness in the order of centimetres can improve out-of-band suppression. However, in their work the SiO_2 shield was not in radiative equilibrium since convective heating and cooling from flue gas and combustion-air was anticipated.

The work reported here focuses in particular on dielectric media in the cavity with an increased thickness and in radiative equilibrium with the radiator and the PV cell. It is also concluded in this work that dielectric solids with increased thickness could be used for the dielectric insulator concept [227]. These solids would require a low absorption coefficient in the in-band wavelength range, a high absorption in the out-of-band wavelength range, a high maximum operation temperatures and a low thermal conductivity.

8.3.2 Dielectric material options in the cavity

The discussion in the last subsection established the figures of merit for dielectric solids in a TPV cavity. Both crystalline (e.g. sapphire or yttrium aluminium garnet) and amorphous (e.g. SiO_2) materials can fulfil these requirements [446].

An example of a **crystalline** material is sapphire with a melting point of 2319 K [447] and an absorption coefficient below 1 m^{-1} in a wavelength range from about 1 to 3.3 μm assuming a sapphire temperature lower than 1473 K [448]. Also yttrium aluminium garnet (YAG) has a melting point of approximately 2200 K [115,447] and an absorption coefficient below 500 m^{-1} in the wavelength range from 0.19 to 6 μm [115]. This absorption coefficient is expected here to be lower in a more narrow wavelength range but no values were available for this work. The disadvantages of such crystalline materials are high costs (single crystal growth), high thermal conductivity (13.4 W/mK for YAG and 46 W/mK for Sapphire at 300 K [447]) and low absorption (respectively high transmission) in the out-of-band wavelength range (e.g. above 2 μm).

Alternatively, **amorphous** materials (glasses) offer many of the required characteristics. For high-temperature applications SiO_2 has typically suitable thermo-physical properties (high operation temperature, good thermal shock resistance)

[447,449]. Also the costs and the thermal conductivity are lower compared to the two crystalline example materials. Finally the absorption edge in the infrared is at a shorter wavelength compared to the crystalline examples due to absorption bands at 2.22 and 2.73 μm. SiO_2 has generally promising properties. However, one possible problem is that devitrification may occur for high-temperature cycling [449]. Here the white opaque mass of cristobalite forms in the SiO_2 surface layer and proceeds inwards [449,450]. There are various factors influencing the rate of devitrification, such as the SiO_2 type, operation temperature, exposure time, thermal history and surface contamination [449].

8.3.3 Focus of this work

For the work reported here SiO_2 has been selected as a dielectric solid in the cavity. SiO_2 is regarded superior compared to crystalline material options, although some limitation in terms of SiO_2 devitrification and maximum operation temperature can be expected. Reasons for the selection include the common usage in TPV cavities, the low costs, wide availability, a suitable absorption edge and a low thermal conductivity of SiO_2. The modelling focuses on the SiO_2 aspects in the cavity and includes absorption and re-emission of radiation, as well as conduction within the SiO_2. There are several SiO_2 parameters of interest that influence the radiative heat transfer from the radiator to the PV cells. Also the general configuration of the SiO_2 in the TPV cavity is of interest. These aspects have not been examined in detail previously and are the subject of the remaining part of this chapter.

8.4 Modelling procedure and assumptions

8.4.1 General assumptions

Different software packages are available for heat transfer modelling using approximation methods listed in Table 8-1. For this work a commercially available computational fluid dynamics software package, Fluent, was used [451]. The Fluent software can be applied to model fluid flow and combined modes of heat transfer in complex geometries and offers different radiation models. This software has been previously used to model heat transfer in glass tank furnaces [451]. Hence, it can be expected that the software is also suitable to model coupled heat transfer within SiO_2. For this generic type of study, the 2D Discrete Ordinates radiation model for an infinite plate arrangement of radiator, SiO_2 and PV cells was utilised (1D steady-state heat transfer). Radiative heat transfer is generally dependent on the geometry of the cavity. The 1D heat transfer case is usually regarded as the most general case and has been selected to examine the role of SiO_2 in the cavity.

Throughout the modelling, the radiator and PV cells have been assumed as non-transparent boundaries with a constant temperature. The modelling assumption of a constant radiator temperature is commonly made [260,436,443] and allows the heating of the radiator to be treated independently using other models. For example detailed combustion modelling with heat transfer and mass transfer with heat generation can be regarded as complex to model. It is generally accepted that TPV radiator temperatures range from about 1300 to 2000 K. In this work an intermediate temperature of 1500 K has been assumed. Temperatures around 1500 K can be considered as typical for currently examined TPV generators using GaSb cells and combustion sources [47,376,396]. Planck's radiation law for a temperature of 1500 K defines that about

99.5% of all radiation occurs within the wavelength range from 0.5 to 20 μm, which is thus the range of interest for this work.

As pointed out in the discussion about Equation 8-1, the PV cell temperature should have a minor impact on the radiative heat transfer considering the low operation temperatures of the cells (e.g. typically below 323 K). The PV cell temperature has been assumed constant slightly above room temperature (T_c = 300 K). Water-cooling of the PV cell heat sink commonly maintains a constant cell temperature at the desired value (see Subsection 3.7.3).

Radiator and PV cell surface properties have both angular and spectral dependence. For the generic type of this study, a blackbody characteristic has been assumed for radiator and cell surface (diffuse angle dependence and emissivity $\varepsilon = 1$). This allows modelling of an upper limit of radiative heat transfer and analytical verification for the infinite plate arrangement without SiO_2, as well as some general insights of radiative heat transfer in TPV using SiO_2. Realistic modelling of TPV cavities is more complex and includes aspects such as the geometry, surface properties (angular and spectral dependence) and parasitic heat transfer (conduction and convection). Hence, conclusions drawn from the modelling results obtained in this work need to take these simplifications into account.

8.4.2 Fused silica (SiO_2) assumptions

SiO_2 is available in different grades and these can be classified in electrically-fused (or water-free or infrared-grade), flame-fused and vitreous synthetic silica [449]. The grades differ in their hydroxyl content: electrically-fused (low), flame-fused (intermediate) and vitreous synthetic (high) [449]. Assuming a SiO_2 thickness in the range of centimetres, three wavelength range intervals for the transmission can be distinguished for SiO_2. These are below 2 μm (optically-thin), from 2-5 μm (semitransparent) and above 5 μm (optically-thick). The non-infrared-grade SiO_2 absorption coefficient data $\alpha_{(\lambda)}$ were taken from various sources [452,453]. The absorption coefficient $\alpha_{(\lambda)}$ for longer wavelengths was calculated from the extinction coefficient $k_{(\lambda)}$ given by Philipp using $\alpha_{(\lambda)} = 4\pi \cdot k_{(\lambda)} / \lambda$ [454,455]. In Figure 8-1 data of all sources are shown.

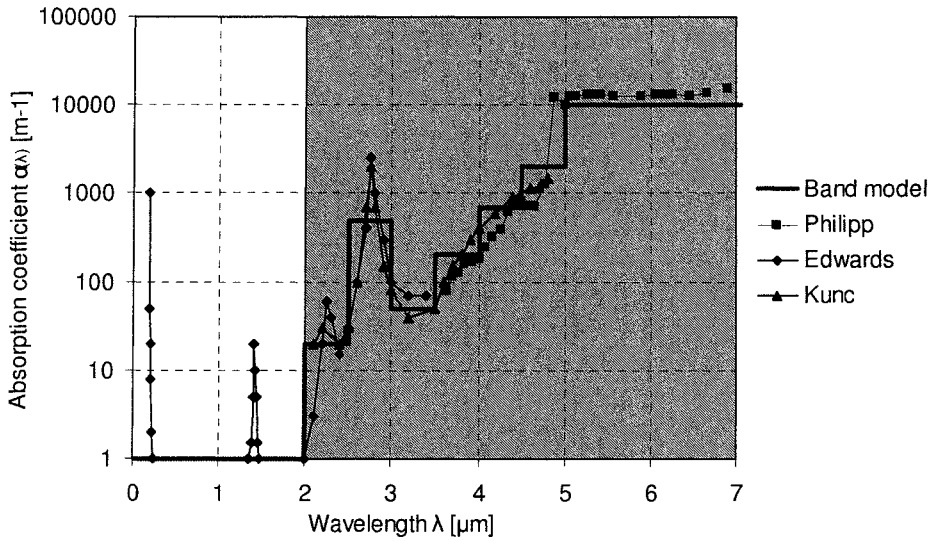

Wavelength λ (μm)	-2	2-2.5	2.5-3	3-3.5	3.5-4	4-4.5	4.5-5	5-
Absorption coefficient $\alpha_{(\lambda)}$ (m^{-1})	1	20	500	50	200	700	2000	10000

Figure 8-1: Absorption coefficient of non-water free SiO_2 and the band model. In this and subsequent figures, the out-of-band wavelength range has been indicated by grey shading. Also, only the wavelength range up to 7 μm has been shown in order to allow the detail to be seen, since this is the range where most of the radiation occurs. The band model data are not only given in the figure but also in the table underneath.

For the modelling, the SiO_2 absorption coefficient was approximated by a band model in 0.5 μm steps in the semitransparent wavelength range (Figure 8-1). The absorption coefficient up to $\lambda = 2$ μm has been assumed to have a value of 1 m^{-1} and considered as the **in-band transmission** range. This definition is approximately in agreement with the GaSb PV cell conversion range up to about 1.8 μm. Actual SiO_2 absorption coefficient values in the window from around 1.2 to 1.6 μm are lower than 1 m^{-1}. This spectral window is utilised for long-distance optical fibre transmission. [455]. For this low absorption wavelength region, losses by scattering need to be taken into account. For the thicknesses in the order of centimetres, considered within this work, scattering can be neglected. Hence, in-band transmission would be expected to be predicted rather too low using an absorption coefficient of 1 m^{-1}. An exception is the absorption peak at 1.38 μm, which has been neglected for the coarse band model. Infrared (IR) grade SiO_2 with reduced absorption for this peak is available.

The wavelength range above 2 μm has been defined as the **out-of-band range** (marked grey in Figure 8-1). Major SiO_2 absorption peaks occur at wavelengths of λ = 2.73 and 2.22 μm [449]. These peaks are also caused by water in the form of hydroxyl groups in the SiO_2 [449]. Here, in contrast to the in-band range, a high absorption coefficient is desirable in order to suppress out-of-band radiation.

Non infrared-grade SiO_2 is thought to be a suitable compromise with a small undesirable in-band absorption peak at the 1.38 μm and stronger wanted out-of-band peaks at 2.22 and 2.73 μm [449,456]. Non infrared-grade flame-fused SiO_2 (Vitreosil®) has been utilised for the experimental work. For this grade more thermo-physical data were available from the manufacturer and the annealing point was higher compared to

the two other grades [456]. Figure 8-2 shows the transmission characteristics of Vitreosil® SiO_2 with its absorption peaks at 2.22 and 2.73 μm.

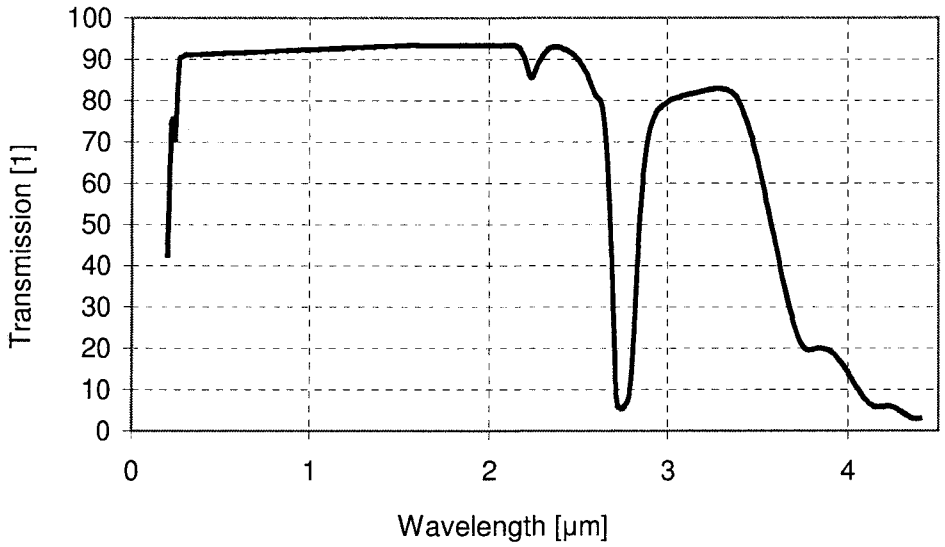

Figure 8-2: Typical transmission of Vitreosil® fused silica with 10 mm path length. The graph has been reproduced from [456]. Data for the wavelength range from 300 to 1600 nm were not available. This range has been interpolated linearly. Note that the reduction in the in-band transmission range is mainly from surface reflections.

The radiative heat transfer within the glass was modelled using the Radiative Transfer Equation (RTE) assuming no scattering (Equation 8-2)[8,9,11,437,451]. The RTE is based on the conservation of radiant energy along a direction $\vec{s}$ at position $\vec{r}$ in a small absorbing and emitting volume element [11]. Physically, the first term on the right-hand side of Equation 8-2 accounts for emission of radiation per unit volume, where Planck's functions $i_{b\lambda(\lambda,Ts)}$ has been defined in Subsection 2.4.2. The second term accounts for the absorption of radiation per unit volume [437].

$$\nabla \cdot \left(I_{(\lambda,\vec{r},\vec{s})} \vec{s} \right) = \alpha_{(\lambda)} \left(n^2 i_{b\lambda(\lambda,T_s)} - I_{(\lambda,\vec{r},\vec{s})} \right) \tag{8-2}$$

In the modelling coupled radiative and conductive heat transfer in the SiO_2 was assumed. Coupling of the two heat transfer modes was taken into account by overall energy conservation according to Equation 8-3. Here, S_r is the radiation source term and

the remaining two terms of the equation describe the transient conductive heat transfer. Since the modelling assumes steady state conditions the left side of Equation 8-3 becomes zero.

$$\rho c_p \frac{\partial T}{\partial t} = k\nabla^2 T + S_r \tag{8-3}$$

The SiO_2 absorption coefficient, refractive index and thermal (molecular) conductivity do not show strong temperature dependence [452] and were assumed constant with temperature for the modelling in this work. The SiO_2 refractive index decreases only slightly in the intermediate wavelength range and was assumed spectrally constant [454]. Typically glass shields used in TPV have optically smooth surfaces. This was taken into account by the modelling assuming specular reflection at the surface by Fresnel's equations and refraction across the surface by Snell's law. Combining these two equations gives the reflected radiation travelling from vacuum into glass depending on the angle of incidence and polarisation (this work assumes non-polarised radiation) [8], so that radiation for angles with large zenith angles is increasingly reflected.

8.4.3 Methodology

First a **base case** arrangement without SiO_2 has been modelled. Modelling results of the radiative heat transfer agreed with the analytical value of 28.7 W/cm^2 according to Equation 8-1. For this base case the computed radiative heat transfer in Fluent within the spectral bands was also successfully verified with blackbody data computed in Matlab (see Blackbody table in the Appendix B). For this and all following cases air

conduction[29] and free convection have been neglected (vacuum conditions). Hence, the total heat transfer from the radiator to the PV cell consists only of radiative components and this makes the modelling results independent of the assumed air gap distances. An exception is the RG arrangement without gap, where the total heat transfer consists of conductive and radiative components.

First the **RAGA** arrangement was modelled and different parameters were varied to gain understanding of how the shield influences the radiative heat transfer from the radiator to the PV cell. They included the absorption coefficient (e.g. total transparent, greybody), the refractive index, the SiO_2 thickness and the SiO_2 temperature (free-floating, external cooling). The latter two are of particular interest, since engineering can be used to alter them. Also the consequences of reflections at the air-glass surface on the radiative heat transfer are of interest.

Modelling results of the RAGA arrangement indicated that the alternative arrangement **RGA** and using an increased SiO_2 thickness should be advantageous. In physically thick semitransparent layers with coupled radiative and conductive heat transfer, non-linear temperature gradients can occur. For the RGA arrangement the impact of SiO_2 thickness and temperature distribution on the out-of-band suppression are of particular interest.

Finally, the **RG** arrangement is proposed and examined in this work. As for the other two arrangements, the dependence of out-of-band suppression on the SiO_2 thickness is relevant. The RG arrangement eliminates air-glass surface reflections. However, the

[29] Modelling in Fluent did not allow zero air conduction. Hence, a value of $1 \cdot 10^{-6}$ W/mK has been selected, which compares small to the real air value between $1 \cdot 10^{-2}$ W/mK and $1 \cdot 10^{-1}$ W/mK shown in Figure 8-3.

total heat transfer not only consists of radiative components, but also of undesirable conductive components. Specifically, the influence of the SiO_2 thickness on the ratio of radiative and conductive components is examined.

The assumptions made have been summarised in the following:

- 1D heat transfer from the radiator to the PV cell boundary
- Blackbody surfaces with constant temperature for the PV cell (300 K) and radiator (1500 K) boundaries
- Air layer: No participation in heat transfer (conduction neglected)
- SiO_2 bulk phenomena: coupled conductive and radiative heat transfer, spectral band model for the absorption coefficient, refractive index wavelength independent, absorption coefficient, refractive index and thermal conductivity temperature independent.
- SiO_2 surface phenomena: specular surface, reflection and refraction according to Fresnel's equations and Snell's law

Figure 8-3 defines the three reference cases for the parametric study.

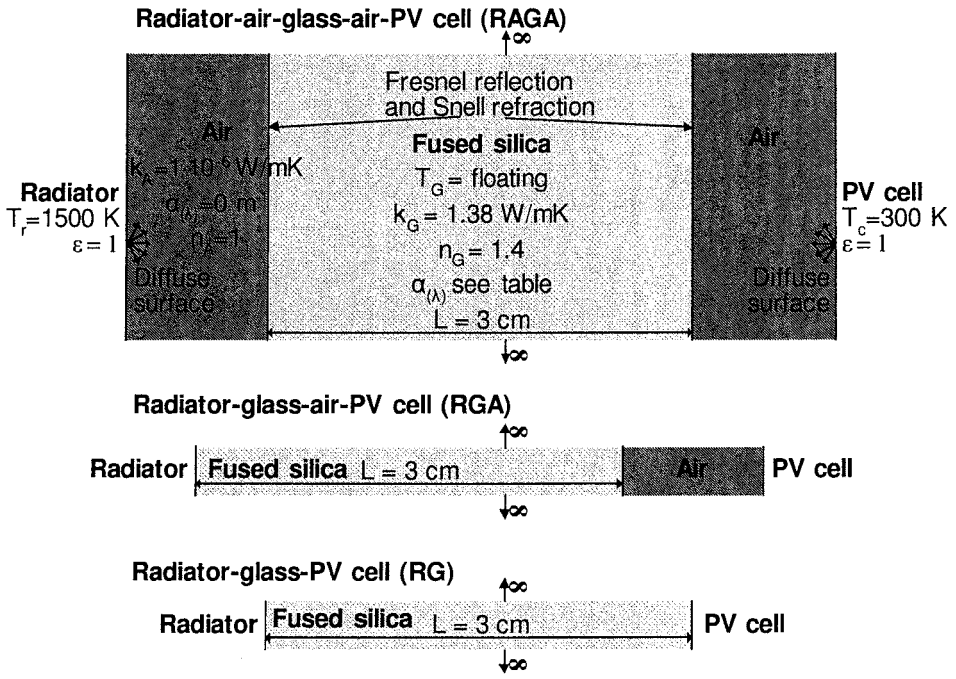

Figure 8-3: Modelling assumptions for the RAGA, RGA and RG reference cases. Note that the air gap is not shown to scale and the thickness does not affect the modelling result since the plates are assumed to be infinite and only radiative transfer across the air gap is considered.

8.5 Modelling results

For the modelling of the three arrangements, the figures of merit for heat transfer from the radiator to the PV cell have been defined as follows:

- A high radiative in-band heat transfer resulting in a high electrical power density
- A high ratio of radiative in-band to total heat transfer resulting in a high efficiency

8.5.1 Results Radiator-Air-Glass-Air-PV cell (RAGA)

For the RAGA arrangement, modelling shows that both in-band and out-of-band radiative heat transfer from the radiator to the cell is reduced, compared to the arrangement without SiO_2 (Figure 8-5).

In-band transmission can be generally high, since SiO_2 has a low absorption coefficient below 2 μm. For a small SiO_2 thickness (below 1 cm), SiO_2 absorption can be neglected and the in-band transmission is only reduced by glass surface reflections. Assuming a diffuse radiator, analytical modelling by Kumano and Hanamura resulted in an in-band transmission of about 86% [95], which is similar to the modelling result here with a value of about 80% (Table 8-2). This reduction has been attributed to a sharp increase of the glass reflectivity for zenith angles larger than 60 ° [95].

	Radiative heat transfer from radiator to PV cell				Total transfer (W/cm^2)	In-band to total (%)
	In-band		Total			
	(W/cm^2)	% of the Base case	(W/cm^2)	% of the Base case		
Base case no glass	**7.8**	100	28.7	100	28.7	**27**
RAGA Ref. case (L=3cm):	**6.1**	78	14.3	50	14.3	**43**
Parameter changes from the RAGA reference case:						
L=0.5 cm	**6.3**	80	18.2	63	18.2	**35**
L=1 cm	**6.3**	80	16.9	59	16.9	**37**
L=10 cm	**5.8**	74	11.2	39	11.2	**52**
L20 cm	**5.4**	69	9.3	32	9.3	**58**
T_G=900K cooling	**6.1**	78	11.5	40	11.5	**53**
T_G=600K cooling	**6.1**	77	8.9	31	8.9	**68**
T_G=300K cooling	**6.1**	77	8.3	29	8.3	**73**

Table 8-2: Heat transfer modelling results of the RAGA arrangement. Note that a base case without SiO_2 has been defined (first data line). The percentage values for all other cases refer to this base case.

In the reference case, the resulting SiO_2 temperature T_G dropped from about 1320 K to 1000 K across its thickness. The impact of shield **cooling** has been modelled by setting the temperature of the entire shield to a constant value instead of the thermal equilibrium case (Figure 8-4). As expected, the cooling impact on the in-band transmission is small, because the in-band reduction is determined by surface reflection.

In contrast to this the **out-of-band suppression** improves for SiO_2 cooling (see Figure 8-4). In practical systems the SiO_2 shield may be cooled due to parasitic losses, or deliberately. However, radiation absorbed and transferred out from the TPV system decreases the overall TPV efficiency. The trade-off between improved spectral control and SiO_2 cooling losses has been not considered further here, since Fluent only gives the absorbed heat of the glass in volumetric units. A 3D modelling in Fluent should allow determination of the absorbed heat by the SiO_2 fixed to a constant temperature, but this was not in the scope of this general study.

Modelling showed that using a physically thin SiO_2 shield allows some moderate **suppression of out-of-band radiation**. For example for a thickness of 0.5 cm the figure of merit for the efficiency, defined as the ratio of in-band to total radiative heat transfer, results in 35% compared to 27% for no SiO_2 (Table 8-5). The out-of-band suppression improves with increasing SiO_2 thickness (Figure 8-5) and this is of particular interest for the subsequent work reported here.

From the RAGA modelling results it was concluded that the alternative RGA arrangement could utilise the out-of-band suppression using increased SiO_2 thickness and should have advantages in terms of in-band transmission due to lower surface reflection losses.

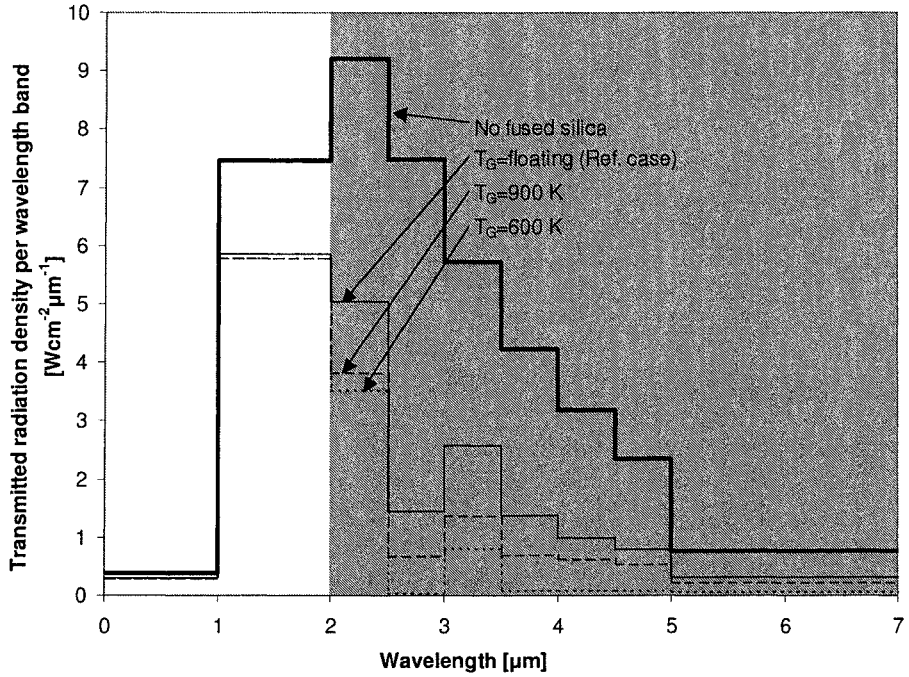

Figure 8-4: RAGA arrangement radiative transfer modelling results, cooled SiO_2. For the reference case the SiO_2 temperature is floating. For the cooling case the SiO_2 temperature was set to a constant temperature of 600 and 900 K in the modelling.

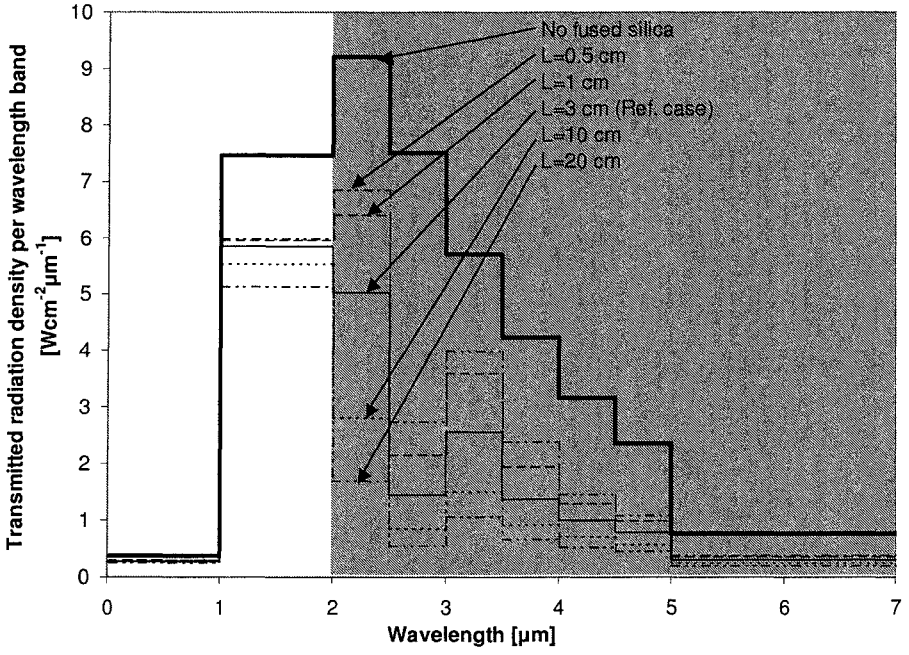

Figure 8-5: RAGA arrangement radiative transfer modelling results, SiO_2 thickness.

8.5.2 Results Radiator-Glass-Air-PV Cell (RGA)

The anticipated increase in **in-band** radiative heat transfer for the RGA compared to that for the RAGA arrangement was confirmed by the modelling (Figure 8-6). This can be explained by the avoidance of reflection at the first air-glass surface.

The **out-of-band** radiative heat transfer of the RGA arrangement is also slightly higher compared to the RAGA arrangement. However, the efficiency figure of merit is similar for both arrangements (Table 8-3). Modelling shows that a SiO_2 thickness of around 10 to 20 cm can suppress a large share of the out-of-band radiation (Figure 8-6).

	Radiative heat transfer from radiator to PV cell				Total transfer (W/cm^2)	In-band to total (%)
	In-band		Total			
	(W/cm^2)	% of the Base case	(W/cm^2)	% of the Base case		
RGA Ref. case (L= 3cm):	**7.5**	95	18.5	64	18.5	**40**
Parameter changes from the RGA reference case:						
L = 1 cm	**7.6**	97	22.6	79	22.6	**34**
L = 10 cm	**7.1**	91	14.3	50	14.3	**50**
L = 20 cm	**6.6**	83	10.8	38	10.8	**60**

Table 8-3: Heat transfer modelling results of the RGA arrangement. Note that a base case without SiO_2 has been defined (first data line).

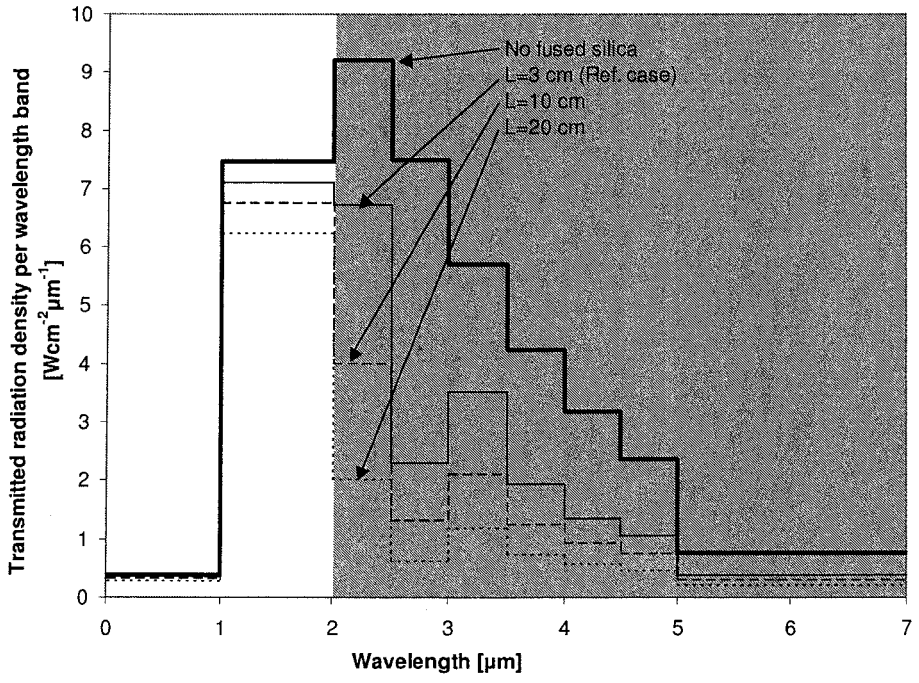

Figure 8-6: RGA arrangement radiative transfer modelling results, SiO_2 thickness.

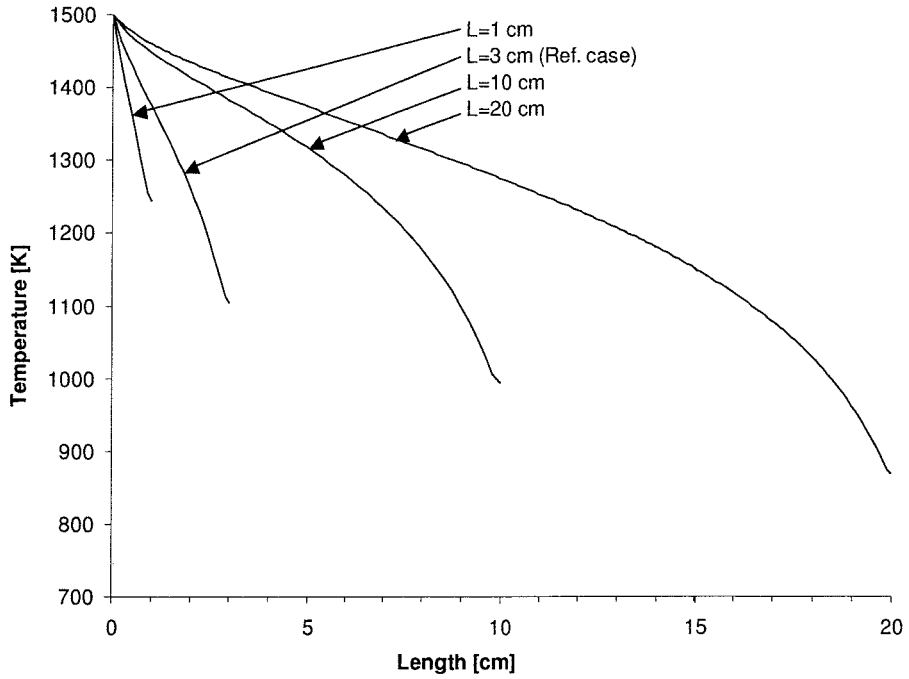

Figure 8-7: RGA arrangement temperature gradient modelling results.

At a thickness of 10 cm the temperature drops from 1500 K to about 1000 K across the SiO_2 (Figure 8-7) and this temperature drop should explain improved suppression for an increased SiO_2 thickness. The volumetric (out-of-band) emission of radiation within the SiO_2 near the air surface at around 1000 K is largely reduced compared to the radiator side (1500 K), because volumetric emission is proportional to the fourth power of the temperature. Other modelling of coupled radiative and conductive heat transfer [8,93] reported similar non-linear temperature gradients as shown in Figure 8-7. The advantage of an air gap in the RAGA and RGA arrangement is the thermal insulation. On the other hand in-band transmission should increase without gap (RG arrangement).

8.5.3 Results Radiator-Glass-PV Cell (RG)

For the RG arrangement, the radiative heat transfer increases to a theoretical value of 56.2 W/cm^2 ($n_G^2\sigma T_h^4$- $n_G^2\sigma T_c^4$) assuming n_G = 1.4 for SiO_2. This value is however not achieved for the RG arrangements since radiation is reduced for out-of-band radiation where the SiO_2 absorption coefficient is high. This phenomenon is beneficial, since improved out-of-band suppression enhances the efficiency of TPV conversion. Additionally it has to be considered that the total heat transfer for the RG arrangement consists of radiation and conduction through the SiO_2. An increased SiO_2 thickness can make the parasitic conductive heat transfer small compared to radiative heat transfer.

The in-band radiative heat transfer is approximately doubled due to the refractive index enhancement (n_G^2=1.96) compared to the previous arrangements assuming a fixed radiator and cell temperature (Figure 8-8). Artificially increasing and decreasing the SiO_2 refractive index n_G in the modelling compared to the reference case shows that in-band radiative heat transfer is correlated with n_G^2 (Figure 8-9). Hence, it can be concluded that high refractive index materials are desirable for the RG arrangement.

The conductive heat transfer for a linear temperature gradient can be calculated analytically as $k_G \cdot \Delta T/L$. For example a SiO_2 thickness of L = 3 cm results in a conductive heat transfer of 5.5 W/cm^2 assuming ΔT = 1500 – 300 K and k_G = 1.38 W/mK. Computational modelling of a SiO_2 thickness of 3 cm resulted in a conductive heat transfer of 10.6 W/cm^2. The higher conductive heat transfer of the computational modelling compared to the analytical calculation can be explained by some additional radiative heat transfer contributing to a higher conductive heat transfer. This combined heat transfer results in a non-linear temperature gradient throughout the SiO_2.

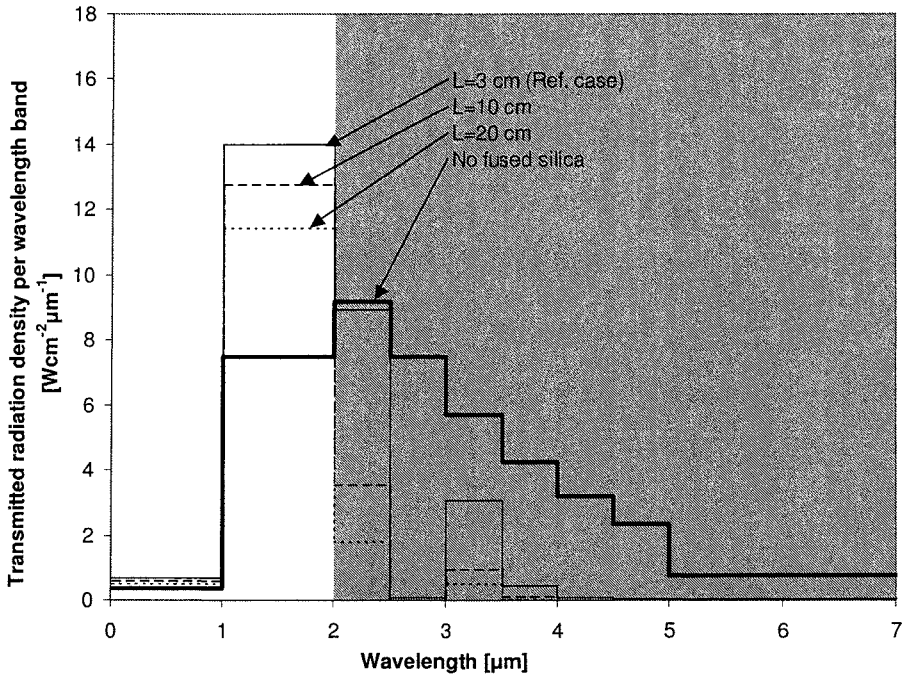

Figure 8-8: RG arrangement radiative transfer modelling results, SiO_2 thickness. The case of no fused silica using an air gap is the same as for the other two arrangements.

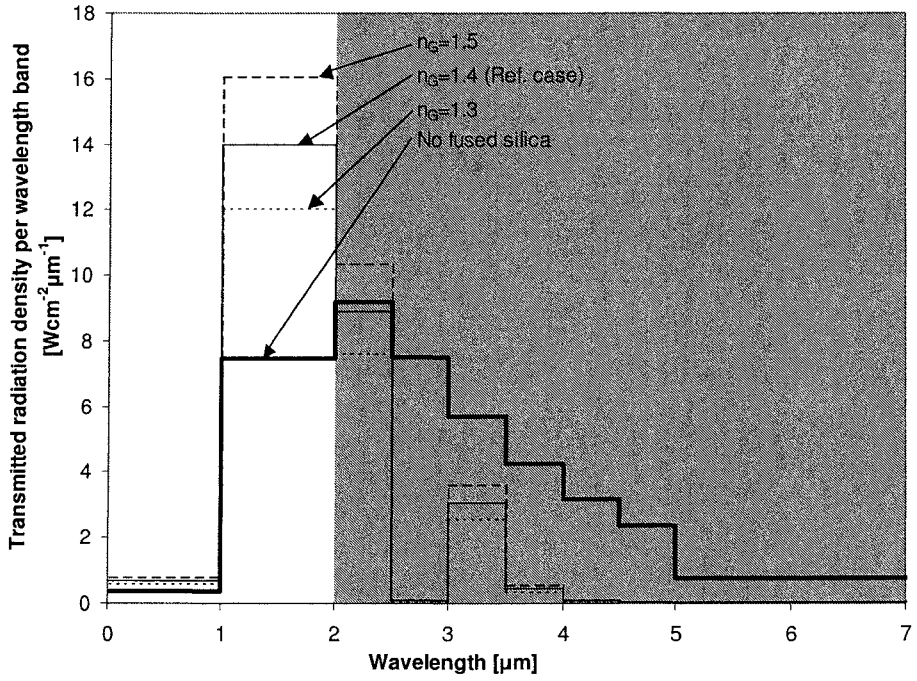

Figure 8-9: RG arrangement radiative transfer modelling results, refractive index.

The share of conductive heat transfer compared to the total heat transfer depends on the SiO_2 thickness. In order to minimise the parasitic conductive heat transfer the SiO_2 thickness needs to be increased. For a thickness of 10 cm the conductive heat transfer is reduced to 5.8 W/cm^2 compared to a value of 10.6 W/cm^2 for a thickness of 3 cm (Table 8-4).

	Radiative heat transfer from radiator to PV cell				Total transfer (W/cm^2)	In-band to total (%)
	In-band		Total			
	(W/cm^2)	% of the Base case	(W/cm^2)	% of the Base case		
RG Ref. case (L= 3cm):	**14.7**	187	21.3	74	31.9	**46**
Parameter changes from the RG reference case:						
L = 10 cm	**13.4**	171	15.9	56	21.7	**62**
L = 20 cm	**12.0**	153	13.4	47	19.0	**63**
n_G= 1.3	**12.7**	161	18.3	64	28.2	**45**
n_G= 1.5	**16.9**	215	24.7	86	35.8	**47**

Table 8-4: Heat transfer modelling results of the RG arrangement. Note that a base case without SiO_2 has been defined (first data line). The percentage values for all other cases refer to this base case. Hence in-band radiative heat transfer can have higher percentage values than 100% for the RG arrangement.

The efficiency figure of merit, defined as the ratio of in-band radiative to the total heat transfer, is found to be higher for the RG arrangement compared to the other two arrangements for a SiO_2 thickness range 3 to 20 cm (Table 8-5). It is believed that this improved ratio is due to the larger temperature difference in the SiO_2 for the RG arrangement, which is fixed by the radiator and PV cell boundaries to 1200 K.

8.6 Summary and conclusions

Table 8-5 sums up all results of the parametric modelling for the three arrangements.

	Radiative heat transfer from radiator to PV cell				Total transfer (W/cm^2)	In-band to total (%)
	In-band		Total			
	(W/cm^2)	% of the Base case	(W/cm^2)	% of the Base case		
Base case no glass	**7.8**	100	28.7	100	28.7	**27**
RAGA Ref. case (L=3cm):	**6.1**	78	14.3	50	14.3	**43**
Parameter changes from the RAGA reference case:						
L=0.5 cm	**6.3**	80	18.2	63	18.2	**35**
L=1 cm	**6.3**	80	16.9	59	16.9	**37**
L=10 cm	**5.8**	74	11.2	39	11.2	**52**
L=20 cm	**5.4**	69	9.3	32	9.3	**58**
T_G=900K cooling	**6.1**	78	11.5	40	11.5	**53**
T_G=600K cooling	**6.1**	77	8.9	31	8.9	**68**
T_G=300K cooling	**6.1**	77	8.3	29	8.3	**73**
RGA Ref. case (L= 3cm):	**7.5**	95	18.5	64	18.5	**40**
Parameter changes from the RGA reference case:						
L = 1 cm	**7.6**	97	22.6	79	22.6	**34**
L = 10 cm	**7.1**	91	14.3	50	14.3	**50**
L = 20 cm	**6.6**	83	10.8	38	10.8	**60**
RG Ref. case (L= 3cm):	**14.7**	187	21.3	74	31.9	**46**
Parameter changes from the RG reference case:						
L = 10 cm	**13.4**	171	15.9	56	21.7	**62**
L = 20 cm	**12.0**	153	13.4	47	19.0	**63**
n_G= 1.3	**12.7**	161	18.3	64	28.2	**45**
n_G= 1.5	**16.9**	215	24.7	86	35.8	**47**

Table 8-5: Heat transfer modelling results of the RAGA, RGA and RG arrangement. The important figures of merits are shown bold. These are the in-band radiative heat transfer for high power densities and the ratio of in-band radiative to total heat transfer for high efficiencies.

In this chapter, radiative heat transfer modelling in TPV has been reviewed and three SiO_2 arrangements in a cavity have been modelled using the Discrete Ordinates method. A commonly used arrangement, radiator-air-glass-air-PV cell (RAGA) has been modelled using SiO_2. Practical systems using this arrangement have achieved some moderate suppression of out-of-band radiation, which could be confirmed by the modelling. Modelling results suggest that increasing the SiO_2 thickness could further improve out-of-band suppression. From the RAGA modelling it was concluded, that an alternative arrangement radiator-glass-air-PV cell (RGA) using an increased SiO_2 thickness should have advantages. Modelling of the RGA confirmed benefits in terms of

enhanced in-band transmission due to lower reflection losses compared to the RAGA arrangement. The out-of-band suppression of the RGA arrangement was slightly lower but generally similar to the RAGA arrangement. The RGA arrangement is expected to have the advantage of simple and practical implementation using total internal reflection in the SiO_2 instead of challenging high-temperature mirror design.

Recently, it has been proposed, that the photon flux is limited by the lowest refractive index in the photonic cavity and is proportional to the minimum refractive index squared [227,228]. An arrangement without gap using dielectric solids was proposed in the work reported here and this was modelled as the radiator-glass-PV cell (RG) arrangement. For a SiO_2 thickness from 3 to 20 cm, modelling results show that the RG arrangement is superior compared to the two other arrangements in terms of enhanced in-band transmission and improved out-of-band suppression. The in-band transmission is enhanced by a factor of about two for SiO_2. This could potentially double the power density compared to TPV systems using gaps. For high efficiencies it is important to minimise out-of-band radiative and parasitic conductive heat transfer. Both can be minimised by increased SiO_2 thickness, while in-band radiation is mostly transmitted through the SiO_2. The results in bold, shown in Table 8-5 multiplied by the PV cell in-band conversion efficiency can be used to estimate the power density and efficiency for an infinite plate TPV arrangement. For example, assuming a GaSb cell efficiency of around 31% (e.g. see Subsection 3.6.3) results in a maximum power density of about 4.6 W/cm^2 for the RG arrangement and an efficiency η_{PV} of up to about 19% for the RGA arrangement. In the next chapter, experiments of the RGA arrangement are reported.

9 Experimental work

9.1 Aims and methodology

This work has identified optical control, and spectral control in particular, within TPV cavities as an aspect where system performance can be improved. This work focused then on the use of bulk SiO_2 to achieve this. In Chapter 3, the disadvantages of various other spectral control options were discussed. The SiO_2 approach selected here is regarded as a robust engineering option (e.g. compared to thermally unstable or evaporating radiator structures) and SiO_2 is commercially available in a range of grades and shapes. Physically thin SiO_2 shields are widely utilised in TPV systems. Modelling showed that these thin shields already provide some spectral control and that this should improve for an increased SiO_2 thickness. In order to verify the modelled SiO_2 arrangement described in Chapter 8, **fundamental decisions about the experimental set-up** need to be made (Section 9.2). These included not only the selection of one of the modelled arrangements, but also the practical cavity design and component selection (e.g. choice of radiator and high-temperature thermal insulation). Additionally, components for an experimental set-up were developed to measure the absorbed heat of the PV cell in order to calculate the cell efficiency. Differences between the 1D

modelling and the experimental implementation were also identified and assessed as to their impact on the verification procedure (Section 9.2).

The design challenges identified led to the development of two experimental set-ups. First, a **preliminary self-made test furnace** was designed and experiments on this furnace were carried out in order to demonstrate the feasibility of the selected approach and to gain experience with high-temperature system design. In Section 9.3 the experimental procedure, results and limitations of this furnace are reported.

Lessons learned from the self-made test furnace were valuable and were used in a more sophisticated second design using a commercial radiant tube furnace. Since this furnace was utilised for the first time, its **characterisation** (Section 9.4) was an essential requirement before experiments on this furnace could be carried out.

In Section 9.5 the implementation of a suitable **experimental set-up** using the radiant tube furnace is presented. This section also discusses the verification of critical parts of this set-up. For the radiant tube furnace, the **experimental procedure** was selected such that relevant characterisation quantities were obtained in order to assess the performance of the set-up. Examples of these quantities are the heat and electricity output of the PV cell, the radiation output spectrum from the SiO_2 and the temperature distribution along the SiO_2 thickness, or rod length (Section 9.6). In Section 9.7 the performance of the **experimental set-up is assessed** and improvements for future system designs are discussed. The **experimental results** in Section 9.8 are presented and discussed in the same order as the experimental procedure. With regard to the modelling, of particular interest are the high TPV figures of merit for the electrical power density and the efficiency. These figures were determined indirectly from experimental results. In Section 9.9 the most important results are **summarised**.

9.2 Fundamental decisions about the experiments

9.2.1 Modelling arrangement selected for experimental verification

In the previous chapter the modelling results of three approaches have been examined: RAGA, RGA and RG arrangement. Although the RG arrangement showed the most promising modelling results, practical implementation of this arrangement was regarded as very challenging.

Considering the RG arrangement, in theory **perfectly smooth SiO_2 and PV cell surfaces** could be arranged to have intimate contact between the surfaces to allow full optical coupling. From MTPV system design it is known that distances in the order of 0.1 μm do not allow full coupling of near infrared radiation (see Section 3.8). Hence, the surface finishing would have to be better than this value and remain in this condition during use.

Another option could be the attachment of the PV cell to the SiO_2 using **optical glue** between the two surfaces [457]. Bearing in mind that the PV cell needs to be fixed to a cooling unit and the SiO_2 expands such experimental arrangement is thought to be also challenging. In addition optical glue may or may not be suitable for an operation at high radiative and conductive heat fluxes. Finally, in the case of PV cell overheating it would be not possible to remove the cell into a safe operation environment, whereas the RAGA and RGA arrangement allow a mechanically independent design of the PV cell and SiO_2 parts. Given these engineering challenges that would need to be overcome to verify the RG arrangement and that the general principle of spectral control using physically thick SiO_2 could be also demonstrated using the RGA arrangement, it was decided to approach experimental verification of the modelling using the RGA arrangement.

9.2.2 Cavity design selected for experimental verification

From the modelling in the previous chapter, it became clear that a SiO_2 thickness in the order of 100 mm or more should give a suitable suppression of the out-of-band radiation. On the other hand, the selected single GaSb PV cell with an area of about 1.33 cm^2 compares small to this SiO_2 thicknesses [177]. Hence, the 1D modelling assumptions differ considerably from the experiment. In the experiment, there is the requirement of a 3D cavity design using a physically small PV cell compared to the SiO_2 thickness. As already discussed in the chapter about optical control (Chapter 4), there are different approaches to design TPV cavities such as lining of the entire cavity with PV cells, the use of mirrors or utilisation of total internal reflection in dielectric materials. Previous experiments by Goldstein and DeShazer et al. [115-117] as well as Horne et al. [269] indicate that TPV systems using total internal reflection approaches have the potential of low optical losses (or high electrical power density). Goldstein et al. used 200 mm long yttrium aluminium garnet (YAG) rods as a light guide and demonstrated electrical power densities of around 1.6 W/cm^2 [115]. Horne applied SiO_2 prisms as optical concentrators (4 times concentration) and projected electrical power densities of around 2 W/cm^2. The power density was estimated within the work reported here from a cell area of 216 cm^2 and an output power 425 W [269]. Also high GaSb cells electrical power densities up to 4.2 W/cm^2 have been reported [357,358]. Hence, SiO_2 rods together with GaSb PV cells have been selected in this work. The rod forms the major part of the TPV cavity and should guide the radiation to the PV cell using total internal reflection. Information regarding total internal reflection is generally available from areas such as long-distance optical fibre transmission [446] and blackbody tipped optical fibre thermometers [458].

In the latter device, an opaque blackbody enclosure can be for example sputtered (e.g. iridium) on the end of the fibre (e.g. sapphire). The fibre then guides the radiation to the detector [458]. The principle of this device has been adopted for the TPV system design in this work, since an implementation holds the promise of coupling a large share of (in-band) radiation into the rod.

Siegel and Howell [9] describe the design of an enclosure emitting blackbody radiation as follows:

> If the cavity is assumed perfectly isothermal and perfectly insulated, and if the exit hole is infinitesimally small so that it does not disturb the radiative equilibrium in the enclosure, then the radiation from the hole is blackbody radiation and hence **the cavity is completely filled with blackbody radiation**. An interesting feature is that under these conditions, the local radiation leaving the cavity wall will be blackbody radiation even though the wall is not a perfect emitter.

A cylindrical enclosure with a finite depth and one open end can be a good approximation of a blackbody (apparent emissivity ε_a close to 1) provided the ratio of depth L to radius R and the wall emissivity ε_w have high enough values (Table 9-1)[8]

	L/R = 2	**L/R = 4**	**L/R = 8**
ε_w = 0.25	0.640	0.844	0.965
ε_w = 0.5	0.839	0.946	0.989
ε_w = 0.75	0.939	0.982	0.996

Table 9-1: Apparent emissivity at the bottom centre of an isothermal cylinder cavity.

The blackbody tipped optical fibre thermometer [458] with a relatively low enclosure wall emissivity (e.g. iridium, platinum) has not been optimised for high values of ε_a. For thermometer applications, a more important design parameter is a constant emissivity for different cavity temperatures. On the other hand, for a TPV system a high ε_a of the enclosure is desirable in order to couple a large share of radiation into the rod. In the publication concerning the fibre thermometer [458] it was concluded that the radiation coupled into the fibre is simply $A \cdot \varepsilon_a$ multiplied with the blackbody radiation without n^2 enhancement, where n is the refractive index and A is the cross-sectional area of the

fibre. This conclusion was based on a paper from 1926 and may be only empirically valid for the special case of the fibre thermometer.

In the following discussions the blackbody tipped arrangement is assumed for an **idealised TPV system** (Figure 9-1, top). It is believed here that heat transfer within the rod is generally complex. As already modelled and discussed in Chapter 8 for the 1D case, heat transfer within the rod takes place by radiation coupled with conduction. Radiative heat transfer is generated and enhanced by n^2 within the medium in wavelength regions where the semitransparent medium is optically thick. Also radiative heat transfer from the opaque enclosure surface into the medium is enhanced by a factor of n^2 [8,9]. However, for the 1D heat transfer case, the radiation leaving the medium into air was not enhanced by n^2 (RGA arrangement). For this infinite plate case, Siegel and Howell explain the phenomenon by the reflection of some radiation with large zenith angle at the inside surface of the medium-air interface [9]. For the idealised arrangement (Figure 9-1, top) radiation should be directed within the rod and incident at the medium-air interface under small zenith angles where reflection is lower than for large zenith angles. Therefore this effect may lead to a radiative heat transfer enhancement in the experimental design compared to the one-dimension modelling. The idealised arrangement also has some radiative heat transfer loss from the rod to the surroundings. One possible ray from the enclosure and one possible ray from a bulk emission are shown in the example in Figure 9-1 (top) as thick grey arrows. Such radiative heat transfer is generally dependent on the surroundings. By designing the thermal insulation so that the temperature of the SiO_2 rod and the insulation are close to each other along the rod length, radiative as well as parasitic conductive and free convective heat transfer losses are reduced.

For the **selected design** a silicon nitride bonded SiC cup was chosen to form an enclosure containing the SiO_2 rod (Figure 9-1). The advantages of SiC compared to other broadband radiator materials have been already discussed in the literature review (Subsection 3.5.2). The cup containing the 25 mm diameter rod was designed with a hole depth of 70 mm and a hole diameter of 27 mm (L/R = 5.2). The L/R ratio was selected to be as large as possible for the given furnace geometry assuming the entire cup needs to be placed in the furnace chamber for a uniform cup temperature. The SiC cup design without SiO_2 would then have an apparent emissivity of more than 0.98 assuming a SiC emissivity higher than $\varepsilon_w = 0.75$ (Table 9-1). A radial gap of 1 mm was chosen to allow for manufacturing tolerances of the components and possibly the future use of one-inch diameter rods.

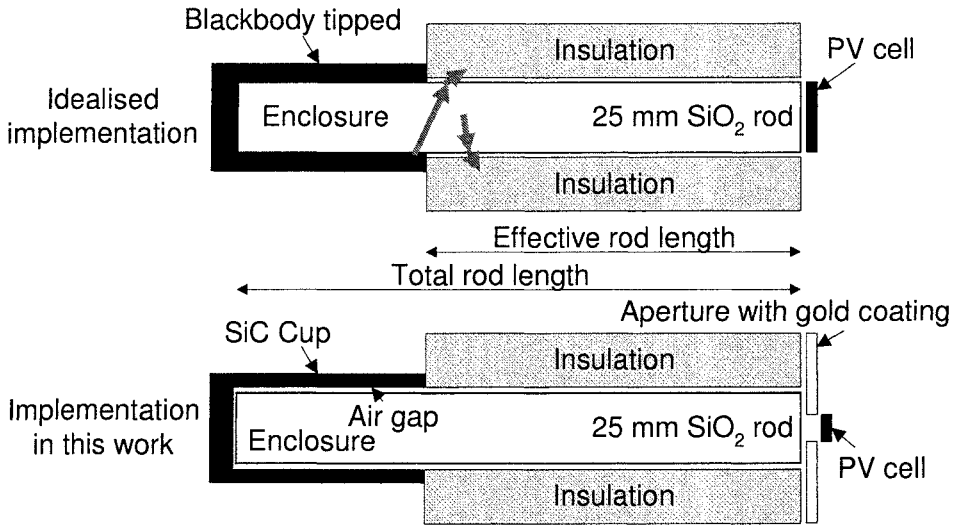

Figure 9-1: Comparison between idealised and selected implementation. The ideal implementation (top) has no air gap between SiC cup and SiO_2 rod and thick grey arrows show two examples of possible radiation rays leading to some radiative heat transfer losses. The selected implementation of this work (bottom) has an air gap and also uses an additional aperture.

Comparing the idealised arrangement and the implemented design (Figure 9-1), there is some uncertainty as to what extent the additional air gap reduces the radiation coupled into the rod due to glass-air surface reflections. However, bearing in mind that

the blackbody enclosure is completely filled with blackbody radiation and the SiC cup is similar to a blackbody enclosure in terms of its apparent emissivity ($\varepsilon_a > 0.98$), it was predicted that radiation coupled into the rod would not be significantly reduced compared to the idealised design.

The surface finish of the as-drawn rods appeared promising for guiding light by total internal reflection. All rod-ends facing the PV cell were ground and polished using SiC paper (240, 400, 600 and 1200 water cooled grit) and subsequent diamond lapping (6, 1 and ¼ micron grades) for all experiments.

Another difference between the selected and idealised designs (Figure 9-1) is the use of a gold-coated aperture in between the larger round SiO_2 rod and the smaller rectangular active PV cell area. The gold coating has been favoured because it is highly reflective in the IR and was used to reduce the cooling demand for the aperture. However, the high IR reflectivity of gold over a wide wavelength range would also be expected to lead to multiple reflections between the SiO_2 surface and the aperture. It seems likely that these multiple reflections enhance the radiation absorbed by the PV cell compared to the idealised design where the SiO_2 rod and the PV cell surface match.

Hence, the experimental implementation includes several additional aspects, which may impact on the heat transfer, if compared to the 1D modelling arrangement. Some of these aspects are expected to increase and some should decrease the radiative heat transfer to the PV cell. Therefore, the radiative heat transfer may be predicted to be too high or too low depending on the their impact.

9.2.3 Measurement of the efficiency

As already discussed in the literature review, there are several efficiency definitions in TPV conversion depending on the input and output assumptions (Section 3.3). For

the waste heat application considered here it is of interest to maximise the ratio of electricity output to extracted process heat. Within this work it was not feasible to measure TPV cavity losses along the SiO_2 rod. Also, the air gap between the SiO_2 rod and the PV cell is not an optimised TPV cavity design. Hence, cavity losses are not assessed here and the efficiency discussion is restricted to the PV cell level. This efficiency η_{PV} has been already defined as the ratio of electricity output to the sum of absorbed heat and electricity output (Equation 3-3, Chapter 3). From the modelling it is expected that η_{PV} increases for longer SiO_2 rods. The following requirements were identified in order to determine the efficiency η_{PV} experimentally:

1. The heat output of the PV cell P_{heat} needs to be transferred away from the cell and quantified (heat flux measurement).
2. Only radiation absorbed by the active PV cell area should contribute to P_{heat}.
3. The PV cell temperature is a parameter of η_{PV}. Hence, this temperature needs to be fixed during the experiment. The impact of the cell temperature is also of interest.
4. The electricity output of the PV cell P_{el} needs to be quantified. This requires determination of the maximum power point of the PV cell.
5. The absorbed heat should increase if the PV cell is replaced by a black surface, since the PV cell reflects back some of the radiation.

9.2.4 Measurement of the absorbed heat

There are several methods to measure heat fluxes and these methods are reviewed elsewhere [459-462]. The approaches of heat flux measurement used in TPV experiments can be broadly classified into three groups: spatial temperature difference (1), temperature change with time - Calorimeter (2) and energy supply and removal with heat balance (3).

For the **first method** the PV cell was mounted on a copper pedestal with two thermocouple sensors mounted along its length [228,439,463]. The thermal power transferred through the pedestal is given by Equation 9-1, where k is the thermal

conductivity, A is the cross-sectional area of the pedestal, d the distance of the temperature sensors and ΔT the temperature difference between the two sensors [463].

$$P = \frac{k \cdot A}{d} \Delta T \tag{9-1}$$

The **second method** (Calorimeter) measures the transient behaviour of an insulated thermal mass [96,357]. One advantage is that only one temperature sensor is required. A drawback is that no steady state measurements can be made, since the mass increases its temperature with time. Equation 9-2 allows calculation of the thermal power absorbed by the mass, where m is the weight and c_p the specific heat capacity of the mass. The transient behaviour of the mass temperature dT/dt is discussed elsewhere [459,461].

$$P = m \cdot c_p \cdot \frac{dT}{dt} \tag{9-2}$$

The **third method** is commonly used in TPV systems with water-cooled PV cells [46,91,463]. Here the heat absorbed is measured indirectly by measuring the water flow rate V_w and the water temperature difference before and after the PV cell ΔT. The water density and the heat capacity were assumed temperature constant in this work (ρ_w = 1003 kg/m^3, $c_{p,w}$ = 4187 J/kgK at 298 K).

$$P = V_w \cdot \rho_w \cdot c_{p,w} \cdot \Delta T \tag{9-3}$$

In this work steady state conditions are anticipated and hence the calorimeter method was not utilised. Instead a similar approach as described by Gethers et al. [463] using the first and last method simultaneously was adapted for this work.

In order to demonstrate the feasibility of the SiO_2 rod approach, preliminary experiments were designed.

9.3 Preliminary furnace tests

9.3.1 Experimental procedure

This experiment aimed to demonstrate the feasibility of the SiO_2 rod approach and to gain experience with high-temperature system designs, where engineering challenges were expected to be greater for temperatures higher than about 1300 K (Section 5.6). Three preliminary furnace chambers were developed enclosing a SiC cup. This cup contained a 10 mm diameter SiO_2 rod with one ground and polished end standing out of the furnace. Initially a jeweller's blowtorch using a propane-air flame heated the chamber. This set-up only achieved a maximum temperature of about 1400 K inside the SiC cup. The desired temperature of 1500 K was obtained using a jeweller blowtorch operating with bottled propane and oxygen. For both gases a flashback arrestor was used for safety reasons. In the final furnace design, the furnace chamber was made from one insulating firebrick. Another complete firebrick covered the chamber. The flue gas was extracted at the top of the chamber using a fan (Figure 9-2).

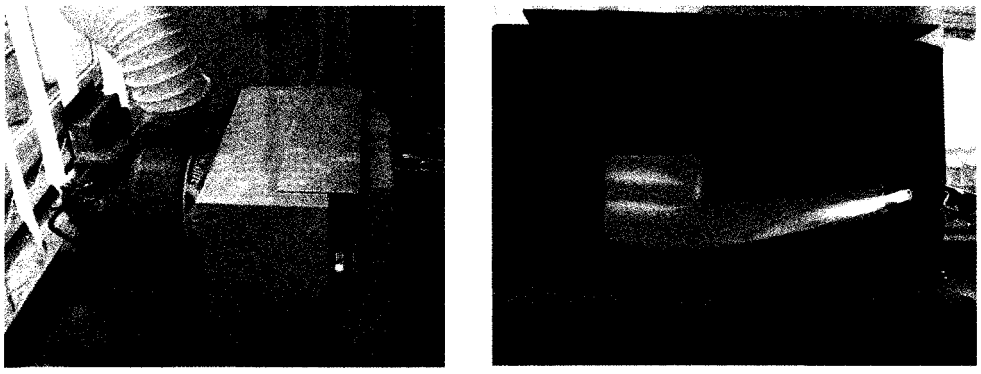

Figure 9-2: Two photographs of the preliminary test furnace.
The furnace was made of insulating firebricks. The left hand picture shows the entire furnace with the fan exhaust extraction unit on the left and the 10 mm SiO_2 rod at the front. The right hand picture was taken immediately after opening the furnace. The blowtorch, the glowing SiC cup and the SiO_2 rod are visible.

The pyranometer CM3 from Kipp & Zonen was utilised to estimate the quality of the light guidance (or losses of radiation from the rod surface) [464]. The pyranometer measures a maximum radiation of 0.15 W/cm^2 in a wavelength range from about 0.3 to 2.8 μm. At a constant reading of 0.1 W/cm^2 the distance between the SiO_2 rod-end and the pyranometer was used as a measure of the radiation output of the rod.

9.3.2 Experimental results and discussion

The experiments highlighted in general the importance of suitable cavity design for temperatures above around 1300 K. The flexibility of this experimental set-up allowed several furnace designs to be constructed. The initial designs were found to possess too many un-insulated regions that enabled significant loss of radiation such that the target temperature of 1500 K was not reached. The final design (Figure 9-2) took account of this and also allowed rapid heating (10 minutes) from room temperature to 1523 K.

The radiation guidance of the **SiO_2 rods** appeared to be promising. Almost no radiation leaving the rod surface was observed and the end face of the rod was bright orange. This is visible in Figure 9-2 to some extent. At a constant pyranometer reading of 0.1 W/cm^2 the distance between the SiO_2 rod-end and the pyranometer was 32 mm and 31 mm for a total rod length of 170 mm and 270 mm respectively (effective rod length outside the cup 100 and 200 mm). This slight decrease in radiation intensity for a 100 mm increase in rod length may have been due to furnace temperature variation or due to desired absorption in the SiO_2. It was concluded that the SiO_2 surface finish is suitable for the anticipated rod lengths to guide radiation by total internal reflection to the PV cell. Hence within this work, the SiO_2 surfaces were not further treated, except the end face.

This conclusion is strengthened by an experiment using a 170 mm **sapphire rod** with rough surface finish and a polished end face. The same experimental set-up was used as for the SiO_2 rod and the distance between the sapphire rod-end and the pyranometer was only 20 mm with considerably more visible radiation leaving the rough surface compared to the previous experiment. These results show, as expected, that the light guidance depends critically on the surface finish.

The **insulating firebricks** were found to have suitable thermal insulation properties. Also machining of these bricks to different shapes proved to be straightforward and the bricks seemed to be an appropriate insulation option around the SiO_2 rods and they were considered suitable for the later experimental system design using the radiant tube furnace.

The **uniformity of the temperature inside the SiC cup** was also verified. This was achieved by removing the SiO_2 rod from the cup and closing the opening hole in the furnace using another insulating firebrick. A small hole in this brick allowed measurement of the temperatures inside the SiC cup with an N-type thermocouple. In the hot zone of the furnace (40 mm range from the SiC cup tip) a relatively constant temperature within +/- 5 K was measured along the cup.

9.3.3 Lessons learned from the experiments for further experiments

One major difficulty of the preliminary test furnace was the **control of the furnace temperature** over longer time periods to carry out or reproduce experiments. Small gas flow changes on the manually controlled jeweller's blowtorch resulted in large temperature changes in the furnace (in the range of +/- 50 K). In addition the temperature in the furnace tended to drift and equilibrium conditions were difficult to achieve. The radiant tube furnace used in later experiments was manufactured with a

temperature control and hence was expected to achieve constant and adjustable furnace temperatures. It became clear that the radiant tube furnace needed to be characterised in terms of its temperature distribution before a TPV test system could be implemented. Also the flue gas was analysed along with this characterisation to ensure a correct furnace operation (Section 9.4).

For a long exposure time, the **firebricks** did not withstand the temperature of the propane-oxygen flame. Cracks and surface deformation were observed. Firebricks are available for different temperature classes, where the disadvantage of the higher temperature types is their higher density associated with a higher thermal conductivity (poorer insulation). In order to avoid sharp temperature drops along the SiC cup and the SiO_2 rods, it became clear that the cup and the rod require thermal insulation in a later design. Hence, a suitable insulating firebrick type (grade 23) was selected for the later radiant tube experiments.

The preliminary furnace tests were limited to 10 mm diameter SiO_2 rods. A larger sized redesign of the furnace would have been required to implement the 25 mm rod. It is not clear whether the **blowtorch power** would have been high enough for such a preliminary furnace. For the experiments on the radiant tube furnace, it was decided to calculate a heat balance to obtain information about the maximum available heat for the TPV experiments (Subsection 9.4.2).

The **pyranometer measurements** only measured the total light guidance of radiation with wavelengths below 2.8 μm. In order to examine the suppression of long-wavelength radiation in thick layers of SiO_2, not only the pyranometer measurements, but also additional characterisation methods were required. Measurements of the spectral radiation output of the SiO_2 rods using a spectroradiometer should show

suppression of long wavelength radiation as the SiO_2 thickness increases. Another selected approach for verification was the examination of the installed PV cell performance, namely the electrical and absorbed heat output of the cell. These values can be used to calculate the efficiency and power density of the cell, where the efficiency is expected to improve for an increased rod length. Hence, it was decided to implement a heat flux meter in the experiments with the radiant tube furnace. Such meter was not only be used to measure the absorbed heat of PV cell with a partly reflective surface, but also to measure the absorbed radiation of a highly absorbing (black) surface. The PV cell measurement is of importance for a practical implementation, since ultimately the installed PV cell performance is critical. The black plate measurement is closer to the modelling assumption and therefore should give additional information for the verification process.

Section 9.5 discusses the design and verification of the experimental set-up added to the radiant tube furnace. Section 9.6 then presents the implementation of the characterisation methods. The following section describes the characterisation of the radiant tube furnace (Section 9.4).

9.4 Characterisation of the radiant tube furnace

Radiant tube burners from the WS-Wärmeprozesstechnik GmbH have been used previously in combustion TPV system designs [46]. The smallest of these radiant tube burners (type C80) was selected for this work [465-468]. The burner itself has a thermal power of 5 – 12 kW and can be operated with various fuels[30]. Natural gas from the utility grid was utilised in this work. The limiting factor of the maximum burner power is the thermal stability of the SiC radiant tube. This tube should not exceed a net heat flux of 5 W/cm^2. Hence, according to the manufacturer the burner can only be fired with 9 kW using the SiC radiant tube. Fuel Furnace Engineering LTD[31] manufactured a complete radiant tube furnace with two custom-made openings to incorporate a TPV system. This work utilises the end port opening (Figure 9-3, Figure 9-7) [469].

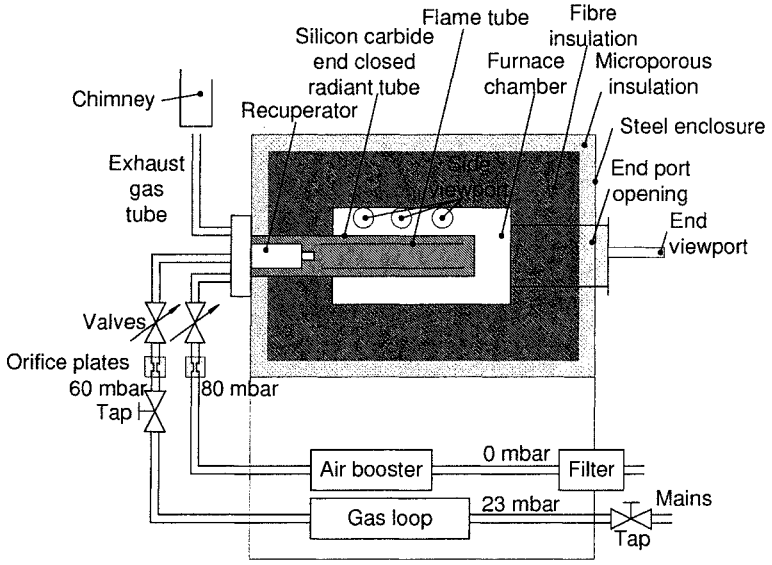

Figure 9-3: Simplified schematic of the radiant tube furnace.
Shown are the radiant tube burner and the air and natural gas supply with the nominal pressures.

[30] These are natural gas, methane, propane, butane and other dust free non-aggressive clean gases.
[31] The previous name is Fuel Furnace Company.

The mains **natural gas** pressure was found to vary in a range from 23 to more than 30 mbar throughout the experiments. A loop consisting of a regulator [470] and a booster [471] normally increases and controls this pressure [468]. The burner manufacturer specifies the pressure before the orifice with 60 mbar +/- 3 mbar (see Figure 9-3)[467]. The regulator in the loop did not allow changing of the pressure and according to the manufacturer a redesign would be required. This problem still exists and the natural gas pressure before the orifice was controlled manually using the gas tap below the orifices throughout the experiments. The natural gas flow into the burner was adjusted using a needle valve after the orifices. This flow was monitored indirectly through the differential pressure across the orifice plate (Figure 9-3).

The ambient **air** is first filtered and then pressurised in an air booster. The air pressure before the orifice was not controlled and varied in a range from 83 to 93 mbar above ambient air pressure in the experiments. These values compare with a nominal air pressure of 80 mbar +/- 4 mbar specified by the burner manufacturer [467]. The airflow was set using the hexagonal needle valve after the orifice. The air then passes through a counter-flow SiC recuperator, which preheats the combustion air and at the same time cools the exhaust gas (Figure 9-3) [467].

The preheated air and the natural gas are burned mainly inside the flame tubes and the combustion products return between the flame tube and the radiant tube, as shown in Figure 9-3. The space between burner end and flame tube is generally critical and is designed such that re-circulation of the combustion gases takes place around the flame tube. A burner breakdown occurred during the experiments and this may have been the result of dislocated flame tubes due to a furnace relocation. The high velocity of the

combustion gases (up to 100 m/s according to the manufacturer) and the re-circulation result in a uniform temperature distribution along the radiant tube [467].

The varying air and gas pressures, and in particular the varying mains gas pressure, required a constant monitoring and adjustment of the pressures in order to achieve combustion conditions with the desired output power and combustion products. The flue gas was also monitored during the experiments, so that the remaining oxygen in the flue gas was in the nominal range from 2 to 4% by dry product volume.

9.4.1 Flue gas analysis

The volumetric flue gas composition on a dry basis was measured using a flue gas analyser (bold values in Table 9-2)[472]. The remaining compositions on a wet and dry basis by weight and volume were calculated using these measured values and assuming a typical North Sea natural gas composition [420,473,474].

	Stoichiometric	**Experiment**			
	By volume	**By volume**		**By weight**	
	Wet	**Dry**	**Wet**	**Dry**	**Wet**
CO_2	9.6%	**10.3%**	8.6%	15.3%	13.6%
O_2	0	**3.0%**	2.2%	3.2%	2.9%
N_2	71.6%	86.7%	72.4%	81.5%	72.7%
H_2O	18.8%	-	16.8%	-	10.8%

Table 9-2: Flue gas analysis on dry and wet basis by volume and weight. The stoichiometric values are from [420]. The measured values are shown bold. All other values have been calculated, where details are in the Appendix E.

9.4.2 Heat balance

For the heat balance a set of values was measured within one experiment. The flue gas temperature of around 773 K (500 °C) was determined by inserting a K-type thermocouple a few centimetres from the top in the exhaust gas tube (Figure 9-3). The differential pressures across the orifices were ΔP_{gas} = 13 mbar and ΔP_{air} = 16 mbar. The volumetric flue gas composition was the same as in Table 9-2 (marked bold).

Furthermore, calorific, density and composition values of a typical North Sea natural gas have been assumed [420][32]:

H_u = 34.91 MJ/m^3, ρ_{gas} = 0.719 kg/m^3
CH_4 = 94.4%, C_2H_6 = 3.22%, C_3H_8 = 0.6%, C_4H_{10} = 0.2%, C_5H_{12} = 0.07%, CO_2 = 0.05%, N_2 = 1.46%

The furnace heat input P_{in} (W) is given by Equation 9-4. The flow rate (m^3/hour) for both natural gas and air were obtained from the measured differential pressure ΔP (mbar) across the orifice using Equation 9-5. The flow coefficient f depends on the hole diameter of the orifice d, the absolute pressure before the orifice P[33], the absolute temperature T and the gas density under normal conditions ρ_N (Equation 9-6)[465]. The orifices for gas and air have a diameter of 2.5 and 9 mm respectively. The two flow coefficients are already given by the burner manufacturer: f_{gas} = 0.25 m^3 hour^{-1} mbar$^{-1/2}$ and f_{air} = 2.4 m^3 hour^{-1} mbar$^{-1/2}$.

$$P_{in} = V_{gas} \cdot H_u \tag{9-4}$$

$$V = f \cdot \sqrt{\Delta P} \tag{9-5}$$

$$f \sim d^2 \sqrt{\frac{P}{T \cdot \rho_N}} \tag{9-6}$$

Initially, the differential pressures of natural gas and air were 4 and 5.5 mbar respectively. The resulting heat input of P = 4.77 kW proved to be too small to achieve a furnace temperature of 1523 K. The heat input was increased to the maximum of 9 kW, when the furnace was commissioned. The furnace temperature of 1523 K[34] was then achieved in 2 to 3 hours, assuming the furnace was heated from room temperature

---

[32] The natural gas net calorific value and density are similar to the burner manufacturer data, in which the composition was not specified [467].
[33] The absolute natural gas pressure before the orifice is the sum of the ambient pressure (e.g. 1013 mbar) and the reported nominal pressures.
[34] The furnace temperature was taken from the control instrument for all experiments.

and the differential natural gas pressure was in the range from 12 to 14 mbar. Once the furnace reached the operation temperature the burner operates in an on-off mode with a cycle time of around 2 to 3 minutes and within a temperature window from 1516 to 1525 K.

The measured values for the differential pressures result in flow rates of V_{gas} = 0.901 m^3/h and V_{air} = 10 m^3/h using Equation 9-5. The ratio V_{air}/V_{gas} = 11.1 is in agreement with the theoretical value of the flue gas analysis V_{air}/V_{gas} = 11.2 (see Appendix E). A furnace power input of P_{in} = 8.8 kW was calculated using Equation 9-4.

The flue gas mass flow rate on a dry basis (kg/hour) was calculated from the density of the natural gas and the mass ratio of combustion products to fuel on a dry basis (see Appendix E). For a stoichiometric combustion the specific enthalpy of the flue gas at 773 K is about 0.6 MJ/kg [420]. It has been assumed that this value represents approximately the enthalpy of the flue gas in this experiment with 3% oxygen. Multiplying the flue gas enthalpy and fuel gas mass flow rate results in a thermal power of about P_{flue} = 1.9 kW (about 22% of P_{in}).

Assuming no other losses and equilibrium conditions, the remaining power of P_{in} - P_{flue} = 6.9 kW (about 78% of P_{in}) is transferred from the radiant burner into the furnace chamber and lost to the surrounding through the furnace insulation. The net heat flux of the radiant burner is then the ratio of 6.9 kW to the effective radiant tube surface area[35] of 2020 cm^2. This results in a value of about 3.4 W/cm^2, safely below the maximum flux of 5 W/cm^2 specified by the burner manufacturer [467].

[35] The radiant tube surface was calculated here from the effective length of the tube (593 mm) and the diameter (100 mm) [467].

9.4.3 Temperature distribution in the furnace

The furnace steel casing is lined with layers of compressed fibre blankets (approximately 220 mm thick) and microporous insulation sheets (75 mm thick) to form the furnace chamber (Figure 9-3) [468]. The temperature in the chamber and insulation was measured using thermocouple probes. Stainless steel thermocouple probes and self-made thermocouples using K-type wire did not withstand the temperatures in the hottest zone (1523 K). In the furnace there are three permanently installed R-type thermocouples for the temperature controller, the alarm and the logger. S-type thermocouple temperature measurements at other locations in the furnace chamber showed values within a few degrees of the R-type values. An older disappearing filament instrument showed temperature values of the furnace chamber about 50 K too low. Above about 1600 K only thermocouples of type R and S containing the noble metal platinum can be used. For the experimental work with several thermocouples, a limited exposure time and a maximum temperature of 1523 K, mineral insulated K-type thermocouple probes proved to be a reliable and economical alternative [475][36]. Below 1300 K Inconel thermocouple probes were also used [475]. Most temperatures were measured with a PC using a temperature data acquisition system [476], but some were also measured manually[37]. This PC based system uses an isothermal block for the cold junction compensation of the thermocouples. The quality of the cold junction

[36] During all experiments only one mineral insulated probe broke under mechanical stress.
[37] A 19" rack with thermocouple reader, switch and 20 thermocouple plugs was made for this purpose.

compensation was tested within this work and drifted by less than +/- 0.1 K for an isothermal block temperature from 293 to 310 K[38].

Figure 9-4 shows the temperature profile at the side and end viewport of the furnace. The temperature within the furnace chamber is approximately constant due to the extensive heat exchange by radiation. Within the insulation the higher temperature of the side viewport may be explained by the large hole in the insulation and heating up of the thermocouple by radiation from the furnace chamber. For the lowest temperature profile (end port with refractory fibre tube), the thermocouple was placed tightly in the fibre insulation. This lower temperature may also be partly due to it being measured before equilibrium conditions had been reached and/or possibly heat loss resulting from some small gaps around refractory fibre tube. The thermal conductivity of the microporous insulation is almost an order of a magnitude lower than that of the ceramic fibre blanket (Subsection 3.7.1). Hence, one may expect that the temperature drop in the thick layer of the ceramic fibre blanket with a relatively high thermal conductivity is small and that the temperature drops steeply in the microporous insulation with a relatively low thermal conductivity. Such a temperature gradient can be found in glass furnaces for example [418]. However, the experimental results indicate rather a linear temperature drop within the insulation.

In addition, the geometry impacts on the temperature gradient. For example, the sidewall of the furnace is approximately radially conductive. This would result in a non-linear temperature gradient due to the difference in heat gain and heat loss area. On the other hand, for the end port the area of heat gain and loss may be approximately the

[38] For this test a thermocouple was placed in ice water. The isothermal block was insulated in Styrofoam and heated using resistance wire.

same so that a linear temperature gradient can be expected, assuming no change in thermal conductivity of the insulation. The combined impact of the described aspects, namely the thermal conductivity and geometry of the insulation, as well as radiation shielding of the measurements, were not further assessed, since this was considered to have a limited contribution for the further experiments.

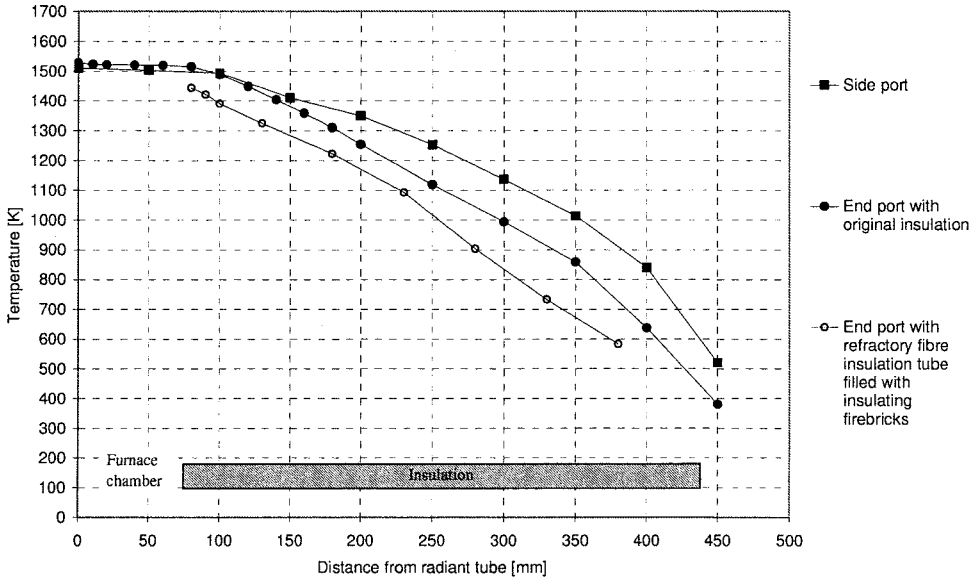

Figure 9-4: Radiant tube furnace temperature versus distance from the radiant tube. The thickness of the furnace insulation is indicated at the bottom of the diagram.

A later experiment measuring four temperatures along a SiO_2 rod placed in the furnace gives an insight into the **transient behaviour** of the furnace (Figure 9-5). As can be seen, the large mass of the furnace requires a long soaking time before equilibrium conditions are reached. This is especially true for the locations further away from the furnace chamber, where a time of more than 10 hours to establish equilibrium conditions is estimated (Figure 9-5). The temperature profiles (Figure 9-4) were taken within a few hours after the furnace temperature was reached. Hence, the measured temperature profiles were additionally influences by the transient behaviour of the

furnace. At least one night of cooling was required before a redesign at the end port opening of the furnace was undertaken.

Several factors indicate that the furnace may not reach the desired temperature, if a large amount of heat would be extracted by a TPV system. These include, the rapid temperature decrease after a furnace shut-off (Figure 9-5), the burner on/off ratio of about 2 (top right hand corner Figure 9-5) and the already increased burner power from about 5 to 9 kW.

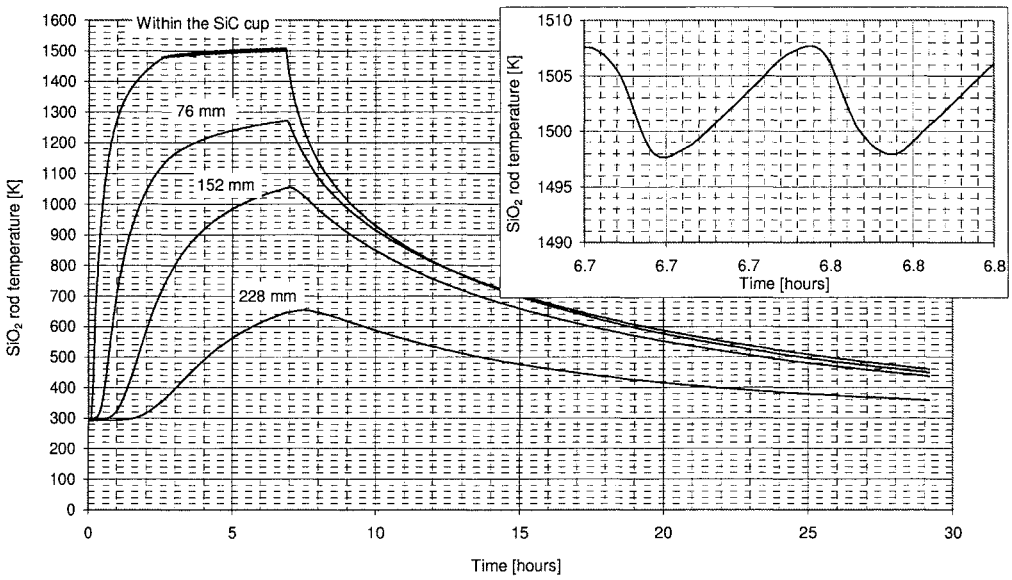

Figure 9-5: Radiant tube furnace transient temperatures of four thermocouples. Heating and cooling temperature curve for four thermocouples along a 10 mm diameter SiO_2 rod placed within the furnace. Details of the furnace on-off cycle are shown in the top right hand corner. The distances of the thermocouples from the SiC cup flange are also shown.

9.5 Configuration and verification of the experiments

In the following subsections, first the installation and verification of the SiO_2 rod and its surrounding components is discussed (Subsection 9.5.1 and 9.5.2). Then, the design, the calibration and the verification of the aluminium tube assembly to characterise the SiO_2 rod is presented (Subsection 9.5.3 and 9.5.4) and the three heat exchangers of this assembly are verified in detail (Subsection 9.5.5 to 9.5.7).

9.5.1 Set-up of SiC cup and SiO_2 rod in the radiant tube furnace

A supportive structure consisting of a refractory ceramic fibre (RCF) tube [477], held by a self-made steel construction, was installed to facilitate the SiC cup and insulating firebricks of grade 23 (Figure 9-6). These firebricks were machined such, that they fitted into the RCF tube and held one or two SiO_2 holding tubes.

These **SiO_2 tubes** held the SiO_2 rod using three SiO_2 support tips on each side of the tube. These tips were made by bending three edges into each side of the heated SiO_2 tubes. The tips had the purpose to hold the SiO_2 rod with a minimum contact area in order to minimise radiation being coupled out and lost from the rod. In addition, it was expected to minimise conductive heat transfer between the SiO_2 rod and the insulation.

SiO_2 rods with three diameters 10, 25 and 50 mm were selected. These rods were cut to different lengths using a diamond saw. For most experiments reported here only the 25 mm diameter rods with the total lengths of 170, 220 and 270 mm (effective rod lengths of 100, 150 and 200 mm) were used with some preliminary tests using the 10 mm diameter and 270 mm long rod.

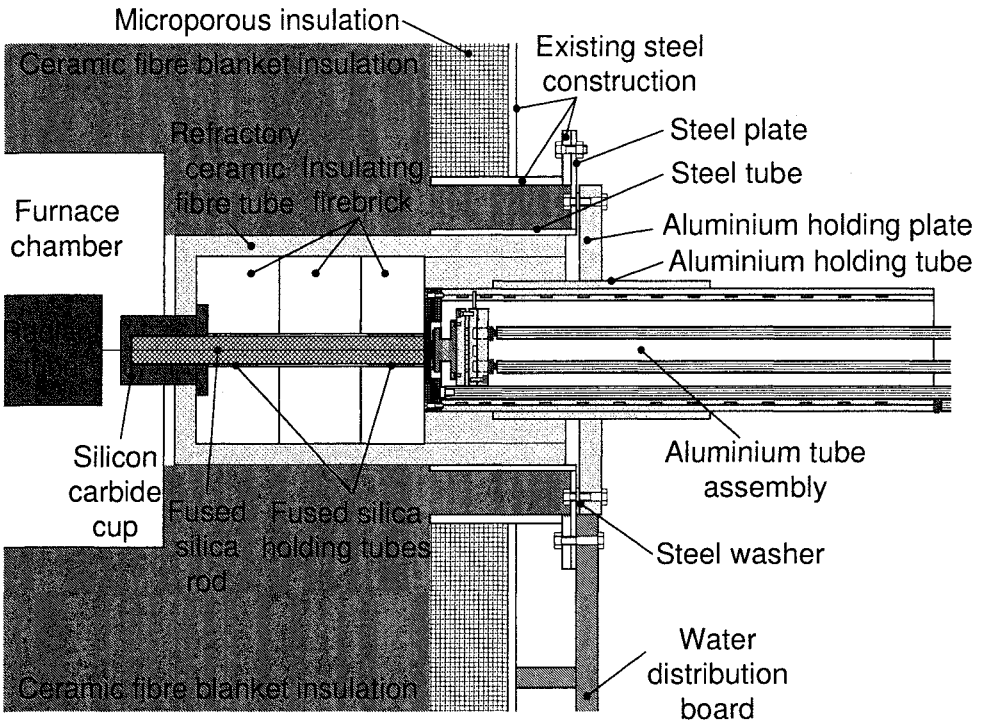

Figure 9-6: Sketch of the experimental set-up in the radiant tube furnace. Details of the aluminium tube assembly are shown in the Figure 9-10.

9.5.2 Verification of the installations in the radiant tube furnace

The steel construction, the RCF tube, insulating firebrick, SiC cup and SiO_2 parts were installed step-by-step. First, only the RCF tube filled with fibre blanket (with and without steel tube) was installed and the temperature distribution was measured using a thermocouple probe. It was found, that a tight fit of the RCF tube within the fibre blanket insulation is important. Localised heating of the steel tube identified gaps in this insulation. For the full installation of the components and heating of the furnace to 1523 K, no experimental high-temperature difficulties were identified.

In order to facilitate precise and repetitive experiments using the installed SiO_2 rod, an aluminium holding tube and plate were installed (Figure 9-6). These two components were permanently fixed using a shrink fit. All further experiments, except the SiO_2 rod

temperature measurements and the pyranometer measurements, utilised the aluminium tube assembly moved into the aluminium holding tube (Figure 9-6). In the following subsection the development of this assembly is discussed.

9.5.3 Design of the aluminium tube assembly with heat flux meter

Initially, cooling of the PV cell using a **forced air-cooled Peltier unit** [478] was considered. Some tests demonstrated the possibility of controlling the cell temperature by applying different voltages to the solid-state heat pump (Peltier element). However, temperature variability of the forced air-cooled heat sink indicated that potential difficulties might occur in PV cell temperature control, because both the heat sink and source temperature varied. Thus, the decision was made to use a **forced water cycle** with a constant inlet temperature as a Peltier heat sink. For this purpose, a water bath kept the inlet temperature constant [479].

As already mentioned (Subsection 9.2.4) two methods have been selected and implemented in order to measure the **absorbed heat of the PV cell**, namely the spatial temperature difference and water heat balance method. The spatial temperature difference method is a more direct measurement method of the two. Thus this method can be expected to be superior in terms of precision, if the required care is taken in the design.

In this work, the **heat flux meter** mass was reduced from that used in the work by Gethers et al. [463] by means of an intermediate stainless steel layer with low thermal conductivity. Two heat flux meters were designed. Difficulties of the first design were overcome by a second design. The second design used a stainless steel layer silver soldered between the two copper pieces and was used for the verification experiments reported in this work. The dimensioning of the stainless steel layer with a thickness of

d = 5 mm was based on Equation 9-1. The assumptions were a minimum temperature difference of $\Delta T = 4$ K[39], a stainless steel thermal conductivity of 0.16 W/mK, a square cross-section of 2 by 2 cm and a minimum power of 5 W[40]. Two K-type thermocouples were glued in holes located on each side of the stainless steel layer (Figure 9-8, left).

Another requirement identified in this work is that only radiation should be measured which is absorbed by the active area of the PV cell. Gethers et al. implemented an independently cooled aperture for this purpose, in which the absorption of radiation by the aperture was reduced using a gold coating [463]. The experimental TPV system in this work has been designed in a similar way but arranged to be horizontal rather than the vertical system used by Gethers et al. (Figure 9-10). This required clamping of the aperture. Also a third cooling water cycle, in addition to the small aluminium heat exchanger and the aperture copper heat exchanger, was introduced, since the PV cell needs to be moved in and out tens of centimetres into the furnace. The third heat exchanger consists of two aluminium tubes, within which cooling water channels were machined into the outside of the inner tube (Figure 9-6, Figure 9-10). A shrink fit permanently fixed the tubes moving the cold inner tube into the heated outer tube.

Each of the three water cycles was designed with a valve to control the **water flow rate** and a flow transducer to measure the flow rate (see Appendix I) [480,481]. The flow rates were measured manually using the frequency output of the transducer and an oscilloscope. K-type thermocouples were installed in the water path entrance and exit of

---

[39] In the dimensioning process it was assumed that the PC data acquisition system has a resolution of 0.04 K. Hence, 100 measurement points can be made for a temperature of 4 K. Later measurements showed an even better resolution of 0.02 K.

[40] Assuming a PV cell with $P_{el} = 1$ W_{el}/cm^2, an active area of 1 cm^2 and an efficiency $\eta_{PV} = 20\%$ results in a maximum absorbed heat of 5 W/cm^2.

each heat exchanger. These installations allow calculation of the thermal power transferred from the heat exchanger to the cooling water using Equation 9-3. The water flows needed to be adjusted, such that the three flow transducer operated within in their specified flow range and that, ideally, temperature differences of a few degrees would be obtained between water inlet and outlet thermocouple measurement. Smaller temperature differences have the disadvantage of a reduced accuracy using the temperature data acquisition system [476].

The aperture was located in close proximity to the PV cell to avoid radiation being absorbed outside the active cell area. It is desirable to keep the aperture and the PV cell at about the same temperature in order to minimise conductive and convective heat transfer between these two components (e.g. through cables or air). There can be a large temperature gradient across the heat flux meter (e.g. for an absorbed power of 20 W the temperature difference is about 20.3 K from Equation 9-1). Hence, the heat sink of the heat flux meter needs to be at a lower temperature compared to the PV cell. This can be for example achieved by using two independent water cycles, where the aperture operates at a higher water cycle temperature than the heat flux meter heat sink. This work employs another novel approach using a Peltier heat pump and only one water cycle. One other TPV publication was identified using a Peltier heat pump to control the PV cell temperature [442]. In the work reported here, the heat sink and the aperture operate at the same temperature using one water bath. The temperature gradient across the heat flux meter is compensated by a temperature gradient with opposite direction across the Peltier element. This also allows control of the PV cell temperature due to regulation of the Peltier power. A control circuit has been realised within this work and is schematically shown in Figure 9-11. An inner control loop maintains a constant

Peltier power and consists of signal conditioning units, the multiplier, the proportional integral (PI) circuit, the H-bridge circuit and the Peltier element. The outer control loop adjusts this Peltier power until the desired PV cell temperature is reached. For this purpose a commercial PID controller [482] was used together with a K-type thermocouple[41] and the inner control loop circuit. A detailed circuit diagram of the Peltier control unit in Figure 9-11 is given in the Appendix H.

9.5.4 Calibration of the heat flux meter

The heat flux meter was calibrated using a heating resistor instead of the PV cell (Figure 9-8, middle). The meter and the resistor were thermally insulated with Styrofoam. Both current and voltage were measured to determine the exact input power of the resistor. The value $A \cdot k/d = 1.0135$ W/K was determined from four measurements at around 5 W and 15 W (see Appendix F). The error of the measured resistor power compared to the calculated power from the temperature difference was always smaller than ± 3.5%[42]. In addition, the entire heat flux meter was placed in an environmental chamber and tested at 253, 273, 293, 313 and 333 K. The values ΔT were found to be always smaller than 0.2 K (or about 0.2 W) for all five steady state temperatures.

---

[41] The temperature of the PV cell was measured and controlled on the copper mounting surface next to the PV cell. Hence, the actual PV cell temperature can be expected higher, but such temperature increase is considered to be small and has not been quantified in this work.

[42] These errors were calculated by the following equation: $(P_{meas} - \Delta T_{meas} \cdot 1.0135 \text{ W/K}) / P_{meas} \cdot 100\%$.

Figure 9-7: Radiant tube furnace photograph, the three side viewports are visible.

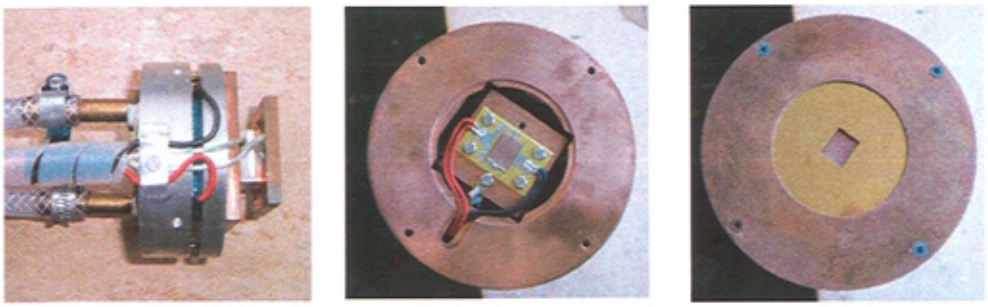

Figure 9-8: Photographs of the heat flux meter unit and aluminium tube assembly. Shown are the single heat flux meter unit (left), the aluminium tube assembly with mounted PV cell (middle) and the aluminium tube assembly with mounted PV cell and aperture (right).

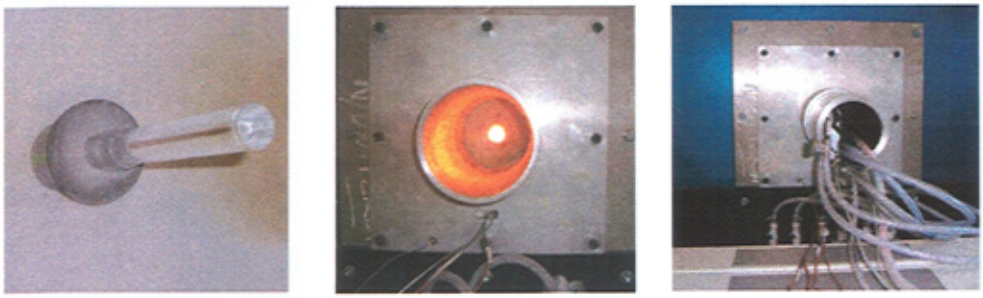

Figure 9-9: Photographs of the experimental set-up in the radiant tube furnace. Shown is the SiC cup with SiO_2 rod and SiO_2 holding tube (left), the complete experimental set-up without aluminium tube assembly (middle) and the set-up with aluminium tube assembly (right).

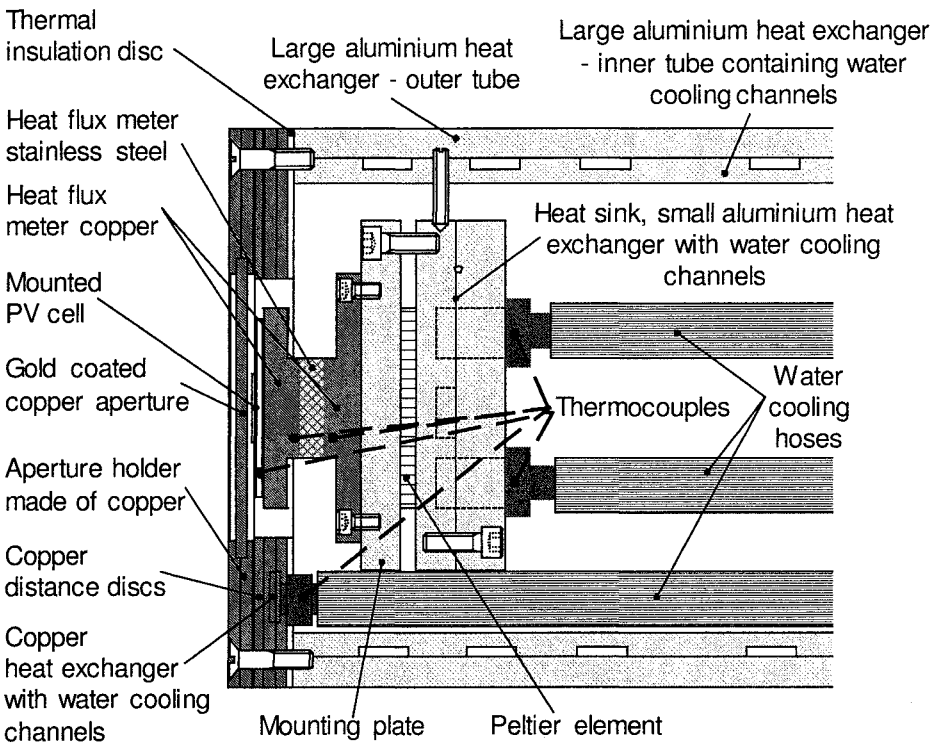

Figure 9-10: Sketch of the experimental set-up, details aluminium tube assembly.

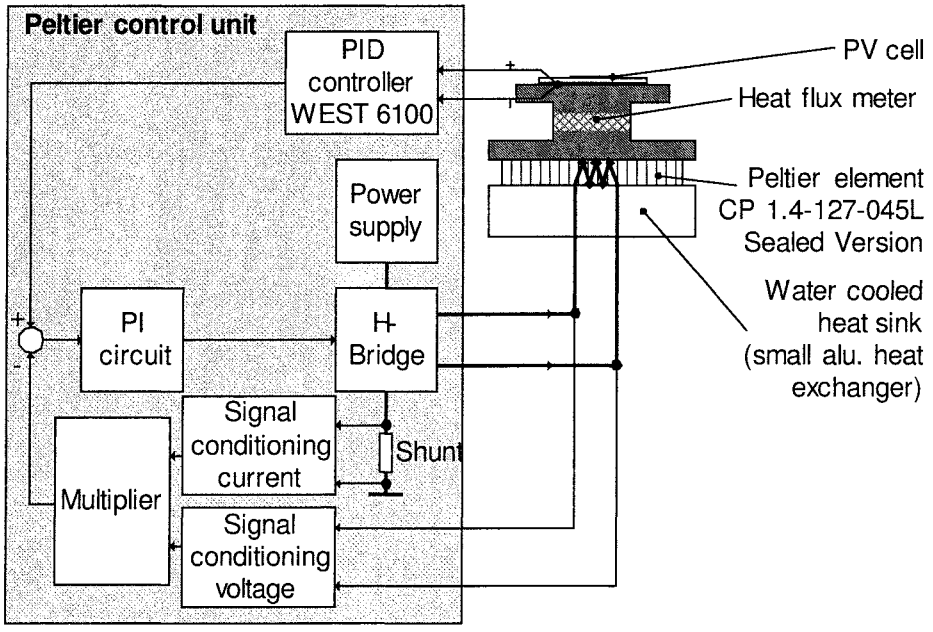

Figure 9-11: Block diagram of the Peltier circuit for PV cell temperature control. The PV cell, the heat flux meter, the Peltier element and the heat sink are also shown on the right hand side. Paths with high currents are drawn with thicker lines. The signal flow is indicated by lines with arrows.

9.5.5 Verification of the large aluminium heat exchanger

In the initial experimental trials unacceptably high heat losses occurred from the large aluminium heat exchanger due to conduction from the aluminium tube exchanger via the aluminium tube holding tube and plate to the furnace steel frame (Figure 9-6). Hence, it was difficult to cool the aluminium tube to low temperatures, such as 283 K (10 °C). To address this, steel washers were used between the aluminium holding plate and the steel plate to minimise this conductive heat transfer (Figure 9-6). These washers were also used to centre the aluminium tube assembly with the fixed SiO_2 rod.

The subsequent four measurements resulted in an absorbed power of about 20 to 30 W for furnace temperatures from 1423 to 1523 K and water bath temperatures from 10 to 293 K. A slow increase of the absorbed power with time was usually observed as result of the length of time the furnace required to reach equilibrium (see Figure 9-5 in Subsection 9.4.3). Another tendency was the increase in absorbed power for lower water bath temperatures (e.g. 283 K) due to the heat absorbed from the surrounding air and the steel frame of the furnace. Other experimental details may have also influenced the absorbed heat of the large aluminium heat exchanger tube (details are in the Appendix J). Their exact influence is difficult to assess, because the conditions were too dissimilar for a reasonable comparison to be made.

For most experiments the space in between the outside of the aluminium tube heat exchanger and the inside of the ceramic fibre tube was filled with ceramic fibre blanket (Figure 9-6). However, this blanket caused scuffing between the aluminium holding tube and the aluminium heat exchanger tube. Removing of the ceramic fibre blanket and the use of anti-scuffing paste overcame this difficulty [483].

9.5.6 Verification of the copper heat exchanger

The copper heat exchanger measures the absorbed heat from the front of the aluminium tube assembly next to the radiating SiO_2 rod (Figure 9-6, Figure 9-10). A change of the SiO_2 rod diameter from 10 to 25 mm increased the absorbed power of the copper heat exchanger from 18 to 29 W. Changes in cooling water temperature had a small impact on the absorbed power. Hence both aspects indicated, that heat absorption is dominated by radiative, conductive and convective heat transfer from the SiO_2 rod to the gold reflector. Multiple photon reflections between the SiO_2 rod and the gold aperture surface should enhance the absorption by radiation. The experiments did not aim to assess this heat absorption in detail (e.g. dominating mode of heat transfer), since an experimental design using a close arrangement of the same-sized SiO_2 face and PV cell could exclude the gold aperture. This would involve a redesign and construction of the set-up, which was not possible within the time constraints of the project.

As already observed for the aluminium tube heat exchanger, the absorbed power of the copper heat exchanger also increased with time, because of the slow thermal response of the furnace.

9.5.7 Verification of the small aluminium heat exchanger (heat balance)

The only heat absorbed by the small aluminium heat exchanger originates from the electrical power to the Peltier element and from the measurement aperture, via the heat flux meter (Figure 9-10). This assumes that no additional heat transfer occurs from the large aluminium heat exchanger tube and the copper heat exchanger. Critical areas in

this assumption are the steel screws mounting the small aluminium heat exchanger[43] and the PV cell cables[44] [177]. The absorbed heat in the water of the small aluminium heat exchanger $P_{small,alu}$ was mainly used to verify the heat measured by the heat flux meter P_{flux}. Knowing the electrical Peltier power $P_{peltier}$ allows calculation of the heat balance for the steady state: $P_{small,alu} = P_{flux} + P_{peltier}$. Experiments at equilibrium confirmed this heat balance.

At a water bath temperature of 283 K (10 °C) condensation on the aperture and aperture holder occurred. At a slightly higher water bath temperature of 288 K (15 °C) no condensation was found during the final experiments. The actual temperatures of the heat exchangers were found to be a few degrees higher than the water bath temperature.

The aluminium tube assembly containing the heat flux meter unit with closed gold-coated copper disc was moved into the furnace in order to test the flux meter at zero heat flux. Here a value of 0.6 W was measured. The most likely cause for this higher value than zero is thought to be some undesirable heat transfer from the hotter aperture via the PV cell cables to the heat flux meter. This effect was compensated by selecting the water bath temperature of the copper heat exchanger (holding the aperture), as well as for the other heat exchangers, to be 5 K lower than the PV cell temperature for all subsequent measurements.

---

[43] The small aluminium heat exchanger is mounted with four M3 steel screws. The heat transfer through these screws between the aluminium tube and the small aluminium heat exchanger is not higher than 0.3 W assuming the thermal conductivity of steel with 0.16 W/Kcm and a temperature difference of not more than 5 K. This heat transfer may be reduced further using stainless steel or plastic screws.

[44] The thermal conductivity of the PV cell lead wires as well as their insulation (Teflon) is not specified by the manufacturer [177]. Also the current arrangement of the cables complicates the calculation of conductive heat transfer through the cables (Figure 9-8). The heat transfer through four copper cables with a length of 2 cm and a copper diameter of 1.5 mm would result in a conductive heat transfer of 0.7 W assuming a temperature difference of 5 K.

9.6 Experimental procedure of the characterisation

9.6.1 Procedure for the pyranometer test with the radiant tube furnace

The radiation output of a SiO_2 rod was compared between the small preliminary furnace, already described in Subsection 9.3.2, and the radiant tube furnace using the same pyranometer. Also the SiO_2 rod dimensions (diameter 10 mm, total length 270 mm) and the SiC cup type and temperature (around 1523 K) were the same for both experiments[45]. For the radiant tube furnace set-up the SiO_2 rod was additionally thermally insulated using insulating firebricks. As for the small preliminary furnace, the radiation output was determined by varying the distance between the SiO_2 rod-end and the pyranometer to obtain a pyranometer reading of 0.1 W/cm^2.

9.6.2 Procedure for the spectral measurement

It was intended that the spectral output of different SiO_2 rod lengths would be characterised in detail with an Optonic Laboratories Inc. OL750 based spectroradiometer [484]. However, due to some measurement difficulties the experiments were limited to one SiO_2 rod with a diameter of 10 mm and a total length of 270 mm. For this measurement, the water-cooled aluminium tube assembly was used[46] without the heat flux meter unit being installed (Figure 9-10, Figure 9-8). The aperture had a diameter of 0.2" (5.1 mm). The distance between the aluminium tube assembly end and the integrating sphere of the spectroradiometer was 25 mm. To prevent stray light effecting the measurements the gap between the tube and integrating

[45] A difference was that the SiO_2 rod was not fully moved into the SiC cup for the radiant tube furnace experiment (1 to 2 cm space).

[46] The water bath temperature was 293 K. Both the aluminium tube and the copper heat exchanger were cooled.

sphere was shielded. The spectroradiometer has two detectors. The first detector is a Si/PbS dual head detector, which measures in the wavelength range from 0.28 to 1.1 μm (silicon) and from 1.0 to 3.2 μm (PbS). The second liquid nitrogen cooled HgCdTe detector has a wavelength range from 1.0 to 14 μm.

9.6.3 Procedure for the black plate measurements

In the modelling chapter the total radiative heat transfer over all wavelengths was computed for the 1D case (Table 8-5). In the experiment a black painted copper plate mounted on the heat flux meter instead of the PV cell has been used to verify this modelling result. In the experiment four different rod lengths were measured using first the 0.2" aperture for the longer and then the 0.4" aperture for the shorter rod lengths, as explained in more detail in Subsection 9.7.7 and Appendix L.

9.6.4 Procedure for the SiO_2 temperature measurements

In order to measure the SiO_2 temperature along the rod three thermocouples were installed for each of the three different SiO_2 installations with a total length of 170, 220 and 270 mm. For the SiO_2 rod with a total length of 100 mm only one thermocouple was installed, because of space limitation in the insulating firebrick. The K-type thermocouple probes had a diameter of 1.5 mm and were arranged into holes in the insulating firebricks so that the side of the thermocouple tip was in contact with the SiO_2 rod. For the two thermocouples measuring the hottest temperatures, mineral insulated types were used [475].

9.6.5 Procedure for short circuit current vs. SiO_2 distance measurements

In this and the following subsections, the PV cell short circuit current or IV curve have been used exclusively or as part of the characterisation of the experimental set-up. The short circuit current has been used in other TPV research work to measure the radiation intensity below the cut-off wavelength of the PV cell [143], since this current is directly proportional to the power generated by the PV cell assuming no change in fill factor and open circuit voltage with varying intensity. The short circuit current was determined by measuring the voltage across a 0.01 Ω shunt resistor with a tolerance of 0.1%.

It is well known that the TPV system performance generally depends on the view factor from the radiator to the PV cell [50]. Hence, the view factor between the SiO_2 rod-end and PV cell can be also expected to have a major impact on the PV cell output in the experimental set-up. Therefore the experimental set-up was designed such that the distance between the SiO_2 rod-end and the PV cell was minimised and offered the flexibility to be increased. For the experiment the case of 'zero distance' was defined, where the aluminium tube assembly was fully moved towards the insulating bricks. At this distance the PV cell was at an actual distance of about 5 mm from the SiO_2 rod-end (Figure 9-6, Figure 9-10). Short circuit current measurements were then made at increased distances of 2, 5, 10, 20, 40, 80 and 160 mm from the 'zero' by positioning of the aluminium tube assembly (Figure 9-6). For the experiment the total rod length was 270 mm and the diameter 25 mm. The short circuit current varied with the on-off cycle of the furnace. Hence, minimum and maximum values of two complete cycles were averaged. After altering the assembly position a time delay of 3 to 4 minutes was add in to allow the current to reach equilibrium conditions.

9.6.6 Procedure for short circuit current vs. SiC temp. measurements

For a TPV heat recovery system, it would be desirable to design a system with a low radiator temperature, since the number of potential processes would increase. However, from the Stefan-Boltzmann law (see Subsection 2.4.3) it is instantly recognizable that the radiation intensity drops sharply for decreasing temperature. For the experimental set-up the sensitivity of the PV cell short circuit current (or electrical power output) depending on the SiC cup temperature is of interest. Measurements at the different temperatures all at thermal equilibrium conditions were regarded as impractical due to the slow response of the furnace (see Figure 9-5). Instead, short circuit current measurements were made during the heating up process of the furnace under non-equilibrium conditions. The SiC cup temperatures were estimated as average values from the furnace temperature at the control instrument and the SiO_2 temperature near the SiC cup. For the experiment the diameter was 25 mm and the total length 270 mm.

9.6.7 Procedure for the electrical output power measurements

Initial tests were made using a **Current Source Measure Unit** to measure the IV curve [485]. This unit cannot be used for currents higher than 1 A. It is possible to reduce the short circuit current, if the distance from the SiO_2 rod-end to PV cell is increased or alternatively the aperture cross-section is decreased (covering of some area of the PV cell). Measurements made with these two reduced current set-ups showed very small fill factors with values around 30%. The reason for these small fill factors was not further examined in this work because of time constraints.

Instead, the IV curve was measured using a range of **resistors** mounted on a cooling plate. The voltage output of the PV cell was determined with sense wires soldered directly onto the PV cell mounting plate [177]. The current was measured using a

0.01 Ω resistor with a tolerance of 0.1%. The resistor load to measure the IV curve had the following values in Ohm: 0.01 (only current shunt), 0.05, 0.1, 0.15, 0.2, 0.25, 1 and open circuits. These eight I-V measurement pairs were averaged for at least one furnace on-off cycle and then matched to curves generated with the one-diode PV cell model (Equation 9-7) [4,5]. Here e_0 is the elementary charge, k the Boltzmann constant and T the absolute temperature of the PV cell. In order to match the curve to the measurement points, four curve parameters were altered, namely the series resistance R_s, the parallel resistance R_p, the saturation current I_s and the photocurrent I_{ph}. The Matlab tool, which has been used for the matching process, is described in more detail in the Appendix G. This tool was also used to compute the maximum power point and the fill factor. The experimental power outputs were divided by the active cell area with grid of 1.33 cm^2 [177] to obtain the electrical power density.

$$I = I_s\left(e^{\frac{e_0(V-I\cdot R_s)}{kT_c}}-1\right)+\frac{V-I\cdot R_s}{R_p}-I_{ph} \tag{9-7}$$

Using this methodology the PV cell IV curves at both 293 K (20 °C) and 313 K (40 °C) for total rod lengths of 170, 220 and 270 mm with 25 mm diameter were measured.

9.6.8 Procedure for the efficiency measurements

For the efficiency calculations the following equation was used: $P_{el} / (P_{el} + P_{heat})$. Here P_{el} is the electricity output and P_{heat} the absorbed heat of the PV cell. This equation was previously defined in Chapter 3 (Equation 3-3). The absorbed heat of the PV cell was measured by two different methods simultaneously, so that two efficiencies were also calculated. Two measurements, rather than one, were preferred to give greater confidence in reassurance of the measurement results.

The first absorbed heat calculations were based on the heat flux meter using the Equation 9-1 with the factor $k \cdot A/d = 1.0135$ W/K determined by the calibration process described in Subsection 9.5.4. Averaged temperatures of the two heat flux meter thermocouples were recorded every 30 seconds with a temperature data acquisition system [476]. The differences of several temperature values were calculated. These differential values were again averaged to obtain the absorbed heat (Equation 9-1).

The second calculation was based on measurements of the Peltier power and the heat absorbed in the cooling water. The absorbed heat by the PV cell was calculated as the absorbed heat in the cooling water minus the Peltier power. This calculation assumes a heat balance, where the only heat in the cooling water originates from electrical power of the Peltier element and the heat absorbed via the aperture. The Peltier power was read manually at the PID control unit from a LCD panel (Appendix H). The absorbed heat in the cooling water was calculated using Equation 9-3 with measured values of the flow rate and temperature difference between inlet and outlet water temperature. The temperature measurement and averaging processes were the same as for the previously discussed heat flux meter.

9.7 Experimental assessment and future work

9.7.1 Assessment of the SiO_2 devitrification

As anticipated some devitrification occurred at the hottest part of the SiO_2. There may be various ways to overcome this engineering challenge. Surface contamination could be minimised by a thorough cleaning process of the SiO_2 (e.g. immersion in hydrofluoric acid and rinsing with distilled water). Also a lower hydroxyl content of the SiO_2 (e.g. electrically fused SiO_2) could reduce devitrification [449]. Possibly a high-temperature stable coating of the SiO_2 surface could overcome devitrification issues. This would also eliminate the air gap of the current design, if a stable coating with a high emissivity could be identified. Experimental results of this work indicate that thermal cycling accelerates devitrification. It has been reported that SiO_2 could operate indefinitely up to 1623 K, and often higher, provided that the temperature is never allowed falling below 573 K after devitrification has been observed [449]. In a high-temperature heat recovery system operating continuously over long time periods a limited number of thermal cycles below 573 K would occur. For example glass tank furnaces typically operate about one decade without a shutdown.

9.7.2 Assessment of the commercial radiant tube furnace

As already described in the characterisation of the radiant tube furnace (Section 9.4), the natural gas pressure could not be controlled to the required burner pre-pressure and had to be manually controlled. Also the air pre-pressure was not within the required range and was not stabilised, but this was tolerated during the experiments. However, in order to ensure a complete combustion the flue gas composition was frequently

monitored using a flue gas analyser during all experiments [472]. Gas pressure control, in particular for the natural gas, could simplify further experiments.

Both the temperature variation due to the on-off cycle and in particular the slow response of the furnace due to the large mass had a direct impact on the quality of the experimental results. Generally the SiO_2 rod required many hours to reach a temperature gradient in thermal equilibrium with its surrounding (Figure 9-5). Possibly a smaller sized experimental furnace with a continuously controlled electrical heating system could be used for more precise and accelerated experiments. Trials on the radiant tube furnace could still give valuable information about the in-situ operation of a TPV heat recovery system, where inconveniences in terms of long tests and combustion monitoring could be tolerated.

9.7.3 Assessment of the experimental data acquisition

For the experiments several physical quantities were measured manually. These included the water flow rates using flow transducers, the Peltier power and the IV curves. For some water cycles the trend of a slowly decreasing water flow was recorded. This trend is considered to be the result of dirt build-up in the water filters and required some flow adjustments. If changes in the experimental set-up were made (e.g. moving out and in of the aluminium tube assembly, changes in water flow rate or changes in Peltier power), all subsequent measurements were made only after equilibrium conditions were re-established. In addition the furnace on-off cycle had to be monitored and considered during the measurements. For future experiments, a data acquisition system recording not only the temperatures but also other physical quantities, and that could visualise meaningful results immediately would simplify the monitoring of the experiments. An example would be the absorbed power of each heat exchanger

calculated through measurements of the flow rate and the temperature difference. Such system could also record data of the radiant tube furnace, such as a burner on-off signal as well as temperatures, pressures and gas flow rates, which also had to be manually monitored during the experiments.

9.7.4 Assessment of the heat flux meter with aperture

Measurements with the heat flux meter were generally obtained, but some difficulties in temperature control and heat flux meter precision occurred. This was partly caused by the large temperature difference over the heat flux meter. It was found that the control of the temperature near the PV cell was generally difficult. Temperature changes from the Peltier element were transferred slowly to the PV cell because of the low conductivity of the stainless steel in the heat flux meter. In most of the final experiments it was possible to control the PV cell temperature using the PID controller [482][47]. In some cases the Peltier cooling power had to be set on the PID controller manually.

The following engineering issues were identified and an implementation should overcome drawbacks of the current design:

- Temperature control of the heat flux meter mounting plate instead of the existing control near the PV cell
- Thermal insulation of the heat flux meter (e.g. styrofoam)
- Mounting of the heat flux meter with low conductive screws (e.g. stainless steel or plastic)
- A modified arrangement of the PV cell cables with a larger distance to the aperture
- The use of another more sensitive heat flux meter with a lower temperature gradient (e.g. thermopile type)

[47] The highest possible integral time constant was selected (99 minutes and 59 seconds). The derivative time constant was zero and the proportional band was usually around 6.0%. The bias was set to 0%. The set point high limit was 333 K (60 °C) and the set point low limit 278 K (5 °C). Other settings were also tested but did not improve the control. Hence other settings remained unchanged from their default values.

For some experiments, the selected water flow rate for the small aluminium heat exchanger was too high and this resulted in a temperature difference smaller than 1 K between the inlet and outlet water temperature of the heat exchanger. Hence, heat balances were assessed to identify errors caused by this small temperature difference. The heat balance consisted of measurements of the Peltier power, the heat flux meter and the absorbed heat in the water. These balances showed that the absorbed heat in the water of the heat exchanger for the temperature difference smaller than 1 K were under predicted (see Appendix K).

Generally the furnace temperature was still achieved although additional losses through the experimental set-up occurred. An extracted heat in the order of tens of watt was estimated. This power is negligible when compared to the thermal input power of 6.9 kW. The water bath [479] also coped with the absorbed power in the heat exchangers, except for the arrangement with the 100 mm SiO_2 rod (30 mm effective length). In this case, a broken RCF tube (Figure 9-6) caused a total absorbed heat of about 250 W, above the specified value of the water bath of 200 W.

9.7.5 Assessment of the pyranometer test with the radiant tube furnace

A pyranometer has been used for relative measurements of the SiO_2 rod radiative output power up to a wavelength of about 2.8 μm [464]. Absolute measurements require calculation of the view factor from the SiO_2 rod-end to the pyranometer. The dome structure of the pyranometer and the non-uniform distribution of the radiation leaving the SiO_2 rod (not diffuse and not completely directed) would make such calculations challenging.

9.7.6 Assessment of the spectral measurements

During the calibration and measurements some software difficulties occurred and the blackbody calibration source failed. As a result, no long wavelength measurements using the nitrogen cooled HgCdTe detector is reported here. The short wavelength range was not fully calibrated and showed a low signal-to-noise ratio in the region 2.7 to 3.2 μm for the PbS sensor. Hence, only spectral data for the wavelength range from 0.6 to 2.7 μm are reported and conclusions from measurement results need to be treated with care. Future spectral measurements are required in the wavelength range from 0.6 to 10 μm and for different rod SiO_2 lengths in order to fully spectrally characterise the set-up. Since the repair schedule did not allow such measurements in the anticipated time frame, the work concentrated on measurements using the installed PV cell for characterisation. This characterisation was initially planned to be undertaken after the spectral measurements had been completed.

9.7.7 Assessment of the black plate measurements

The aperture size was increased during the four experiments (100, 170, 220 and 270 mm total rod length) from 0.2" to 0.4" in order to increase the heat flux and thus improve the accuracy of the heat flux measurement. In theory, it may be expected that the absorbed heat per unit area (W/cm^2) remain unchanged for different aperture sizes and the use of the same rod length. However, measurements indicated that the aperture size impacts on the absorbed heat flux due to changes of the cavity between SiO_2 rod-end and PV cell. Future work could examine this cavity effect using different rod lengths and aperture sizes. Additionally, for the long wavelength radiation range spectral reflectivity measurements of the black plate would need to confirm the assumed black behaviour of the plate.

9.7.8 Assessment of the SiO_2 temperature measurements

The direct contact temperature measurements of the SiO_2 rod should have resulted in underestimated values of the real SiO_2 rod temperatures. This is because the thermocouple cools the SiO_2 rod by conduction. From a measurement directly in the SiC cup given in Figure 9-5 it is estimated that the error of underestimation is smaller than 20 K.

The temperature of the shortest SiO_2 rod (100 mm total length) was lower than expected in comparison with the other rod lengths, although, the thermocouple was placed next to the SiC cup flange. In this experiment the RCF tube broke and the water bath did not cope with the heat load. This points towards a major heat loss of the furnace for this experiment and may account for the lower SiC cup temperature. The lower temperature would also explain why the total heat transfer with the black absorber plate (previous section) did not increase significantly for the 100 mm rod length (30 mm effective).

9.7.9 Assessment of PV cell short circuit current vs. SiO_2 rod distance

The experimental set-up was designed such that the distance between SiO_2 rod-end and PV cell remained the same for the different rod lengths. In the experiments this was ensured by a flush installation of the SiO_2 rod-end and the insulating firebrick. The experimental examination showed that the short circuit current (or power density) critically depends on this distance and that the repetitive accuracy of the experimental set-up may have already had some impact on the precision of the short circuit current measurements. Therefore, there is a need to improve the control of the distance between SiO_2 rod-end and PV cell for the experimental set-up.

As expected, the experimental results cannot be directly compared to the 1D modelling in which the magnitude of the air gap had no influence on the radiative heat transfer (view factor 1). 2D or 3D modelling would be required to predict the experimental radiative heat transfer introduced by the cavity.

9.7.10 Assessment of the short circuit current vs. SiC cup temperature

This experiment includes some uncertainties about the exact temperature of the SiC cup and the non-equilibrium conditions. These experimental restrictions are regarded as minor for the general type of experimental outcome.

9.7.11 Assessment of electrical output power (IV curve, power density)

In total six IV curves were measured due to three different rod lengths and two PV cell temperatures.

The **temperature dependences** of the saturation current and the open circuit voltage were verified. The increase in **saturation current,** I_s, with increasing cell temperature of the experimental values was approximately confirmed using the proportional relation in Equation 9-8 [4].

$$I_s \sim e^{-\frac{h\nu_g}{kT_c}} \tag{9-8}$$

For the three rod lengths using the measurements at 293 and 313 K, the temperature coefficient of the **open circuit voltage** varied in a range from 1 to 1.5 mV/K. The reason for this wide range may be due to difficulties with the temperature control of the PV cell. During the experiments one thermocouple generated unreasonable temperature values. Hence, some PV cell temperatures were not exactly at 293 or 313 K. In an additional experiment using the 270 mm long SiO_2 rod, a linear temperature coefficient for the open circuit voltage of 1.4 mV/K was measured for a temperature range from

288 to 323 K (15 to 50 °C) using measurement points every 5 K (see Appendix M). This is in agreement with values reported in the literature from 1.42 mV/K to 1.69 mV/K for diffused-junction GaSb cells from another manufacturer [211,486,487].

The following discussion focuses on the electrical power densities obtained from the 293 K IV-curves and two additional measurements (details are in the Appendix N).

This temperature selection was made, since the experimental electrical power density of 0.82 W/cm^2 of the GaSb cell at a similar temperature of 298 K (25 °C) using a 1473 K blackbody source was available from the **manufacturer** [177]. Both the radiator and the PV cell temperature can be considered similar to the experimental conditions of this work. Hence, this data point can to some extent be used as a comparison for the case without a SiO_2 rod. The share of 1500 K blackbody radiation below 2.0 and 1.7 μm is 7.9 and 5.0 W/cm^2 respectively (see Appendix B), where the 7.9 W/cm^2 is also approximately[48] consistent with the modelling results without SiO_2 (Section 8.6). These values were multiplied with an in-band conversion efficiency of the GaSb PV cell of 31% to obtain the two theoretical electrical power density values of 2.45 W/cm^2 (2.0 μm) and 1.55 W/cm^2 (1.7 μm). The 1.7 μm value was selected as a realistic cut-off wavelength of a typical GaSb cell [177]. The 2.0 μm value was assumed as the cut-off wavelength of the modelling within this work. For the experimental electrical power density of 0.82 W/cm^2 from the manufacturer, an improvement in electrical power density due to the view factor of 70% is expected[49] (Subsection 3.6.3). This results in a corrected experimental value of 1.39 W/cm^2, which is considered

[48] The small difference of modelling and blackbody data is due to the neglected cell temperature for the blackbody case.

[49] (0.8-0.47)/0.47·100% = 70%

reasonably close to the theoretical value of 1.55 W/cm^2. It needs to be considered that in an experimental system such a high view factor (or close arrangement) between the radiator and the PV cell is regarded difficult to implement due to high conduction and convection losses.

Experimental results of this work point towards a **decay of the short circuit current** (or power density) over the entire experimental sequence. This was clearly seen for the 2nd and 5th measurements, which were repetitions of the 1st measurement using the 25 mm diameter and 270 mm long rod. Since the 5th measurement was a repetition of the first measurement with a new radiant tube furnace set-up (new insulating firebricks, new SiO_2 rod), degradation in performance due to the set-up in the radiant tube furnace was excluded as a possible cause. Hence, it is thought that some form of cell decay was the reason. Accumulation of fibre dust at the cell surface was observed for some experiments. The PV cell surface was subsequently cleaned with iso-propanol, but the initial power level was not obtained again. For the result section, **corrected measurement** values have been calculated in order to estimate the performance without the degradation. The difference δ between the 1st and 5th measurement was used for a correction. The corrected points were then the 2nd measurement point plus ¼ δ, the 3rd measurement point plus ½ δ and the 4th measurement point plus ¾ δ. As described in Subsection 9.7.9, the short circuit current drops rapidly as the distance between SiO_2 rod-end and the PV cell increases. Improvements of around 23% compared to the current power density are expected using a closer arrangement of the PV cell and the SiO_2 rod. For the current experimental set-up, this correction involved extrapolating the short circuit current results in Figure 9-14 to the left by the distance between SiO_2 rod-end and PV cell (5 mm). The entire correction first took the view factor into account

followed by the PV cell decay. It needs to be considered that for a small air gap conduction and convection losses would contribute to some parasitic heat transfer. Such an arrangement would be similar to the RG arrangement and an implementation is regarded promising due to the previously presented modelling results (Section 8.6).

The modelled electrical power density has been calculated from the total in-band radiation of the Radiator-Glass-Air (RGA) arrangement (Section 8.6) multiplied with an in-band conversion efficiency of $\eta_{OC} \cdot \eta_{QE} \cdot \eta_{FF} \cdot \eta_{UE} = 31\%$ for a GaSb PV cell (see Subsection 3.6.3). The modelled cut-off wavelength of the GaSb cell up to about 2 μm instead of the realistic value of 1.7 μm causes significant differences for the modelling results (spectral bands have been assumed in 0.5 μm steps). In order to take these differences into account, a corrected version of the modelling results was calculated. Here, modelling results of the RGA arrangement and blackbody based electrical power density without SiO_2 assuming a 2 μm cut-off wavelength were normalised at the modelling point without SiO_2 and a cut-off wavelength of 1.7 μm.

In the modelling the radiator temperature was 1500 K, whereas in the experiments the furnace temperature was 1523 K. This difference is considered insignificant, since the SiC cup temperature is expected to have a gradient and lower temperature than the temperature of 1523 K within the furnace. This effect is expected to compensate for the higher furnace temperature compared to the modelling, where exact quantification of this effect is difficult because of the described challenges of high-temperature thermocouple measurements (conductive cooling).

9.7.12 Assessment of the efficiency measurements

In total twelve efficiency values were calculated resulting from measurements of three different rod lengths, using two different measurement methods and two PV cell temperatures. Of these twelve values two results were contradictory (see Appendix O for details). The most likely reasons for this is that in one case there were non-equilibrium measurement conditions (270 mm rod with a cell temperature of 313 K (40 °C) using the heat balance method) and in the other case there was condensation at the heat flux meter (220 mm rod with a cell temperature of 293 K (20 °C) using the heat flux meter method).

The 293 K data were selected for a detailed comparison with the modelling results, since in this case experimental data from the manufacturer of the **directly illuminated GaSb cell** at a similar cell temperature (298 K) are available [177]. The efficiency of the JX Crystals cell under blackbody illumination was calculated as $P_{el,meas}/\sigma T_s^4$ = 0.82/26.7·100% = 3.1%. This value potentially increases by about 70% to a value of 5.3% due to the non-ideal view factor within the reported experiment. The two modelled values of a directly illuminated cell have been calculated as follows. The share of 1500 K blackbody radiation below 2.0 and 1.7 μm compared to the total radiation is 27.5% and 17.4% respectively. These values have been multiplied by an in-band conversion efficiency of the GaSb PV cell of 31% to obtain the two modelled efficiencies of 8.5 and 5.4%.

Modelled in-band radiative heat transfer rates of the RGA arrangement (Section 8.6) were also multiplied with the PV cell in-band conversion efficiency of 31% to obtain the modelled efficiency for different SiO_2 thicknesses with a cut-off wavelength of 2.0 μm. Efficiency modelling data versus SiO_2 thickness for the RGA arrangement with

a cut-off wavelength of 1.7 μm were calculated by normalising the 2.0 μm modelling data for the RGA arrangement for the case without SiO_2.

Taking into account the PV cell decay, the efficiency values show the same trends and are only slightly higher compared to the measured values. Hence, these values are not reported in the results of this work (Subsection 9.8.8), but are given in Appendix O. For the efficiency, a correction for the view factor from the SiO_2 rod-face to the PV cell, as for the power density, was not made, because this would have also resulted in higher absorbed heat powers by the PV cell and measurements of these powers would have required another experimental set-up with a reduced distance between SiO_2 rod-end and PV cell.

9.8 Experimental results of the characterisation

9.8.1 Results of the pyranometer test with the radiant tube furnace

One SiO_2 tube was visible during the experiment and had a dark colour. Qualitatively, this indicated that a small share of radiation was transferred and lost from the SiO_2 rod to the SiO_2 holding tubes. At a pyranometer reading of 0.1 W/cm^2 the distance between SiO_2 rod and pyranometer was 60 mm. This is about double the distance compared to the test using the preliminary furnace (Subsection 9.3.2). Hence the radiant tube furnace set-up gives approximately 4 times the radiation output as the preliminary furnace set-up assuming the inverse square law. It is concluded here, that this is the result of a more uniform temperature of the SiC cup within the furnace chamber and similar temperature gradients of the SiO_2 rod and the insulating firebrick.

9.8.2 Results of the spectral measurement

The spectral measurement[50] qualitatively showed the absorption of radiation of the wavelength regions around 2.7, 2.2 and 1.4 μm (Figure 9-12). These peaks are in agreement with absorption coefficient data given in the previous modelling chapter (Figure 8-1, Figure 8-2). The strongest SiO_2 absorption peak around 2.7 μm indicates good suppression of radiation at this wavelength as predicted in the modelling. The peak at 2.2 μm contributes to some suppression. The modelling indicated stronger suppression than was indicated by the spectral measurement. However, without a calibrated measurement this cannot be stated with certainty. The suppression at 1.4 μm seems to be rather weak as already expected from the modelling.

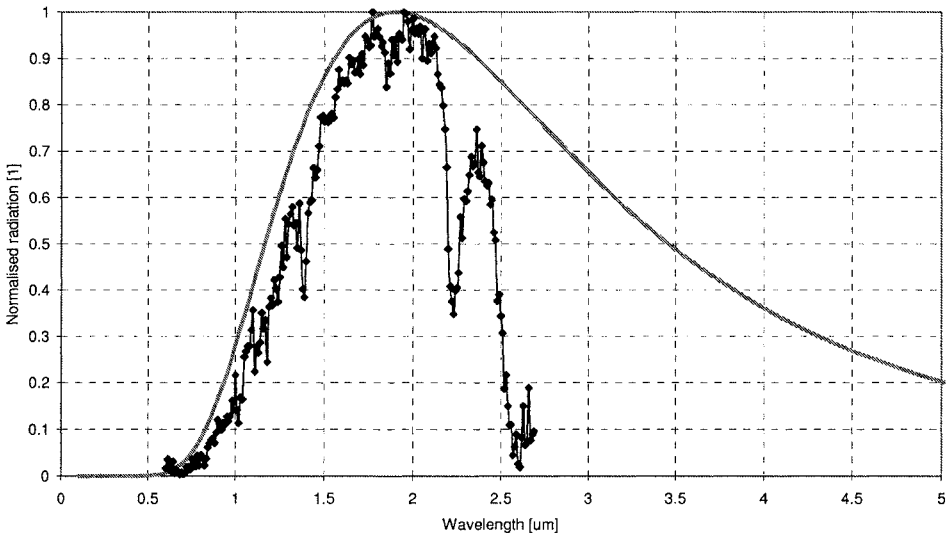

Figure 9-12: Result of the spectral measurement of the SiO_2 rod radiation output. Shown are the normalised radiation of a 1523 K blackbody (grey line) and the spectroradiometer measurement from 0.6 to 2.7 μm (black measurement dots). Measurements data are averaged from three scans. The SiO_2 absorption peaks at 1.4, 2.2 and 2.7 μm are visible. No data are reported for the wavelength range from 2.7 to 3.2 μm, because of the low signal to noise ratio of the PbS detector for the given spectroradiometer set-up.

[50] The measurement interval was set to 10 nm and the signal response time was set to slow. The cut-on wavelength of the PbS detector was 1090 nm.

9.8.3 Results of the black plate measurements

Within the experiments using the same aperture, the tendency of a decreased total radiation for longer rod lengths was measured. For the smaller 0.2" aperture generally larger heat fluxes were measured, even though the rods were longer. This contradictory result should be explained by enhanced multiple reflections between the reflective aperture and the SiO_2 surface for the 0.2" aperture, since the smaller hole results in a large reflective area.

In the experiment conduction and free convection of air occurs and this would be expected to lead to an increase of the experimental values compared to the modelling predictions, where no conduction and convection has been assumed for the gap. For a SiO_2 thickness of 100 and 200 mm, the modelling predicted total heat fluxes of 14.3 and 10.8 W/cm^2 respectively. The measured values ranged from 13 to 14 W/cm^2 indicating that coupling of radiation into the rod and the guiding of radiation by the rod in this experimental arrangement behave similarly to the 1D modelling.

9.8.4 Results of the SiO_2 temperature measurements

The experimental arrangement and the modelling differ considerably from each other. In the 1D modelling it has been assumed that the PV cell is a black absorber. In the experimental arrangement both the PV cell and the gold coated aperture disc reflect back some of the radiation. For the experiment, there may also be a temperature increase or loss due to the insulating firebrick surrounding the rod compared to the 1D modelling. These effects have been not quantified, since this work focussed on the characterisation at the PV cell and not the system level. Considering these differences and the limited number of measurement points, the experimental results and the modelling are in good overall agreement (Figure 9-13).

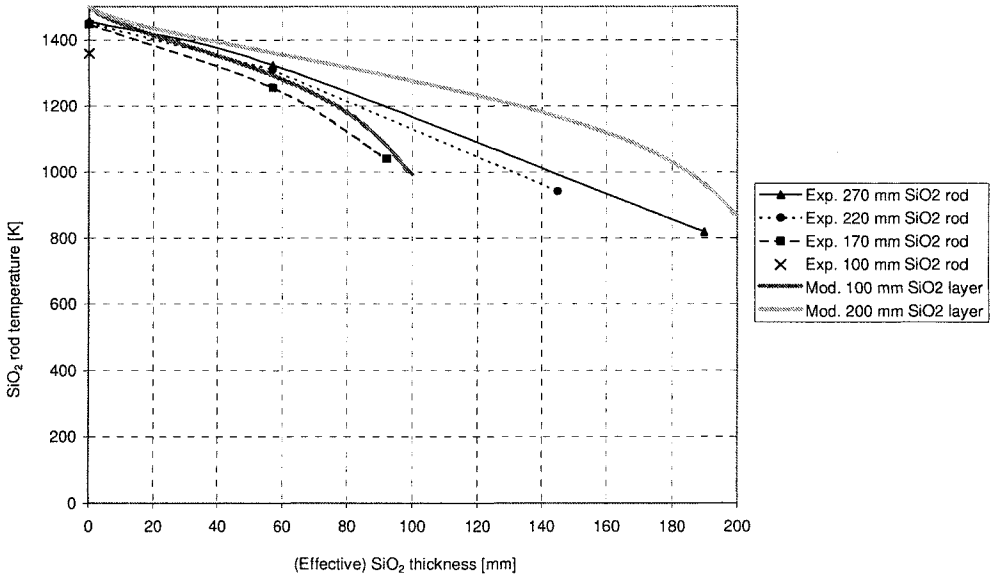

Figure 9-13: Results of the temperature measurements along the SiO_2 rods. For the four different rod lengths, experimental rod temperature values are shown (black). For the rod lengths 270, 220 and 170 mm (200, 150 and 100 mm effective length) the PV cell was installed (held at 293 K) and three temperatures were measured. The x-axis shows the effective rod length, where the distance of 70 mm within the SiC cup is subtracted. For comparison also modelling results for a thickness of 100 and 200 mm are shown (grey).

The cold side temperature of the SiO_2 rod varied by up to 200 K for the same rod length, which is shown by multiple data sets for each rod length in Figure 9-13. This variation occurred for different experimental arrangements. For example, the highest temperatures were measured using the closed gold-coated copper disc. Here, radiation was reflected back into the SiO_2 rod and this is considered to be the most likely cause of the temperature increase. On the other hand the lowest temperatures were observed if the radiation leaving the rod could freely escape (e.g. with the aluminium tube assembly not installed, see Figure 9-6). In addition, the furnace operation time at 1523 K was a major factor of the cold side SiO_2 temperature (see Section 9.4.3, Figure 9-5). The temperature of the hottest part of the SiO_2 rod in the SiC cup varied with the furnace on-off cycle by a few degrees.

In the following section the impact of the distance between the SiO_2 rod-end and the PV cell is discussed. In the experiment also the SiO_2 cold side temperature was measured, the results show that the temperature first increases and then decreases for larger distances (second y-axis in Figure 9-14). The increase in the cold SiO_2 rod temperature is probably due to a decrease in the absorbed power by the PV cell. This is attributed to more radiation being reflected back into the SiO_2 rod, so that the SiO_2 rod temperature increased. For larger distances the view factor between SiO_2 rod-end and the reflective aperture becomes smaller. Hence, less radiation should be reflected back and coupled into the rod and the SiO_2 rod temperature decreases for these distances.

9.8.5 Results of the PV cell short circuit current vs. SiO_2 rod distance

In the experimental set-up distance changes of a few millimetres between the SiO_2 rod-end and the PV cell strongly affected the short circuit current (or electrical power density) of the PV cell (Figure 9-14). Hence, the view factor from the SiO_2 rod-face to the PV cell needs to be considered. The strong drop of the short circuit current I_{sc} with increasing distance indicated that I_{sc} could be enhanced using a shorter distance in the experimental set-up than that used. For example I_{sc} drops by about half for a distance of 10 mm from the initial distance. This can be compared to a built-in distance of about 5 mm for the experimental set-up.

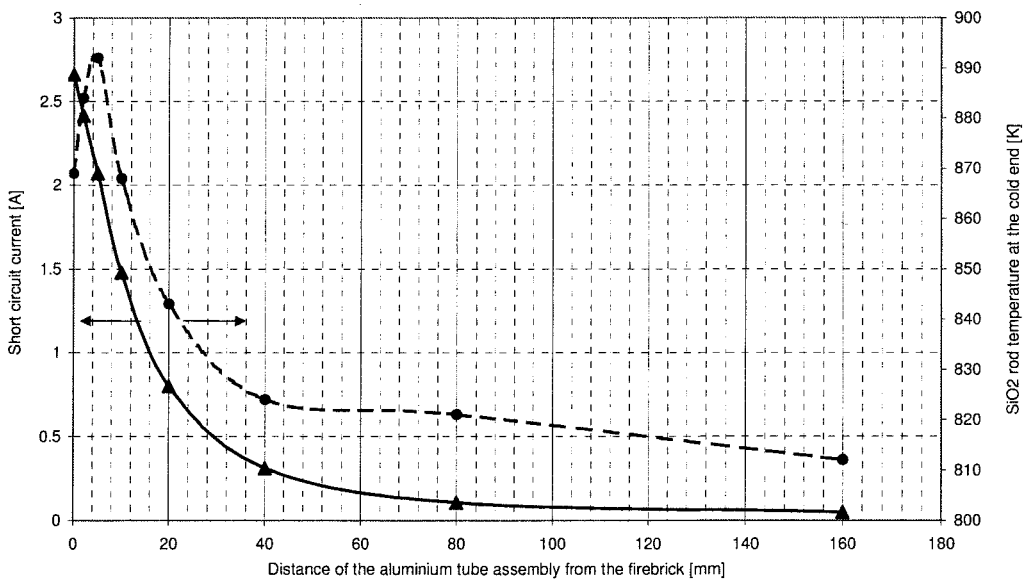

Figure 9-14: Result of the PV cell short circuit current measurement versus gap. The diagram shows the PV cell short circuit current (left y-axis) and SiO_2 rod temperature near the PV cell (right y-axis) as a function of the distance between aluminium tube assembly and the SiO_2 rod. The rod had a total length of 270 mm and a diameter of 25 mm.

9.8.6 Results of the short circuit current vs. SiC cup temperature

The PV cell short circuit current (or electrical power density) dropped by about half for a radiator temperature reduction of 150 K (Figure 9-15). The experimental data correlate with the theoretical blackbody radiation below 1.7 μm. The differences of the theoretical and experimental values for the region above 1400 K may be explained by the non-equilibrium conditions of the experiment. The normalised fourth power temperature dependences is also plotted (Figure 9-15). This curve shows for the electrical power density versus radiator temperature behaviour, that higher than fourth power temperature dependency can be expected. The experiment highlighted not only the importance of high radiator temperatures, but also strengthens the assumption that blackbody radiation up to 1.7 μm is transmitted with low absorption through the SiO_2, because of the correlation of the theoretical blackbody and the experimental data.

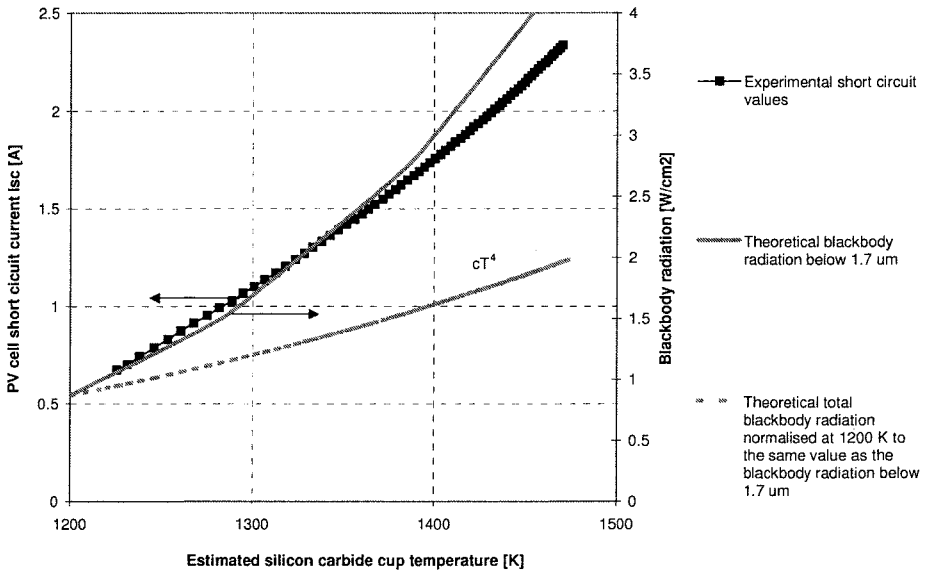

Figure 9-15: Result of the short circuit current measurement vs. SiC temperature. The plot illustrates the PV cell short circuit current (left y-axis) depending on the estimated SiC cup temperature. The blackbody radiation below 1.7 μm (cut-off wavelength of the GaSb cell) is approximately proportional to the short circuit current (right y-axis). The total blackbody radiation over the whole spectrum (normalised at 1200 K) is also shown for comparison.

9.8.7 Results of the electrical output power (IV curve, power density)

Figure 9-16 contains three plots of the six IV curve experiments. In these plots circles and triangles show the measurement points for 293 and 313 K respectively. The curve of the one-diode model matched to these measurement points is also shown (bold line for 293 K and dashed line for 313 K data), where details of the matching process are given in the Appendix G. Generally the model was fitted well to the experimental IV values (Figure 9-16). The IV curves were generally similar for the different rod lengths and also showed similar characteristics to a typical IV curve measured by the manufacturer for the same cell type [177], although the open circuit voltage and the fill factor were slightly lower for the experimental results in this work. The slightly higher photocurrent I_{sc} of this experiment compared to manufacturer value is thought to be the result of a higher view factor for the experimental set-up reported here. The gradient of the modelled IV curves near the open circuit and short circuit case contain information about the PV cell series resistance R_s and the parallel resistance R_p respectively [4]. Measurements of this work indicate a lower R_p and a similar R_s for the cell compared to the manufacturer values, where further details of these resistances were not available from the manufacturer [177]. As already discussed in Subsection 9.7.11, the temperature dependence of the open circuit voltage V_{oc} and the saturation current I_s was verified successfully. Hence, although a limited number of IV-curve measurement points were made, consistent IV-curve results were obtained in this work using a one-diode model.

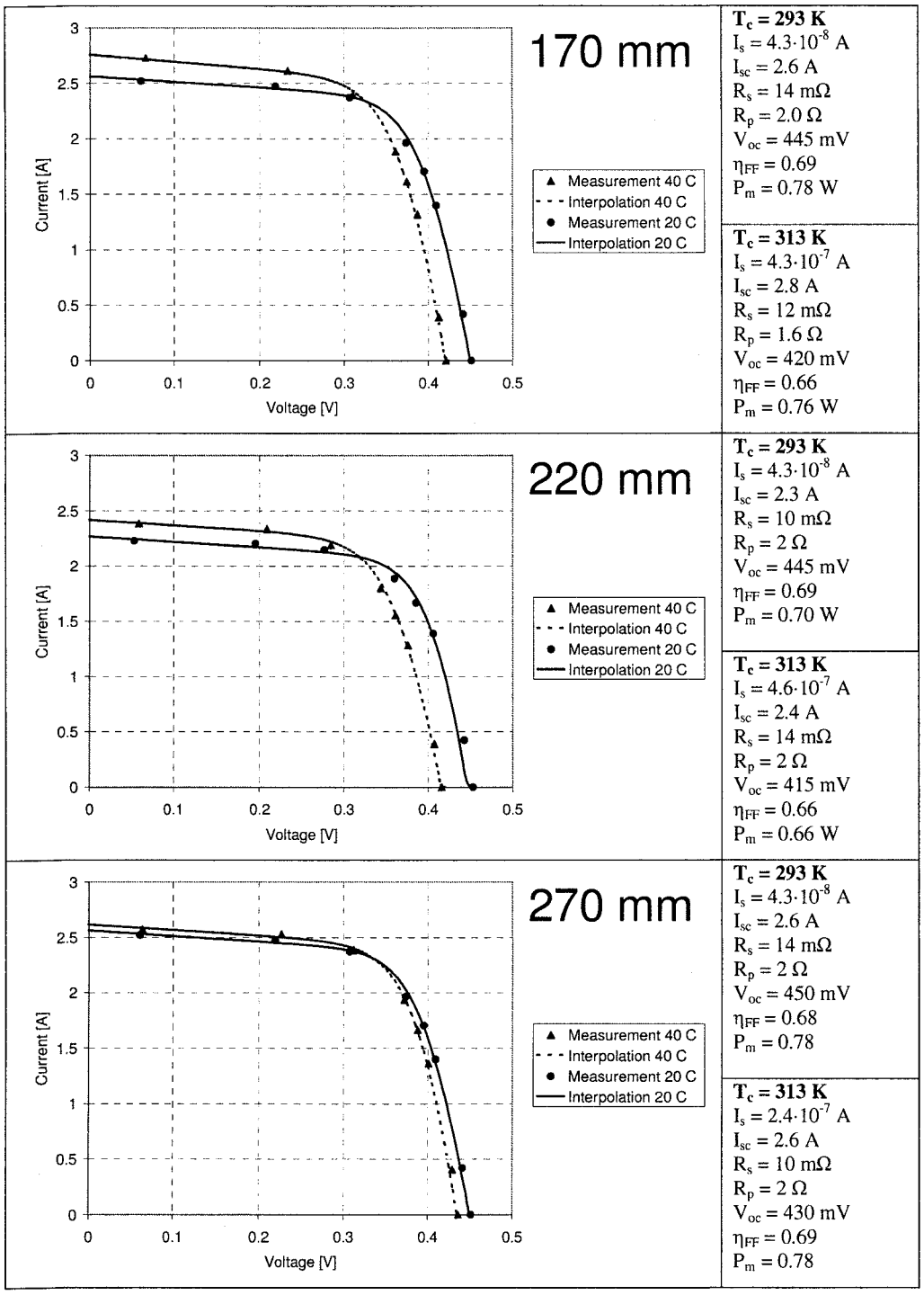

Figure 9-16: Results of the IV curve measurements for the three SiO_2 rod lengths.

Three electrical power densities of the 293 K IV-curves in Figure 9-16 were computed. Two additional experimental power densities, made from one short circuit measurement, were also included, where details are given in the Appendix N. Figure 9-17 shows these five measurements as black squares with their measurement sequence given by a number. Assessing this sequence led to the conclusion that some PV cell decay had occurred. A further reduction in power density due to the view factor from the SiO_2 rod-face to the PV cell was thought to be likely. Both reductions were taken into account to calculate corrected values of the experimental power densities (grey squares in Figure 9-17).

Figure 9-17 also shows as a black triangle a typical power density of the same PV cell type at 298 K measured experimentally under blackbody radiation (1473 K) by the manufacturer without SiO_2. This point was corrected for the view factor (Figure 9-17, grey triangle). Although it may be not possible to implement this correction practically due to a high conductive and convective heat transfer for a close arrangement of radiator and PV cell, this data point is useful for a comparison with the modelling results.

Figure 9-17 shows the RGA arrangement modelling results as grey solid line, where a cut-off wavelength of 2 μm was assumed (Section 8.6). A corrected version for a cut-off wavelength of 1.7 μm is also plotted.

The modelling showed an almost linear drop in electrical power density with increasing rod length. For the case without SiO_2 (effective rod length zero), the corrected modelled and the (view factor) corrected experimental values were in good agreement. For the effective lengths from 100 to 200 mm a discrepancy between the correct modelled and corrected experimental values was observed. There are potentially a number of reasons for these discrepancy and these include the following. First, the

straightforward normalisation assumption for the correction of the modelling results could include some errors. Second, the coupling of radiation into the SiO_2 rod could be imperfect. Third, there may be some radiation guidance losses. Finally a non-uniform illumination of the PV cell area could have also contributed to this reduction.

For an experiment without SiO_2 a reduction of view factor usually requires a certain PV cell to radiator distance to avoid cell overheating by conduction and convection. On the other hand, a small SiO_2 to PV cell distance could be implemented for the experimental RGA arrangement. Hence, practically similar electrical power densities of the PV cell under direct illumination and the use of the RGA arrangement can be expected. This benefit of the RGA arrangement can be seen in Figure 9-17 comparing the corrected experimental values for the effective lengths from 100 to 200 mm (grey squares) with the uncorrected experimental value at distance zero (black triangle).

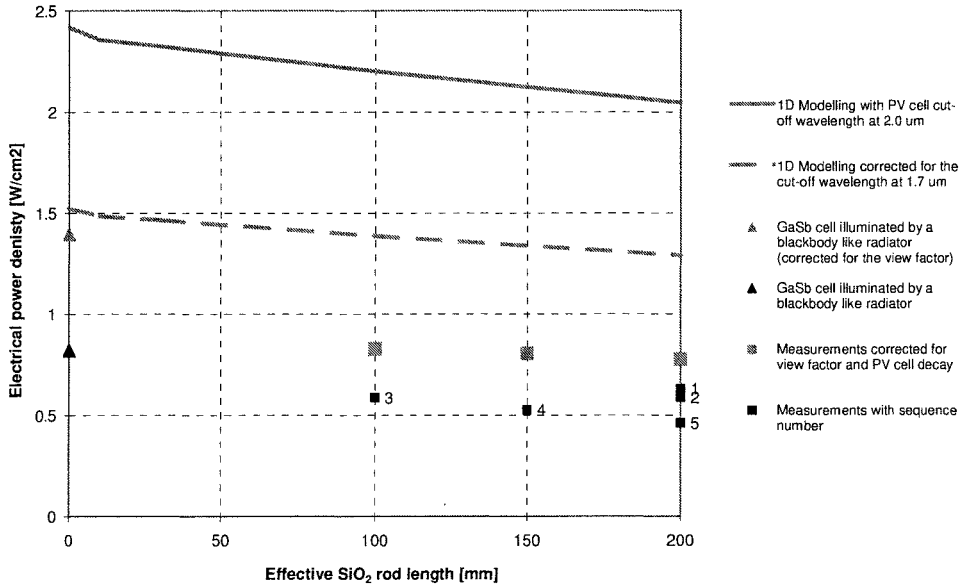

Figure 9-17: Results of the power density measurements versus SiO_2 rod length. Measured power density values with their experimental sequence (squares) and the power density of the same cell type measured under blackbody illumination (triangle). The measured values have been corrected for view factor losses and PV cell decay (grey squares). The measurement by JX-Crystals was corrected for the view factor loss (grey triangle). The modelling is shown as a grey line for the original and cut-off corrected case.

9.8.8 Results of the efficiency measurements

For the experiments in this work, three efficiency values using two different measurement methods were computed (Appendix O). Figure 9-18 gives the resulting values for the heat flux (black squares) and heat balance method (black circles). For the results of each of these methods a black dashed trend line was included. As discussed in the experimental assessment (Section 9.7.12), the measurement of the heat balance method at an effective rod length of 150 mm was measured incorrectly. For comparison the efficiency of the GaSb PV cell, directly illuminated by blackbody radiation not including conductive and convective losses, is shown (Figure 9-18 black triangle, see Section 9.7.12). This efficiency is also shown, corrected for the view factor (grey triangle in Figure 9-18). The grey full line in Figure 9-18 shows the modelled PV cell efficiency of the RGA arrangement assuming an in-band cell efficiency of 31%. For the grey dashed line (Figure 9-18), the modelled cut-off wavelength has been corrected.

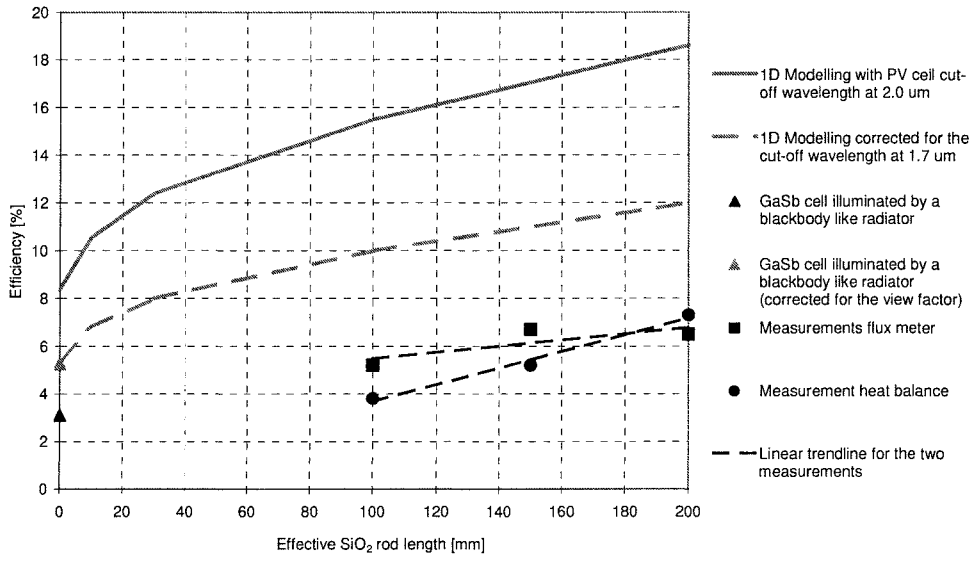

Figure 9-18: Results of the efficiency measurements versus SiO_2 rod length. Measured efficiency values are based on the heat flux meter values (square points) and using a heat balance (round points). The PV cell efficiency under blackbody conditions without conduction and convection losses is also shown (triangle). The modelling is plotted as a grey line for the original (full line) and cut-off corrected (dashed line) case.

Both modelling as well as experimental data based on the heat flux and heat balance method show the tendency of improved efficiency for an increased SiO_2 thickness (Figure 9-18). For the case without SiO_2, the corrected modelled and the (view factor) corrected experimental values were in good agreement. This can be seen in Figure 9-18 for the grey dashed line and the grey triangle point at an effective SiO_2 rod length of zero. On the other hand, for the case with SiO_2, there was a discrepancy between the correct modelled and the corrected experimental values. There are various possible reasons for this discrepancy. These include an inaccuracy in the corrected modelling result, conductive and convective heat transfer not considered in the modelling, a higher experimental out-of-band radiation for the modelling or a non-uniform illumination of the PV cell area in the experiment. The experimental results have approximately the same gradient of the modelled efficiency enhancement. The heat balance measurement over predicts and the heat flux measurement under predicts the modelled gradient.

Additional efficiency calculations were made for a cell temperature of 313 K (Appendix O). Also for this higher cell temperature, for both efficiency measurement methods (heat flux and heat balance) the efficiency improved monotonically with increasing rod length. In addition, the Peltier power decreased as well as the heat absorbed in the water decreased when the rod length increased for both temperature cases (see Appendix O). These additional results, as well as the tendencies already found for the black plate measurements (see Subsection 9.8.3) and SiC cup temperature (see Subsection 9.8.6) further support the experimental outcome of an increased efficiency for an increased SiO_2 thickness (Figure 9-18).

9.9 Summary

This chapter described the selection, implementation and analysis of an experimental Radiator-Glass-Air (RGA) arrangement. The coupling of radiation into the SiO_2 was designed to be similar to that of a blackbody tipped optical fibre thermometer [458]. Other TPV research indicates that thermal radiation can be guided in dielectric materials by total internal reflection with low losses [115,269]. In the work reported here, these concepts have been combined to guide radiation via a SiO_2 rod to a commercially available GaSb cell [177,456]. In terms of spectral control, the SiO_2 rod mainly transmits in-band short wavelength radiation and suppresses a large share of out-of-band long wavelength radiation.

The concept was first tested in a preliminary self-made furnace. The results encouraged a more sophisticated experimental design in a radiant tube furnace. This furnace was first characterised in terms of its combustion products, as well as its heat balance and its temperature distribution in order to carry out further experiments. The TPV system, installed into the radiant tube furnace, was divided into two major parts. Firstly for each experimental rod trial, the SiO_2 rod together with its holding components was installed. A straightforward pyranometer measurement showed that improvements made by using this set-up (insulation of the SiO_2 rod and more uniform SiC cup temperature) lead to about double the radiation output compared to the preliminary self-made furnace. In order to characterise the installed SiO_2 rod further, the second part, an aluminium tube assembly with holding set-up was engineered (see Figure 9-6). This assembly can be removed from the system to facilitate measurements of the spectrum, total radiation (black plate) and PV cell performance. Two heat exchangers located at the assembly top (copper heat exchanger) and side surface

(aluminium tube heat exchanger) shielded the measurements. Both heat exchangers absorbed about the same amount of heat, about 20 to 30 W. The aluminium tube heat exchanger did not only absorb heat from the furnace but also from the environment for the usual water bath temperature of 288 K. Hence, the major source of absorbed heat occurred at the smaller copper heat exchanger at the top. Parasitic radiation absorption of the gold coated aperture discs, enhanced by multiple reflections as well as air conduction and free convection, would all be expected to contribute to the heat absorbed in the copper heat exchanger. The high ratio of absorbed heat power compared to the electrical output power indicates the challenge of a high efficiency mirror design in TPV cavities. Such designs using mirrors were attempted earlier in other TPV work, but are regarded unsuitable (Section 4.3). In this work the purpose of the mirror aperture was to obtain SiO_2 radiation of a defined area and to shield other areas. This allowed illumination of the PV cell area only in order to measure cell efficiency. In a more practical implementation, the SiO_2 face-area and the PV cell area would be designed to match each other (e.g. shaped SiO_2) and arranged closely without the need of a mirror.

The experimental set-up was characterised by several methods. Of particular significance is the spectral and total radiation output of the SiO_2 rods, as well as temperature measurements along the SiO_2, since experimental results can be compared with the 1D modelling reported in Chapter 8. Work on **spectral measurements** did not progress as far as anticipated due to some equipment difficulties. However, those measurement results that were obtained confirmed that there was suppression of radiation at the three known absorption peaks of the SiO_2 at 1.4, 2.2 and 2.7 μm, as predicted. The **total radiation output** was measured using a black painted plate. It was found that the aperture size had a decisive impact on the measurement. Use of two

different aperture sizes showed that absolute values are approximately in agreement with modelling results. Also for both aperture sizes, the tendency of decreased total radiation for longer rod lengths was measured as predicted by the modelling. Although, there are considerable differences in the modelling assumptions and the non-ideal experimental set-up, experimental **temperature gradients along the SiO_2 rod** have been found to be in good agreement with the 1D modelling results.

The sensitivity of the experimental set-up in terms of the distance between the SiO_2 rod-end and the PV cell as well as the SiC cup temperature was assessed. Both aspects had a critical impact on the electrical power density (or short circuit current). For the former, the short circuit current dropped sharply with increasing **distances**. The current experimental set-up should have the potential to increase the power density further using a smaller distance between the SiO_2 rod-end and the PV cell. For the **SiC cup temperature** experiment, the short circuit current (or power density) dropped sharply for lower radiator temperatures. The drop in short circuit current versus temperature was also approximately predicted by computed blackbody radiation below the GaSb cell cut-off wavelength at 1.7 μm. This agreement between experiment and model strengthens the assumption that there is little SiO_2 attenuation of in-band radiation.

A total electrical power of about 0.78 W for an active PV cell area of 1.33 cm^2 was measured within this work corresponding to a **power densities** of 0.59 W/cm^2. A closer arrangement of the SiO_2 rod-end and the PV cell should result in power densities about 23% higher than the current value. Furthermore, some gradual PV cell decay has been observed. From the first to the last measurement this resulted in an estimated drop of 27% in the electrical power density. The power density values corrected for these factors are 0.83, 0.81 and 0.78 W/cm^2 for an effective SiO_2 rod length of 100, 150 and

200 mm respectively. A slight drop of electrical power density with increased SiO_2 thickness is in general agreement with the 1D modelling. The differences in the absolute values between modelling and experiment were to be expected considering the simplifications made in the 1D modelling. Reasons for the different values have also been discussed.

The power absorbed by the PV cell was determined by the heat balance and heat flux method to calculate the efficiency. Both methods showed similar values and the same tendency of enhanced efficiency for increased SiO_2 lengths. The measured efficiencies had about half the values of the corrected 1D modelling results. The previous section gave potential contributing causes of this deviation. For an effective rod length from 100 to 200 mm, a PV cell efficiency η_{PV} in the range from 4 to 7% was measured including conduction and free convection losses. Corrections for the PV cell decay leads to a maximum efficiency value of around 8%. This value can be compared to a theoretical value of 3% for the same PV cell type under blackbody radiation not including conduction and convection losses. Hence, the additional SiO_2 rod is estimated to have at least doubled the efficiency compared to a direct blackbody illumination. The modelled efficiency enhancement is caused by coupled radiation and conduction within the SiO_2 and has now been confirmed by experiment.

Generally, the experimental set-up offers opportunities to optimise angular, spatial and specular radiation distribution further using methods such as different SiO_2 shapes together with total internal reflection (collimator or concentrator), the implementation of the RG arrangement, surface coatings (e.g. metal reflector and AR), SiO_2 doping or crystalline materials with a high refractive index. Also advances in PV cell performance would increase the power density and efficiency (e.g. low and multi-bandgap cells).

10 Conclusion

10.1 Results and contributions

In the UK, several groups have carried out TPV cell research. The work reported here examines for the first time TPV on a system and application level in depth for the UK. The first objective of this work was a comprehensive TPV assessment in order to identify applications with high potential together with critical aspects of TPV system technology. The second objective was then to examine one high potential application in detail. This included an in depth application assessment, the selection of a suitable TPV system approach and the investigation of critical aspects of a system design by modelling and experiment.

Previous conference and journal publications on TPV applications were limited in the publication length and considered specifically the Japanese market or were presented around a decade ago. The work reported here assessed TPV applications comprehensively and in depth for the UK market. Applications have been classified by heat source and CHP mode, whereas other published work used different structuring methods. This classification can be justified because TPV systems vary in their efficiency definition, type of components and competing technologies for differences in the heat source and the CHP mode. For example, TPV systems powered by solar,

nuclear or waste heat have potentially higher efficiencies than combustion systems with their flue gas losses. Also components of TPV systems may be used specifically for one heat source, such as solar concentrators or Welsbach mantle type radiators. On the other hand, technological aspects also impact on the potential applications. For example the current TPV technology status makes it unlikely that applications with combustion efficiency (fuel to electricity) above 15% will become feasible in the near future.

The iterative assessment resulted in twelve application groups considering the technological capabilities of TPV and its competitors, as well as the application requirements. The applications of domestic micro CHP and industrial waste heat recovery were identified to have the highest potential for the UK market. In the short-term, these applications could operate in the niche markets of self- and backup-powering that could sustain higher costs. In the long-term, both applications could have large potential markets and could contribute to considerable primary energy savings.

The requirements for micro CHP include high reliability, low maintenance and low noise, all of which could be met by TPV conversion. Competition from several other dynamically emerging conversion technologies has been identified as the major future challenge.

The high-temperature heat recovery application has been selected for this work. For this application, there have been a few previous experiments on a partially built TPV system and a brief discussion for the Japanese market. The work reported here assesses the potential of TPV industrial high-temperature heat recovery in depth using the UK as an example. The industrial sectors with a suitable temperature for TPV operation include the iron and steel, non-ferrous metal, bricks and refractories, cement, glass and ceramics industries. An overall assessment of TPV in those industries is complex

mainly because of the large process diversity. Hence, one example process for each of the three principal heat loss locations (hot product, flue gas and the insulation wall) has been assessed in detail. Extrapolating the electricity generation capability of the example processes to the entire high-temperature industry in the UK indicates that 30% of the electricity consumed in the high-temperature industry could be supplied by generation from TPV heat recovery. Competition from other technologies is limited to external heat engines and other direct heat-to-electricity conversion devices all with their own disadvantages. TPV systems have been identified to be more suitable to convert high-grade heat into electricity since no intermediate energy conversion or heat transport with high losses occurs and the technology could be applied modularly. In the long-term, direct heat-to-electricity recovery over the entire temperature range may be possible using thermoelectric generators for low-temperature and TPV for high-temperature conversion.

The waste heat recovery application is likely to be more capital cost effective and achieve shorter payback periods than other TPV applications, because of the long operation hours and the low or no costs of the thermal input. Unlike solar PV conversion, TPV conversion can be optimised for high efficiency or high power density. For TPV waste heat recovery, the decisive economic factor is the capital cost per generated watt and not the efficiency because of the advantageous thermal input costs of this application.

TPV technology was reviewed and assessed by its three major components: heat source, radiator and PV cell. It has been found that components and knowledge about them is often available from other research fields. For the heat source, component examples are solar concentrators and radiant burners. Selective radiators have been

developed for both electric and gas lighting, and broadband radiator materials are established in the field of high-temperature ceramics. GaSb PV cells for example have been developed initially as a bottom PV cell for solar conversion. Hence, the emphasis of this work was to examine the interaction of these components and how they influence the important figures of merit for a TPV system.

There is general agreement that high electrical power densities and high efficiencies are the important figures of merit. It is generally accepted that out-of-band bandgap suppression (usually referred to as spectral control) improves the efficiency of TPV conversion and it has been suggested that additional in-band suppression may enhance the efficiency further. This work models for this first time the impact of simultaneous in-band and out-of-band bandgap suppression on an ultimate efficiency level. The modelling showed that additional in-band bandgap suppression does not considerably improve the efficiency and hence gave justification for the common configuration using purely out-of-band suppression.

The work reported here identifies optical control in the cavity, including not only spectral but also angular and spatial radiation control, as the critical aspect of TPV system design. Mirrors directing the radiation from the radiator to the PV cell have been recognised as critical in terms of parasitic absorption by all heat transfer modes and the material requirements (high reflectivity, high temperature stability, thermally insulating). This work reviewed spectral control methods and it was found that each method has its own challenges in areas such as costs, engineering complexity and thermal stability. A few publications indicate that total internal reflection in dielectrics is a promising concept to replace mirrors. Many TPV systems utilise fused silica (SiO_2) shields in the cavity and these shields also take part in the cavity spectral control, but

research work in this area is limited. Therefore, radiative heat transfer in a TPV cavity with a SiO_2 shield was modelled within this work in detail. Results showed that coupled radiative and conductive heat transfer in SiO_2 shields becomes important for thicknesses in the range from centimetres to tens of centimetres and that at enlarged thicknesses the suppression of out-of-band radiation is enhanced. This and previous TPV work conclude that the angular radiation distribution leads to in-band radiation reductions due to SiO_2 surface reflections.

In this work both mechanisms have been considered to propose an alternative arrangement radiator-glass-air-PV cell (RGA) using increased SiO_2 thicknesses. The RGA arrangement has been examined using 1D modelling and verification experiments using the commonly available engineering material SiO_2. Radiation has been directed to the PV cell by total internal reflection in the SiO_2. The measured power densities of about 0.6 W/cm^2 (corrected value of around 0.8 W/cm^2) is about the same value as for direct illumination of the PV cell by blackbody radiation under similar conditions reported elsewhere. Hence, this work concludes that total internal reflection in dielectrics is a promising concept to replace challenging high temperature mirror design. Also the high-temperature processes for the waste heat recovery application may be difficult to access due to thick insulation layers. Placing the PV cells in this high-temperature environment, as suggested by other TPV research (JX-Crystals), requires not only cooling of the PV cell but also cooling of the entire structural support and this should result in low efficiencies. Guiding and filtering of the radiation from the high-temperature processes to the PV cell should result in lower structural losses.

Experimental and modelling results show that the efficiency improves due to the use of SiO_2 and that the efficiency is further enhanced by an increased SiO_2 thickness. For a

SiO_2 thickness of 100 to 200 mm the experimental results showed that the PV cell efficiency could be at least doubled compared to the direct blackbody illumination.

There has been work reported about micron-gap TPV systems and one experiment using oil at low temperatures, where the prediction was made that the photon flux is limited by the lowest refractive index in the photonic cavity and scales with the minimum refractive index squared. The work reported here proposes and models for the first time the radiator-glass-PV cell (RG) arrangement without an air gap for TPV using dielectric solids with the properties of in-band transmission and high operation temperature. For the SiO_2 thicknesses of interest (30 to 200 mm), modelling showed that the RG arrangement is superior in terms of enhanced efficiency and electrical power density compared to the two other arrangements that were examined. For SiO_2 with a refractive index of about 1.4, the electrical power density should approximately double.

10.2 Lessons learned and future work

The application assessment was based on assumptions, which were made from recently reported TPV work, competing technologies and current market demands. The assessment preferentially resulted in applications with the potential of primary energy saving, because these applications tended to also score higher ratings in the areas of funding and market size. Also the rating system tended to lead to a higher result for applications with larger TPV research participation. In this case it was assumed that technology constraints are more likely to be overcome, however, this is not a certainty. It is in the nature of such assessments that the outcome varies depending on the assumptions and other assessments are likely to generate different results in future as technological barriers are overcome. This is especially true since several TPV

applications achieved close ratings compared to the most promising applications. Also, advances in TPV in the areas of costs, efficiency, demonstrated maximum power or power density could lead to new application markets not considered in this work. Finally, applications based on nuclear sources, as well as military and space applications have been briefly discussed, but excluded from this assessment. Although these high value applications are likely to launch first, this is not considered as of major importance within the UK market.

In the selected application of high-temperature heat recovery some technological challenges were identified in the area of process temperature variation. During the experiments reported in this work the furnace temperature varied in a window of about 10 K due to the on-off operation and this is estimated to result in power output variation of a few percent compared to the total output. Some industrial high-temperature processes can show larger temperature variations. An example is the regenerator location in a glass tank furnace with variation of around 100 K. For a TPV system using this heat source, considerable output power variations would be expected. A thermal storage system that would provide a heat buffer to keep the radiator temperature more stable could minimise these variations. The changing output power may be, at least to some extent, tolerable and the heat recovery process may be regarded as similar to the solar PV conversion process with a varying but cost free energy input. Besides the time dependent temperature variation of some processes, also other process specific impacts on the TPV system design were identified. These include differences in process temperature, location dependent energy losses (heat flux differences) and other existing heat recovery methods. Hence, generally a flexible technological TPV approach is required for this application. Potentially the RGA arrangement examined in the

experiments is a flexible design, since different shapes (concentrators or collimators) of the SiO_2 could allow a system design for different heat fluxes and radiator temperatures in future.

In the experimental design reported in this work, some engineering issues of the heat flux meter design and the SiO_2 devitrification were identified and any future work needs to address these issues. Also, the experimental set-up required an aperture, due to the mismatch of the round SiO_2 face and rectangular PV cell area. From the experimental results it is concluded that such aperture is not an ideal set-up, since the aperture brings in some additional cavity effects and does not allow the required close location of SiO_2 rod-face and PV cell in order to demonstrate the full potential of the RGA arrangement. Further experiments may also fully optically connect the SiO_2 face and the PV cell surface by using optical glue (RG arrangement).

Absolute values, and in particular trends of efficiency and power density were in reasonable agreement between modelled and experimental results of the RGA arrangement with the expected differences for a first experimental design and the simplified modelling assumptions. 3D modelling and the improvements in the experimental set-up discussed above should overcome these differences and result in a closer match of modelled and experimental results.

The reported experiments were limited to a cell area of 1.33 cm^2. So far prototypes of complete TPV heat recovery systems have not been demonstrated. Changes in the experimental set-up should allow the demonstration of (part) systems. These could include scaling up of the output power, measurement of the system efficiency and the design of one mechanical unit. Such a unit could be inserted into different high-temperature processes for a comparison.

10.3 Summary and implications

Both TPV applications and technology have been evaluated in detail. The application of industrial high-temperature heat recovery was selected and assessed. Major reasons for this selection include the limited amount of TPV research in this field, the low competition from other technologies, the potential of higher efficiencies than combustion systems, the potential of a niche market for backup power, the potential of a large market with considerable primary energy savings and the advantages in costs (long operation hours, low cost or free heat input).

For this application process specific impacts on the TPV system design were identified. These impacts were considered by selecting a flexible TPV cavity design. The most important challenge of TPV technology was identified to be the area of optical control in the TPV cavity. In this work, the novel RGA and RG arrangements based on an increased thickness of SiO_2 were proposed.

The concept of total internal reflection in dielectrics was adapted in this work for a practical implementation of the RGA arrangement. Silicon carbide radiators and GaSb PV cells are commonly used in TPV systems and have been also selected for this work. Modelling and experimental work examined the efficiency and the power density of the RGA arrangement. The GaSb PV cell efficiency should at least double, if an additional SiO_2 rod with an effective length of 100 to 200 mm is used when compared to the direct blackbody illumination of the PV cell. Methods to improve the efficiency of the experimental set-up further include the optimisation of the rod length, PV cell front filters and back surface reflectors, lower and multi-bandgap PV cells, the use of other dielectric materials or SiO_2 doping.

For the waste heat recovery application, where the heat is mostly available free of costs to the TPV system, the capital cost per power output (£/W) is regarded as the decisive factor rather than the efficiency. Cell costs are expected to decrease with increasing production volume but are considered to be the major cost constraint in the proposed TPV system. Experimental results of the RGA arrangement suggest that there is a path to higher power densities. Extrapolation of the electrical power density results in about the same values as the result reported for a directly illuminated PV cell. Hence, it can be concluded that in-band radiation guidance by total internal reflection using SiO_2 results in low losses and it seems likely that shaped concentrators would have also low losses. This assumption is supported by some recently reported TPV work concerning SiO_2 prisms. Other research also indicates that III-V PV cells are capable of operating at higher electrical power densities than the typical reported value of 1 W/cm^2 for TPV.

The proposed and modelled RG arrangement is another concept with the potential to increase the power density by a further factor of about two for SiO_2. Also experimental results of the RGA arrangement reported in this work lead to the conclusion that the closest arrangement of SiO_2 rod and PV cell leads to the highest performance. These power density enhancements could result in a reduction of the PV cell area for the same power output and hence should allow reduced capital costs for TPV systems. Alternatively, higher power densities may also offer the possibility to reduce the radiator temperature. As a result the number of potential heat recovery processes would increase. The processes considered for the waste heat recovery application operate at different temperatures and also the heat loss per unit area may vary depending on the

application. Here, individual SiO_2 concentrator designs could be used to match the process requirements.

The proposed and examined TPV implementations of this work were considered for the waste heat recovery application, but are not limited to this heat source. Hence findings for this work can also be of interest for other TPV applications.

Appendices

A. Publications and presentations during the PhD

- Bauer, T., Forbes, I., Penlington, R., Pearsall, N. (2005) 'Heat Transfer Modelling in Thermophotovoltaic Cavities Using Glass Media', *Solar Energy Materials and Solar Cells*, 88(3), pp. 257-268.
- Bauer, T. (2005) 'Thermophotovoltaic Applications and Technology', Oral presentation, *Bavarian Center for Applied Energy Research (ZAE Bayern), Division Thermosensorics and Photovoltaics*, Erlangen, 15. April.
- Bauer, T. (2004) 'Thermophotovoltaic Technology and Applications', Oral presentation, *Meeting of the Society of Glass Technology*, Northumbria University, Newcastle upon Tyne, 28. October.
- Bauer, T., Forbes, I., Penlington, R., Pearsall, N. (2004) 'Heat Transfer Modelling of Glass Media within TPV Systems', Poster presentation with publication in the proceedings, *6th International Conference on Thermophotovoltaic Generation of Electricity*. Freiburg, Germany 14-16 June 2004: New York: American Institute of Physics, pp. 153-161.
- Bauer, T., Forbes, I., Penlington, R., Pearsall, N. (2004) 'An Assessment of Potential Thermophotovoltaic Applications in the UK', Poster presentation with publication in the proceedings, *19th European Photovoltaic Solar Energy Conference*. Paris, 7 - 11 June 2004: Munich: WIP, pp. 2984-1987.
- Bauer, T., Forbes, I., Pearsall, N. (2003) 'The Potential of Thermophotovoltaic Heat Recovery for the UK Industry', Poster presentation with publication in the proceedings, *Conference of the UK International Solar Energy Society C79*, Loughborough, 3 - 4. April. Selected publication: (2004) *International Journal of Ambient Energy*, 25, pp. 19-25.
- Bauer, T. (2003) 'Thermophotovoltaic Technology and Applications', Oral presentation, *Research Seminar*, Northumbria University, Newcastle upon Tyne, 14. Mai.
- Bauer, T. (2002) 'Summary of the 5th Conference on Thermophotovoltaic Generation of Electricity', *Summary for the UK PV Network*.
- Bauer, T., Forbes, I., Penlington, R., Pearsall, N. (2002) 'The Potential of Thermophotovoltaic Heat Recovery for the Glass Industry', Oral presentation with publication in the proceedings, *5th Conference on Thermophotovoltaic Generation of Electricity*. Rome, Italy 16-19 September 2002: New York: American Institute of Physics, pp. 101-110.
- Bauer, T., Forbes, I., Penlington, R., Pearsall, N. (2002) 'Thermophotovoltaic Electric Power Generation for High-Temperature Processes', Poster presentation, *Meeting of the Society of Glass Technology*, Durham, 17 - 19. April.

B. Blackbody table

T(K)	Blackbody radiation in W/cm^2 below the given wavelength in μm												σT^4
	1.0	1.1	1.2	1.3	1.4	1.5	1.6	1.7	1.8	1.9	2.0	2.5	100
700	2.74E-6	1.33E-5	4.89E-5	1.44E-4	3.61E-4	7.87E-4	1.54E-3	2.77E-3	4.63E-3	7.26E-3	1.08E-2	4.65E-2	1.36E+0
773	2.12E-5	8.69E-5	2.76E-4	7.21E-4	1.62E-3	3.23E-3	5.86E-3	9.82E-3	1.54E-2	2.29E-2	3.26E-2	1.16E-1	2.03E+0
800	4.13E-5	1.60E-4	4.84E-4	1.22E-3	2.65E-3	5.13E-3	9.06E-3	1.48E-2	2.28E-2	3.34E-2	4.66E-2	1.57E-1	2.32E+0
873	2.05E-4	6.92E-4	1.87E-3	4.29E-3	8.61E-3	1.56E-2	2.59E-2	4.02E-2	5.90E-2	8.27E-2	1.11E-1	3.25E-1	3.30E+0
900	3.47E-4	1.12E-3	2.93E-3	6.51E-3	1.27E-2	2.25E-2	3.67E-2	5.60E-2	8.09E-2	1.12E-1	1.49E-1	4.14E-1	3.72E+0
973	1.26E-3	3.66E-3	8.75E-3	1.80E-2	3.30E-2	5.53E-2	8.59E-2	1.26E-1	1.75E-1	2.34E-1	3.02E-1	7.54E-1	5.09E+0
1000	1.93E-3	5.49E-3	1.26E-2	2.53E-2	4.55E-2	7.48E-2	1.14E-1	1.65E-1	2.27E-1	3.00E-1	3.84E-1	9.23E-1	5.68E+0
1073	5.58E-3	1.44E-2	3.11E-2	5.88E-2	1.00E-1	1.58E-1	2.32E-1	3.23E-1	4.31E-1	5.55E-1	6.93E-1	1.53E+0	7.52E+0
1100	7.99E-3	2.00E-2	4.22E-2	7.82E-2	1.31E-1	2.03E-1	2.94E-1	4.06E-1	5.37E-1	6.85E-1	8.48E-1	1.81E+0	8.31E+0
1173	1.95E-2	4.53E-2	9.01E-2	1.59E-1	2.55E-1	3.81E-1	5.35E-1	7.18E-1	9.25E-1	1.15E+0	1.40E+0	2.79E+0	1.07E+1
1200	2.64E-2	5.99E-2	1.17E-1	2.02E-1	3.20E-1	4.72E-1	6.57E-1	8.72E-1	1.12E+0	1.38E+0	1.67E+0	3.23E+0	1.18E+1
1273	5.63E-2	1.21E-1	2.24E-1	3.71E-1	5.67E-1	8.10E-1	1.10E+0	1.42E+0	1.78E+0	2.17E+0	2.58E+0	4.71E+0	1.49E+1
1300	7.31E-2	1.53E-1	2.79E-1	4.58E-1	6.90E-1	9.76E-1	1.31E+0	1.69E+0	2.10E+0	2.54E+0	2.99E+0	5.36E+0	1.62E+1
1373	1.41E-1	2.81E-1	4.90E-1	7.75E-1	1.13E+0	1.56E+0	2.05E+0	2.59E+0	3.16E+0	3.77E+0	4.38E+0	7.47E+0	2.02E+1
1400	1.77E-1	3.46E-1	5.96E-1	9.30E-1	1.35E+0	1.84E+0	2.40E+0	3.00E+0	3.65E+0	4.32E+0	5.01E+0	8.39E+0	2.18E+1
1473	3.14E-1	5.88E-1	9.75E-1	1.48E+0	2.08E+0	2.78E+0	3.55E+0	4.38E+0	5.24E+0	6.13E+0	7.02E+0	1.13E+1	2.67E+1
1500	3.83E-1	7.06E-1	1.16E+0	1.73E+0	2.43E+0	3.21E+0	4.08E+0	5.00E+0	5.95E+0	6.93E+0	7.90E+0	1.25E+1	2.87E+1
1573	6.35E-1	1.13E+0	1.79E+0	2.61E+0	3.57E+0	4.64E+0	5.80E+0	7.00E+0	8.23E+0	9.47E+0	1.07E+1	1.63E+1	3.47E+1
1600	7.58E-1	1.33E+0	2.09E+0	3.02E+0	4.09E+0	5.28E+0	6.56E+0	7.88E+0	9.23E+0	1.06E+1	1.19E+1	1.79E+1	3.72E+1
1673	1.19E+0	2.02E+0	3.08E+0	4.35E+0	5.79E+0	7.35E+0	8.99E+0	1.07E+1	1.24E+1	1.40E+1	1.57E+1	2.29E+1	4.45E+1
1700	1.39E+0	2.34E+0	3.53E+0	4.95E+0	6.54E+0	8.26E+0	1.00E+1	1.19E+1	1.37E+1	1.55E+1	1.72E+1	2.49E+1	4.74E+1
1773	2.09E+0	3.40E+0	5.02E+0	6.89E+0	8.95E+0	1.11E+1	1.34E+1	1.56E+1	1.79E+1	2.00E+1	2.21E+1	3.12E+1	5.61E+1
1800	2.41E+0	3.88E+0	5.68E+0	7.74E+0	9.99E+0	1.24E+1	1.48E+1	1.72E+1	1.96E+1	2.19E+1	2.42E+1	3.37E+1	5.96E+1
1873	3.48E+0	5.45E+0	7.81E+0	1.05E+1	1.33E+1	1.62E+1	1.92E+1	2.21E+1	2.50E+1	2.77E+1	3.04E+1	4.14E+1	6.99E+1
1900	3.96E+0	6.14E+0	8.73E+0	1.16E+1	1.47E+1	1.79E+1	2.11E+1	2.42E+1	2.72E+1	3.02E+1	3.29E+1	4.45E+1	7.40E+1
1973	5.52E+0	8.37E+0	1.17E+1	1.53E+1	1.91E+1	2.29E+1	2.67E+1	3.05E+1	3.40E+1	3.75E+1	4.07E+1	5.39E+1	8.60E+1
2000	6.21E+0	9.34E+0	1.29E+1	1.68E+1	2.09E+1	2.50E+1	2.91E+1	3.31E+1	3.69E+1	4.05E+1	4.39E+1	5.77E+1	9.08E+1
2073	8.42E+0	1.24E+1	1.69E+1	2.17E+1	2.66E+1	3.15E+1	3.63E+1	4.09E+1	4.53E+1	4.94E+1	5.33E+1	6.89E+1	1.05E+2
2100	9.38E+0	1.37E+1	1.86E+1	2.37E+1	2.89E+1	3.42E+1	3.93E+1	4.41E+1	4.88E+1	5.31E+1	5.72E+1	7.34E+1	1.10E+2
2173	1.24E+1	1.78E+1	2.37E+1	2.99E+1	3.61E+1	4.22E+1	4.82E+1	5.38E+1	5.91E+1	6.40E+1	6.86E+1	8.67E+1	1.27E+2
2200	1.37E+1	1.95E+1	2.59E+1	3.25E+1	3.91E+1	4.56E+1	5.18E+1	5.77E+1	6.33E+1	6.84E+1	7.32E+1	9.20E+1	1.33E+2
2273	1.77E+1	2.48E+1	3.25E+1	4.03E+1	4.80E+1	5.55E+1	6.27E+1	6.94E+1	7.57E+1	8.15E+1	8.68E+1	1.08E+2	1.52E+2
2300	1.94E+1	2.71E+1	3.52E+1	4.35E+1	5.17E+1	5.96E+1	6.71E+1	7.41E+1	8.07E+1	8.67E+1	9.23E+1	1.14E+2	1.59E+2
2373	2.47E+1	3.39E+1	4.35E+1	5.31E+1	6.26E+1	7.16E+1	8.01E+1	8.81E+1	9.54E+1	1.02E+2	1.08E+2	1.32E+2	1.80E+2
2400	2.69E+1	3.67E+1	4.69E+1	5.71E+1	6.70E+1	7.65E+1	8.54E+1	9.37E+1	1.01E+2	1.08E+2	1.15E+2	1.39E+2	1.88E+2
2473	3.36E+1	4.52E+1	5.71E+1	6.88E+1	8.02E+1	9.09E+1	1.01E+2	1.10E+2	1.19E+2	1.26E+2	1.33E+2	1.60E+2	2.12E+2
2500	3.64E+1	4.87E+1	6.12E+1	7.36E+1	8.55E+1	9.67E+1	1.07E+2	1.17E+2	1.26E+2	1.34E+2	1.41E+2	1.68E+2	2.22E+2
2573	4.48E+1	5.92E+1	7.36E+1	8.78E+1	1.01E+2	1.14E+2	1.25E+2	1.36E+2	1.46E+2	1.55E+2	1.63E+2	1.92E+2	2.49E+2

C. Ultimate efficiency: relation between x+ and r+

		r+									
		0	**0.1**	**0.2**	**0.3**	**0.4**	**0.5**	**0.6**	**0.7**	**0.8**	**0.9**
x_g	**0.1**	0.1	1.5	2.1	2.6	3.0	3.5	4.0	4.6	5.4	6.6
	0.5	0.5	1.6	2.1	2.6	3.0	3.5	4.0	4.6	5.4	6.6
	1	1.0	1.7	2.2	2.7	3.1	3.6	4.1	4.7	5.4	6.6
	1.5	1.5	2.0	2.5	2.9	3.3	3.7	4.2	4.8	5.6	6.7
	2	2.0	2.4	2.8	3.2	3.5	4.0	4.4	5.0	5.7	6.9
	2.5	2.5	2.8	3.2	3.5	3.9	4.3	4.7	5.3	6.0	7.1
	3	3.0	3.3	3.6	3.9	4.2	4.6	5.0	5.6	6.2	7.3
	3.5	3.5	3.8	4.0	4.3	4.6	5.0	5.4	5.9	6.6	7.6
	4	4.0	4.2	4.5	4.7	5.0	5.4	5.8	6.3	6.9	8.0
	4.5	4.5	4.7	4.9	5.2	5.5	5.8	6.2	6.6	7.3	8.3
	5	5.0	5.2	5.4	5.7	5.9	6.2	6.6	7.0	7.7	8.7
	5.5	5.5	5.7	5.9	6.1	6.4	6.7	7.0	7.5	8.1	9.1
	6	6.0	6.2	6.4	6.6	6.8	7.1	7.5	7.9	8.5	9.5
	6.5	6.5	6.7	6.9	7.1	7.3	7.6	7.9	8.4	8.9	9.9
	7	7.0	7.2	7.4	7.6	7.8	8.1	8.4	8.8	9.4	10.3
	7.5	7.5	7.7	7.8	8.0	8.3	8.5	8.9	9.3	9.8	10.8
	8	8.0	8.2	8.3	8.5	8.8	9.0	9.3	9.7	10.3	11.2
	8.5	8.5	8.7	8.8	9.0	9.2	9.5	9.8	10.2	10.7	11.7
	9	9.0	9.2	9.3	9.5	9.7	10.0	10.3	10.7	11.2	12.1
	9.5	9.5	9.7	9.8	10.0	10.2	10.5	10.8	11.1	11.7	12.6
	10	10.0	10.2	10.3	10.5	10.7	10.9	11.2	11.6	12.1	13.0

D. Conversion for the band model with examples

The modelling results have allowed general statements about TPV efficiency, power density and ideal PV cell bandgap. However, practical spectral control approaches do not follow the assumed idealised band model. An equivalent spectral band (values of x+ and x-) can be calculated, which generates the same amount of heat and electricity as the practical spectral control approach. The values x- and x+ can be calculated for the practical spectral control approach and then compared with the model. The two unknowns x+ and x- can be found by one equation for electricity conservation (Equation D-1) and one for heat conservation (Equation D-2) assuming a known value T_s and hv_g (or x_g).

$$hv_g \int_{v_g}^{\infty} \frac{R_{real(v)}}{hv} dv = hv_g \cdot \frac{2\pi}{c_0^2} \int_{v_g}^{v+} \frac{v^2}{e^{\frac{hv}{kT_s}} - 1} dv \tag{D-1}$$

$$\int_0^{\infty} R_{real(v)} dv = \frac{2\pi h}{c_0^2} \int_{v-}^{v+} \frac{v^3}{e^{\frac{hv}{kT_s}} - 1} dv = \frac{2\pi h}{c_0^2} \int_{v-}^{v_g} \frac{v^3}{e^{\frac{hv}{kT_s}} - 1} + \frac{2\pi h}{c_0^2} \int_{v_g}^{v+} \frac{v^3}{e^{\frac{hv}{kT_s}} - 1} \tag{D-2}$$

Equation D-1 allows calculation of v+, which can be then used in Equation D-2 to find v-. This methodology was applied to different practical spectral control approaches and equivalent values x_g, x+, x-, r+, r-, max. η_{TPV} and max. P_{TPV} were computed. Spectral radiation values have been scanned and converted in vector data using Matlab. For some spectra, this process also included interpolated of some data outside the given frequency range (respectively wavelengths range). Estimations given in TPV literature are marked with # in the following table.

	T_s (K)	hv_g (eV)	x_g (1)	x- (1)	x+ (1)	r- (1)	r+ (1)	max. η_{TPV} (%)	η_{real} (%)	max. P_{TPV} (W/ cm^2)	P_{real} (W/ cm^2)
Model of a SiC radiator with two quartz shields and a 18-layer dielectric filter [46]	1473	0.69	5.43	4.72	6.68	0.111	0.522	48	8.5[51] 10#	2.44	1.14[52]
Monte Carlo model of a Antireflection tungsten radiator and a 9-layer dielectric filter [46]	1573	0.69	5.09	4.64	6.01	0.081	0.405	57	15#	3.08	0.79#
FSS filter transmission multiplied with blackbody radiation [96]	1673	0.69	4.78	4.47	5.51	0.064	0.323	63	9.7[53] 16#[54]	3.67	0.86 2.48#[55]
Co-doped MgO matched radiator [143]	1474	0.69	5.43	3.81	7.94	0.304	0.790	34	No sys.	3.49	No sys.
Double quartz shield with a blackbody radiator [138]	1573	0.69	5.09	3.26	7.93	0.412	0.825	32	No sys.	5.62	No sys.
Yb_2O_3 mantel radiator [260]	1735	1.12	7.49	5.42	8.52	0.148	0.500	15	2.4[56]	1.33	0.1[57] 0.3#
Yb_2O_3 fibre radiator [262]	2000	1.12	6.50	5.47	7.05	0.096	0.295	25	2 4#[58]	2.74	.76[59]
Yb_2O_3 radiator with a single crystal YAG rod [115]	2407	1.12	5.40	5.08	5.90	0.046	0.250	54	6.8[60]	9.12	1.04[61]
Erbium aluminium garnet radiator [145][62]	1523	0.62	4.72	3.31	5.42	0.359	0.311	24	No sys.	2.57	No sys.

[51] Tests with SiC glowbar and one quartz shield with a total cell area of 396 cm^2. At a radiator temperature of 1873 K the electrical power output was 990 W and the water heat load 10532 W. The efficiency was then calculated as $\eta = 990 / 10532 = 9.4\%$. In the work reported here, the efficiency is calculated as $\eta = 990 / (990+10532) = 8.6\%$ assuming no other losses. A correction factor of 8.6/9.4 = 0.92 has been used here for the efficiency at 1573 K: $\eta = 0.92 \cdot 7.8\% = 7.2\%$.

[52] 450 W / 396 cm^2 = 1.14 W/cm^2

[53] At 1473 K radiator temperature and a recuperator leakage without housekeeping power.

[54] At 1673 K radiator temperature and without recuperator leakage and without housekeeping power.

[55] At 1473 K radiator temperature without housekeeping power. 216 cm^2 of PV cells and an output of 185W.

[56] This includes the combustion efficiency, so a higher efficiency η_{real} can be expected.

[57] Power density P_{real} = 47.9 W / 480 cm^2 = 0.1 W/cm^2.

[58] With air preheating including combustion efficiency

[59] Assuming no housekeeping power P_{real} = 110 W / 144 cm^2 = 0.76 W/cm^2

[60] Total radiation power leaving the rod was computed as 15.2 W/cm^2. Using P_{real} = 1.04 W/cm^2 leads to ηreal = 1.04/15.2 = 6.8%

[61] At 1973 K instead of 2407 K.

[62] Computed from 2 μm bandgap, hv_g = 1.24 / 2 eV = 0.62 eV

E. Analysis of the radiant tube burner combustion

In the following calculations a typical North Sea natural gas composition by volume is assumed [420]: CH_4 = 94.4%, C_2H_6 = 3.22%, C_3H_8 = 0.6%, C_4H_{10} = 0.2%, C_5H_{12} = 0.07%, CO_2 = 0.05% and N_2 = 1.46%. The flue gas analyser measures the volumetric composition on a dry basis. The following composition was measured: CO_2 = 10.3%, O_2 = 3.0%. Unburned hydrocarbons and carbon monoxide (CO) were close to zero and within the tolerance of the flue gas analyser. Hence unburned hydrocarbons and CO have been neglected.

The volumetric composition of the combustion products by percentage **volume on dry basis** is then: CO_2 = 10.3%, O_2 = 3.0% and N_2 = 86.7%. The combustion equation can then be written as the reaction of natural gas reaction with air to the products of CO_2, O_2, H_2O and N_2.

$$0.944CH_4+0.0322C_2H_6+0.006C_3H_8+0.002C_4H_{10}+0.0007C_5H_{12}+0.0005CO_2+0.0146N_2 +AF_V\cdot(0.21O_2+0.79N_2) \rightarrow X_{meas}\cdot(0.103CO_2+0.03O_2) + X_{H2O}\cdot H_2O+ X_{N2}\cdot N_2$$

The balance for each element allows calculation of the four unknowns AF, X_{meas}, X_{H2O} and X_{H2O} [474].

C: $0.944+2\cdot0.0322+3\cdot0.006+4\cdot0.002+5\cdot0.0007+0.0005= X_{meas}\cdot0.103 \rightarrow \underline{X_{meas}= 10.082}$
H: $4\cdot0.944+6\cdot0.0322+8\cdot0.006+10\cdot0.002+12\cdot0.0007= X_{H2O}\cdot2 \rightarrow \underline{X_{H2O} = 2.023}$
O: $2\cdot0.0005+ AF_V\cdot2\cdot0.21= X_{meas}\cdot(2\cdot0.103+2\cdot0.03)+X_{H2O}$
$0.001+ AF_V\cdot0.42 = 10.082\cdot(2\cdot0.103+2\cdot0.03)+2.023$
$0.001+ AF_V\cdot0.42 =2.682+2.023=4.705$
$\underline{AF_V=11.2}$
N: $2\cdot0.0146+AF\cdot2\cdot0.79= 2\cdot X_{N2} \rightarrow \underline{X_{N2} = 8.726}$

The complete combustion equation reads then:

$$0.944CH_4+0.0322C_2H_6+0.006C_3H_8+0.002C_4H_{10}+0.0007C_5H_{12}+0.0005CO_2+0.0146N_2 +11.2\cdot(0.21O_2+0.79N_2) \rightarrow 10.082\cdot(0.103CO_2+0.03O_2) + 2.023H_2O+ 8.726N_2$$
$$(\rightarrow 1.038CO_2+0.302O_2 + 2.023H_2O+ 8.726N_2)$$

If all gases are assumed to be ideal gases this equation can be used to determine the composition of the combustion products by percentage **volume on a wet basis** [473]:

Total kmoles of the products in the equation: 1.0384+0.26636+8.726+2.0228=12.05356
CO_2 =1.0384/12.05356=8.6%
O_2 =0.26636/12.05356=2.2%
N_2=8.726/12.05356=72.4%
H_2O=2.0228/12.05356=16.8%

The combustion equation can also be written in terms of masses [473]:

$16 \cdot 0.944 kgCH_4 + 30 \cdot 0.0322 kgC_2H_6 + 44 \cdot 0.006 kgC_3H_8 + 58 \cdot 0.002 kgC_4H_{10} + 72 \cdot 0.0007 kgC_5H_{12}$
$+ 44 \cdot 0.0005 kgCO_2 + 28 \cdot 0.0146 kgN_2$
$+ 11.2 \cdot (32 \cdot 0.21 kgO_2 + 28 \cdot 0.79 kgN_2)$
$\rightarrow 10.082 \cdot (44 \cdot 0.103 kgCO_2 + 32 \cdot 0.03 kgO_2) + 18 \cdot 2.023 kgH_2O + 28 \cdot 8.726 kgN_2$
$(\rightarrow 45.692 kgCO_2 + 9.679 kgO_2 + 36.414 kgH_2O + 244.328 N_2)$

The combustion products composition **by weight on wet basis** is then:

Total weight of the products in the equation: 336.113kg
CO_2 =45.692/336.113=13.6%
O_2 =9.679/336.113=2.9%
N_2=244.328/336.113=72.7%
H_2O=36.414/336.113=10.8%

The combustion products composition **by weight on dry basis** is:

Total weight of the products in the equation: 299.699kg
CO_2 =45.692/ 299.699=15.3%
O_2 =9.679/ 299.699=3.2%
N_2=244.328/ 299.699=81.5%

The volumetric air flue ratio AF_V can be verified experimentally.

ΔP_{gas} = 13 mbar $\rightarrow$ V_{gas} = 0.901 m^3/h
ΔP_{air} = 16 mbar $\rightarrow$ V_{air} = 10 m^3/h
$AF_V = V_{air} / V_{gas}$ 10m^3/h /0.901m^3/h = 11.1 compared to the calculated AF_V = 11.2

The air to fuel ratio by weight is:

Total fuel weight in the equation: 16.931kg, Total air weight in the equation: 323.008kg
Air fuel ratio by weight: $\underline{AF_w = 19.078}$

The ratio combustion products to fuel by weight on dry basis is:

CF = 299.699kg/16.931kg = 17.702

Assuming the composition of typical North Sea natural gas [420], the total power into the furnace is:

$P_{in} = V_{gas} \cdot H_u$ = 0.901$m^3/h \cdot$34.91 MJ/m^3 = 8.74kW

Using the density of typical North Sea natural gas [420] gives the total fuel input weight per hour:

$V_{gas} \cdot \rho_{gas} = 0.901 m^3/h \cdot 0.719 kg/m^3 = 0.648$ kg/h

This allows calculation of the flue gas mass output per hour on dry basis

$V_{gas} \cdot \rho_{gas} \cdot CF = 0.648$ kg/h $\cdot 17.702 = 11.468$ kg/h

A flue gas temperature of around 770 K was measured by inserting a K-type thermocouple a few centimetres from the top in the exhaust gas tube (Figure 9-3). The specific enthalpy of stoichiometric combustion products is about 0.6 MJ/kg at this temperature [420]. It is assumed here that the combustion products of the furnace have the same value, since no specific enthalpy for other flue gas compositions was available here. The thermal power in the flue gas in total and as a percentage of the input is then:

$P_{flue} = 11.468$ kg/h $\cdot$ 0.6 MJ/kg = 1.91 kW, $P_{flue}/P_{in} \sim 22\%$

F. Calibration of the heat flux meter

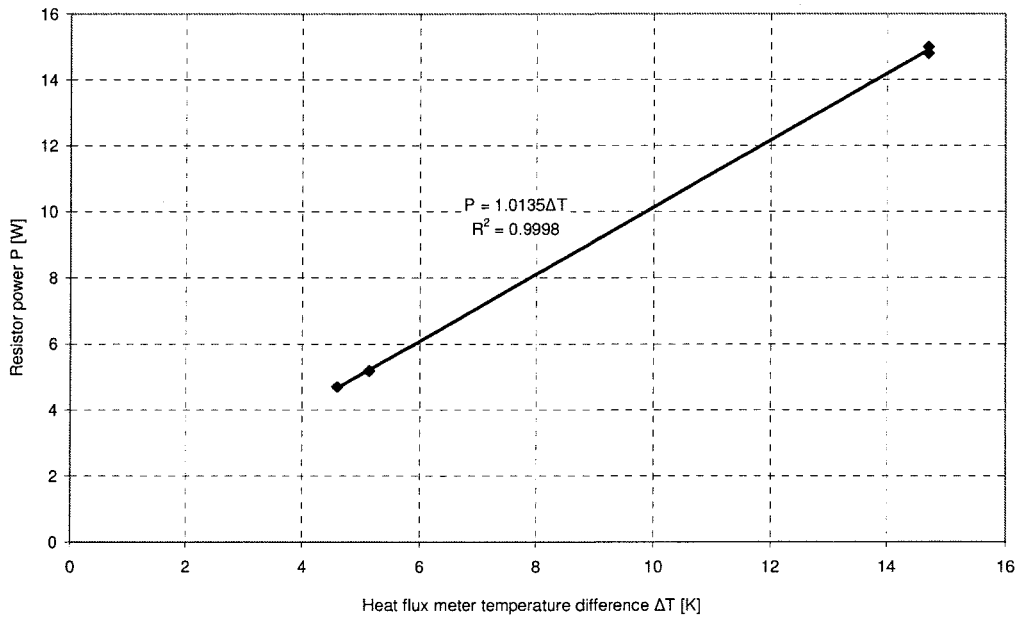

G. IV curve matching using a Matlab tool

The matching of the one-diode model approximation to the measurement points was a manual and iterative process using a Matlab tool. The PV cell temperature was fixed either to 293 or 313 K. The major influences of the remaining parameters are the following:

- The saturation current I_s influences the open circuit voltage V_{oc}
- The photocurrent I_{ph} influences the short circuit current I_{sc}
- The series resistance R_s influences the gradient near open circuit operation
- The parallel resistance R_p influences the gradient near short circuit operation

The example plot is for a PV cell operating at 293 K together with a SiO_2 rod with 25 mm diameter a total length of 170 mm. The x-axis shows the voltage (V) and the y-axis the current (A). The measurement points are plotted as stars and the one-diode model approximation as solid line. The current (I_m) and voltage (V_m) values for maximum power (P_m) are also shown as a grey line in the plot. The five varying parameters were I_s, I_{ph}, R_s, R_p T_c. The program was used to calculate then I_{sc}, V_{oc}, I_m, V_m and η_{FF}.

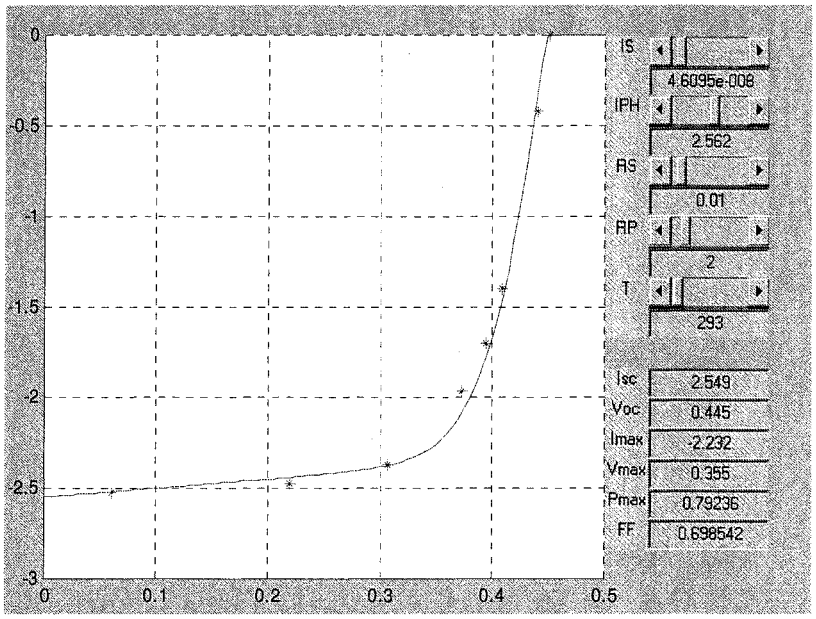

H. Peltier circuit to control the PV cell temperature

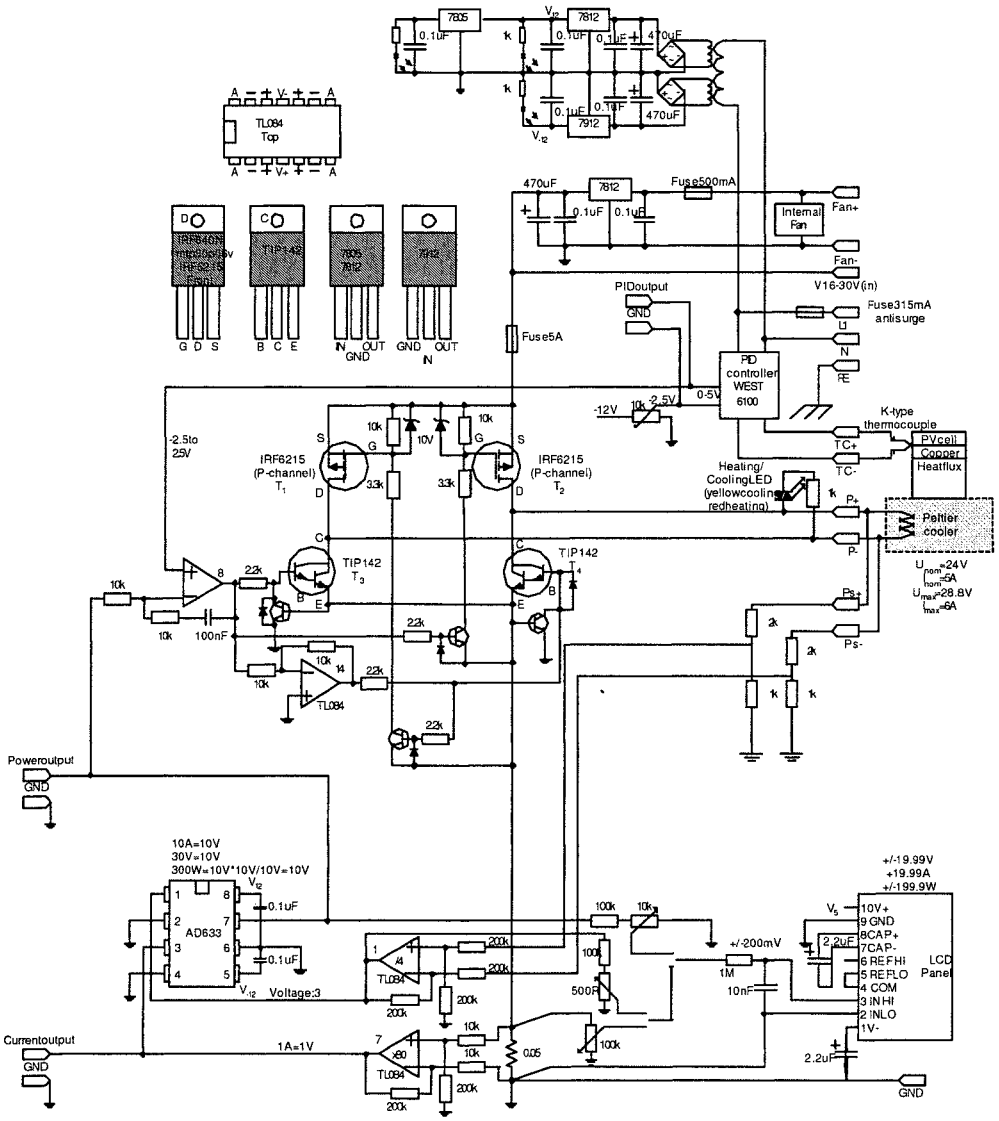

I. Data of the water flow meters

	Dual range transducer (low flow) [481]	Dual range transducer (high flow) [481]	Flow transducer V8189 [480]
RS Order code	256-225	256-225	257-133
Flow range	3 – 90 litre/hour	12 – 540 litre/hour	90 – 1800 litre/hour
Frequency range	5.75 – 172.5 Hz	4 – 180 Hz	30 – 600 Hz
Period time range	174 – 5.8 ms	250 – 5.6 ms	33 – 1.7 ms

J. Details of the heat exchanger measurements

Large aluminium heat exchanger

Date	Flow meter	Power absorbed	Water bath temperature	Glass rod dimens.	Comment
2.7.2004	Dual range low	26 W	293 K	270 x 10 mm	Without steel washer and aluminium tube only, furnace only 1423 K
20.7.2004	Dual range high	29 W	283 K	270 x 10 mm	From now always with steel washer, 0.2" aperture and black plate installed, furnace at 1423 K
10.1.2005	Dual range high	21 W	293 K	270 x 25 mm	0.2" aperture installed, black plate installed with uncontrolled cell temperature, furnace 1523 K
11.1.2005	Dual range high	30 W	288 K	270 x 25 mm	PV cell installed, 1.5 hours at 1523 K before that bath temperature at 293 K and furnace at 1373 K
14.1.2005	Dual range high	24 W	288 K	270 x 25 mm	PV cell installed, 2 hours at 1523 K

Copper heat exchanger

Date	Flow meter	Power absorbed	Water bath temperature	Glass rod dimens.	Comment
20.7.2004	V8189	18 W[63]	283 K	270 x10 mm	From now always with steel washer, 0.2" aperture installed, black plate installed and controlled to 288 K, furnace at 1423 K
10.1.2005	V8189	29 W	293 K	270 x 10 mm	0.2" aperture installed, black plate installed with uncontrolled temperature, furnace at 1523 K
11.1.2005	V8189	29 W	288 K	270 x 25 mm	PV cell installed, 1.5 hours at 1523 K before that bath temperature at 293 K and furnace at 1373 K
14.1.2005	V8189	25 W	288 K	270 x 25 mm	PV cell installed, 2 hours at 1523 K

[63] The temperature difference of water inlet and outlet was only 0.4 K and the temperatures were read manually with a resolution of 0.1 K. An increase of the differential temperature of 0.1 K results in a power increase of about 4 W. Hence, this value can show larger errors.

Small aluminium heat exchanger

Date	Flow meter	$P_{small,alu}$	P_{flux}	$P_{peltier}$	Water bath temp.	Glass rod dim.	Comment
28.1.04	Dual range low	5.7W	4.7W	2W	293 K	-	Heat flux meter unit only, P_{flux} is the known power of a resistor
28.1.04	Dual range low	36W	14.9W	29W	293 K	-	Same as above, the disagreement of the heat balance may be explained by heat transferred to the environment (e.g. laboratory table) and not the cooling water.
20.7.04	Dual range low	2.8W	1W	Too small	283 K	270x 10mm	From now always with steel washer, 0.2" aperture and black plate installed, furnace at 1423 K
10.1.05	Dual range low	2.8 W	2.7W	~0W	293 K	270x 25mm	0.2" aperture installed, black plate installed with uncontrolled temperature, furnace at 1523 K
10.1.05	Dual range low	0.9W	0.7W	~0W	293 K	270x 25mm	Closed aperture installed, black plate installed with uncontrolled temperature, furnace at 1523 K
11.1.05	Dual range low	13.5W	10.4W	2.9W	288 K	270x 25 mm	PV cell installed, 1.5 hours at 1523 K before that bath temp. at 293 K and furnace at 1373 K
18.1.05	Dual range low	20W[64]	10.6W	4.2W	288 K	170x 25 mm	Black plate with 0.2" aperture installed, plate temp. controlled to 293 K, furnace at 1523 K
18.1.05	Dual range low	27W[64]	14.3W	6.8W	288 K	170x 25 mm	PV cell installed, PV cell temperature controlled to 293 K, furnace at 1523 K
18.1.05	Dual range low	24W[64]	14.1W	5.4W	308 K	170x 25 mm	PV cell installed, PV cell temperature controlled to 313 K, furnace at 1523 K
21.1.05	Dual range low	2.8W[64]	2.9W	~0	288 K	220x 25 mm	Black plate with 0.2" aperture installed, plate temperature controlled 293 K, furnace 1523 K
21.1.05	Dual range low	17W[64]	9.0W	1.3W	288 K	220x 25 mm	Black plate with 0.4" aperture installed, plate temperature controlled 293 K, furnace 1523 K
21.1.05	Dual range low	16W[64]	9.8W	2.9W	288 K	220x 25 mm	PV cell installed, PV cell temperature controlled to 293 K, furnace at 1523 K
21.1.05	Dual range low	2.6W[64]	1.9W	~0	288 K	220x 25 mm	Closed aperture, PV cell temperature controlled to 293 K, furnace at 1523 K
21.1.05	Dual range low	13W[64]	9.6W	1W	308 K	220x 25 mm	PV cell installed with aperture, PV cell temperature controlled to 313 K, furnace at 1523 K

[64] This calculation was based on temperature difference below 1 K and may show high errors.

K. Analysis of the quality of the heat balance

The quality of the heat balance ($P_{small,alu} = P_{flux} + P_{peltier}$) is shown graphically. $P_{small,alu}$ forms the y-axis and $P_{flux} + P_{peltier}$ the x-axis. The ideal balance is shown as a doted line. The measurements taken with a small temperature difference for the inlet and outlet water temperature result in values too low (triangles). All other measurement points are shown as squares and are in good agreement with the theoretical value (dotted line).

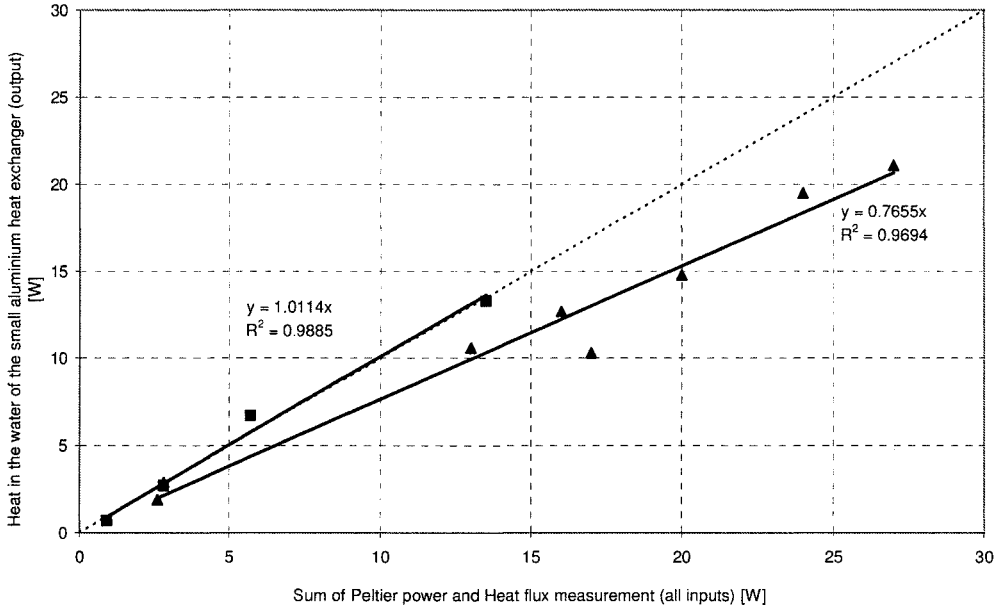

L. Details of the black absorber plate measurements

SiO_2 dimension	Measured heat flux	Aperture diameter	Heat flux experiment	Modelled heat flux
100, Ø 25 mm	10.5 K[65]	0.4"	10.5 K/0.8103 cm^2 · 1.0135 W/K=13.1W/cm^2	
170, Ø 25 mm	10.4 K	0.4"	10.4 K/0.8103 cm^2 · 1.0135 W/K=13.0W/cm^2	
100 mm 1D Modelling				14.3W/cm^2
220, Ø 25 mm	2.8 K	0.2"	2.8K/0.2027cm^2 · 1.0135 W/K=14.0W/cm^2	
270, Ø 25 mm	2.7 K	0.2"	2.7K/0.2027cm^2 · 1.0135 W/K=13.5W/cm^2	
200 mm 1D Modelling				10.8 W/cm^2

[65] Increased water bath temperature to 291 K (18 °C).

M. Open circuit voltage vs. temperature measurement

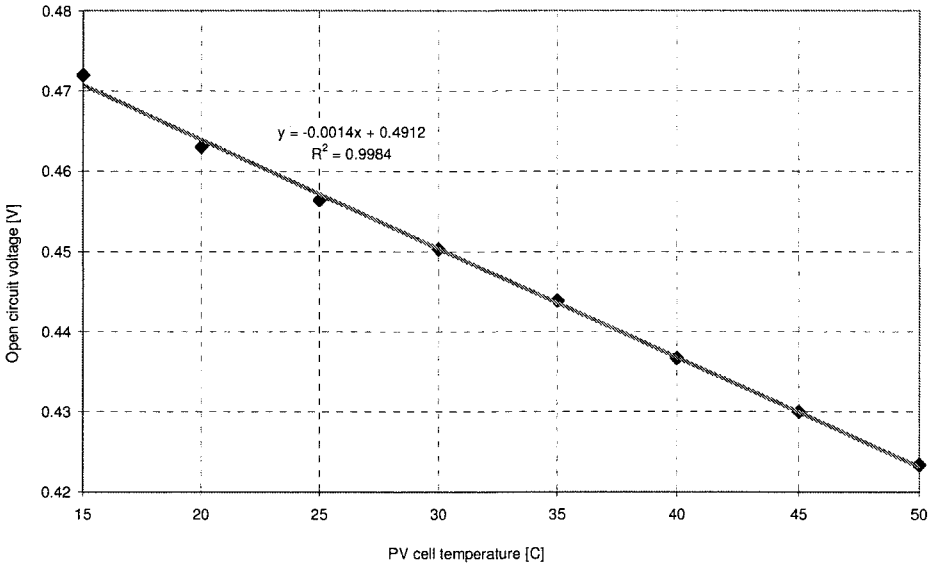

N. Details of the power density calculations

For the 270 mm SiO_2 rod, the complete set-up of the rod has been repeated at the end of the experiments. Here, only one measurement point near the short circuit case has been measured (Figure last). Also one additional measurement was made before the first complete IV curve measurement (Figure first). The interpolation is based on R_s = 12 mΩ, R_p = 2 Ω and $I_s = 4.3 \cdot 10^{-8}$ A selected from the previous experiments using the same Matlab tool as in Apendix G.

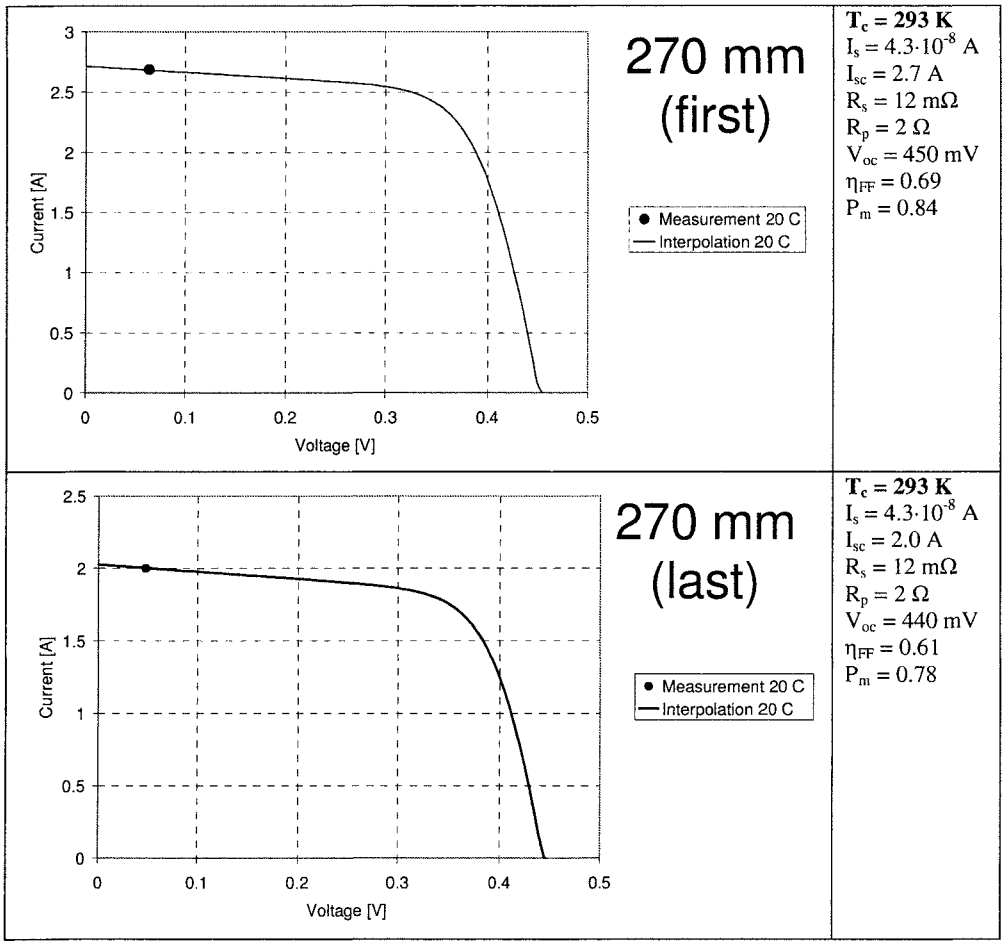

O. Details of the efficiency calculations

Total rod length	**170 mm**	**220 mm**	**270 mm**
Effective rod length	**100 mm**	**150 mm**	**200 mm**
PV cell temp. 293 K			
$T_{avg.\ PV\ cell}$	293.6 K	290.6 K	297.4 K
P_{el}	0.78 W	0.70 W	0.78 W
$P_{el,corrected}$[66]	0.90 W	0.87 W	0.84 W
P_{heat_meter}	14.3 W	9.8 W[67]	11.2 W
P_{water}	26.7 W[68]	15.7 W[68]	10.3 W
$P_{Peltier}$	- 6.8 W	- 2.9 W	- 0.5 W
P_{heat_water}[69]	19.9 W	12.8 W	9.8 W
$\eta_{PV,meter}$[70]	5.2%	6.7%	6.5%
$\eta_{PV,meter,\ corrected}$	5.9%	8.2%	7.0%
$\eta_{PV,water}$	3.8%	5.2%	7.3%
$\eta_{PV,water,\ corrected}$	4.3%	6.4%	7.9%
PV cell temp. 313 K			
P_{el}	0.76 W	0.66 W	0.78 W
P_{heat_meter}	14.1 W	9.6 W	10.6 W
P_{water}	23.8 W	12.8 W	6.24 W
$P_{Peltier}$	- 5.4 W	- 0.98 W	- 0.5 W
P_{heat_water}	18.4 W	11.8 W	5.7 W[71]
$\eta_{PV,meter}$	5.1%	6.4%	6.8%
$\eta_{PV,water}$	4.0%	5.3%	12%[71]

[66] Corrected for PV cell decay as described for the power density. View factor losses have been not corrected.

[67] In an analysis of the measurement data it was found that the heat flux meter temperature was below 273 K (0 °C) in a black absorbed plate experiment immediately before the heat flux measurement of interest. This should have caused condensation on the heat flux meter influencing the heat flux measurement. The condensed water on the heat flux meter is thought to have predicted the heat flux measurement too low. This conclusion can be strengthened through a second verification measurement of the heat flux meter value at 200 mm effective SiO_2 thickness.

[68] Small temperature differences of inlet and outlet may have resulted in errors.

[69] $P_{heat\_flux\_water} = P_{water} - P_{Peltier}$

[70] $\eta_{PV,meter} = P_{el} / (P_{el} + P_{heat\_meter})$

[71] The experiment was not in equilibrium for this measurement.

List of references

1. Great Britain. Department of Trade and Industry (2002) *Energy Consumption in the United Kingdom*. London: Department of Trade and Industry.
2. Nelson, R. (2003) 'TPV Systems and state-of-the-art development', *5th Conference on Thermophotovoltaic Generation of Electricity*. Rome, Italy 16-19 September 2002: New York: American Institute of Physics, pp. 3-17.
3. Coutts, T.J. (1999) 'A review of progress in thermophotovoltaic generation of electricity', *Renewable and Sustainable Energy Reviews*, 3(2-3), pp. 77-184.
4. Sze, S.M. (1981) *Physics of Semiconductor Devices*, 2nd edn. New York Chichester Brisbane Toronto Singapore: Wiley & Sons.
5. Würfel, P. (1995) *Physik der Solarzellen*. (in German), 2nd edn. Heidelberg Berlin: Spektrum Akademischer Verlag.
6. Doyle, E.F., Becker, F.E., Shukla, K.C., Fraas, L.M. (1999) 'Design of a thermophotovoltaic battery substitute' *4th NREL Conference on Thermophotovoltaic Generation of Electricity*. Denver, Colorado, US 11-14 October 1998: New York: American Institute of Physics, pp. 351-361.
7. Durisch, W., Grob, B., Mayor, J. C., Panitz, J. C., Rosselet, A. (1999) 'Interfacing a small thermophotovoltaic generator to the grid' *4th NREL Conference on Thermophotovoltaic Generation of Electricity*. Denver, Colorado, US 11-14 October 1998: New York: American Institute of Physics, pp. 403-414.
8. Modest, M.M. (1993) *Radiative Heat Transfer*, New York: McGraw-Hill.
9. Siegel, R., Howell, J. (2001) *Thermal Radiation Heat Transfer*, 4th edn. Washington London: Taylor & Francis.
10. Biter, P. J., Georg, K. A., Phillips, J. E. (1997) 'A TPV system using a gold filter with $CuInSe_2$ solar cells' *3rd NREL Conference on Thermophotovoltaic Generation of Electricity*. Denver, Colorado, US 18-21 May 1997: New York: American Institute of Physics, pp. 443-459.
11. Howell, J.R., Mengüç, M. P. (1998) 'Chapter 7: Radiation', in Rohsenow, W.M. et al. (ed.) Handbook of Heat Transfer, 3rd edn. New York: McGraw-Hill, pp. 7.1-7.100.
12. Les, J., Borne, T., Cross, D., Gang Du, Edwards, D.A., Haus, J., King, J., Lacey, A., Monk, P., Please, C., Hoa Tran (2000) 'Interference filters for thermophotovoltaic applications', Fifteenth Workshop on Mathematical Problems in Industry, Delaware, US June 1999.
13. Modest, M.F. (1999) 'Section 3.3: Radiation' in Kreith, F. (ed.) *CRC Handbook of Thermal Engineering*, London: CRC Press, pp. 65-91.
14. Gombert, A. (2003) 'An overview of TPV emitter technologies' *5th Conference on Thermophotovoltaic Generation of Electricity*. Rome, Italy 16-19 September 2002: New York: American Institute of Physics, pp. 123-131.
15. Licciulli, A., Diso, D., Torsello, G., Tundo, S., Maffezzoli, A., Lomascolo, M. Mazzer, M. (2003) 'The challenge of high-performance selective emitters for thermophotovoltaic applications' *Semiconductor Science and Technology*, 18, pp. 174-183.
16. Archer, M. D., Hill, R. (ed.) (2001) *Clean Electricity from Photovoltaics (Series on Photoconversion of Solar Energy, Volume 1)*, London: Imperial College Press.
17. Benner, J.P., Coutts, T.J. (2000) 'Section 60.3 Thermophotovoltaics', in Dorf, R.C. (ed.) *The Electrical Engineering Handbook*, Boca Raton: CRC Press.
18. Fahrenbruch, A.L., Bube, R.H. (1983) 'Chapter 12: Concentrators, Concentrator Systems, and Photoelectrochemical Cells', in Fahrenbruch, A. L., Bube, R. H. (ed.) *Fundamentals of Solar Cells*, pp. 505-540.
19. Green, M.A. (2003) 'Chapter 9: Thermophotovoltaic and Thermophotonic Conversion' in Green, M.A. (ed.) *Third generation photovoltaics - advanced solar energy conversion*, New York: Springer Press, pp. 112-123.

20. Würfel, P. (1995) 'Chapter 8: Konzepte zur Verbesserung des Wirkungsgrads (in German)' in Würfel, P. (ed.) *Physik der Solarzellen* 2nd edn. Heidelberg Berlin: Spektrum Akademischer Verlag, pp. 167-185.
21. Decher, R. (1997) *Direct Energy Conversion Fundamentals of electric power production*, New York Oxford: Oxford University Press.
22. Angrist, S.W. (1976) *Direct Energy Conversion*, 3rd edn., Boston: Allyn and Bacon.
23. Kassakian, J.G. (1967) *A planar germanium thermophotovoltaic energy converter*, PhD thesis. Massachusetts Institute of Technology.
24. Whale, M.D. (1997) *A fluctuational electrodynamic analysis of microscale radiative transfer and the design of microscale thermophotovoltaic devices*, PhD thesis. Massachusetts Institute of Technology.
25. Griffin, P.R. (1997) *An investigation of quantum well solar cells for concentrator and thermophotovoltaic applications*, PhD thesis. Imperial College of Science, Technology and Medicine.
26. Rohr, C. (2000) *InGaAsP quantum well cells for thermophotovoltaic applications*, Imperial College of Science, Technology and Medicine.
27. Höfler, H. (1984) *Thermophotovoltaische Konversion der Sonnenenergie* (in German), Doctoral thesis. Universität Karlsruhe (TH).
28. Zenker, M. (2001) *Thermophotovoltaische Konversion von Verbrennungswärme* (in German), Doctoral thesis. Albert-Ludwigs-Universität Freiburg im Breisgau.
29. Lindberg, E. (2002) *TPV optics studies - on the use of non-imaging optics for improvement of edge filter performance in thermophotovoltaic applications*, Doctoral thesis. Swedish University of Agricultural Science, Uppsala.
30. Hampe, C. (2002) *Untersuchung influenzierter und diffundierter pn-Übergänge von Terrestrik- und Thermophotovoltaik-Siliciumsolarzellen* (in German), Doctoral thesis. Institut für Solarenergieforschung GmbH Hameln/Emmerthal (ISFH).
31. Volz, W. (2001) *Entwicklung und Aufbau eines thermophotovoltaischen Energiewandlers* (in German), Doctoral thesis. Universität Gesamthochschule Kassel, Institut für Solare Energieversorgungstechnik (ISET).
32. Schmid, J. (2004) *Energiewandlungsverfahren* (in German), Universität Gesamthochschule Kassel, Institut für Solare Energieversorgungstechnik (ISET).
33. Broman, L. (1995) 'Thermophotovoltaics bibliography', *Progress in Photovoltaics: Research and Applications*, 3(1), pp. 65-74.
34. Barnham, K., Connolly, J., Rohr, K. (ed.)(2003) 'Thermophotovoltaic Special Issue', *Semiconductor Science and Technology*, 18.
35. European Patent Office (2005) [Online]. Available at: http://ep.espacenet.com.
36. United States Patent and Trademark Office (2005) [Online]. Available at: http://www.uspto.gov/.
37. Ralph, E.L., FitzGerald, M.C. (1995) 'Systems/marketing challenges for TPV', *1st NREL Conference on Thermophotovoltaic Generation of Electricity*. Copper Mountain, Colorado, US 24-28 July 1994: New York: American Institute of Physics, pp. 315-321.
38. Noreen, D.L., Honghua, D. (1995) 'High power density thermophotovoltaic energy conversion', *1st NREL Conference on Thermophotovoltaic Generation of Electricity*. Copper Mountain, Colorado, US 24-28 July 1994: New York: American Institute of Physics, pp. 119-132.
39. Nelson, R.E. (2003) 'A brief history of thermophotovoltaic development', in Barnham, K., Connolly, J., Rohr, K. (ed.), *Semiconductor Science and Technology*, 18, pp. 141-143.
40. Aigrain, P. (1956) Lecture 'Thermophotovoltaic conversion of radiant energy', Massachusetts Institute of Technology.
41. Kolm, H.H. (1956) 'Solar-battery power source', *Quarterly Progress Report*, pp. 13.
42. Wedlock, B.D. (1963) 'Thermal photovoltaic effect', *3rd IEEE Photovoltaic Specialists Conference*, New York: IEEE, pp. A4.1-A4.13.

43. Guazzoni, G.E. (1972) 'High-temperature spectral emittance of oxides of erbium, samarium, neodymium and ytterbium' *Applied Spectroscopy*, 26, pp. 60-65.
44. Werth, J.J. (1963) *Thermo-photovoltaic converter with radiant energy reflective means.* U.S. Pat. 3,331,707.
45. Nelson, R.E. (1992) *Fibrous emissive burners Selective and Broadband.* Annual Report. Gas Research Inst. (GRI-92/0347).
46. Fraas, L., Avery, J., Malfa, E., Wuenning, J.G., Kovacik, G., Astle, C. (2003) 'Thermophotovoltaics for combined heat and power using low NOx gas fired radiant tube burners', *5th Conference on Thermophotovoltaic Generation of Electricity.* Rome, Italy 16-19 September 2002: New York: American Institute of Physics, pp. 61-70.
47. Fraas, L.M., Avery, J.E., Huang, H.X., Martinelli, R.U. (2003) 'Thermophotovoltaic system configurations and spectral control', in Barnham, K., Connolly, J., Rohr, K. (ed.), *Semiconductor Science and Technology*, 18, pp. 165-173.
48. West, E.M., Connelly, W.R. (1999) 'Integrated development and testing of multi-kilowatt TPV generator systems', *4th NREL Conference on Thermophotovoltaic Generation of Electricity.* Denver, Colorado, US 11-14 October 1998: New York: American Institute of Physics, pp. 446-456.
49. Morrison, O., Seal, M., West, E., Connelly, W. (1999), 'Use of a thermophotovoltaic generator in a hybrid electric vehicle', *4th NREL Conference on Thermophotovoltaic Generation of Electricity.* Denver, Colorado, US 11-14 October 1998: New York: American Institute of Physics, pp. 488-496.
50. White, D.C., Hottel, H.C. (1995) 'Important factors in determining the efficiency of TPV systems', *1st NREL Conference on Thermophotovoltaic Generation of Electricity.* Copper Mountain, Colorado, US 24-28 July 1994: New York: American Institute of Physics, pp. 425-454.
51. Regan, T.M., Martin, J.G., Riccobono, J. (1995) 'TPV conversion of nuclear energy for space applications, *1st NREL Conference on Thermophotovoltaic Generation of Electricity.* Copper Mountain, Colorado, US 24-28 July 1994: New York: American Institute of Physics, pp. 322-330.
52. Vicente, F.A., Kelly, C.E., Loughin, S. (1996) 'Thermophotovoltaic (TPV) applications to space power generation', *31th Intersociety Energy Conversion Engineering Conference*, New York: IEEE, pp. 635-640.
53. Day, A.C., Horne, W.E., Morgan, M.D. (1990) 'Application of the GaSb solar cell in isotope-heated power systems', *21th IEEE Photovoltaic Specialists Conference*, New York: IEEE, 2, pp. 1320-1325.
54. Schock, A., Kumar, V. (1995) 'Radioisotope thermophotovoltaic system design and its application to an illustrative space mission', *1st NREL Conference on Thermophotovoltaic Generation of Electricity.* Copper Mountain, Colorado, US 24-28 July 1994: New York: American Institute of Physics, pp. 139-152.
55. Schock, A., Mukunda, M., Or, C., Summers, G. (1995) 'Analysis, optimization, and assessment of radioisotope thermophotovoltaic system design for an illustrative space mission', *1st NREL Conference on Thermophotovoltaic Generation of Electricity.* Copper Mountain, Colorado, US 24-28 July 1994: New York: American Institute of Physics, pp. 331-356.
56. Schock, A., Or, C., Mukunda, M. (1996) 'Effect of expanded integration limits and measured infrared filter improvements on performance of RTPV system', *2nd NREL Conference on Thermophotovoltaic Generation of Electricity.* Colorado Springs, Colorado, US 16-20 July 1995: New York: American Institute of Physics, pp. 55-80.
57. Schock, A., Or, C., Kumar, V. (1996) 'Small radioisotope thermophotovoltaic (RTPV) generators', *2nd NREL Conference on Thermophotovoltaic Generation of Electricity.* Colorado Springs, Colorado, US 16-20 July 1995: New York: American Institute of Physics, pp. 81-97.
58. Schock, A., Or, C., Kumar, V. (1997) 'Design and integration of small RTPV generators with new millennium spacecraft for outer solar system', *Acta Astronautica*, 41(12), pp. 801-816.

59. Murray, C.S., Crowley, C.J., Murray, S., Elkouh, N.A., Hill, R.W., Chubb, D.E. (2004) 'Thermophotovoltaic Converter Design for Radioisotope Power Systems', *6th International Conference on Thermophotovoltaic Generation of Electricity*. Freiburg, Germany 14-16 June 2004: New York: American Institute of Physics, pp. 123-132.
60. Cassedy, E. S., Grossman, P. Z. (1998) 'Chapter 7: Nuclear fission technology' and 'Chapter 8: The nuclear fuel cycle', in *Introduction to Energy - Resources, Technology, and Society*, 2nd edn. Cambridge: Cambridge University Press, pp. 169-209, pp. 210-229.
61. Bryan, K., Smith, M.S. (2003) *Definition, expansion and screening of architectures for planetary exploration class nuclear electric propulsion and power systems*, MSc thesis. Massachusetts Institute of Technology.
62. Foster, A.R., Wright Jr., R.L. (1983) 'Chapter 7: Radioisotope Application' in *Basic Nuclear Engineering*, 4th edn., Boston: Allyn and Bacon, pp. 168-194.
63. Kulcinski, G.L. (2001) Lecture 21-Nuclear power in space, 22 October [Online]. Available at: http://silver.neep.wisc.edu/~neep533/FALL2001/lecture21.pdf (Accessed: 7 May 2004)
64. Meschede, D. (2002) *Gerthsen Physik* (in German), 21. edn., Berlin Heidelberg New York: Springer Press.
65. AM0 ASTM E-490-00 (2004) *Renewable Resource Data Center, supported by the National Center for Photovoltaics at the National Renewable Energy Laboratory, US* [Online]. Available at: http://rredc.nrel.gov/solar/spectra/ (Accessed: 1 September 2004).
66. AM1.5 ASTM G173-03 (2004) *Renewable Resource Data Center, supported by the National Center for Photovoltaics at the National Renewable Energy Laboratory, US* [Online]. Available at: http://rredc.nrel.gov/solar/spectra/ (Accessed: 1 September 2004).
67. Dang, A (1986) 'Concentrators: a review', *Energy Conversion and Management*, 26(1), pp. 11-26.
68. Winston, R., Cooke, D., Gleckman, P., Krebs, H., O'Gallagher, J., Sagie, D. (1990) 'Sunlight brighter than the sun', *Nature*, 346, pp. 802.
69. Stone, K.W., Kusek, S.M., Drubka, R.E., Fay, T.D. (1995) 'Analysis of solar thermophotovoltaic test data from experiments performed at McDonnell Douglas', *1st NREL Conference on Thermophotovoltaic Generation of Electricity*. Copper Mountain, Colorado, US 24-28 July 1994: New York: American Institute of Physics, pp. 153-162.
70. Stone, K., McLellan, S. (1996) 'Utility market and requirements for solar thermophotovoltaic system', *2nd NREL Conference on Thermophotovoltaic Generation of Electricity*. Colorado Springs, Colorado, US 16-20 July 1995: New York: American Institute of Physics, pp. 238-250.
71. Stone, K.W., Leingang, E.F., Kusek, S.M., Drubka, R.E., Fay, T.D. (1994) 'On-sun test results of McDonnell Douglas` prototype solar thermophotovoltaic power system', *24th IEEE Photovoltaic Specialists Conference*, 2, New York: IEEE, pp. 2010-2013.
72. Fatemi, N.S. (1996) *A solar thermophotovoltaic electrical generator for remote power applications*. Final Report. Essential Research Inc., Cleveland, US (NAS3-27779).
73. Swanson, R.M. (1979) 'A proposed thermophotovoltaic solar energy conversion system', *Proceedings of the IEEE*, 67(3), New York: IEEE, pp. 446-447.
74. Thermophotovoltaic research (2004) Presentation, *Space Power Institute Auburn University, Space Research Institute* [Online]. (Accessed: 10 May 2004).
75. Chubb, D.L., Good, B.S., Lowe, R.A. (1996) 'Solar thermophotovoltaic (STPV) system with thermal energy storage', *2nd NREL Conference on Thermophotovoltaic Generation of Electricity*. Colorado Springs, Colorado, US 16-20 July 1995: New York: American Institute of Physics, pp. 181-198.
76. Yugami, H., Sai, H., Nakamura, K., Nakagawa, N., Ohtsubo, H. (2000) 'Solar thermophotovoltaic using $Al_2O_3/Er_3Al_5O_{12}$ eutectic composite selective emitter', *28th IEEE Photovoltaic Specialists Conference*, New York: IEEE, pp. 1214-1217.
77. Guazzoni, G.E., Rose, M.F. (1996) 'Extended use of photovoltaic solar panels', *2nd NREL Conference on Thermophotovoltaic Generation of Electricity*. Colorado Springs, Colorado, US 16-20 July 1995: New York: American Institute of Physics, pp. 162-176.

78. Stone, K. W., Chubb, D. L., Wilt, D. M., Wanlass, M. W. (1996) 'Testing and modelling of a solar thermophotovoltaic power system', *2nd NREL Conference on Thermophotovoltaic Generation of Electricity.* Colorado Springs, Colorado, US 16-20 July 1995: New York: American Institute of Physics, pp. 199-209.

79. Stone, K.W., Fatemi, N.S., Garverick, L.M. (1996) 'Operation and component testing of a solar thermophotovoltaic power system', *25th IEEE Photovoltaic Specialists Conference*, New York: IEEE, pp. 1421-1424.

80. Davies, P.A., Luque, A. (1994) 'Solar thermophotovoltaics: brief review and a new look', *Solar Energy Materials and Solar Cells*, 33, pp. 11-22.

81. Demichelis, F., Minetti-Mezzetti, E. (1980) 'A solar thermophotovoltaic converter', *Solar Cells*, 1(4), pp. 395-403.

82. Khvostikov, V.P., Rumyantsev, V.D., Khvostikova, O.A., Gazaryan, P.Y., Kaluzhniy, N.A., Andreev, V.M. (2004) 'TPV cells based on Ge, GaSb and InAs related compounds for solar powered TPV systems', *19th European Photovoltaic Solar Energy Conference.* Paris, 7 - 11 June 2004: Munich: WIP.

83. Imenes, A. G., Mills, D. R. (2004) 'Spectral beam splitting technology for increased conversion efficiency in solar concentrating systems: a review', *Solar Energy Materials and Solar Cells,* 84, pp. 19-69.

84. Andreev, V.M., Grilikhes, V.A., Khvostikov, V.P., Khvostikova, O.A., Rumyantsev, V.D., Sadchikov, N.A., Shvarts, M. Z. (2004) Concentrator PV modules and solar cells for TPV systems, *Solar Energy Materials and Solar Cells*, 84(1-4), pp. 3-17.

85. Nielsen, O.M., Arana, L.R., Baertsch, C.D., Jensen, K.F., Schmidt, M.A., (2003) 'A thermophotovoltaic micro-generator for portable power applications', *12th International Conference on Solid State Sensors, Actuators and Microsystems*, Boston, June 8-12.

86. Yang Wenming, Chou Siawkiang, Shu Chang, Xue Hong, Li Zhiwang (2004) 'Effect of wall thickness of micro-combustor on the performance of micro-thermophotovoltaic power generators', *Sensors and Actuators A*, 119(2), pp. 441-445.

87. Yang, W.M., Chou, S.K., Shu, C., Li, Z. W., Xue, H. (2003) 'Research on micro-thermophotovoltaic power generators', *Solar Energy Materials and Solar Cells*, 80, pp. 95-104.

88. Yang, W.M., Chou, S.K., Shu, C., Xue, H., Li, Z.W. (2004) 'Development of a prototype micro-thermophotovoltaic power generator', *Journal of Physics D: Applied Physics*, 37, pp. 1017-1020.

89. Williams, D.J., Fraas, L.M. (1996) 'Demonstration of a candle powered radio using GaSb thermophotovoltaic cells' *2nd NREL Conference on Thermophotovoltaic Generation of Electricity.* Colorado Springs, Colorado, US 16-20 July 1995: New York: American Institute of Physics, pp. 134-137.

90. Broman, L., Marks, J. (1994) 'Development of a TPV converter for co-generation of electricity and heat from combustion of wood powder', *24th IEEE Photovoltaic Specialists Conference*, 2, New York: IEEE, pp. 1764-1766.

91. Fraas, L., Avery, J., Malfa, E., Venturino, M. (2002) 'TPV tube generators for apartment building and industrial furnace applications', *5th Conference on Thermophotovoltaic Generation of Electricity.* Rome, Italy 16-19 September 2002: New York: American Institute of Physics, pp. 38-48.

92. DeBellis, C.L., Scotto, M.V., Scoles, S.W., Fraas, L. (1997) 'Conceptual design of 500 watt portable thermophotovoltaic power supply using JP-8 fuel', *3rd NREL Conference on Thermophotovoltaic Generation of Electricity.* Denver, Colorado, US 18-21 May 1997: New York: American Institute of Physics, pp. 355-367.

93. Hanamura, K., Kumano, T. (2003) 'Thermophotovoltaic power generation by super-adiabatic combustion in porous quartz glass', *5th Conference on Thermophotovoltaic Generation of Electricity.* Rome, Italy 16-19 September 2002: New York: American Institute of Physics, pp. 111-120.

94. Hanamura, K., Kumano, T. (2004) 'TPV power generation system using super-adiabatic combustion in porous quartz glass', *6th International Conference on Thermophotovoltaic Generation of Electricity*. Freiburg, Germany 14-16 June 2004: New York: American Institute of Physics, pp. 88-95.
95. Kumano, T., Hanamura, K. (2004) 'Spectral control of transmission of diffuse irradiation using piled AR coated quartz glass filters', *6th International Conference on Thermophotovoltaic Generation of Electricity*. Freiburg, Germany 14-16 June 2004: New York: American Institute of Physics, pp. 230-236.
96. Horne, W.E., Morgan, M.D., Sundaram, V.S., Butcher, T. (2003) '500 watt diesel fueled TPV portable power supply', *5th Conference on Thermophotovoltaic Generation of Electricity*. Rome, Italy 16-19 September 2002: New York: American Institute of Physics, pp. 91-100.
97. Weinberg, F. (1996) 'Heat recirculating burners: principles and some recent developments', *Combustion Science and Technology*, 121, pp. 3-22.
98. Weinberg, F. (1986) *Advanced Combustion Methods*, London, New York: Academic Press.
99. DeBellis, C.L., Scotto, M.V., Fraas, L., Samaras, J., Watson, R.C., Scoles, S.W. (1999) 'Component development for 500 watt diesel fueled portable thermophotovoltaic (TPV) power supply', *4th NREL Conference on Thermophotovoltaic Generation of Electricity*. Denver, Colorado, US 11-14 October 1998: New York: American Institute of Physics, pp. 362-370.
100. Adair, P.L., Rose, M.F. (1995) 'Composite emitters for TPV systems', *1st NREL Conference on Thermophotovoltaic Generation of Electricity*. Copper Mountain, Colorado, US 24-28 July 1994: New York: American Institute of Physics, pp. 245-262.
101. Baukal, C.E. (2000) 'Chapter 8: Heat transfer from burners' in *Heat Transfer in Industrial Combustion*. London: CRC Press, pp. 285-343.
102. Gaydon, A. G. (1974) *The Spectroscopy of Flames*, 2nd edn., London: Chapman and Hall.
103. Nelson, R.E. (1995) 'Thermophotovoltaic emitter development', *1st NREL Conference on Thermophotovoltaic Generation of Electricity*. Copper Mountain, Colorado, US 24-28 July 1994: New York: American Institute of Physics, pp. 80-96.
104. Bitnar, B., Durisch, W., Mayor, J.-C., Sigg, H., Tschudi, H. R. (2002) 'Characterisation of rare earth selective emitters for thermophotovoltaic applications', *Solar Energy Materials and Solar Cells*, 73, pp. 221-234.
105. Wünning J.G. (2003) 'FLOX® - flameless oxidation', *Thermprocess Symposium*, Düsseldorf: VDMA.
106. Dryden, I.G.C. (1975) *The Efficient use of energy*, London: IPC Science and Technology Press.
107. Fraas, L.M., Avery, J.E., Daniels, W.E., Huang, H.X., Malfa, E., Testi, G. (2001) 'TPV tube generators for apartment building and industrial furnace applications', *17th European Photovoltaic Solar Energy Conference*. Munich, 22-26 October 2001, Munich: WIP.
108. *Glass project fact sheet - thermophotovoltaic electric power generation using exhaust heat* (2001) US. Department of Energy, Office of Industrial Technologies [Online]. Available at: www.oit.doe.gov/inventions (Accessed: 25 September 2001).
109. Yamaguchi, H., Yamaguchi, M. (1999) 'Thermophotovoltaic potential applications for civilian and industrial use in Japan', *4th NREL Conference on Thermophotovoltaic Generation of Electricity*. Denver, Colorado, US 11-14 October 1998: New York: American Institute of Physics, pp. 17-29.
110. Yugami, H. Sasa, H., Yamaguchi, M. (2003) 'Thermophotovoltaic systems for civilian and industrial applications in Japan', *Semiconductor Science and Technology*, 18, pp. 239-246.
111. Durisch, W., Bitnar, B., Roth, F., Palfinger, G. (2003) 'Small thermophotovoltaic prototype systems', *Solar Energy*, 75, pp. 11-15.

112. Fraas, L., Ballantyne, R., She-Hui, Shi-Zhong Ye, Gregory, S., Keyes, J., Avery, J., Lamson, D., Daniels, B. (1999) 'Commercial GaSb cell and circuit development for the Midnight Sun(R) TPV stove', *4th NREL Conference on Thermophotovoltaic Generation of Electricity*. Denver, Colorado, US 11-14 October 1998: New York: American Institute of Physics, pp. 480-487.

113. Kushch, A.S., Skinner, S.M., Brennan, R., Sarmiento, P.A. (1997) 'Development of a cogenerating thermophotovoltaic powered combination hot water heater/hydronic boiler', *3rd NREL Conference on Thermophotovoltaic Generation of Electricity*. Denver, Colorado, US 18-21 May 1997: New York: American Institute of Physics, pp. 373-386.

114. Palfinger, G., Bitnar, B., Durisch, W., Mayor, J.-C., Grützmacher, D., Gobrecht, J. (2003) 'Cost estimate of electricity produced by TPV', *Semiconductor Science and Technology*, 18, pp. 254-261.

115. Goldstein, M. K., DeShazer, L.G., Kushch, A. S., Skinner, S. M. (1997) 'Superemissive light pipe for TPV applications', *3rd NREL Conference on Thermophotovoltaic Generation of Electricity*. Denver, Colorado, US 18-21 May 1997: New York: American Institute of Physics, pp. 315-326.

116. DeShazer, L.G., Kushch, A.S., Chen, K.C. (2001) 'Hot dielectrics as light sources for TPV devices and lasers', *NASA Tech Briefs magazine*, [Online]. Available at: www.nasatech.com (Accessed: 10 September 2004).

117. Goldstein, M.K. Quantum Group Inc. (1996) *Superemissive light pipes and photovoltaic systems including same*. U.S. Pat. 5,500,054.

118. Coutts, T.J., Guazzoni, G. Luther, J. (2003) 'An overview of the fifth conference on thermophotovoltaic generation of electricity', *Semiconductor Science and Technology*, 18, pp. 144-150.

119. Cockeram, B.V., Hollenbeck, J.L. (1999) The spectral emittance and stability of coatings and textured surfaces for thermophotovoltaic (TPV) radiator applications, *US Department of Energy Report* (DE-AC11-98PN38206).

120. Roth, A. (1990) *Vacuum Technology*, 3rd edn., Amsterdam: Elsevier science.

121. Darling, R. (2003) 'Film deposition - physical vapor deposition', Lecture notes, University of Washington College of Engineering, US, [Online]. Available at: www.engr.washington.edu (Accessed 26 July 2004).

122. Marsden, M.A., Cayless, A.M. (1984) *Lamps and Lighting: A Manual of Lamps and Lighting*, 3rd edn., London: Routledge.

123. Richerson, D. W. (1992) *Modern Ceramic Engineering: Properties, Processing, and Use in Design*, 2nd edn., New York: Marcel Dekker.

124. Lay, L.A. (1991) *Corrosion Resistance of Technical Ceramics*, London: Her Majesty's Stationery Office (HMSO).

125. Pernisz, U.C., Saha, C.K. (1995) 'Silicon carbide emitter and burner elements for a TPV converter', *1st NREL Conference on Thermophotovoltaic Generation of Electricity*. Copper Mountain, Colorado, US 24-28 July 1994: New York: American Institute of Physics, pp. 99-105.

126. Guazzoni, G., McAlonan, M. (1997) 'Multifuel (liquid hydrocarbons) TPV generator', *3rd NREL Conference on Thermophotovoltaic Generation of Electricity*. Denver, Colorado, US 18-21 May 1997: New York: American Institute of Physics, pp. 341-354, 1997.

127. Ferguson, L.G., Dogan, F. (2002) 'Spectral analysis of transition metal-doped MgO "matched emitters" for thermophotovoltaic energy conversion', *Journal of Materials Science*, 37(7), pp. 1301-1308.

128. Chubb, D. L. (1990) 'Reappraisal of solid selective emitters', *21th IEEE Photovoltaic Specialists Conference*, 2, New York: IEEE, pp. 1326-1333.

129. Dieke, G. H. (1968) *Spectra and energy levels of rare earth ions in crystals*, New York Chichester Brisbane Toronto Singapore: Wiley & Sons.

130. Touloukian, Y.S., DeWitt, D.P. (1972) *Thermophysical Properties of Matter, Vol. 8, Thermal Radiative Properties*: Nonmetallic Solids, New York: Plenum Press.

131. Chubb, D.L., Pal, A-M.T., Patton, M.O., Jenkins, P.P. (1999) 'Rare earth doped high temperature ceramic selective emitters', *Journal of the European Ceramic Society* 19, pp. 2551-2562.

132. Diso, D., Licciulli, A., Bianco, A., Lomascolo, M., Leo, G., Mazzer, M., Tundo, S., Torsello, G., Maffezzoli, A. (2003) 'Erbium containing ceramic emitters for thermophotovoltaic energy conversion', *Materials Science and Engineering B*, 98(2), pp. 144-149.

133. Ferguson, L.G., Dogan, F. (2001) 'Spectrally selective, matched emitters for thermophotovoltaic energy conversion processed by tape casting', *Journal of Materials Science*, 36(1), pp.137-146.

134. Schubnell, M., Gabler, H., Broman, L. (1997) 'Overview of European activities in thermophotovoltaics', *3rd NREL Conference on Thermophotovoltaic Generation of Electricity*. Denver, Colorado, US 18-21 May 1997: New York: American Institute of Physics, pp. 3-22.

135. Ortabasi, U., Lund, K. O., Seshadri, K. (1996) 'A fluidized bed selective emitter system driven by a non-premixed burner', *2nd NREL Conference on Thermophotovoltaic Generation of Electricity*. Colorado Springs, Colorado, US 16-20 July 1995: New York: American Institute of Physics, pp. 469-487.

136. Adair, P.L., Zheng-Chen, Rose, F. (1997) 'TPV power generation prototype using composite selective emitters', *3rd NREL Conference on Thermophotovoltaic Generation of Electricity*. Denver, Colorado, US 18-21 May 1997: New York: American Institute of Physics, pp. 277-291.

137. Nelson, R.E. (1997) 'Temperature measurement of high performance radiant emitters', *3rd NREL Conference on Thermophotovoltaic Generation of Electricity*. Denver, Colorado, US 18-21 May 1997: New York: American Institute of Physics, pp. 189-202.

138. Pierce, D.E., Guazzoni, G. (1999) 'High temperature optical properties of thermophotovoltaic emitter components', *4th NREL Conference on Thermophotovoltaic Generation of Electricity*. Denver, Colorado, US 11-14 October 1998: New York: American Institute of Physics, pp. 177-190.

139. Licciulli, A., Maffezzoli, A., Diso, D., Tundo, S., Rella, M., Torsello, G., Mazzer, M. (2003) 'Sol-gel preparation of selective emitters for thermophotovoltaic conversion', *Journal of Sol-Gel Science and Technology*, 26(1), pp. 1119-1123.

140. Panitz, J-C., Schubnell, M., Durisch, W., Geiger, F. (1997) 'Influence of ytterbium concentration on the emissive properties of Yb:YAG and Yb:Y_2O_3' *3rd NREL Conference on Thermophotovoltaic Generation of Electricity*. Denver, Colorado, US 18-21 May 1997: New York: American Institute of Physics, pp. 265-276.

141. Panitz, J-C (1999) 'Characterization of ytterbium-yttrium mixed oxides using Raman spectroscopy and X-ray powder diffraction', *Journal of Raman Spectroscopy*, 30(11), pp. 1035-1042.

142. Chubb, D.L., Lowe, R.A. (1996) 'A small particle selective emitter for thermophotovoltaic energy conversion', *2nd NREL Conference on Thermophotovoltaic Generation of Electricity*. Colorado Springs, Colorado, US 16-20 July 1995: New York: American Institute of Physics, pp. 263-277.

143. Ferguson, L., Fraas, L. (1997) 'Matched infrared emitters for use with GaSb TPV cells', *3rd NREL Conference on Thermophotovoltaic Generation of Electricity*. Denver, Colorado, US 18-21 May 1997: New York: American Institute of Physics, pp. 169-179.

144. Crowley, C.J., Elkouh, N.A., Magari, P.J. (1999) 'Thermal spray approach for TPV emitters', *4th NREL Conference on Thermophotovoltaic Generation of Electricity*. Denver, Colorado, US 11-14 October 1998: New York: American Institute of Physics, pp. 197-213.

145. Diso, D., Licciulli, A., Bianco, A., Leo, G., Torsello, G., Tundo, S., Sinisi, M., Larizza, P., Mazzer, M. (2003) 'Selective emitters for high efficiency TPV conversion: materials preparation and characterisation', *5th Conference on Thermophotovoltaic Generation of Electricity*. Rome, Italy 16-19 September 2002: New York: American Institute of Physics, pp. 132-141.

146. Höfler, H., Würfel, P., Ruppel, W. (1983) 'Selective emitters for thermophotovoltaic solar energy conversion', *Solar Cells*, 10(3), pp. 257-271.

147. Good, B.S., Chubb, D.L. (2003) 'Theoretical comparison of erbium-, holmium- and thulium-doped aluminum garnet selective emitters', *5th Conference on Thermophotovoltaic Generation of Electricity*. Rome, Italy 16-19 September 2002: New York: American Institute of Physics, pp. 142-154.

148. Zheng Chen, Adair, P. L., Rose, M. F. (1997) 'Multiple-dopant selective emitter', *3rd NREL Conference on Thermophotovoltaic Generation of Electricity*. Denver, Colorado, US 18-21 May 1997: New York: American Institute of Physics, pp. 181-188.

149. Wyatt, L. (1993) 'Chapter 1: Materials Properties and Selection', in Koshal, D. (ed.) *Manufacturing Engineer's Reference Book*. 13th edn. Oxford, Boston: Butterworth-Heinemann.

150. *Metals handbook - Vol. 13 Corrosion* (1987) 9th edn., Ohio: ASM International.

151. Doyle, E., Shukla, K., Metcalfe, C. (2001) Development and demonstration of a 25 Watt thermophotovoltaic power source for a hybrid power system, NASA Report (TR04-2001).

152. *Bekaert Combustion Technology*, US and Netherlands [Online]. Available at: www.acotech.com.

153. *Eclipse, Inc.*, US, [Online]. Available at: www.eclipsenet.com.

154. Rumyantsev, V.D., Khvostikov, V.P., Sorokina, O., Vasil'ev, A.I., Andreev, V.M. (1999) 'Portable TPV generator based on metallic emitter and 1.5-amp GaSb cells', *4th NREL Conference on Thermophotovoltaic Generation of Electricity*. Denver, Colorado, US 11-14 October 1998: New York: American Institute of Physics, pp. 384-393.

155. Wheeler, M.J. (1983) 'Chapter 17: Radiating properties of metals', in Brandes, E.A. (ed.) *Smithells Metals Reference Book*, 6th edn., Oxford: Butterworth-Heinemann.

156. Fraas, L.M., Magendanz, G., Avery, J.E. JX-Crystals Inc. (2001) *Antireflection coated refractory metal matched emitters for use in thermophotovoltaic generators*, U.S. Pat. 6,177,628.

157. Fraas, L.M., Samaras, J.E., Avery, J.E. JX-Crystals Inc. (2001) *Antireflection coated refractory metal matched emitters for use in thermophotovoltaic generators*, U.S. Pat. 6,271,461.

158. Hitoshi Sai, Hiroo Yugami, Yoshiaki Kanamori, Kazuhiro Hane (2003) 'Spectrally selective emitters with deep rectangular cavities fabricated with fast atom beam etching', *5th Conference on Thermophotovoltaic Generation of Electricity*. Rome, Italy 16-19 September 2002: New York: American Institute of Physics, pp. 155-163.

159. Schlemmer, C., Aschaber, J., Boerner, V., Gombert, A., Hebling, C., Luther, J. (2003) 'Thermal stability of microstructured selective tungsten emitters', *5th Conference on Thermophotovoltaic Generation of Electricity*. Rome, Italy 16-19 September 2002: New York: American Institute of Physics, pp. 164-173.

160. H. Sai, T. Kamikawa, H. Yugami (2004) 'Thermophotovoltaic generation with microstructured tungsten selective emitters', *6th International Conference on Thermophotovoltaic Generation of Electricity*. Freiburg, Germany 14-16 June 2004: New York: American Institute of Physics, pp. 206-214.

161. Pralle, M.U., Moelders, N., McNeal, M.P., Puscasu, I., Greenwald, A.C., Daly, J.T., Johnson, E.A., George, T., Choi, D.S., El-Kady, I., Biswas, R. (2002) 'Photonic crystal enhanced narrow-band infrared emitters', Applied Physics Letters, 81, pp. 4685-4687.

162. McCarthy, D.C. (2002) 'Photonic crystals: a growth industry', *Photonics Spectra*, June, pp, 54-60.

163. Fleming, J.G., Lin, S.Y., El-Kady, I. Biswas, R., Ho, K.M. (2002) 'All-metallic three-dimensional photonic crystals with a large infrared bandgap', *Nature* 417, pp. 52-55.

164. Narayanaswamy, A., Cybulski, J., Gang Chen, '1D metallo-dielectric photonic crystals as selective emitters for thermophotovoltaic applications' *6th International Conference on Thermophotovoltaic Generation of Electricity*. Freiburg, Germany 14-16 June 2004: New York: American Institute of Physics, pp. 215-220.

165. Chubb, D.L., Wolford, D.S., Meulenberg, A., DiMatteo, R.S. (2003) 'Semiconductor silicon as a selective emitter', *5th Conference on Thermophotovoltaic Generation of Electricity*. Rome, Italy 16-19 September 2002: New York: American Institute of Physics, pp. 174-200.

166. Cockeram, B.V., Measures, D.P., Mueller, A.J. (1999) 'The development and testing of emissivity enhancement coatings for themophotovoltaic (TPV) radiator applications', *Thin Solid Films*, 355-356, pp. 17-25.

167. Andreev, V.M. (2003) 'An overview of TPV cell technologies', *5th Conference on Thermophotovoltaic Generation of Electricity*. Rome, Italy 16-19 September 2002: New York: American Institute of Physics, pp. 289-304.

168. Bhat, I.B., Borrego, J.M., Gutmann, R.J., Ostrogorsky, A.G. (1996) 'TPV energy conversion: a review of material and cell related issues', *31th Intersociety Energy Conversion Engineering Conference*, New York: IEEE, pp. 968-973.

169. Iles, P.A. (1990) 'Non-solar photovoltaic cells', *21th IEEE Photovoltaic Specialists Conference*, New York: IEEE, pp. 420-425.

170. Shockley, W., Queisser, H.J. (1961) 'Detailed balance limit of efficiency of p-n junction solar cells', *Applied Physics*, 32, pp. 510-519.

171. Yeargan, J.R., Cook, R.G., Sexton, F.W. (1976) 'Thermophotovoltaic systems for electrical energy conversion', *12th IEEE Photovoltaic Specialists Conference*, New York: IEEE, pp. 807-813.

172. Baldasaro, P.F., Brown, E.J., Depoy, D.M., Campbell, B.C., Parrington, J.R. (1995) 'Experimental assessment of low temperature voltaic energy conversion', *1st NREL Conference on Thermophotovoltaic Generation of Electricity*. Copper Mountain, Colorado, US 24-28 July 1994: New York: American Institute of Physics, pp. 29-43.

173. Charache, G.W, Egley, J.L., Depoy, D. M., Danielson, L.R., Freeman, M.J., Dziendziel, R.J. Moynihan, J.F., Baldasaro, P.F., Campbell, B.C., Wang, C.A., Choi, H.K., Turner, G.W., Wojtczuk, S.J., Colter, P., Sharps, P., Timmons, M., Fahey, R.E., Zhang, K. (1998) 'Infrared materials for thermophotovoltaic applications', *Journal of Electronic Materials*, 27, pp.1038-1042.

174. Baldasaro, P.F., Raynolds, J.E., Charache, G.W., DePoy, D.M., Ballinger, C.T., Donovan, T., Borrego, J. M. (2001) 'Thermodynamic analysis of thermophotovoltaic efficiency and power density tradeoffs', *Applied Physics*, 89, pp. 3319-3327.

175. Murray, S., Aiken, D., Stan, M., Murray, C., Newman, F., Hills, J., Siergiej, R. R., Wernsman, B. (2002) 'Effect of metal coverage on the performance of 0.6-eV InGaAs monolithic interconnected modules', *5th Conference on Thermophotovoltaic Generation of Electricity*. Rome, Italy 16-19 September 2002: New York: American Institute of Physics, pp. 424-433.

176. Green, M.A., Emery, K., King, D.L., Igari, S., Warta, W. (2003) 'Solar cell efficiency tables (Version 22)', *Progress in Photovoltaics: Research and Applications*, 11, pp. 347-352.

177. GaSb sales item (2004) *JX-Crystals Inc., US* [Online]. Available at: www.jxcrystals.com

178. Partain, L.D. (1995) 'Chapter 1: Solar Cell Fundamentals', in *Solar Cells and Their Applications*, New York: Wiley Interscience, pp. 1-51.

179. Coutts, T.J., Ward, J.S. (1999) 'Thermophotovoltaic and photovoltaic conversion at high-flux densities', *IEEE Transactions on Electron Devices*, 46(10), pp. 2145-2153.

180. Fraas, L., Samaras, J., Han-Xiang Huang, Seal, M., West, E. (1999) 'Development status on a TPV cylinder for combined heat and electric power for the home', *4th NREL Conference on Thermophotovoltaic Generation of Electricity*. Denver, Colorado, US 11-14 October 1998: New York: American Institute of Physics, pp. 371-383.

181. Bitnar, B. (2003) Silicon, germanium and silicon/germanium photocells for thermophotovoltaics applications, *Semiconductor Science and Technology*, 18, pp. 221-227.

182. Qiu, K., Hayden, A. (2004) 'A novel integrated TPV power generation system based on a cascaded radiant burner', *6th International Conference on Thermophotovoltaic Generation of Electricity*. Freiburg, Germany 14-16 June 2004: New York: American Institute of Physics, pp. 105-113.

183. Swanson, R.M. (2000) 'The promise of concentrators', *Progress in Photovoltaics: Research and Applications*, 8, pp. 93-111

184. Charache, G.W., DePoy, D.M., Baldasaro, P.F., Campbell, B.C. (1996) 'Thermophotovoltaic device utilizing a back surface reflector for spectral control', *2nd NREL Conference on Thermophotovoltaic Generation of Electricity*. Colorado Springs, Colorado, US 16-20 July 1995: New York: American Institute of Physics, pp. 339-350.

185. Hampe, C., Metz, A., Hezel, R. (2001), Innovative silicon-concentrator solar cell for thermophotovoltaic application, *17th European Photovoltaic Solar Energy Conference*. Munich, 22-26 October 2001, Munich: WIP.

186. Posthuma, N., Heide, J., Flamand, G., Poortmans, J. (2004) 'Development of low cost germanium photovoltaic cells for application in TPV using spin-on diffusants', *6th International Conference on Thermophotovoltaic Generation of Electricity*. Freiburg, Germany 14-16 June 2004: New York: American Institute of Physics, pp. 337-344.

187. Andreev, V.M., Khvostikov, V.P., Khvostikova, O.V., Oliva, E.V., Rumyantsev, V.D., Shvarts, M.Z., Tabarov, T.S. (2003) 'Low band gap Ge and InAsSbP/InAs-based TPV cells', *5th Conference on Thermophotovoltaic Generation of Electricity*. Rome, Italy 16-19 September 2002: New York: American Institute of Physics, pp. 383-391.

188. Mauk, M.G., Andreev, V.M. (2003) 'GaSb-related materials for TPV cells', *Semiconductor Science and Technology*, 18, pp. 191-201.

189. Contreras, M., Wiesner, H., Webb, J. (1997) 'Thin-film polycrystalline $Ga_{1-x}In_xSb$ materials', *3rd NREL Conference on Thermophotovoltaic Generation of Electricity*. Denver, Colorado, US 18-21 May 1997: New York: American Institute of Physics, pp. 403-410.

190. Dhere, N.G. (1997) 'Appropriate materials and preparation techniques for polycrystalline-thin-film thermophotovoltaic cells', *3rd NREL Conference on Thermophotovoltaic Generation of Electricity*. Denver, Colorado, US 18-21 May 1997: New York: American Institute of Physics, pp. 423-442.

191. Wanlass, M.W., Schwartz, R.J. (1995) 'Introduction to workshop spectral control and converters', *1st NREL Conference on Thermophotovoltaic Generation of Electricity*. Copper Mountain, Colorado, US 24-28 July 1994: New York: American Institute of Physics, pp. 6-12.

192. Zheng, L., Sweileh, G.M., Haywood, S.K., Scott, C.G., Lakrimi, M., Mason, N.J., Walker, P.J. (1999) 'p-GaSb/n-GaAs heterojunctions for thermophotovoltaic cells grown by MOVPE', *4th NREL Conference on Thermophotovoltaic Generation of Electricity*. Denver, Colorado, US 11-14 October 1998: New York: American Institute of Physics, pp. 525-534.

193. Bett, A.W., Dimroth, F., Stollwerck, G., Sulima, O. V. (1999) 'III-V compounds for solar cell applications', *Applied Physics A*, A69 (2), pp.119-129.

194. Bett, A.W., Sulima, O.V. (2003) GaSb photovoltaic cells for applications in TPV generators, *Semiconductor Science and Technology*, 18, pp. 184-190.

195. Wojtczuk, S., Gagnon, E., Geoffroy, L., Parodos, T. (1995) '$In_xGa_{1-x}As$ thermophotovoltaic cell performance vs. bandgap', *1st NREL Conference on Thermophotovoltaic Generation of Electricity*. Copper Mountain, Colorado, US 24-28 July 1994: New York: American Institute of Physics, pp. 177-187.

196. Karlina, L.B., Blagnov, P.A., Kulagina, M.M., Vlasov, A.S., Vargas-Aburto, C., Uribe, R.M. (2003) 'Zinc (P) diffusion in $In_{0.53}Ga_{0.47}As$ and GaSb for TPV devices', *5th Conference on Thermophotovoltaic Generation of Electricity*. Rome, Italy 16-19 September 2002: New York: American Institute of Physics, pp. 373-382.

197. Wilt, D.M., Fatemi, N.S., Jenkins, P.P., Weizer, V.G., Hoffman, R.W. Jain, R.K., Murray, C.S., Riley, D.R. (1997) 'Electrical and optical performance characteristics of 0.74 eV pin InGaAs monolithic interconnected modules', *3rd NREL Conference on Thermophotovoltaic Generation of Electricity*. Denver, Colorado, US 18-21 May 1997: New York: American Institute of Physics, pp. 237-247.

198. Ginige, R., Kelleher, C., Corbett, B., Hilgarth, J., Clarke, G. (2002) 'The design, fabrication and evaluation of InGaAs/InP TPV cells for commercial applications', *5th Conference on Thermophotovoltaic Generation of Electricity*. Rome, Italy 16-19 September 2002: New York: American Institute of Physics, pp. 354-362.

199. Murray, S.L., Newman, F.D., Murray, C.S., Wilt, D.M., Wanlass, M.W., Ahrenkiel, P., Messham, R., Siergiej, R.R. (2003) 'MOCVD growth of lattice-matched and mismatched InGaAs materials for thermophotovoltaic energy conversion', *Semiconductor Science and Technology*, 18, pp. 202-208.

200. Wanlass, M.W., Carapella, J.J., Duda, A., Emery, K., Gedvilas, L., Moriarty, T., Ward, S., Webb, J., Wu, X., Murray, C.S. (1999) 'High-performance, 0.6-eV, $GA_{0.32}In_{0.68}As/In_{0.32}P_{0.68}$ thermophotovoltaic converters and monolithically interconnected modules', *4th NREL Conference on Thermophotovoltaic Generation of Electricity*. Denver, Colorado, US 11-14 October 1998: New York: American Institute of Physics, pp. 132-141.

201. Wilt, D., Wehrer, R., Palmisiano, M., Wanlass, M., Murray, C. (2003) 'Monolithic interconnected modules (MIMs) for thermophotovoltaic energy conversion', *Semiconductor Science and Technology*, 18, pp. 209-215.

202. Siergiej, R.R., Wernsman, B., Derry, S.A., Wehrer, R.J., Link, S.D., Palmisiano, M.N., Messham, R.L., Murray, S., Murray, C.S., Newman, F., Hills, J., Taylor, D. (2003) '20 % Efficient InGaAs/InPAs Thermophotovoltaic Cells', *5th Conference on Thermophotovoltaic Generation of Electricity*. Rome, Italy 16-19 September 2002: New York: American Institute of Physics, pp. 414-423.

203. Ringel, S.A., Sacks, R.N., Qin, L., Clevenger, M.B., Murray, C.S. (1999) 'Growth and properties of InGaAs/FeAl/InAlAs/InP heterostructures for buried reflector/interconnect applications in InGaAs thermophotovoltaic devices', *4th NREL Conference on Thermophotovoltaic Generation of Electricity*. Denver, Colorado, US 11-14 October 1998: New York: American Institute of Physics, pp. 142-151.

204. Ward, J.S., Duda, A., Wanlass, M.W., Carapella, J.J., Wu, X., Matson, R.J., Coutts, T.J., Moriarty, T., Murray, C.S., Riley, D.R. (1997) 'Novel design for monolithic interconnected modules (MIMS) for thermophotovoltaic power conversion', *3rd NREL Conference on Thermophotovoltaic Generation of Electricity*. Denver, Colorado, US 18-21 May 1997: New York: American Institute of Physics, pp. 227-236.

205. Shellenbarger, Z., Taylor, G., Martinelli, R., Carpinelli, J. (2004) 'High performance InGaAsSb thermophotovoltaic cells via multi-wafer OMVPE growth', *6th International Conference on Thermophotovoltaic Generation of Electricity*. Freiburg, Germany 14-16 June 2004: New York: American Institute of Physics, pp. 314-323.

206. Wang, C.A., Murphy, P.G., O'Brien, P.W., Shiau, D.A., Anderson, A.C., Liau, Z.L., Depoy, D.M., Nichols, G. (2003) 'Wafer-bonded internal back-surface reflectors for enhanced TPV performance', *5th Conference on Thermophotovoltaic Generation of Electricity*. Rome, Italy 16-19 September 2002: New York: American Institute of Physics, pp. 473-481.

207. Mauk, M.G., Shellenbarger, Z.A., Gottfried, M.I., Cox, J.A., Feyock, B.W., McNeely, J.B., DiNetta, L.C., Mueller, R.L. (1997) 'New concepts for III-V antimonide thermophotovoltaics', *3rd NREL Conference on Thermophotovoltaic Generation of Electricity*. Denver, Colorado, US 18-21 May 1997: New York: American Institute of Physics, pp. 129-137.

208. Wilt, D.M., Wehrer, R.J., Maurer, W.F., Jenkins, P.P., Wernsman, B., Schultz. R.W. (2004) 'Buffer layer effects on tandem InGaAs TPV Devices', *6th International Conference on Thermophotovoltaic Generation of Electricity*. Freiburg, Germany 14-16 June 2004: New York: American Institute of Physics, pp. 453-461.

209. Siergiej, R.R., Sinharoy, S., Valko, T., Wehrer, R.J., Wernsman, B., Link, S.D., Schultz, R.W., Messham, R.L. 'InGaAsP/InGaAs tandem TPV device', *6th International Conference on Thermophotovoltaic Generation of Electricity*. Freiburg, Germany 14-16 June 2004: New York: American Institute of Physics, pp. 480-488.

210. Connolly, J.P., Rohr, C. (2003) 'Quantum well cells for thermophotovoltaics', *Semiconductor Science and Technology*, 18, pp. 216-220.

211. Sulima, O.V., Bett, A.W., Mauk, M.G., Mueller, R.L., Dutta, P.S., Ber, B. Y. (2003) 'GaSb-, InGaAsSb-, InGaSb- and InAsSbP TPV cells with Zn-diffused emitters', *5th Conference on Thermophotovoltaic Generation of Electricity*. Rome, Italy 16-19 September 2002: New York: American Institute of Physics, pp. 434-441.

212. Sater, B.L. (1995) 'Vertical multi-junction cells for thermophotovoltaic conversion', *1st NREL Conference on Thermophotovoltaic Generation of Electricity*. Copper Mountain, Colorado, US 24-28 July 1994: New York: American Institute of Physics, pp. 165-176.

213. Microtherm® insulation - product and performance data (2004) *Microtherm International Ltd., UK.* [Online]. Available at: www.microtherm.uk.com.

214. Clean thermal insulation with Wacker WDS® (2004) *Wacker-Chemie GmbH, Germany*, [Online]. Available at: www.wacker.com.

215. MICROSIL microporous insulation (2004) *ZIRCAR Ceramics, Inc., US.* [Online]. Available at: www.zircarceramics.com.

216. Insulating firebricks JM (2004) *Thermal Ceramics Europe, UK.* [Online]. Available at: www.thermalceramics.com.

217. Quartzel® rigid silica for insulation & reflection in infrared applications (2004) *Saint-Gobain Quartz SAS, France.* [Online]. Available at: www.quartz.saint-gobain.com.

218. Williams, D. (2004) 'Thermal conductivity data Ceramic fibre blanket (Fiberfrax Durablanket Z, 96 kg/m^3, 0.24 W/mK @ 800 °C, 0.34 W/mK @ 1000 °C, 0.44 W/mK @ 1200 °C)', *Warren Insulation Newcastle, UK*, Telephone conversation with Thomas Bauer, 7 January.

219. Yarbrough, D.W., Nowobilski, J. (1999) 'Section 4.5 Thermal insulation' in Kreith F. (ed.) *CRC Handbook of Thermal Engineering*, London: CRC Press.

220. Swet, C.J. (1991) 'Chapter 14 Energy Storage for Solar System - Overview ' in deWinter F. (ed.) *Solar Collectors, Energy Storage, and Materials*, Cambridge*: MIT Press.*

221. Dincer, I. (2002) 'Thermal energy storage systems as a key technology in energy conservation', *International Journal of Energy Research*, 26, pp. 567-588.

222. Stöcker, H. (2000) *Taschenbuch der Physik* (in German), 4th edn., Thun and Frankfurst am Main: Verlag Harri Deutsch.

223. Broman, L., Marks, J. (1995) 'Co-generation of electricity and heat from combustion of wood powder utilizing thermophotovoltaic conversion', *1st NREL Conference on Thermophotovoltaic Generation of Electricity*. Copper Mountain, Colorado, US 24-28 July 1994: New York: American Institute of Physics, pp. 133-138.

224. Osborn, P.D. (1985) *Handbook of Energy Data and Calculations: Including Directory of Products and Services*, Oxford: Butterworth-Heinemann.

225. Schroeder, K.L., Rose, M.F., Burkhalter, J.E. (1995) 'An experimental investigation of hybrid kerosene burner configurations for TPV applications', *1st NREL Conference on Thermophotovoltaic Generation of Electricity*. Copper Mountain, Colorado, US 24-28 July 1994: New York: American Institute of Physics, pp. 106-118.

226. Raynolds, J.E. (1999) 'Enhanced electro-magnetic energy transfer between a hot and cold body at close spacing due to evanescent fields', *4th NREL Conference on Thermophotovoltaic Generation of Electricity*. Denver, Colorado, US 11-14 October 1998: New York: American Institute of Physics, pp. 49-57.

227. Baldasaro, P.F., Fourspring, P.M. (2003) Improved Thermophotovoltaic (TPV) Performance Using Dielectric Photon Concentrations (DPC), Lockheed Martin Inc., US, Technical Report (LM-02K136).

228. DiMatteo, R., Greiff, P., Seltzer, D., Meulenberg, D., Brown, E., Carlen, E., Kaiser, K., Finberg, S., Nguyen, H., Azarkevich, J., Baldasaro, P., Beausang, J., Danielson, L., Dashiell, M., DePoy, D., Ehsani, H., Topper, W., Rahner, K., Siergiej, R. (2004) 'Micron-gap ThermoPhotoVoltaics (MTPV)', *6th International Conference on Thermophotovoltaic Generation of Electricity*. Freiburg, Germany 14-16 June 2004: New York: American Institute of Physics, pp. 42-51.

229. Ashcroft, J., DePoy, D. (1997) Design considerations for a thermophotovoltaic energy converter using heat pipe radiators, Kapl Atomic Power Laboratory, US (Report KAPL-P-000236).

230. Brougham, R.P., Whale, M.D. (2001) 'Feasibility of hybrid the thermophotovoltaic and reformer/fuel cell energy conversion systems', *11th Canadian Hydrogen Conference - Building the Hydrogen Economy*, Victoria, Canada June 17-20.

231. Erickson, T.A., Lindler, K.W., Harper, M.J. (1997) 'Design and construction of a thermophotovoltaic generator using turbine combustion gas', *32th Intersociety Energy Conversion Engineering Conference*, New York: IEEE, pp. 1101-1106.

232. Steinhüser, A., Hille, G., Kügele, R., Roth, W., Schulz, W. (1999) 'Photovoltaic-hybrid power supply for radio network components', *Intelec'99*, Kopenhagen, 6-9 Juni.

233. Zheng Chen, Brandhorst, H.W. (1999) 'Effect of elevated temperatures on the performance of an InP cell illuminated by a selective emitter', *4th NREL Conference on Thermophotovoltaic Generation of Electricity*. Denver, Colorado, US 11-14 October 1998: New York: American Institute of Physics, pp. 438-445.

234. Chen Zhen, Brandhorst, H.W., Wells, B.K. (2001) 'InAsP cells for solar thermophotovoltaic applications', *IEEE Aerospace and Electronic Systems Magazine*, 16(4), pp. 39-43.

235. Brandhorst, H.W., Zheng Chen Auburn University (2000) *Thermophotovoltaic conversion using selective infrared line emitters and large band gap photovoltaic devices*, U.S. Pat. 6,072,116.

236. Harder, N.P., Green, M.A. (2003) 'Thermophotonics', *Semiconductor Science and Technology*, 18, pp. 270-278.

237. Luque, A., Martí, A., Cuadra, L., Algora, C., Wahnon, P., Sala, G., Benítez, P., Bett, A.W., Gombert, A., Andreev, V.M., Jassaud, C., Van Roosmalen, J.A.M., Alonso, J., Räuber, A., Strobel, G., Stolz, W., Bitnar, B., Stanley, C., Conesa, J.C., Van Sark, W., Barnham, K., Danz, R., Meyer, T., Luque-Heredia, I., Kenny, R., Christofides, C. (2004) 'FULLSPECTRUM: A new PV wave making more efficient use of the solar spectrum', *19th European Photovoltaic Solar Energy Conference and Exhibition*, Paris 7-11 June.

238. Corkish, R., Green M.A., Puzzer, T. (2002) 'Solar energy collection by antennas', *Solar Energy*, 73, pp. 395-401.

239. Goswami, D.Y., Vijayaraghavan, S., Lu, S., Tamm, G. (2004) 'New and emerging developments in solar energy', *Solar Energy*, 76, pp. 33-43.

240. Cody, G.D. (1999) 'Theoretical maximum efficiencies for thermophotovoltaic devices', *4th NREL Conference on Thermophotovoltaic Generation of Electricity*. Denver, Colorado, US 11-14 October 1998: New York: American Institute of Physics, pp. 58-67.

241. Woolf, L.D. (1986) 'Optimum efficiency of single and multiple bandgap cells in thermophotovoltaic energy conversion', *Solar Cells*, 19(1), pp.19-38.

242. Woolf, L.D. (1985) 'Optimum efficiency of single and multiple band gap cells in TPV energy conversion', *18th IEEE Photovoltaic Specialists Conference*, New York: IEEE, pp. 1731-1732.

243. Wanlass, M.W., Emery, K.A., Gessert, T.A., Horner, G.S., Osterwald, C.R., Coutts, T.J. (1989) 'Practical considerations in tandem cell modelling', *Solar Cells*, 27, pp. 191-204.

244. Horner, G.S., Coutts, T.J., Wanlass, M.W. (1995) 'Proposal for a second-generation, lattice matched, multiple junction Ga_2/AsSb TPV converter', *1st NREL Conference on Thermophotovoltaic Generation of Electricity*. Copper Mountain, Colorado, US 24-28 July 1994: New York: American Institute of Physics, pp. 390-403.

245. Caruso, A., Piro, G. (1986) 'Theoretical efficiency of realistic solar cells intended for thermophotovoltaic applications', *Solar Cells*, 19(2), pp. 123-130.

246. Iles, P.A., Chu, C.L., Linder, E. (1996) 'The influence of bandgap on TPV converter efficiency', *2nd NREL Conference on Thermophotovoltaic Generation of Electricity*. Colorado Springs, Colorado, US 16-20 July 1995: New York: American Institute of Physics, pp. 446-457.

247. Würfel, P, Ruppel, W (1980) 'Upper limit of thermophotovoltaic solar-energy conversion', *IEEE Transactions on Electron Devices*, 27(4), pp. 745-750.

248. Harder, N.P., Würfel, P. (2003) 'Theoretical limits of thermophotovoltaic solar energy conversion', *Semiconductor Science and Technology*, 18, pp. 151-157.

249. Bell, R.L. (1979) 'Concentration ratio and efficiency in thermophotovoltaics', *Solar Energy*, 23(3), pp. 203-210.

250. Edenburn, M.W. (1980) 'Analytical evaluation of a solar thermophotovoltaic (TPV) converter', *Solar Energy*, 24(4), pp. 367-371.

251. Duomarco, J.L., Kaplow, R. (1984) 'Theoretical estimations of the efficiency of thermophotovoltaic systems using high-intensity silicon solar cells', *Solar Energy*, 32(1), pp. 33-40.

252. Badescu, V. (2001) 'Thermodynamic theory of thermophotovoltaic solar energy conversion', *Applied Physics*, 90(12), pp. 6476-6486.

253. De Vos, A. (1992) *Endoreversible Thermodynamics of Solar Energy Conversion*, New York Oxford: Oxford University Press.

254. De Vos, A. (1993) 'The endoreversible theory of solar energy conversion: a tutorial', *Solar Energy Materials and Solar Cells*, 31, pp. 75-93.

255. Baruch, P., de Vos, A., Landsberg, P.T., Parrott, J.E. (1995) 'On some thermodynamic aspects of photovoltaic solar energy conversion', *Solar Energy Materials and Solar Cells*, 36, pp. 201-222.

256. Gray, J. L., El-Husseini, A. (1996) 'A simple parametric study of TPV system efficiency and output power density including a comparison of several TPV materials', *2nd NREL Conference on Thermophotovoltaic Generation of Electricity*. Colorado Springs, Colorado, US 16-20 July 1995: New York: American Institute of Physics, pp. 3-15.

257. Zenker, M., Heinzel, A., Stollwerck, G., Ferber, J., Luther, J. (2001) 'Efficiency and power density potential of combustion-driven thermophotovoltaic systems using GaSb photovoltaic cells', *IEEE Transactions on Electron Devices*, 48(2), pp. 367-376.

258. Heinzel, A., Luther, J., Stollwerck, G., Zenker, M. (1999) 'Efficiency and power density potential of thermophotovoltaic systems using low bandgap photovoltaic cells', *4th NREL Conference on Thermophotovoltaic Generation of Electricity*. Denver, Colorado, US 11-14 October 1998: New York: American Institute of Physics, pp. 103-112.

259. Kittl, E. (1974) 'Unique correlation between blackbody radiation and optimum energy gap for a photovoltaic conservation device', *10th IEEE Photovoltaic Specialists Conference*, New York: IEEE, pp. 103-106.

260. Bitnar, B., Durisch, W., Mayor, J.-C., Sigg, H., Tschudi, H.R., Palfinger, G., Gobrecht, J. (2003) 'Record electricity-to-gas power efficiency of a silicon solar cell based TPV system', *5th Conference on Thermophotovoltaic Generation of Electricity*. Rome, Italy 16-19 September 2002: New York: American Institute of Physics, pp. 18-28.

261. Bitnar, B., Durisch, W., Mayor, J.-C., Sigg, H., Tschudi, H.R., Palfinger, G., Gobrecht, J. (2001) 'Development of a small TPV prototype system with an efficiency >2%' *17th European Photovoltaic Solar Energy Conference*.

262. Becker, F.E., Doyle, E.F., Shukla, K. (1999) 'Operating experience of a portable thermophotovoltaic power supply', *4th NREL Conference on Thermophotovoltaic Generation of Electricity*. Denver, Colorado, US 11-14 October 1998: New York: American Institute of Physics, pp. 394-402.

263. Andreev, V.M., Khvostikov, V.P., Khvostikova, O.A., Rumyantsev, V.D., Gazarjan, P.Y., Vlasov, A.S. (2004) 'Solar thermophotovoltaic converters: efficiency potentialities', *6th International Conference on Thermophotovoltaic Generation of Electricity*. Freiburg, Germany 14-16 June 2004: New York: American Institute of Physics, pp. 96-104.

264. Sarraf, D.B., Mayer, T.S. (1996) 'Design of a TPV Generator with a durable selective emitter and spectrally matched PV cells', *2nd NREL Conference on Thermophotovoltaic Generation of Electricity*. Colorado Springs, Colorado, US 16-20 July 1995: New York: American Institute of Physics, pp. 98-108.

265. Good, B.S., Chubb, D.L. (1997) 'Effects of geometry on the efficiency of TPV energy conversion', *3rd NREL Conference on Thermophotovoltaic Generation of Electricity*. Denver, Colorado, US 18-21 May 1997: New York: American Institute of Physics, pp. 487-503.

266. Schroeder, K.L., Rose, M.F., Burkhalter, J.E. (1997) 'An improved model for TPV performance predictions and optimization', *3rd NREL Conference on Thermophotovoltaic Generation of Electricity.* Denver, Colorado, US 18-21 May 1997: New York: American Institute of Physics, pp. 505-519.

267. Adachi, Y., Yugami, H. Shibata, K., Nakagawa, N. (2004) 'Compact TPV generation system using Al2O3/Er3Al5O12 eutectic ceramics selective emitters', *6th International Conference on Thermophotovoltaic Generation of Electricity.* Freiburg, Germany 14-16 June 2004: New York: American Institute of Physics, pp. 198-205.

268. Fraas, L.M., Huang, H.X., Shi-Zhong Ye, She Hui, Avery, J., Ballantyne, R. (1997) 'Low cost high power GaSb photovoltaic cells', *3rd NREL Conference on Thermophotovoltaic Generation of Electricity.* Denver, Colorado, US 18-21 May 1997: New York: American Institute of Physics, pp. 33-40.

269. Horne, E. (2002) Hybrid thermophotovoltaic power systems, *EDTEK, Inc., US*, Consultant Report (P500-02-048F).

270. Fourspring, P.M., DePoy, D.M., Beausang, J.F., Gratrix, E.J., Kristensen, R.T., Rahmlow, T.D., Talamo, P.J., Lazo-Wasem, J.E., Wernsman, B. (2004)'Thermophotovoltaic spectral control', *6th International Conference on Thermophotovoltaic Generation of Electricity.* Freiburg, Germany 14-16 June 2004: New York: American Institute of Physics, pp. 171-179.

271. Rahmlow, T.D., Lazo-Wasem, J.E., Gratrix, E.J., Fourspring, P.M., DePoy, D.M. (2004) 'New performance levels for TPV front surface filters', *6th International Conference on Thermophotovoltaic Generation of Electricity.* Freiburg, Germany 14-16 June 2004: New York: American Institute of Physics, pp. 180-188.

272. Good, B.S., Chubb, D.L., Lowe, R.A. (1997) 'Comparison of selective emitter and filter thermophotovoltaic systems', *2nd NREL Conference on Thermophotovoltaic Generation of Electricity.* Colorado Springs, Colorado, US 16-20 July 1995: New York: American Institute of Physics, pp. 16-34.

273. Chubb, D., Nelson, R. (1995) 'Workshop 3: Emission & spectral control', *1st NREL Conference on Thermophotovoltaic Generation of Electricity.* Copper Mountain, Colorado, US 24-28 July 1994: New York: American Institute of Physics, pp. 13-16.

274. Gruenbaum, P.E., Kuryla, M.S., Sundaram, V.S. (1995) 'Technical and economic issues for gallium antimonide based thermophotovoltaic systems', *1st NREL Conference on Thermophotovoltaic Generation of Electricity.* Copper Mountain, Colorado, US 24-28 July 1994: New York: American Institute of Physics, pp. 357-367.

275. Horne, W.E., Morgan, M.D., Sundaram, V.S. (1996) 'IR filters for TPV converter modules', *2nd NREL Conference on Thermophotovoltaic Generation of Electricity.* Colorado Springs, Colorado, US 16-20 July 1995: New York: American Institute of Physics, pp. 35-51.

276. Vardaxoglou, J.C. (1997) 'Chapter 1: Introduction to Frequency Selective Surfaces', in Vardaxoglou, J.C. (ed.) *Frequency Selective Surfaces: Analysis and Design*, New York Chichester Brisbane Toronto Singapore: Wiley & Sons, pp. 1-13.

277. Jefimovs, K., Vallius, T., Kettunen, V., Kuittinen, M., Turunen, J., Vahimaa, P., Kaipiainen, M., Nenonen , S. (2004) 'Inductive grid filters for rejection of infrared radiation', *Journal of Modern Optics*, 51, pp. 1651-1661.

278. Reed, J. A. (1997) *Frequency selective surfaces with multiple periodic elements*, PhD thesis. University of Texas at Dallas.

279. Spector, S.J., Astolfi, D.K., Doran, S.P., Lyszczarz, T.M., Raynolds, J.E. (2001) Infrared frequency selective surfaces fabricated using optical lithography and phase-shift masks, Report, *Lockheed Martin Corporation, US* (LM-01K062).

280. Horne, W.E., Morgan, M.D. EDTEK Inc. (1995) *Filter array for modifying radiant thermal energy*, U.S. Pat. 5,611,870.

281. Horne, W., Morgan, M., Horne, W., Sundaram, V. (2004) 'Frequency selective surface bandpass filters applied to thermophotovoltaic applications', *6th International Conference on Thermophotovoltaic Generation of Electricity.* Freiburg, Germany 14-16 June 2004: New York: American Institute of Physics, pp. 189-197.

282. Kristensen, R.T., Beausang, J.F., DePoy, D.M. (2004) 'Frequency selective surfaces as near-infrared electromagnetic filters for thermophotovoltaic spectral control', *Applied Physics*, 95, pp. 4845-4851.

283. Silberglitt, R., Le, H.K. (1991) 'Chapter 21: Materials for Solar Collector Concepts and Designs' in de Winter, F. (ed.) *Solar Collectors, Energy Storage, and Materials*, Cambridge: MIT Press.

284. Lampert, C.M. (1991) 'Chapter 22: Theory and Modeling of Solar Materials' in de Winter, F. (ed.) *Solar Collectors, Energy Storage, and Materials*, Cambridge: MIT Press.

285. Anna Selvan, J.A., Grützmacher, D., Hadorn, M., Bitnar, B., Durisch, W., Stutz, S., Neiger, T., Gobrecht, J. (2000) 'Tuneable plasma filters for TPV systems using transparent conducting oxides of tin doped indium oxide and Al doped zinc oxide', *16th European Photovoltaic Solar Energy Conference*, London: James and James Science-Publ., pp. 187-190.

286. Bitnar B., Durisch W., Grützmacher D., Mayor J.-C., von Roth F., Anna Selvan J.A., Sigg, H., Gobrecht J. (2000) 'Photovoltaic cells for a thermophotovoltaic system with a selective emitter', *16th European Photovoltaic Solar Energy Conference*, London: James and James Science-Publ., pp. 191-194.

287. Murthy, S.D., Langlois, E., Bath, I., Gutmann, R., Brown, E., Dzeindziel, R., Freeman, M., Choudhury, N. (1996) 'Characteristics of indium oxide plasma filters deposited by atmospheric pressure CVD', *2nd NREL Conference on Thermophotovoltaic Generation of Electricity*. Colorado Springs, Colorado, US 16-20 July 1995: New York: American Institute of Physics, pp. 290-311.

288. Charache, G.W., DePoy, D.M., Raynolds, J.E., Baldasaro, P.F., Miyano, K.E., Holden, T., Pollak, F.H., Sharps, P.R., Timmons, M.L., Geller, C.B., Mannstadt, W., Asahi, R., Freeman, A.J., Wolf, W. (1999) 'Moss-Burstein and plasma reflection characteristics of heavily doped n-type $In_xGa_{1-x}As$ and $InPyAs_{1-y}$', *Journal of Applied Physics*, 86, pp. 452-258.

289. Wu, X., Mulligan, W.P., Webb, J.D., Coutts, T. J. (1996) 'TPV plasma filters based on cadmium stannate', *2nd NREL Conference on Thermophotovoltaic Generation of Electricity*. Colorado Springs, Colorado, US 16-20 July 1995: New York: American Institute of Physics, pp. 329-338.

290. Ehsani, H., Bath, I., Borrego, J., Gutmann, R., Brown, E., Dzeindziel, R., Freeman, M., Choudhury, N. (1996) 'Characteristics of degenerately doped silicon for spectral control in thermophotovoltaic systems', *2nd NREL Conference on Thermophotovoltaic Generation of Electricity*. Colorado Springs, Colorado, US 16-20 July 1995: New York: American Institute of Physics, pp. 312-328.

291. Höfler, H., Paul, H.J., Ruppel, W., Würfel, P. (1983) 'Interference filters for thermophotovoltaic solar energy conversion', *Solar Cells*, 10(3), pp. 273-286.

292. Demichelis, F., Minetti-Mezzetti, E., Agnello, M., Perotto, V. (1982) 'Bandpass filters for thermophotovoltaic conversion systems', *Solar Cells*, 5, pp. 135-141.

293. Abbott, P., Bett, A.W. (2004) 'Cell-mounted spectral filters for thermophotovoltaic applications', *6th International Conference on Thermophotovoltaic Generation of Electricity*. Freiburg, Germany 14-16 June 2004: New York: American Institute of Physics, pp. 244-251.

294. Ortabasi, U., Bovard, B.G. (2003) 'Rugate technology for thermophotovoltaic (TPV) applications a new approach to near perfect filter performance', *5th Conference on Thermophotovoltaic Generation of Electricity*. Rome, Italy 16-19 September 2002: New York: American Institute of Physics, pp. 249-258.

295. Ortabasi, U., Friedman, H.W. (2004) 'PowerSphere: A novel photovoltaic cavity converter using low bandgap TPV cells for efficient conversion of high power laser beams to electricity', *6th International Conference on Thermophotovoltaic Generation of Electricity*. Freiburg, Germany 14-16 June 2004: New York: American Institute of Physics, pp. 142-152.

296. Fraas, L.M., Daniels, W.E., Muhs, J. (2001) 'Infrared photovoltaics for combined solar lighting and electricity for buildings', *17th European Photovoltaic Solar Energy Conference*. Munich, 22-26 October 2001, Munich: WIP.

297. Iles, P.A. (1995) 'Photovoltaic principles used in thermophotovoltaic generators', *1st NREL Conference on Thermophotovoltaic Generation of Electricity*. Copper Mountain, Colorado, US 24-28 July 1994: New York: American Institute of Physics, pp. 67-79.

298. Rose, M.F. (1996) 'Competing Technologies for Thermophotovoltaic', *2nd NREL Conference on Thermophotovoltaic Generation of Electricity*. Colorado Springs, Colorado, US 16-20 July 1995: New York: American Institute of Physics, pp. 213-220.

299. Johnson, S. (1997) 'TPV Market Review', *3rd NREL Conference on Thermophotovoltaic Generation of Electricity*. Denver, Colorado, US 18-21 May 1997: New York: American Institute of Physics, pp. xxv-xxvii.

300. Kruger, J.S. (1997), 'Review of a workshop on thermophotovoltaics organized for the Army Research Office', *3rd NREL Conference on Thermophotovoltaic Generation of Electricity*. Denver, Colorado, US 18-21 May 1997: New York: American Institute of Physics, pp. 23-30.

301. 'Chapter 3: Energy Sources and Systems' (1997) in *Energy-Efficient Technologies for the Dismounted Soldier*, Washington, DC: National Academy Press.

302. Milton, B.E. (1995) *Thermodynamics, Combustion and Engines*, Cheltenham: Stanley Thornes Pub Ltd.

303. Theiss, T.J., Conklin, J.C., Thomas, J.F., Armstrong, T.R. (2000) *Comparison of Prime Movers Suitable for USMC Expeditionary Power Sources*, Oak Ridge National Laboratory, US, Report (ORNL/TM-2000/116).

304. *Honda specialist* (2004) East Yorkshire, UK, [Online]. Available at: www.honda-uk.com.

305. Kusko, A. (1989) Emergency Standby Power Systems. New York: McGraw-Hill.

306. Capstone C30 Product Datasheet (2004) Capstone Microturbine Corporation, US [Online]. Available at: www.microturbine.com.

307. Price information about Capstone C30 (2004) [Online]. Available at: www.globalmicroturbine.com.

308. Peirs, J., Reynaerts, D., Verplaetsen, F. (2004) 'A microturbine for electric power generation', *Sensors and Actuators A*, 113, pp. 86-93.

309. WhisperGen AC Technical Specifications (2003) Whisper Tech Ltd, New Zealand, [Online]. Available at: www.whispergen.com.

310. Price information about WhisperGen AC unit (2004) E.ON, UK, [Online]. Available at: www.eon-uk.com.

311. Solo Stirling 161 CHP Module Technical Documentation (2003) Solo Stirling GmbH, Germany [Online]. Available at: www.stirling-engine.de.

312. STM Power - The clean energy choice (2004) STM Power, Inc., US [Online]. Available at: www.stmpower.com.

313. Deakin, R.I. (2000) 'Chapter 12: Batteries and fuel cells', in Warne, D.F. (ed.) *Newnes Electrical Engineer's Handbook*, Oxford: Newnes.

314. Linden, D. (1995) 'Chapter 6: Selection and application of batteries', Linden, D. (ed.) *Handbook of Batteries*, 2nd edn., New York: McGraw-Hill, pp. 6.1-6.15.

315. Datasheet Nickel-Cadmium VSE 4/5 A HIGH ENERGY SERIES (2002) Saft Energy Unlimited, France [Online]. Available at: www.saftbatteries.com.

316. Srinivasan, S., Dave, B.B., Murugesamoorthi, K.A., Parthasarathy, A.., Appleby, A.J. (1994) 'Chapter 2, Overview of fuel cell technology', in Blomen, L.J.M.J., Mugerwa, M.N. (ed.) *Fuel Cell Systems*, New York: Plenum Press, pp. 37-72.

317. Williams, M.C. (ed.) (2000) Fuel Cell Handbook, 5th edn., U.S. Department of Energy, Office of Fossil Energy, National Energy Technology Laboratory (DE-AM26-99FT40575).

318. Great Britain. Department of Trade and Industry (2003) *Sustainable energy technology route maps - Fuel cells*, London: Department of Trade and Industry.

319. Acres, G.J.K. (2001) 'Recent advances in fuel cell technology and its applications', *Journal of Power Sources*, 100, pp. 60-66.
320. Chunshan Song (2002) 'Fuel processing for low-temperature and high-temperature fuel cells - Challenges, and opportunities for sustainable development in the 21st century', *Catalysis Today*, 77, pp. 17-49.
321. Transportation Fuel Cells - Technical Info (2003) The online fuel cell information resource [Online]. Available at: www.fuelcells.org.
322. Prater, K.B. (1996) 'Solid polymer fuel cells for transport and stationary applications', *Journal of Power Sources*, 61, pp. 105-109.
323. Pinkerton, F.E., Wicke, B.G. (2004) 'Bottling the hydrogen genie', *The Industrial Physicist*, New York: American Institute of Physics, February/March, pp. 20-23.
324. Great Britain. Department of Trade and Industry (2003) *Sustainable energy technology route maps - Hydrogen*, London: Department of Trade and Industry.
325. Fuel Cells for Portable Power: Markets, Manufacture and Cost (2003) Darnell Group Inc., US, US Fuel Cell Council, Revised Final Report (4) for Breakthrough Technologies & [Online]. Available at: www.usfcc.com.
326. SFC A25 Smart Fuel Cell (2004) Fuel cell store, US [Online]. Available at: www.fuelcellstore.com (Accessed: 9 August 2004).
327. A50 Smart Fuel Cell (2004) Fuel cell store, US [Online]. Available at: www.fuelcellstore.com (Accessed: 9 August 2004).
328. VE100 v2 (2004) Fuel cell store, US [Online]. Available at: www.fuelcellstore.com (Accessed: 9 August 2004).
329. VE1000 (2004) Fuel cell store, US [Online]. Available at: www.fuelcellstore.com (Accessed: 9 August 2004).
330. AirGen™ Fuel Cell Generator Specifications (2003) Ballard Power Systems Inc., Canada.
331. Nexa Power Module Specifications (2004) Ballard Power Systems Inc., Canada.
332. Ebara Ballard News Release (2004), Ebara Corporation, Japan, 28 January.
333. C. Lok (2004) 'In Japan beginnt die Brennstoffzellen-Ära' (in German), *Technology Review - Das M.I.T.-Magazin fuer Innovation*, 9, pp. 10.
334. Independence 1000 (2004) Fuel cell store, US [Online]. Available at: www.fuelcellstore.com (Accessed: 9 August 2004).
335. 200kW Fuel Cell Power Plant : PC25C (2004) Toshiba, Japan [Online]. Available at: www.toshiba.co.jp/product/fc/fce/index.htm (Accessed: 9 August 2004).
336. Goulding, P.S., Fry, M.R. (2003) Woking Park PAFC Chp Monitoring Phase 1: Planning, Installation and Commissioning, Department of Trade and Industry, UK (DTI/Pub URN 03/879).
337. Rowe, D.M. (1994) 'Chapter 10: Thermoelectric generation', in Crook A.W. (ed.) *Profiting from low-grade heat: thermodynamic cycles for low-temperature heat sources*, Institution of Electrical Engineers.
338. Cobble, M.H. (1995) 'Chapter 39: Calculation of Generator Performance', in Rowe, D.M. (ed.) *CRC Handbook of Thermoelectrics*, London: CRC Press.
339. Riffat, S.B., Xiaoli Ma (2003) 'Thermoelectrics: a review of present and potential applications', *Applied Thermal Engineering*, 23, pp. 913-935.
340. Lambrecht, A., Böttner, H., Nurnus, J. (2004) 'Thermoelectric Energy Conversion - Overview Of A TPV Alternative', *6th International Conference on Thermophotovoltaic Generation of Electricity*. Freiburg, Germany 14-16 June 2004: New York: American Institute of Physics, pp. 24-32.
341. Vining, C.B. (1994) *Thermoelectric Technology of the Future*, Presentation, Defense Science Research Council Workshop, La Jolla, California, 21 July.
342. Product Summary - Thermoelectric generator (2004) Global Thermoelectric, Canada [Online]. Available at: www.globalte.com.

343. HZ-20 Thermoelectric Module, Hi-Z Technology, Inc., US [Online]. Available at: www.hi-z.com (Accessed: 9 June 2004).

344. Hall, W.C. (1995) 'Chapter 40: Terrestrial Applications of Thermoelectric Generators', in Rowe, D.M. (ed.) *CRC Handbook of Thermoelectrics*, London: CRC Press.

345. Cardiff Thermoelectric Group, About us (2004) University of Cardiff [Online]. Available at: www.thermoelectrics.com (Accessed: 13 September 2004).

346. Advanced Thermoelectric Materials for Efficient Waste Heat Recover very in Process Industries (2004) Industrial Technologies Program, U.S. Department of Energy [Online]. Available at: www.eere.energy.gov

347. Lyon, H.B. (2002) *Domestic and International Activities in Thermoelectrics*, Marlow industries, Inc., Presentation. [Online]. Available at: www.osti.gov/fcvt/darpa2002/darpa2002wkshp.html

348. Matsuura, K., Rowe, D.M. (1995) 'Chapter 44:Low-temperature heat conversion', in Rowe, D.M. (ed.) *CRC Handbook of Thermoelectrics*, London: CRC Press.

349. Lodhi, M.A.K., Vijayaraghavan, P., Daloglu, A. (2001) 'An overview of advanced space/terrestrial power generation device: AMTEC', *Journal of Power Sources*, 103(1), pp. 25-33.

350. El-Genk, M.S., Tournier, J.-M.P. (2004) 'AMTEC/TE static converters for high energy utilization, small nuclear power plants', *Energy Conversion and Management*, 45, pp. 511-535.

351. Macauley, M. K., Davis, J. F. (2001) *An Economic Assessment of Space Solar Power as a Source of Electricity for Space-Based Activities*, Discussion Paper, Resources for the Future, Washington, US [Online]. Available at: www.rff.org.

352. Oman, H. (1999) 'AMTEC Cells Challenge Energy Converters', *IEEE Aerospace and Electronic Systems Magazine*, 14, pp. 43-46.

353. 'Chapter 3: Overview of Technology' (2001) in *Thermionics Quo Vadis? An Assessment of the DTRA's Advanced Thermionics Research and Development Program*, Washington, DC: National Academy Press, pp. 15-32, [Online] Available at: http://books.nap.edu/.

354. Massie, L.D. (1991) 'Future trends in space power technology', *IEEE Aerospace and Electronic Systems Magazine*, 6(11), pp. 8-13.

355. Hagelstein, P.L., Kucherov, Y. (2002) 'Enhanced figure of merit in thermal to electrical energy conversion using diode structures', *Applied Physics Letters*, 81, pp. 559-561.

356. Woolf, L.D. (1987) 'Solar photothermophotovoltaic energy conversion', *19th IEEE Photovoltaic Specialists Conference*, New York: IEEE, pp. 427-432.

357. Fraas, L., Groeneveld, M., Magendanz, G., Custard, P. (1999) 'A single TPV cell power density and efficiency measurement technique', *4th NREL Conference on Thermophotovoltaic Generation of Electricity*. Denver, Colorado, US 11-14 October 1998: New York: American Institute of Physics, pp. 312-316.

358. Seal, M. (1998) Report to the US Department of Energy on the thermophotovoltaic research at Western Washington University 1994-1997.

359. Fraas, L. M., Avery, J. E., Nakamura, T. (2002) 'Electricity from concentrated solar IR in solar lighting applications', *29th IEEE Photovoltaic Specialists Conference*, New York: IEEE.

360. Dashiell, M.W., Beausang, J.F., Nichols, G., Depoy, D.M., Danielson, L.R., Ehsani, H., Rahner, K.D., Azarkevich, J., Talamo, P., Brown, E., Burger, S., Fourspring, P., Topper, W., Baldasaro, P.F., Wang, C.A., Huang, R., Connors, M., Turner, G., Shellenbarger, Z., Taylor, G., Jizhong Li, Martinelli, R., Donetski, D., Anikeev, S., Belenky, G., Luryi, S., Taylor, D.R., Hazel, J. (2004) '0.52 eV Quaternary InGaAsSb Thermophotovoltaic Diode Technology', *6th International Conference on Thermophotovoltaic Generation of Electricity*. Freiburg, Germany 14-16 June 2004: New York: American Institute of Physics, pp. 404-414.

361. Shellenbarger, Z.A., Taylor, G.C., Martinelli, R.U., Carpinelli, J.M. (2004) 'High Performance InGaAsSb TPV Cells', *6th International Conference on Thermophotovoltaic Generation of Electricity*. Freiburg, Germany 14-16 June 2004: New York: American Institute of Physics, pp. 345-352.

362. Wanlass, M.W., Ahrenkiel, S.P., Ahrenkiel, R.K., Carapella, J.J., Wehrer, R.J., Wernsman, B. (2004) 'Recent Advances in Low-Bandgap, InP-Based GaInAs/InAsP Materials and Devices for Thermophotovoltaic (TPV) Energy Conversion', *6th International Conference on Thermophotovoltaic Generation of Electricity*. Freiburg, Germany 14-16 June 2004: New York: American Institute of Physics, pp. 427-435.

363. Fraas, L.M., Avery, J.E., Huang, H. X. (2003) 'Thermophotovoltaic furnace-generator for the home using low bandgap GaSb cells', *Semiconductor Science and Technology*, 18, pp. 247-253.

364. Solar Power Unit 7 (2000) Postgraduate Distance Learning Series in Renewable Energy Systems Technology, Centre for Renewable Energy Systems Technology (CREST), Loughborough University, UK [Online] Available at: http://crestdl.lboro.ac.uk/.

365. Krist, K. (1995) 'GRI research on thermophotovoltaics', *1st NREL Conference on Thermophotovoltaic Generation of Electricity*. Copper Mountain, Colorado, US 24-28 July 1994: New York: American Institute of Physics, pp. 54-63.

366. Ostrowski, L.J., Pernisz, U.C., Fraas, L.M. (1996) 'Thermophotovoltaic Energy Conversion: Technology and Market Potential', *2nd NREL Conference on Thermophotovoltaic Generation of Electricity*. Colorado Springs, Colorado, US 16-20 July 1995: New York: American Institute of Physics, pp. 251-260.

367. Kohler Power Systems (2004) Kohler Power Systems, US, [Online]. Available at: www.kohlerpowersystems.com.

368. West, C. (1986) *Principles and Applications of Stirling Engines*, New York: Van Nostrand Reinhold.

369. Batteries to 2007 - Market Size, Market Share, Demand Forecast and Sales (2003) only abstract and list of contents available, Freedonia Group, Inc., Ohio, US [Online]. Available at: www.freedoniagroup.com.

370. Weston, M., Matcham, J. (2002) *Portable Power Applications of fuel cells*, London: Department of Trade and Industry, UK (ETSU F/03/00253/00/REP).

371. Oil and Gas Applications and Telecom uses (2005) Global Thermoelectric, Canada [Online]. Available at: www.globalte.com (Accessed: 4 May 2005).

372. Hi-Z module applications (2005) Hi-Z Technology, Inc., US [Online]. Available at: www.hi-z.com (Accessed: 4 May 2005).

373. Solar applications (2002) BP Solar International, US [Online]. Available at: www.bpsolar.com (Accessed: 22 September 2004).

374. 'Chapter 4: Spacecraft Electric Power' (1994), in *Technology for Small Spacecraft*, Washington, DC: National Academy Press.

375. Baker, A.M. (2002) Future Power Systems for Space Exploration: Executive summary, QinetiQ UK [Online].

376. Fraas, L., Minkin, L., She Hui, Avery, J., Howells, C. (2004) 'TPV Power Source Using Infrared-Sensitive Cells with Commercially Available Radiant Tube Burner', *6th International Conference on Thermophotovoltaic Generation of Electricity*. Freiburg, Germany 14-16 June 2004: New York: American Institute of Physics, pp. 52-60.

377. Hess, H.L. (2002) Front End Analysis of Mobile Electric Power Research and Development for the 2015-2025 Time Frame, Fort Monmouth, US [Online]. Available at: www.ee.uidaho.edu/ee/power/hhess/FrontEndAnalysis.pdf (Accessed: 21 August 2004).

378. Uninterruptible Power Supplies: Global Market Forecasts, Emerging Technologies and Competitive Environment (2001) Brochure, 3rd edn., Darnell Group, Inc., US. [Online]. Available at: www.darnell.com.

379. Aubyn, J., Platts, J., Aubyn, J.D. (1992) *Uninterruptible Power Supplies (IEE Power Series 14)*, London: Peter Peregrinus.

380. Brownlie, G.D. (1998) 'Battery requirements for uninterruptible power-supply applications', *Journal of Power Sources*, 23(1-3), pp. 211-220.

381. Section 4.8 Remote area power supply (RAPS) (2002) *Renewable Energy Technology Roadmap*, Department of Industry, Tourism and Resources, Australia [Online]. Available at: www.industry.gov.au/retr.

382. Mazzer, M, de Risi, A., Laforgia, D., Barnham, K., Rohr, C. (2000) 'High Efficiency Thermophotovoltaics for Automotive Applications', *World Congress of the Engineerung Society for advanced mobility land sea air and space (SAE)*, Detroit, Michigan, 6-9 March.

383. Vázquez, J, Sanz-Bobi, M.A., Palacios, R., Arenas, A. (2002) 'State of the Art of Thermoelectric Generators Based on Heat Recovered from the Exhaust Gases of Automobiles', *7th European Workshop on Thermoelectrics*, Pamplona, Spain, October.

384. Tompsett, G.A., Finnerty, C., Kendall, K., Alston, T., Sammes, N.M. (2000) 'Novel applications for micro-SOFCs', *Journal of Power Sources*, 86, pp. 376-382.

385. Nelson, R., Doyle, E., Hurley, J. (1997) Utility Thermophotovoltaic Cogeneration, only Abstract available, Final Report, Gas Research Institute, US (GRI-97/0416).

386. Kassakian, J.G. (2000) 'Automotive Electrical Systems – The Power Electronics Market of the Future', *Applied Power Electronics Conference and Exposition*, New Orleans, Louisiana, February 6-10.

387. Hebling, C. (2002) 'Presentation as a chairman (not published)', *5th Conference on Thermophotovoltaic Generation of Electricity*. Rome, Italy 16-19 September 2002: New York: American Institute of Physics.

388. Wang, C.A. (2004) 'Audience comment', *6th International Conference on Thermophotovoltaic Generation of Electricity*. Freiburg, Germany 14-16 June 2004: New York: American Institute of Physics.

389. Caton, J.A., Turner, W.D. (1996) 'Chapter 17: Cogeneration', in Kreith, F., West, R.E. (ed.) *CRC Handbook of Energy Efficiency*, London: CRC Press, pp. 669-711.

390. Combined Heat and Power (1994) An Appraisal of UK Energy Research, Development, Demonstration & Dissemination, ETSU R83, London: Her Majesty's Stationery Office (HMSO), pp. 465-480.

391. A Guide to Cogeneration (2001) The European Association for the Promotion of Cogeneration, Brussels, Belgium [Online]. Available at: www.cogen.org.

392. MICRO - MAP Mini and Micro CHP - Market Assessment And Development Plan Summary Report (2002) Summary report, FaberMaunsell Ltd, UK [Online]. Available at: www.cogen.org/projects/micromap.htm.

393. Iles P., Hindman, D. (1995) 'Workshop 4: Converter Cooling & Recuperation', *1st NREL Conference on Thermophotovoltaic Generation of Electricity*. Copper Mountain, Colorado, US 24-28 July 1994: New York: American Institute of Physics, pp. 17-22.

394. Graham, G., Cruden, A., Hart, J. (2002) *Assessment of the Implementation Issues for Fuel Cells in Domestic and Small Scale Stationary Power Generation and CHP Applications*, Report, Department of Trade and Industry, UK (ETSU F/03/00235/REP, DTI/Pub URN 02/1349).

395. Crozier-Cole, T., Jones, G. (2002) *The potential market for micro CHP in the UK*, Report to the Energy Saving Trust, Energy for Sustainable Development Limited, UK (P00548) [Online]. Available at: www.est.org.uk.

396. Aicher, T., Kästner, P., Gopinath, A., Gombert, A., Bett, A. W., Schlegl, T., Hebling, C., Luther, J. (2004) 'Development of a Novel TPV Power Generator', *6th International Conference on Thermophotovoltaic Generation of Electricity*. Freiburg, Germany 14-16 June 2004: New York: American Institute of Physics, pp. 71-78.

397. Mattarolo, G., Bard, J., Schmid, J. (2004) 'TPV-Application As Small Back-up Generator For Standalone Photovoltaic Systems', *6th International Conference on Thermophotovoltaic Generation of Electricity*. Freiburg, Germany 14-16 June 2004: New York: American Institute of Physics, pp. 133-141.

398. The Micro-CHP Technologies Roadmap - Meeting 21 Century Residential Energy Needs (2003), United States Department of Energy, Office of Energy Efficiency and Renewable Energy, Distributed Energy Program [Online].

399. Slowe, J. (2004) *Micro-CHP Technologies and Markets*, Presentation, Micro-CHP Workshop, Milan, Italy, 13 September [Online].

400. Pehnt, M., Praetorius, B., Schumacher, K., Fischer, C., Schneider, L., Cames, M., Voß, J.-P. (2004) *Discussion Paper 4 - Micro CHP – a sustainable innovation?*, Transformation and Innovation in Power Systems (TIPS), Socio-ecological Research Framework, Germany [Online]. Available at: www.tips-project.de.

401. Butcher, T. (2003) *MicroCHP The Next Level in Efficiency*, Presentation, National Oilheat Research Alliance Technology Symposium, New England Fuel Institute Convention, Boston, 9 June.

402. A Technical and Economic Assessment of Small Stirling Engines for Combined Heat and Power (1993), Future Practice Report No. 32, Energy Efficiency Enquiries Bureau (ETSU), UK.

403. Introduction to Small - Scale Combined Heat and Power (1995) Good Practice Guide 3, Energy Efficiency Enquiries Bureau (ETSU), UK.

404. Mills, D. (2004) 'Advances in solar thermal electricity technology', *Solar Energy*, 76, pp. 19-31.

405. Laing, D., Pålsson, M. (2002) 'Hybrid Dish/Stirling Systems: Combustor and Heat Pipe Receiver Development', *Journal of Solar Energy Engineering*, 124, pp. 176-181.

406. Universal® Portable Heaters - A Scheu Company (2003) Product Catalog, Univeral Portable Heater, A Scheu Company, California, US [Online]. Available at: www.universal-heaters.com.

407. Waste heat recovery from high temperature gas streams (1999) Good Practice Guide 13, Energy Efficiency Enquiries Bureau (ETSU), UK.

408. Rowe, D.M., Gao Min (1998) 'Evaluation of thermoelectric modules for power generation', *Journal of Power Sources*, 73, pp. 193-198.

409. Korobitsyn, M. (2002) 'Industrial applications of the air bottoming cycle', *Energy Conversion and Management*, 43, pp. 1311-1322.

410. Larjola, J. (1995) 'Electricity from Industrial Waste Heat Using High-Speed Organic Rankine Cycle (ORC)', *International Journal of Production Economics*, 41, pp. 227-235.

411. Brown, H.L. (1996) *Energy Analysis of 108 Industrial Processes*, Lilburn: Fairmont Press.

412. Phylipsen, G.J.M., Blok, K., Worrell, E. (1998) *Handbook on International Comparisons of Energy Efficiency in the Manufacturing Industry*, Department of Science, Technology and Society, Utrecht University, The Netherlands.

413. Energy use and energy efficiency in UK manufacturing industry up to the year 2000 - Energy efficiency series (1984) Excecutive Summary and Main Report, 1, London: Her Majesty's Stationery Office (HMSO).

414. An Appraisal of UK Energy Research, Development, Demonstration and Dissemination (1994), ETSU R83, Vol. 2, London: Her Majesty's Stationery Office (HMSO).

415. de Beer, J., Worrell, E., Blok, K. (1998) 'Future technologies for energy-efficient iron and steel making', *Annual Review of Energy and the Environment*, 23, pp. 123-205.

416. Chih Wu (1996) 'Analysis of waste heat thermoelectric power generators', *Applied Thermal Engineering*, 16, pp. 63-69.

417. Hultgren, R., Desai, P.D., Hawkins, D.T., Gleiser, M., Kelley, K.K., Wagman, D.D. (1973) 'Selected values of the thermodynamic properties of elements', Ohio: American Society for metals.

418. Trier, W. (1987) *Glass Furnaces, Design construction and operation*, translated by Loewenstein, K.L., Sheffield: Society of Glass Technology.

419. Touloukian, Y. S. (1967) *Thermophysical properties of high temperature solid materials, Vol. 4, Oxides and their solutions and mixtures*, New York: MacMillan.

420. Rhine, J.M., Tucker, R.J. (1991) *Modelling of Gas-Fired Furnaces and Boilers and other industrial heating processes*, New York: McGraw-Hill.

421. Irving, W.R. (1993) *Continuous casting of steel*, Aldershot: Ashgate Publishing.

422. UK Iron and Steel Industry: Annual Statistics (1996) Iron and Steel Statistics Bureau, UK.

423. Technology Benchmarking in the UK Glass Sector (2000) General Information Report 75, Energy Efficiency Enquiries Bureau (ETSU), UK.

424. Picture without naming (2002) SEPR Group, France [Online]. Available at: www.sefpro.saint-gobain.com.

425. Glass Industry of the future, Energy and Environmental Profile of the U.S. Glass Industry (2002) US. Department of Energy, Office of Industrial Technologies [Online]. Available at: www.oit.doe.gov.

426. Beerkens, R. (1992) 'Application of Energy Saving Technologies for Glass Furnaces: A comparative study', *European Seminar on Improved technologies for the rational use of energy in the glass industry*, Wiesbaden, Germany, 4-6 February, Fachinformationszentrum Karlsruhe, pp. 325-339.

427. The Use of Refractories for Container Glass Furnaces - Bonded Refractories, Fused-Cast Refractories, Product catalogue, SEPR Group, France, 2000. Available at: www.sefpro.saint-gobain.com.

428. Hayes, R.R., Brewster, S., Webb, B.W., McQuay, M.Q., Huber, A.M. (2001) 'Crown incident radiant heat flux measurements in an industrial regenerative, gas-fired, flat-glass furnace', *Experimental Thermal and Fluid Science*, 24, pp. 35-46.

429. Tooley, F.V. (1984) *The Handbook of Glass Manufacture*, 3rd. edn., New York: Ashlee Publishing.

430. Bredehoeft, R., Hammer, E.E., Unger, K.-D. (1986) 'Umbau eines 80-t-Lichtbogenofens der Tyssen Edelstahlwerke AG – Kuehlkreislaeufe unter besonderer Beruecksichtigung der Verdampfungskuehlung fuer Wand- und Deckenelemente' (in German), *Stahl und Eisen*, 106(19), pp. 1011-1015.

431. Energy and Environmental Profile of the U.S. Iron and Steel Industry (2000) US. Department of Energy, Office of Industrial Technologies [Online]. Available at: www.oit.doe.gov.

432. Great Britain. Department of Trade and Industry (1997) Energy Consumption in the United Kingdom (Energy Paper 66), London: Department of Trade and Industry.

433. UK 2002 - The Official Yearbook of the United Kingdom of Great Britain and Northern Ireland (2002) Office for National Statistics, [Online]. Available at: www.statistics.gov.uk.

434. Aschaber, J., Hebling, C., Luther, J. (2001) 'Modelling of a thermophotovoltaic system including radiation and conduction heat transfer', *17th European Photovoltaic Solar Energy Conference*, pp. 186-189.

435. Aschaber, J., Hebling, C., Luther, J. (2002) 'The Challenge of Realistic TPV System Modelling', *5th Conference on Thermophotovoltaic Generation of Electricity*. Rome, Italy 16-19 September 2002: New York: American Institute of Physics, pp. 79-90.

436. Aschaber, J., Hebling, C., Luther, J. (2003) 'Realistic modelling of TPV systems', *Semiconductor Science and Technology*, 18, pp. 158-164.

437. Viskanta, R., Anderson, E.E. (1975) 'Heat transfer in semitransparent solids', *Advances in Heat Transfer*, 11, pp. 317-441.

438. Burger, D.R. (1997) 'Modeling the TPV system optical cavity', *3rd NREL Conference on Thermophotovoltaic Generation of Electricity*. Denver, Colorado, US 18-21 May 1997: New York: American Institute of Physics, pp. 535-546.

439. Gethers, C.K., Ballinger, C.T., Postlethwait, M.A., DePoy, D.M., Baldasaro, P.F. (1997) 'TPV efficiency predictions and measurements for a closed cavity geometry', *3rd NREL Conference on Thermophotovoltaic Generation of Electricity*. Denver, Colorado, US 18-21 May 1997: New York: American Institute of Physics, pp. 471–486.

440. Ballinger, C.T., Charache, G.W., Murray, C.S. (1999) 'Monte Carlo analysis of a monolithic interconnected module with a back surface reflector', *4th NREL Conference on Thermophotovoltaic Generation of Electricity*. Denver, Colorado, US 11-14 October 1998: New York: American Institute of Physics, pp. 161-174.

441. Thomas, R.M., Wernsman, B.R. (2001) 'Thermophotovoltaic devices and photonics modeling', *Optics and Photonics News*, 12(8), pp. 40-44.

442. Wernsman, B., Mahorter, R.G., Thomas, R.M. (2002) 'Optical Cavity Effects on TPV Efficiency', *5th Conference on Thermophotovoltaic Generation of Electricity*. Rome, Italy 16-19 September 2002: New York: American Institute of Physics, pp. 277-286.

443. Gopinath, A., Aschaber, J., Hebling, C., Luther, J. (2004) 'Modeling of Radiative Energy Transfer and Conversion in a TPV Power System', *6th International Conference on Thermophotovoltaic Generation of Electricity*. Freiburg, Germany 14-16 June 2004: New York: American Institute of Physics, pp. 162-168.

444. Gardon, R. (1961) 'A Review of Radiant Heat Transfer in Glass', *Journal of the American Ceramic Society*, 44, pp. 305-311.

445. Fraas, L.M., Ferguson, L., McCoy, L.G., Pernisz, U.C. (1996) 'SiC IR Emitter Design for Thermophotovoltaic Generators', *2nd NREL Conference on Thermophotovoltaic Generation of Electricity*. Colorado Springs, Colorado, US 16-20 July 1995: New York: American Institute of Physics, pp. 488-494.

446. Zubia, J., Lomer, M. (2001) 'Chapter 4: Optical waveguides and their manufacture' in Lopez-Higuera, J.M. (ed.) *Handbook of optical fibre sensing technology*, New York Chichester Brisbane Toronto Singapore: Wiley & Sons, pp. 57-79.

447. Tropf, W.J., Thomas, M.E., Harris, T.J. (1995) 'Chapter 33: Properties of Crystals and Glasses', in Bass, M. (ed.) *Handbook of Optics*, 2, New York: McGraw-Hill.

448. *Agate product catalogue*, Agate Products Ltd, UK, www.agateproducts.co.uk.

449. Hetherington, G., Jack, K.H. (1963) *Fused Quartz and Fused Silica*, TSL Wallsend Northumberland England, translated and reprinted from Ullmanns Encyklopädie der technischen Chemie, 14, 3rd edn., München Berlin: Urban & Schwarzberg, pp. 511-524.

450. Doremus, R.H. (1973) 'Chapter Crystallization', in *Glass Science*, New York Chichester Brisbane Toronto Singapore: Wiley & Sons, pp. 74-97.

451. Fluent, Version 6.1, *Fluent Europe Ltd.*, Sheffield, UK, www.fluent.com.

452. Kunc, T., Lallemand, M., Saulnier, J. B. (1984) 'Some new developments on coupled radiative-conductive heat transfer in glasses - experiments and model', *International Journal of Heat and Mass Transfer*, 27, pp. 2307-2319.

453. Edwards, O.J. (1966) 'Optical transmittance of fused silica at elevated temperatures', *Journal of the Optical Society of America*, 56, pp. 1314-1319.

454. Philipp, H.R. (1985) 'Silicon dioxide (SiO_2) (Glass)', in Palik E. D. (ed.) *Handbook of optical constants of solids*, New York: Academic Press, pp. 749-763.

455. Barsoum, M. (1997) 'Chapter 16: Optical Properties', in *Fundamentals of Ceramics*, New York: McGraw-Hill, pp. 611-649.

456. Vitreosil Product datasheet (2001) Saint-Gobain Quartz PLC, Wallsend, UK [Online]. Available at: www.quartz.saint-gobain.com.

457. DiMatteo, R. (2004) Conversation with Thomas Bauer, DiMatteo from the Charles Stark Draper Laboratory briefly suggested the optical glue possibility, *6th International Conference on Thermophotovoltaic Generation of Electricity*. Freiburg, Germany 14-16 June 2004: New York: American Institute of Physics, pp. 255-266.

458. Dils, R.R. (1983) 'High-temperature optical fiber thermometer', *Journal of Applied Physics*, 54, pp. 1198-1201.

459. Diller, T.E. (1993) 'Advances in Heat Flux Measurements', in Hartnett, J.P., Irvine, F.I., Cho, Y.I. (ed.) *Advances in heat transfer*, 23, New York: Academic Press, pp. 279-368.

460. Childs, P.R.N. (2001) 'Chapter 12: Heat flux measurement', in *Practical temperature measurement*, Oxford, Boston: Butterworth-Heinemann, pp. 324-361.

461. Doebelin, E.O. (1990) 'Section 8.10: Heat-Flux Sensors', in *Measurement systems – application and design*, 4th edn. New York: McGraw-Hill, pp. 706-711.

462. Clayton, W.A. (1999) 'Part 12: Thermal Sensor, Chapter 11: Heat-Flow Transducers', in Guyer, E.C., Brownell, D.L. (ed.) *Handbook of Applied Thermal Design*, Washington London: Taylor & Francis.

463. Gethers, C.K., Ballinger, C.T., DePoy, D.M. (1999) 'Lessons learned on closed cavity TPV system efficiency measurement', *4th NREL Conference on Thermophotovoltaic Generation of Electricity*. Denver, Colorado, US 11-14 October 1998: New York: American Institute of Physics, pp. 335-348.

464. Instruction manual CM3 pyranometer (2004) Kipp & Zonen, Netherlands [Online]. Available at: www.kippzonen.com.

465. Brennereinstellung + Berechnungsformeln, WS-Waermeprozesstechnik GmbH (2000) WS-Wärmeprozesstechnik GmbH, Renningen, Germany, www.flox.com, http://wsgmbh.de.

466. Drawing of the Rekumat radiant tube burner C Za 80 (2003) WS Wärmeprozesstechnik GmbH, Renningen, Germany, www.flox.com, www.wsgmbh.de.

467. Technical documentation and operating instructions – Rekumat C radiant tube, WS-Wärmeprozesstechnik GmbH, Renningen, Germany, www.flox.com, http://wsgmbh.de.

468. Furnace Drawings (2003) Fuel Furnace Engineering LTD, AldridgeWalsall, UK, www.fuelfurnace.com.

469. Fuel Furnace Engineering LTD, Aldridge Walsall, UK, www.fuelfurnace.com.

470. Pressure regulator FRU 505 (2004) Karl Dungs GmbH & Co. KG, Urbach, Germany www.dungs.com.

471. Installation Operation Maintenance Instructions, Model 675 Series, Centrifugal Blowers, Exhausters & Gas Boosters (2003) The Utile Engineering Co. Ltd, Irthlingborough, UK.

472. Flue gas tester Longus LS5000, Grundig.

473. El-Mahallawy, F., Habik El-Din, S. (2002) *Fundamentals and Technology of Combustion*, Amsterdam: Elsevier Science.

474. Eastop, T.D., McConkey, A. (1986) *Applied Thermodynamics for Engineering Technologists: S.I. Units*, 4th edn. London: Longman Publishing Group.

475. High Temperature Thermocouple Assemblies, Omega, UK.

476. PCI-DAS-TC 16-Channel Thermocouple Input Board (2002) Measurement Computing Corporation, www.measurementcomputing.com, www.MCCDaq.com.

477. Stanley, J. (2004) 'Refractory ceramic fibres VF1260 datasheet', *Tekniform Ltd. UK*, E-mail to Thomas Bauer, 1 March.

478. Solid-state plate-to-air heat pump assembly using a Peltier element, MPA200-24, manufactured by Melcor, www.melcor.com and ordered via Thermo Electric Devices, UK.

479. F3C Operating Instructions (German) (1994) Thermo Haake, Karlsruhe, Germany, www.thermohaake.com.

480. Flow transducer V8189 (2000), ordered via RS UK, Order code 257-133.

481. Flow transducer dual range, ordered via RS UK, Order code 256-225.

482. PID controller 6100 West, ordered via Farnell UK, Order code 3080092.

483. Anti-scuffing paste with a high content of MoS_2 (-100 to 450 °C), Rocol Ltd., Leeds, UK ordered via RS 691-274.

484. OL 750, Optonic Laboratories Inc., US, www.olinet.com.

485. 238 High Current Source Measure Unit, Keithley, US, www.keithley.com.

486. Sulima, O.V., Bett, A.W. (2001) 'Fabrication and simulation of GaSb thermophotovoltaic cells', *Solar Energy Materials and Solar Cells*, 66, pp. 533-540.

487. Wang, C.A. (2004) 'Antimony-Based III–V Thermophotovoltaic Materials and Devices', *6th International Conference on Thermophotovoltaic Generation of Electricity*. Freiburg, Germany 14-16 June 2004: New York: American Institute of Physics, pp. 255-266.